The Pathophysiology of Retinal Ganglion Cell Death in Glaucoma

Sarah Farrant

School of Optometry and Vision Sciences, Cardiff University

Supervisors: Julie Albon, Jon Erichsen and James Morgan

A dissertation submitted to Cardiff University in candidature for the degree of Doctor of Philosophy

September, 2005

ProQuest LLC
789 East Eisenhower Parkway
P.O. Box 1346
Ann Arbor, MI 48106-1346

Summary

The optic nerve represents an important model for neurodegenerative diseases in addition to a number of neurodestructive ocular conditions. Among these, glaucoma is a common cause of optic nerve damage usually associated with an elevated intraocular pressure (IOP), retrodisplacement of the lamina cribrosa, reduced retrograde neurotrophic support and pathological cellular changes. Retinal ganglion cell (RGC) loss can continue after reduction of IOP to normal levels, indicating attenuated secondary neurodegeneration during which glia activate and proliferate. Activated glia may exacerbate glaucoma during secondary degeneration.

Experimental glaucoma was induced in Brown Norway rats using episcleral drainage vessel sclerosis. Neurodegeneration and cell death were assessed as a function of IOP variables. The effects of ocular hypertension on optic nerve microglia, immune cells, astrocytes and nitric oxide synthase (NOS) were determined by qualitative analysis of label-specific immunofluorescence

Ocular hypertension induced significant RGC death ($P<0.05$) and degeneration. Significant astrocytic GFAP elevation occurred following initiation of disease ($P<0.05$). Correlation of macrophage and microglial marker alterations indicated significant increases in both cell types following the induction of ocular hypertension and RGC death ($P<0.05$). Initial microglial up regulation appeared to be regulated by CD200 axis activity. Peripheral immune cells, including B lymphocytes, may have infiltrated the optic nerve during late stages of disease. Significant upregulation of nitric oxide synthase isoforms 1 and 2 in the optic nerve head, also demonstrated a positive correlation with microglial/macrophage increases ($P<0.05$). NOS3 was not upregulated following the induction of ocular hypertension.

Disrupted neuroglial interactions via the CD200 axis are likely to be involved in the initial glial response to ocular hypertension. Astrocytic and microglial activation may play a role in initiating and maintaining RGC death during chronic glaucoma. The production of NOS by these cells, particularly NOS2 by microglia, may serve to either promote or prevent optic nerve neurodegeneration.

Acknowledgements

I would like to acknowledge the assistance and support of my supervisors, Dr Jon Erichsen and Dr James Morgan. I would especially like to thank my supervisor Dr Julie Albon who has been a great friend and shoulder to cry on, as well as a patient supervisor throughout my PhD.

Furthermore I am indebted to Dr Saeed Aktar for his guidance with electron microscopy techniques, as well as his advice with many other matters including the politics of the School of Optometry and badminton.

I am very grateful to Martin Taylor for his patience and support with tonometry and surgery. Thank you Martin for all your hard work. I also thank my family for their continued support throughout my studies. In particular my sister, Rachel, without whom none of my pictures would have appeared at such high resolution or on such good quality photographic paper! Also, thank you to Bethan for temporary binding.

Last of all I would like to thank my post-doctoral research supervisors, Dr Derek Lang, and Prof Malcom Lewis. Thank you for putting up with me secretly working at correcting my PhD during the few occasions when I had time at work.

Declaration

This work has not previously been accepted in substance for any degree and is not being concurrently submitted in candidature for any degree.

SIGNED S. Carroll (candidate)

Date 30-9-05

STATEMENT 1

This thesis is the result of my own investigations, except where otherwise stated. Other sources are acknowledged by footnotes giving explicit references. A bibliography in appended.

SIGNED S. Carroll (candidate)

Date 30-9-05

STATEMENT 2

I hereby give consent for my thesis, if accepted, to be available for photocopying and for inter-library loan, and for the title and summary to be made available to outside organisations.

SIGNED S. Carroll (candidate)

Date 30-9-05

List of abbreviations

A one-way analysis of variance	ANOVA
Adenosine triphosphate	ATP
Aquired immunodeficiency syndrome	AIDS
Blood-brain barrier	BBB
Blood-retinal barrier	BRB
Bovine serum albumin	BSA
Brain-derived neurotropic factor	BDNF
CD200 ligand	CD200L
CD200 receptor	CD200R
Calmodulin	CaM
Carbon dioxide	CO_2
Central nervous system	CNS
1,4-Diazabicyclo[2.2.2]octane	DABCO
Deoxyribose nucleic acid	DNA
Diaminobenzoate	DAB
Di-sodium hydrogen phosphate	Na_2HPO_4
Endothelial nitric oxide synthase	NOS3
Extracellular matrix	ECM
Flavin adenine dinucleotide	FAD
Flavin mononucleotide	FMN
γ-amino butyric acid	GABA
Ganglion cell layer	GCL
Glial fibrillary acidic protein	GFAP
Glutamate receptor 1	GLAST-1
Growth factor	GF
Guanylyl cyclase	GC
Hydrochloric acid	HCl
Inducible nitric oxide synthase	NOS2
Industrial methylated spirit	IMS
Interferon-γ	IF-γ
Intraocular pressure	IOP

Lateral geniculate nucleus	LGN
Leukocyte common antigen	CD45
Lipopolysaccharide	LPS
Major histocompatability complex II	MHCII
NMDA receptors	NMDAR
NOS1 inhibiting protein	PIN
N-methyl-D-aspartate	NMDA
Nerve fibre layer	NFL
Neural cell adhesion molecule	N-CAM
Neuronal class III β-tubulin	TUJ-1
Neuronal nitric oxide synthase	NOS1
Neutral buffered formalin	NBF
Nitric oxide	NO
Normal donkey serum	NDS
Normal goat serum	NGS
Paraformaldehyde	PFA
Phosphate buffered saline	PBS
Polyoxyethylenesorbitan monolaurate	Tween-20
Posterior segment	PS
Potassium di-hydrogen phosphate	KH_2PO_4
Primary open-angle glaucoma	POAG
Proteinase K	PK
Retinal ganglion cell	RGC
Revolutions per minute	rpm
Ribose nucleic acid	RNA
Sodium chloride	NaCl
Sodium hydroxide	NaOH
Superior colliculus	SC
Suprachiasmatic nucleus	SCN
Terminal deoxynucleotidyl transferase-mediated deoxyuridine triphosphate nick end labelling	TUNEL
Tris buffered saline	TBS
Transforming growth factor	TGF

Tyrosine kinase	Trk
Water	H_2O

List of figures

List of tables

List of contents

Chapter I
General Introduction

1.1 The Human and Rat Optic Nerve

1.1.1 The course and nature of the optic nerve

Despite its relative structural simplicity, the rat optic nerve has anatomic parallels with that of humans and other primates. Although optic nerve features are similar across species, the rat optic nerve comprises only around 120,000 fibres (Hughes, 1977) as compared to the 1.1 to 1.3 million fibres of the human and 1.5 to 1.8 million fibres of the rhesus monkey optic nerve (Potts *et al.*, 1972a).

The optic nerve is an extension of the central nervous system, beginning at the retina as the optic nerve head or disc, and extending to the optic chiasm. On leaving the globe, nerve circumference increases due to individual fibre myelination and acquisition of a three-layered connective tissue meningeal sheath (Anderson, 1969). The optic nerve is devoid of a neurolemmal sheath, unlike peripheral nerves, which compromises its regenerative capacity. Damage to the optic nerves, similar to the brains white matter, is mostly irreversible (Scharenberg, 1953). The rodent and human optic nerves travel through the optic foramen and optic canal to enter the cranium. The nerves unite at the sub-thalamic optic chiasm where fibres of the human nerve semi-decussate. Semi-decussation is only partial in the rat. Visual fibres then proceed as oval bands to the peduncles where they diverge. The vast majority (90%) of human visual fibres terminate in the lateral geniculate nucleus (LGN) of the thalamus, while only few rat visual fibres project to this region. Some human visual fibres continue to the superior colliculi to form the superior brachium (Yamadori and Yamauchi, 1983), while the majority of rat visual fibres terminate here. Other fibres leave the optic tract before reaching the LGN and terminate in mid and hind brain oculomotor centres. The majority of human fibres take the retinogeniculocortical pathway as simplified in Figure 1.1.

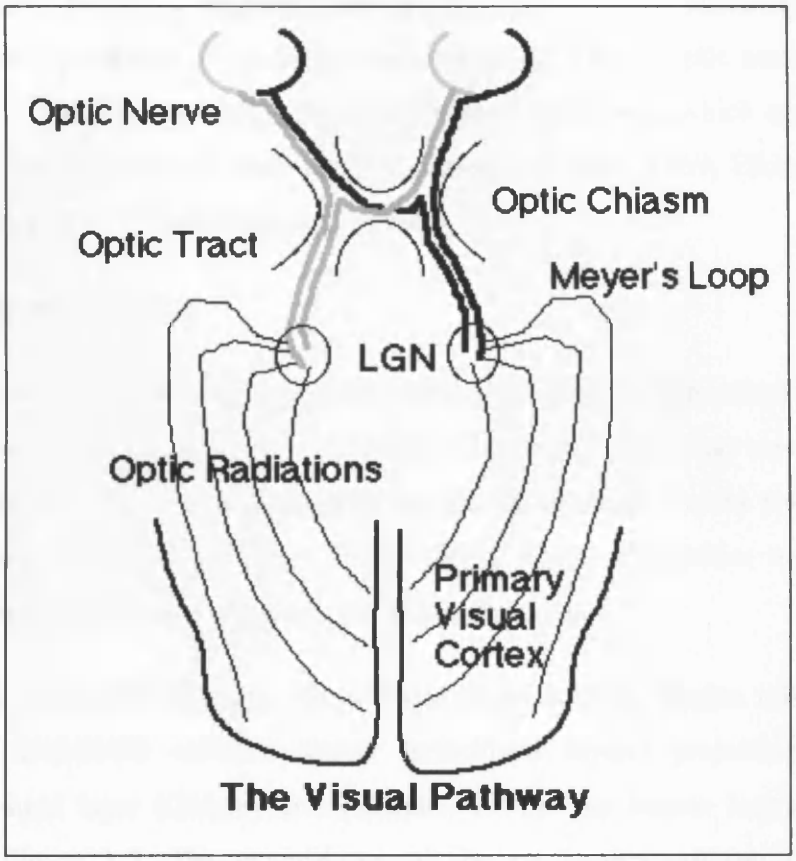

Figure 1.1 The retinogeniculocortical pathway *This route is taken by the majority of human retinal neurons from the retina, through the optic nerve to higher brain centres. The optic nerve projects from the eye and enters the brain. Partial decussation occurs at the optic chiasm, from where the majority of fibres project in the optic tract to the LGN. From here, fibres progress in their optic radiations to deliver visual information to higher brain centres in the cortex (Zigmond* et al.*, 2000).*

1.1.2 The optic nerve head

The optic nerve head or neck is formed from a coalescence of unmyelinated retinal ganglion cell (RGC) axons as they enter the optic disc from the retina. The rat optic nerve head has a distinctive architecture (Morrison *et al.*, 1995) and is horizontally oval in shape, compared with the more circular human optic nerve head (Anderson and Hoyt, 1969). All retinal layers terminate at the optic nerve head, excluding the nerve fibre axons, which pass through from ambient intraocular pressure (IOP) to lower pressure in the optic nerve (Ernest and Potts, 1968). The inner layer of the optic

disc is concave, forming a physiological cup, lined with residual intraorbital astroglia of the limiting membrane of Elschnig (Anderson *et al.*, 1967). Optic nerve axons are separated into fascicles by these specialised support astrocytes, which are orientated similarly to lamina cribrosa astrocytes (Anderson and Hoyt, 1969; Elkington *et al.*, 1990; Ogden *et al.*, 1988; Trivino *et al.*, 1996).

1.1.3 The lamina cribrosa

The collagenous projections of the lamina cribrosa, through which retinal axons pass, occupies the optic nerve head almost entirely. The rat equivalent has a conical shape with the beginnings of myelination and an almost identical protein content to the human lamina cribrosa (Morrison *et al.*, 1995). These similarities are useful in modelling human optic nerve disease, including glaucoma.

The human optic nerve becomes divided into bundles at the lamina cribrosa by 10 successive fenestrated collagen sheets (cribriform layers) projecting from the meningeal dural layer (Quigley and Addicks, 1981). The human lamina is shown clearly in Figure 1.2. The prominence of the rat lamina cribrosa in terms of collagenous material is less than that of the human (Morrison *et al.*, 1995).

Both the neck and transition zone of the rodent optic nerve exhibit transverse vessels with wide collagen filled perivascular spaces and astrocytic borders. These collagenous structures are ultrastructurally similar to primate lamina beams, and consist mainly of collagen types I, III and VI with some elastin (Morrison *et al.*, 1995). Chondroitin and dermatan sulphate-containing proteoglycans, with collagens I, III and VI, make up the lamina core surrounded by laminin and collagen IV (Morrison *et al.*, 1995).

Collagen IV and laminin are produced by astrocytes and vascular endothelial cells of the lamina cribrosa, as well as cultured lamina cribrosa cells (Hernandez *et al.*, 1988). The specialised supportive lamina cribrosa astrocytes also contain glial filaments including glial fibrillary acidic protein (GFAP). The lamina sheets are separated by astrocytes, whose processes are perpendicular to optic nerve axons, and directly contact the unmyelinated axons by entering the nerve fibre bundles (Anderson, 1969; Elkington *et al.*, 1990; Trivino *et al.*, 1996).

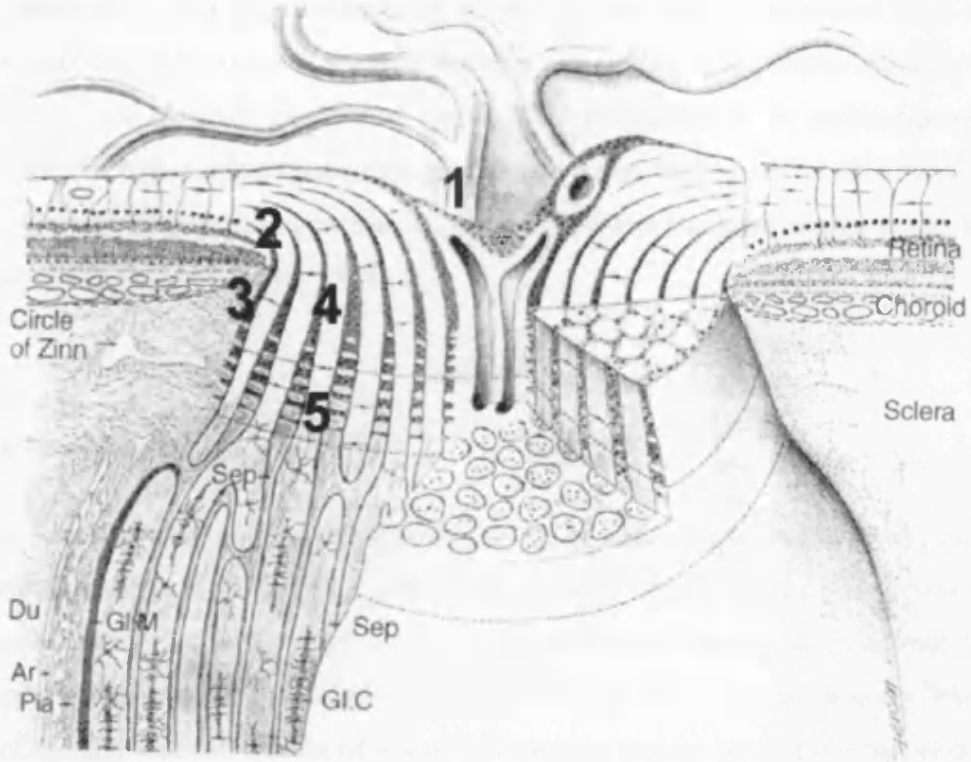

Figure 1.2 The human lamina cribrosa *This structure consists of collagenous projections into the nerve which separate the nerve fibre bundles into fasicles. Numbered regions: 1, central retinal vessels; 2, intermediary tissue of Kuhnt; 3, border tissue of Elschnig; 4, anterior lamina cribrosa; 5, posterior lamina cribrosa. Abbreviations: Du, dura mater; Ar, arachnoid; Pia, pia mater; GlM, periperal glial mantle of Fuchs; GlC, glial columns; Sep, pial septa. (Anderson and Hoyt, 1969).*

The lamina cribrosa provides support to optic nerve axons and protects them upon exit from the globe. Collagenous projections into the nerve at the lamina cribrosa constitute a threat to ganglion cell survival under conditions of stress. The role of the lamina cribrosa in resisting pressure from within the eye may become compromised, and give rise to diseases such as glaucoma (Quigley and Addicks, 1981). The site of RGC axonal damage in glaucomatous optic neuropathy is indeed the lamina cribrosa (Quigley, 1981).

1.1.4 The post laminar region

The optic nerve proper begins posterior to the lamina cribrosa, where individual axons become myelinated by oligodendrocytes. Consequently, nerve diameter increases, and

the measurement or quantification of nerve fibre loss can be performed more easily. The supportive framework alters to become pial septae, with similar constituents to the cribriform plates of the laminal region. Collagen types I, II, IV and V, laminin and fibronectin have all been localised here. Postlaminar regions differ structurally from the lamina cribrosa; less compact septae are orientated at right angles to the lamina supports (Sawaguchi *et al.*, 1994).

1.2 Glaucoma

1.2.1 Introduction to glaucoma

The glaucomas are a heterogeneous group of optic neuropathies with differing pathophysiological mechanisms. All share common characteristics of excessive optic disc excavation, accompanied by a specific pattern of retinal ganglion cell (RGC) degeneration and loss. Photoreceptors and retinal interneurons rely on RGCs to package and transmit quanta of visual information for use by higher brain structures. During glaucoma, RGC death results in a functional deficit over time. Normally this deficit is associated with an increased intraocular pressure (IOP), but vascular and structural alterations at the optic nerve head can also contribute. Visual field loss begins with peripheral vision, advances to the remaining visual field, and eventually compromises central vision (Sears, 1979).

1.2.2 History of glaucoma

The first recorded incidence of glaucoma by Sams-ed-Din, a fourteenth century Arab physician, described blindness accompanied by pain, immobile pupils and elevated IOP. Glaucoma was not described in Europe until the seventeenth century. Sir William Lawrence coined the term during the early nineteenth century, and in 1830, William Mackenzie associated the disease changes with IOP. Ophthalmoscopy enabled the discovery that glaucomatous optic disc cupping, and not disc elevation, resulted from IOP elevation (Duke-Elder, 1940).

1.2.3 Diagnosis

The glaucomas can be differentiated between and from other ocular conditions by an elevated IOP of over 21 mmHg (which occurs frequently, but not always),

accompanied by excessive optic disc excavation, and a specific pattern of visual field defect. Symptoms such as pain or deterioration of visual function can occur at any level from normal vision to complete blindness. However, pathophysiology can begin in a preceding asymptomatic phase (Quigley *et al.*, 1982[1]), diagnosed by a nasal step in the visual field, a notch in the optic disc, angle pathological signs, or afferent pupillary defect (Hitchings and Spaeth, 1976). The presence of pathological signs does not always indicate that symptoms will develop further, as although most glaucomas are progressive, some are stable (Martinez-Bello *et al.*, 2000).

1.2.4 Forms of glaucoma

Glaucoma can be divided into three primary categories: open-angle, closed-angle and congenital, as well as secondary, dependent on the primary defect.

1.2.4.1 Primary open-angle glaucoma

During primary (or idiopathic) open-angle glaucoma (POAG), chronic elevated IOP is partly responsible for bilateral optic nerve atrophy with an unknown initiation factor. As many as 25% of POAG patients have a normal IOP below 21 mmHg (Sommer, 1996). POAG can be subdivided by optic disc characteristics into focal, diffuse and vasospastic glaucoma, and typically has a late onset age. Open-angle glaucoma can also be secondary to vasospasm, trauma, and many other factors.

1.2.4.2 Primary angle-closure glaucoma

Narrow anterior chamber angles are associated with primary angle-closure glaucoma. Effects of angle-closure include mechanical blockage of aqueous outflow from the eye with associated IOP elevation. Inherited in a multifactorial manner, with a late onset age, angle-closure glaucoma can be divided into subtypes of acute, subacute and chronic. Angle-closure can also occur due to secondary insults such as ocular trauma.

1.2.4.3 Primary congenital glaucoma

Primary congenital glaucoma is an autosomal recessive disease with a higher incidence in males. The inheritance rate of primary congenital glaucoma is low, with

an incidence in siblings of 3-11%. Developmental aberrations in the anterior chamber angle, trabecular meshwork, iris and/or ciliary body are responsible for this disease.

1.2.5 Incidence

Glaucoma has serious implications for public health, accounting for 13% of all new registrations of blindness annually (Evans and Bird, 1996). Susceptibility to the disease depends on age, race and family history. It is estimated that 2% of Europeans and around 8% of African-Americans and African-Caribbeans over the age of 40 are affected (Egbert, 2002), making it the most common cause of blindness for the latter. Table 1.1 below shows the incidence of the different types of glaucoma.

Table 1.1 The incidence of glaucoma

Category of glaucoma	**Proportion of glaucoma patients**
Primary open-angle	66%
Primary closed-angle	28%
Primary congenital	1%
Secondary	5%

POAG has the highest rate of occurrence of all the glaucomas in a normal population, with an incidence of 0.5%. Acute angle closure glaucoma, the next most prevalent form of the disease, has an incidence of 0.1%. Congenital glaucoma has the lowest prevalence, occurring in 1 in every 30,000 live births.

1.2.6 Risk factors

Elevated IOP is considered one of the most important predisposing factors to glaucoma other than age (Armaly *et al.*, 1980; Wilson *et al*, 1987). Increased IOP can produce many optic nerve alterations, including compromise of vascularisation, reduced retrograde transport, and glial scarring (Yucel *et al.*, 1999), all of which may contribute to neurodegeneration (Soares *et al.*, 2003). However, IOP varies naturally, and glaucoma often occurs in normotensive eyes (Sommer *et al.*, 1991), with the majority of hypertensive eyes not developing glaucoma. Despite the importance of

elevated IOP, predisposition to glaucoma can result from a number of other factors (Georgopoulos *et* al., 1997; Le *et al.*, 2003; Wilson *et al.*, 1987).

Ocular conditions not associated with IOP may render affected eyes more susceptible to glaucomatous damage, for example myopia (Georgopoulos *et* al., 1997; Grodum *et al.*, 2001; Le *et al.*, 2003; Perkins and Phelps, 1982). Social factors can also be important (Fraser *et al.*, 2001; Wilson *et al.*, 1987). These factors are covered comprehensively in Table 1.2.

Table 1.2 Risk factors for glaucoma

Demographic factors	Age Race Family history (heredity)
Ocular risk factors	Angle configuration Large cupping of the optic nerve head Ocular ischaemia Glaucomatous damage to the fellow eye Elevated intraocular pressure Myopia Pigment dispersion Exfoliation syndrome Angle recession
Systemic risk factors	Peripheral vascular diseases Hyperviscosity states Arteriosclerotic and ischemic vascular diseases Malnutrition Hypotension or hypertension Diabetes mellitus Migraine
Lifestyle	Obesity Lack of exercise Smoking

1.2.7 Aqueous humor dynamics and intraocular pressure

An increased basal IOP is a major treatable risk factor for glaucomatous damage (Brubaker, 1996). IOP maintenance is a function of the aqueous humor, the drainage and production of which helps maintain globe structure and eye functions. Average ocular tensions of 19mmHg for the human (Armaly, 1965) and 15mmHg for the rat are considered average normal pressures. Deviation from these levels may be a result of increased production and/or limited drainage of the intraocular aqueous.

1.2.7.1 Aqueous humor production

Aqueous is produced at a rate of 2.4 +/- 0.6 µl/hour. Circadian variation reduces production during the night for diurnal and during the day for nocturnal species (Gharagozloo *et al.*, 1988; Pointer, 1997). Control of aqueous humor diffusion or active secretion from the ciliary body is a function of the suprachiasmatic nucleus (SCN). The SCN receives a direct retinal projection and belongs to a system responsible for circadian timing, to which it is connected by sparse efferent hypothalamic projections (Stephan and Zucker, 1972). Coupled oscillator SCN neurons form a pacemaker within the core or ventrolateral SCN (Moore *et al*, 1996).

Core SCN neurons contain vasoactive intestinal polypeptide, calretinin, somatostatin, substance P, gastrin releasing peptide (Karatsoreos *et al.*, 2004) and γ-amino butyric acid (GABA). All may have a role in the complex sympathetic control of circadian rhythm. The core SCN receives primary entraining afferents and contains pacemaker neurons responsible for circadian oscillations including that of IOP. The sympathetic nervous system and β-adrenergic receptors are important in control of these oscillations and circadian aqueous flow (Nii *et al.*, 2001). Epinephrine can reduce IOP (Wang *et al.*, 2002), and selective β-receptor antagonists can increase aqueous production.

1.2.7.2 Aqueous humor drainage

Aqueous humor exits the eye via two main drainage routes. The direct outflow pathway accounts for 80% of drainage via the trabecular meshwork, Schlemm's canal, and collector channels into the intrascleral and episcleral venous plexus (Figure

1.3). The uveoscleral outflow pathway allows 10% of indirect outflow, with the remaining 10% accounted for by aqueous humor outflow via the iris stroma.

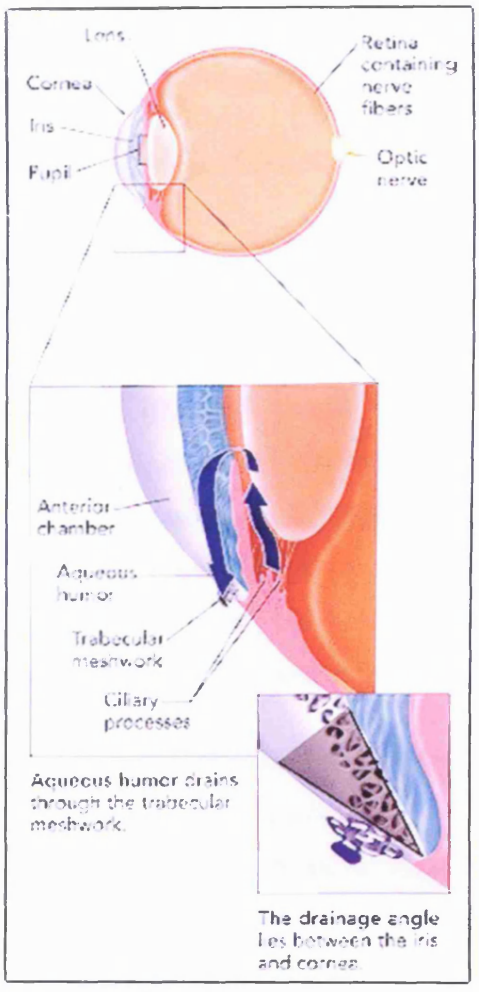

Figure 1.3 The direct aqueous drainage pathway *The direct outflow pathway that accounts for 90% of aqueous leaving the eye is shown to the left. The upper diagram shows the eye and subsequent images are of ocular areas with relevance to aqueous drainage. The ciliary processes just below the iris produces aqueous humor, which travels around the iris to rest behind the cornea in the anterior chamber. Aqueous is drained mainly through the trabecular meshwork which lies at the irido-corneal junction. For alternative aqueous drainage pathways see text (*www.harthosp.org/eyes/ procedures /glaucoma.htm*).*

1.2.7.3 The trabecular meshwork and glaucoma

The posterior trabecular meshwork forms a self-cleaning filter over Schlemm's canal, consisting of a uveal, corneoscleral, and endothelial meshwork. Glaucoma may affect this filter, reducing aqueous outflow, and increasing IOP. Plaques of extracellular debris around the endothelial meshwork increase in abundance with age, and even more so with glaucoma (Rohen, 1983). The cellular component of the trabecular meshwork is also decreased with POAG (Alvarado *et al.*, 1984). In advanced glaucoma, uveal and corneoscleral meshworks become completely obstructed through

trabecular beam hyalinisation. Lack of endothelial lining causes the subendothelial basement membranes to thicken and fuse. Uveal meshwork trabecular cells also become enlarged (Lutjen-Drecoll 1996). Other glaucoma types, exluding juvenile and normotensive glaucoma, all have aqueous humor outflow defects contributing to an increased IOP (Furuyoshi *et al*, 1997).

1.2.8 Heredity and genetics

Glaucoma is passed on to a certain degree by inheritance (Georgopoulos *et* al., 1997). First-degree relatives of glaucoma sufferers have a six-fold greater prevalence than others (Davies, 1968). However, inherited mutations are not common causes of glaucoma (Richards *et al*, 1998). Various disease attributes can have a genetic component, including increased IOP, cup-to-disc ratio, ocular dimensions, as well as decreased aqueous humor drainage. Particular forms of glaucoma are associated with other diseases or phenotypes, for example diabetes, suggesting inheritance (Le *et al.*, 2003; Wilson *et al.*, 1987). Genetic markers of glaucoma are not inherited in simple Mendelian fashion, and the disease is multifactorial.

For example, myocilin (also known as trabecular meshwork-inducible glucocorticoid response protein) is found in RGC axons and astrocytes at the lamina cribrosa (Karali *et* al., 2000). Mutations in this protein are associated with juvenile open-angle glaucoma (Sheffield *et al.*, 1993; Wiggs *et al.*, 1994). Elevated IOP upregulates other physiologically relevant trabecular meshwork genes; the products suggest a homeostatic mechanism in the regulation of aqueous humor drainage similar to the regulation of blood vessel permeability (Gonzalez *et al.*, 2000). Elevated genes include transcripts for proteins involved in vascular permeability, secretion, extracellular matrix remodelling, cytoskeleton reorganisation and reactive oxygen species scavengers (Gonzalez *et al.*, 2000).

1.2.9 Treatment

Glaucoma treatments are numerous and varied, as might be expected from such a multi-faceted disease (reviewed by Schwartz and Budenz, 2004 and Sung and Barton, 2004). Despite the high incidence of glaucoma, no treatment exists which can prevent or repair the continued RGC loss typical of the disease. At present the most a patient

can hope for is a delay in the loss of visual field. Similar treatments are used for patients with hypertensive and normotensive glaucoma (Goldberg, 2003), as reduction of IOP for relatively normotensive eyes is also beneficial. The specific course of treatment does vary to some extent with the type of glaucoma.

Pharmaceutical glaucoma treatment most commonly targets reduction of aqueous production and secretion in combination therapies. Prostaglandin analogues, such as latanoprost, increase uveoscleral aqueous outflow. Alpha(2)-adreonoreceptor agonists and beta-adrenoreceptor antagonists can reduce aqueous production by interaction with the neuroendocrine epinephrine system responsible for aqueous secretion.

Drug treatments are commonly complemented by surgical treatment when no improvements are found. Surgical treatment similarly focuses on IOP reduction. Laser trabeculoplasty and filtration surgery are often used to reduce resistance to aqueous outflow in the trabecular meshwork or to create a new direct outflow route. These procedures will often need to be repeated to sustain IOP reduction.

Less invasive and more effective treatments are sought for the prevention of RGC loss, and possible restoration of visual function. New therapeutic strategies need to be explored due to surgical side effects (such as loss of vision), and the progression of glaucoma despite a reduction in IOP. Once the exact mechanisms of RGC pathophysiology during glaucoma are known, it will be much simpler to devise appropriate and efficient therapeutics. These will need to be used in conjunction with early clinical detection for optimal patient outcome.

1.3 Pathophysiology of the Optic Nerve Head

Glaucomatous degeneration of the optic nerve head is heterogeneous. However, damage always affects the retinal nerve fibre layer (NFL) and the visual field. Depending on the optic nerve head pathology or type of glaucoma, the NFL is targeted in either a focal or diffuse manner.

1.3.1 Optic disc changes

The optic nerve head is often the first and most commonly affected tissue during glaucoma (Quigley and Addicks, 1981) Non-sequential characteristic changes of the optic disc occur. Generally these involve an increasingly enlarged physiologic cup, which retrogradely displaces the optic disc (Burgoyne *et al.*, 1995), increasing the cup-to-disc ratio.

1.3.1.1 Optic disc pallor

The normal optic disc is a pink-orange colour. Disc pallor occurs during glaucoma (Tuulonen *et al.*, 1987), indicating that IOP has persistently risen causing capillary drop out. Optic nerve damage, and/or neuroretinal rim tissue degeneration can also be indicated by pallor (Caprioli and Miller, 1988; Quigley *et al.*, 1982b).

1.3.1.2 Optic cup changes

The optic nerve head surface can become altered in a three-dimensional fashion during normal development and glaucoma. Overpass cupping, where the material between the inner limiting membrane of Elschnig and the lamina cribrosa are destroyed (Hitchings and Spaeth, 1976), and optic cup asymmetry are common in glaucoma. Concentric enlargement of the optic cup from loss of neuroretinal rim tissue and vertical enlargement due to loss of laminar tissue with a similar cup/disc ratio in all axes can be associated with glaucoma (Figure 1.4). Sometimes optic cup enlargement includes notching at the superior and inferior poles. During glaucoma the optic cup becomes large compared to the total disc size.

1.3.1.3 Vascular changes in and around the optic disc

Optic disc blood vessels can become altered or insufficient in association with glaucoma (Cioffi and Sullivan, 1999). Haemorrhages at the outer edge of the inferotemporal sector of the optic disc are found in 4 to 7% of glaucomatous eyes (Drance *et al.*, 1977; Drance, 1989; Healey *et al.*, 1998). This frequently results in localised nerve damage, notching of the disc, or aquired pit of the optic nerve and occurs most often in normotensive glaucoma (Airaksinen *et al.*, 1981). Haemorrhage

may be due to chronic ischemia or to structural optic nerve alterations causing damage to blood vessels.

Elevated IOP can compromise normal blood flow producing vascular looping on the optic disc and a nasal shift in the optic disc's blood supply (Jonas *et al.*, 1989). Decreased blood flow may also result in dilation of retinal veins and narrowing of retinal arteries (Rader *et al.*, 1994). Retinal pigment epithelium and choriocapillaries can sometimes deteriorate adjacent to the optic disc (the β zone), which becomes enlarged and atrophied during glaucoma. Peripheral to this area, irregular pigmentation can occur (the α zone) in peripapilliary chorioretinal atrophy, characteristic of glaucoma.

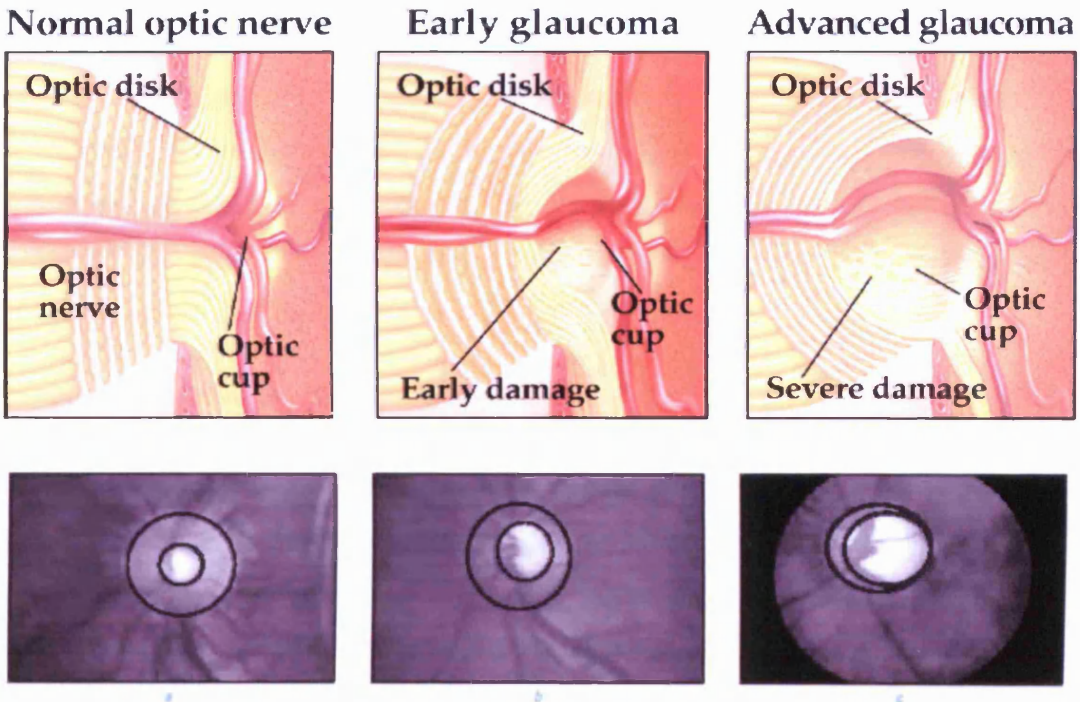

Figure 1.4 Progressive glaucomatous changes at the lamina cribrosa and optic disc
In the normal optic nerve the optic cup is relatively small, and the lamina cribrosa appears straight. The ratio of rim to disc area is normal. In early glaucoma slight enlargement of the cup, with a reduction in the rim to disc ratio is seen. This is accompanied by retrograde bowing of the lamina cribrosa. In advanced glaucoma the lamina cribrosa suffers severe retrograde displacement. The optic cup is typically enlarged, and the ratio of rim to disc is further reduced (www.merckfrosst.ca/.../what_is/home.html).

1.3.1.4 Lamina cribrosa

Lamina cribrosa pathophysiology can involve collapse and rotation of the cribriform plates due to elevated IOP, leading to crush injury of RGC axons (Quigley *et al.*, 1981b; Quigley *et al.*, 1982a). Retrograde bowing and degeneration of the lamina cribrosa can also occur (Bellezza *et al.*, 2003), which is more likely with increasing age (Albon *et al.*, 1995; Albon *et al.*, 2000). This leads to increased optic cup depth (Figure 1.4). During glaucomatous degeneration the lamina pores become visible and compressed due to elevated IOP and death of nerves (Maeda *et al.*, 1999).

1.3.2 Visual field loss

A characteristic pattern of visual field loss is followed during glaucoma (Quigley *et al.*, 1982a). Visual acuity remains unaffected, and early detection of the disease can be difficult. Visual field degeneration begins as general or localised, eventually becoming advanced. During ocular hypertension loss of vision begins in the periphery, and progresses eventually to the central vision. However, in normotensive glaucoma central defects can precede those of the periphery.

1.3.2.1 Generalized visual field defects

Generalised decreased sensitivity to visual stimuli can often occur early in glaucoma and other forms of visual degeneration due to diffuse loss of RGCs. Asymmetric visual field loss occurs frequently during glaucoma, for example in hemifield asymmetry where the extent of optic disc damage varies between superior and inferior poles. Characteristically, the upper nasal quadrant of the field is first affected, and the last area to remain unaffected in advanced glaucoma is the temporal inferior visual field (Ferandez *et al.*, 1993).

1.3.2.2 Localised visual defects

The first detectable localised glaucomatous defect is acute scotoma, when arcuate (or bow shaped) RGCs have suffered damage resulting in insensitivity to stimuli. Damage then progresses to the superonasal periphery, followed by inferior arcuate scotoma and then damage to the inferonasal periphery (Kitazawa and Yamamoto, 1997).

1.3.2.3 Advanced field loss

Advanced visual field loss or tunnel vision involves preservation of only central and/or temporal vision, with complete loss of vision in the periphery. Eventually central and temporal vision will be lost, should the disease remain and persist untreated.

1.3.3 Retinal nerve fibre defects

RGC axons, astrocytes, blood vessels and Muller cell processes comprise the retinal NFL, where abnormalities associated with glaucoma may occur. It is proposed that larger diameter RGC axons localised in the majority to superior and inferior retinal poles degenerate more quickly than smaller diameter axons, possibly due to less resistance to ischemic damage or IOP (Yablonski and Asamoto, 1993).

Defects in the NFL can appear as small, narrow slits or grooves, which extend to the optic disc margin. Peripherally enlarged wedges of the disc (Jonas and Papastathopoulos, 1996; Quigley, 1987), represent areas of localised nerve damage, and often occur as a result of haemorrhage. The glaucomatous NFL also suffers diffuse atrophy frequently accompanied by concentric enlargement of the optic cup and reduced retinal sensitivity. Loss of neuroretinal rim, including retinal nerve fibres, can be diffuse and affect any sector of the optic disc, appearing as notching or acquired pit of the optic nerve (Jonas and Papastathopoulos, 1996).

The presentation of NFL defects depends on the stage of glaucoma (Javitt *et al.*, 1990). Normally, defects do not occur until the rim tissue is less than 0.5 as part of the rim/disc ratio (Jonas *et al.*, 1988) and then correlate with the pattern of visual field loss.

1.4 Mechanisms of Retinal Ganglion Cell Death

1.4.1 Introduction

Glaucomatous degeneration coincides with considerable loss of RGCs, normally via apoptosis (Kerrigan-Baumrind *et al.*, 2000). Subsequent to initial damage and primary RGC loss, secondary damage occurs, which may be initiated by factors separate to

those involved in primary loss (Schwartz *et al.*, 1996). RGCs normally respond to injury with a low regenerative capacity. Thus there is virtually no return of function following degeneration.

1.4.1.1 Elevated intraocular pressure

Elevated IOP is a major risk factor for glaucoma. However, other disease features may define the role of IOP during initiation and chronic RGC degeneration. These other factors, such as vasospasm or mechanical properties of the lamina cribrosa, may also have a role during initiation of cell death. During chronic glaucoma, RGC degeneration continues despite reduction of IOP to normal levels, indicating that other factors may be involved in secondary degeneration (Brubaker, 1996; Cockburn *et al.*, 1983). This is supported by a similar loss of RGCs during normotensive glaucoma.

1.4.2 Axonal transport blockade

Axoplasmic transport involves bi-directional organelle and metabolite movement along the axon. Both orthograde and anterograde components, as well as fast and slow phases can become blocked during glaucoma. The degree of axonal blockage can be correlated with duration and magnitude of IOP elevation (Johansson, 1983; Samuelson and Spaeth, 1983). However, axoplasmic obstruction has been found in some normotensive, low perfusion pressure eyes, and it does not always occur in conditions of high IOP or ischaemia (Sugiyama *et al.*, 1995; Cincaglini, 2001).

The lamina cribrosa is the anatomical barrier between the IOP and subarachnoid pressure that commonly becomes obstructed when axoplasmic transport is blocked (Quigley *et al.*, 1981[1]). Pressure gradient alterations distort the lamina cribrosa beam structure leading to mechanical axonal injury and accumulation of mitochondria and microvessels (Minckler and Spaeth, 1981; Yablonski and Asamoto, 1993). Axons at the periphery of a bundle are more likely to suffer damage, as are bundles at the poles of the disc. These areas are populated by arcuate fibres, which are therefore more likely to suffer initial damage (Fizgibbon and Taylor, 1996; Quigley and Anderson, 1977).

1.4.3 The neurotrophin hypothesis

The neurotrophins are polypeptide growth factors involved in development, differentiation and survival. Neurotrophins signal through either tyrosine kinase (trk) or p75 receptors. Trk A, B and C bind specifically to different neurotrophins, while p75 binds is non-neurotrophin specific. Normally, neurotrophic factors, produced by the LGN and superior colliculus (SC), travel retrogradely to RGC bodies. The RGC response to neurotrophins is likely to be modulated by astrocytes and lamina cribrosa cells through paracrine signalling (Lambert *et al.*, 2001).

The axonal transport blockade leads to deprivation of neurotrophins and RGC death from lack of neurotrophic support (Quigley and Anderson, 1977). This is thought to involve specific and sequential changes in receptor and neurotrophin distribution at the optic nerve head, RGCs, LGN and superior colliculus. The temporal response to IOP indicates that cessation of neurotrophin transport should be considered, amongst other pathological factors, to contribute to RGC death (Johnson *et al.*, 2000). However, neurotrophic support is not the only or principal factor involved.

Neurotrophin-3, neurotrophin4/5, nerve growth factor, ciliary-derived neurotrophic factor and fibroblast growth factors are neuroprotective, and reduce apoptotic death of RGCs previously deprived of neurotrophic factors (Quigley *et al.*, 1995). However, RGC supporting growth factors can compensate for each other (Cellerino *et al.*, 1997). If a particular neurotrophin is present in the cell, it will compensate for the loss of another due to redundancy among the neurotrophin family. Also, the Trk B receptor is not essential for adult neuronal survival (Rohrer *et al.*, 2001). The effect of neurotrophin deprivation is therefore unlikely to be the primary cause of damaging glaucomatous changes (Nickells, 1996).

1.4.4 Vascular factors and ischemia

Disturbance of vascular circulation is involved in RGC death in glaucoma. Decreased blood flow, or low blood pressure and its consequences are important predisposing factors frequently associated with glaucoma (Johnson and Matsumoto, 2000). Decreased blood pressure in the retina, leading to ischaemic damage is responsible for disease pathology, particularly in normal-tension glaucoma (Drance *et al.*, 1973; Gasser, 1999). Reduced blood flow in the choroid and optic nerve head can also produce damage (Wolf *et al.*, 1993).

1.4.4.1 Endothelin in vasospasm

Endothelin-1 levels are important in maintaining vascular tone. During normotensive and hypertensive glaucoma endothelin-1 levels are increased (Michaelson, 1996; Tezel *et al.*, 1997). This promotes vasoconstriction in the ocular circulation, particularly at the optic nerve, resulting in ischaemic damage. This vasospasm is thought to be localised to ciliary or choroidal vessels, and can be prevented by calcium-channel blockers (Toriu *et al.*, 2001), which also improve the visual field. These antagonists are believed to prevent the normal response to endothelin-1, but various other factors could be involved due to the complex physiology of calcium channels, and the many different causes of glaucoma. Also, astrocytes synthesise and are targets for endothelin-1, and thus endothelin levels may affect their proliferation in glaucoma (Prasanna *et al.*, 2002; Ripodas *et al.*, 2001).

1.4.4.2 Ischaemia

Evidence suggests that ischaemia participates in prevention of axoplasmic transport and subsequent RGC death, during increased IOP (Luo *et al.*, 2001). Optic nerve head ischaemia in experimental hypertension can produce morphological alterations in RGCs. These changes include accumulation of organelles in the lamina region, and swelling of axons at the optic disc. Attempts to prevent ischaemia under conditions of elevated IOP do not alleviate axonal blockage (Hayreh *et al.*, 1979). Therefore, it is

likely that other factors are more paramount in the prevention of axonal transport during glaucoma.

Haemodynamics can contribute to optic nerve head damage independent of the IOP level. The role of chronic or acute ischaemia in the glaucomatous axonal transport blockade is uncertain, and may involve excitotoxicity or free-radical damage. It is possible that neurotoxins such as nitric oxide (NO), released during ischaemia, are involved in cell death.

1.4.5 Excitotoxicity

Glutamate is an excitatory amino acid neurotransmitter, which is excitotoxic at high concentrations. Glutamate is likely to be the excitatory neurotransmitter used by RGCs, and it also has a role in neuronal plasticity and survival (Kleinschmidt, Bear and Singer, 1987; Lipton and Kater, 1989). Glutamate from damaged neurons can accumulate in the synaptic cleft to a toxic concentration during growth factor deprivation, hypoxia, ischaemia or excitotoxicity. Excess activation of N-methyl-D-aspartate (NMDA) receptors by increased glutamate results in over-stimulation of calcium channels; intracellular calcium concentration elevates, and overloads the cell. Apoptosis of RGCs can be caused by the neurotoxicity of excess glutamate (Varma 1996). However, survival is improved by the presence of retinal glia, particularly Muller cells as well as NMDA receptor inhibition (Kitano, Morgan and Caprioli, 1996). Muller cells are thought to have a role in excitatory signalling in the normal retina (Rauen *et al.*, 1998). It is likely that the protective action of these cells is mediated through the glutamate receptor GLAST-1, which has a high affinity for glutamate (Rauen *et al.*, 1998).

Toxic levels of glutamate have been shown in monkey and human glaucoma in the optic nerve (Dreyer *et al.*, 1996). Glutamate-mediated excitotoxicity may also be involved in other central disorders such as stroke. However, prevention of excitotoxicity through NMDA receptor antagonism is not an effective neuroprotective strategy following stroke. This may be due to the interference with normal neuronal signalling as well as the induction of excitotoxicity very early in disease (reviewed by

Hoyt *et al.*, 2004; Ikonomidou and Turski, 2002). Therefore, this type of intervention following glaucoma should be approached with caution.

1.4.6 Neurodegeneration

Following lethal insult to the RGC, death will ensue via processes typical of classical neurodegeneration in a retrograde manner (Richardson *et al.*, 1982). This includes Wallerian degeneration, the chromatolytic reaction and apoptosis or necrosis.

1.4.6.1 The pattern and rate of neurodegeneration

Neurodegeneration typically begins in the superior retina during rodent experimental glaucoma, indicated by reduction of neurotrophins and loss of RGCs (Johnson *et al.*, 2000). The superior retina is the focus of RGC damage, with other areas becoming affected only in severe cases (Johnson *et al.*, 2000). RGC degeneration is detectable twenty hours after the induction of elevated IOP in rodent experimental glaucoma (Naskar *et al.*, 2002), and continues at a rate whereby 4% of cells are lost per week (Laquis *et al.*, 1998).

1.4.6.2 Wallerian degeneration

Axotomy involves transection of axons by either cutting or crushing (Wall, 1979), for example, when the damaged lamina cribrosa crushes optic nerve fibres. Axons distal to the site of injury slowly degenerate due to detachment from the cell body. Neurotransmission is prevented, myelin is degraded and surrounding glia are affected. Phagocytic peripheral macrophages and glial cells eventually remove fragmented glia and axonal remains from the degenerating nerve (Lassmann *et al.*, 1978; Ling, 1989; Mueller *et al.*, 2003; Shen and Liu, 1984). This process is called Wallerian degeneration and proceeds in a protracted retrograde manner (Liu *et al.*, 2000; Richardson *et al.*, 1982).

1.4.6.3 Chromatolysis

After injury, the proximal RGC axon and cell body show features typical of the chromatolytic reaction (Gennarelli *et al.*, 1989; Maxwell *et al.*, 1994; Shibuya *et al.*, 1993). Chromatolysis involves a sequential set of changes occurring in the perikaryon, beginning with swelling, eccentric positioning of the nucleus, and fragmentation of rough endoplasmic reticulum. These changes are accompanied by metabolic alterations including an increase in protein and RNA synthesis as well as altered gene expression. Survival of chromatolysis normally occurs at a high rate in peripheral nerves in stark contrast to the neurons in the central nervous system (Ahmed *et al.*, 2001), including the optic nerve (Kermer *et al.*, 2001).

1.4.6.4 Apoptosis and Necrosis

Neuronal death in disease is usually via apoptosis or necrosis. Apoptosis is an active process involving induction of certain genes, and is the most common form of cell death (Schulze-Osthoff *et al.*, 1998). However, some neurodegenerative diseases involve nerve death via neither of these routes, for example, Huntington's disease (Turmaine *et al.*, 2000).

Apoptosis classically begins with a reduction in ATP levels, DNA fragmentation and condensation of chromatin at the inner nuclear envelope to fill the nucleus, and cell shrinkage. The cell degrades into small membrane-bound vesicles. Neighbouring cells phagocytose cellular remains without causing an immune response. Necrosis involves swelling of the cell, disruption of membrane integrity and DNA fragmentation. Unlike apoptosis, cellular contents are released into the surrounding area, eliciting an immune response. Most often the process of cell death will follow an intermediate route between apoptosis and necrosis (Nicotera *et al.*, 1997; Bonfoco *et al.*, 1995).

Apoptosis, or programmed cell death is the likely pathway of neuronal loss in glaucoma. Similarly optic nerve transection induces loss of 80-90% of RGCs within 14 days. In the majority, death is via apoptosis, with necrosis occurring to a lesser extent (Kermer *et al.*, 2001).

1.5 Animal Models Used to Study Retinal Ganglion Cell Death

1.5.1 Introduction

Research into the precise mechanisms of glaucomatous damage to RGCs has progressed with the development of appropriate and suitable laboratory animal models in which to study this phenomenon. Various animal models of glaucoma exist, which utilise a range of species and techniques. The main focus of experimentally induced glaucoma involves rat and primate models developed to assess the effect of high IOP on optic nerve axonal damage. These models can be used to investigate therapeutic measures for preventing such damage.

1.5.2 Animal models of ocular hypertension

Models of ocular hypertension provide insights on optic disc cupping pathophysiology and optic nerve degeneration found in human glaucoma (Sawada and Neufeld, 1999). Considerable evidence exists to this effect. For example, information on lamina cribrosa distortion, axonal transport blockade and neurotrophin deprivation (Johnson *et al.*, 2000) has been supplied by such models. Axoplasmic transport is blocked following hypertension in the optic nerve many glaucoma models including mammals and primates (Quigley and Addicks, 1980). Rodent and primate models are the most widely used and where possible findings are compared to and confirmed in human eyes.

1.5.2.1 Primate experimental glaucoma

The monkey eye and optic nerve are very similar to that of the human. Costly primate glaucoma models are particularly informative, and well suited to pharmaceutical testing.

Methods for the induction of elevated IOP in primates include injection of α-chymotrypsin into the posterior chamber. Chymotrypsin causes lysis of zonular fibres which blocks the trabecular meshwork, minimising drainage from the eye (Chee and

Hamasaki, 1971). More commonly, laser-induced chronic IOP-dependant primate glaucoma is induced by laser scarification of the trabecular meshwork (Carter-Dawson *et al.*, 2002; Lam *et al.*, 2003; May *et al.*, 1997; Pederson and Gaasterland, 1984; Radius and Pederson, 1984; Wang *et al.*, 1998). Trabecular meshwork outflow can also be compromised by the injection of sterile latex microspheres into the anterior chamber (Weber and Zelenak, 1991).

In primate experimental glaucoma, as in the human disease, elevated IOP can result in axonal transport blockade and consequent nerve damage (Anderson and Davis 1974; Quigley and Addicks, 1980), including alterations in viability and size of both the axon and soma (Lampert *et al.*, 1968; Weber *et al.*, 1998). Primate models also exhibit glial changes in the prelaminar region (Furuyoshi *et al.*, 2000), oligodendrocyte degeneration, phagocyte increase, and astrocyte activation (Varela and Hernandez, 1997; Lampert *et al.*, 1968). Neuronal loss extends to the LGN and primary visual cortex (Vickers *et al.*, 1997; Yucel *et al.*, 2003). Primary visual cortical plasticity can also be affected (Lam *et al.*, 2003a).

1.5.2.2 Lapine glaucoma models

Rabbit glaucoma models are not commonplace due to low structural prominence of the lamina cribrosa, myelination of the retinal nerve fibre layer and a lack of central retinal vasculature (Sugiyama *et al.*, 1992). IOP-lowering drugs and the pathways of aqueous control are investigated in the rabbit. Ocular hypertension can be induced in the rabbit using laser-induced trabecular meshwork photocoagulation with consequent size-dependent RGC death. However, the absence of NFL loss in early disease means that NFL thickness cannot be used as an accurate diagnostic measure of glaucoma in this model.

1.5.2.3 Murine models and genetics

The potential genetic causes and molecular pathways of glaucomatous degeneration can be elucidated using mouse glaucoma models (John *et al.*, 1999). Screening and characterisation of glaucomatous mouse strains with various phenotypes have helped

to improve our understanding of glaucoma despite the lack of a lamina cribrosa (May and Lutjen-Drecoll, 2002).

In particular inbred AKXD-28/Ty and DBA/2J mouse strains are affected by inherited glaucoma (Anderson *et* al, 2001; John *et al.*, 1998). Both strains develop IOP-induced age-related glaucoma with optic nerve damage and RGC degeneration (Anderson *et al.*, 2001). DBA/2J is genetically very homogenous, allowing extremely accurate assessment of glaucoma-associated phenotypes.

1.5.2.4 Modelling glaucoma in the rat

The rat optic nerve is similar in structure to that of the human, unlike other rodents, such as the mouse (May and Lutjen-Drecoll, 2002; Morrison *et al.*, 1995). Consequently the rat is useful in studies of glaucoma. This is supported by the fact that experimentally elevated IOP in the rat produces changes homologous to those found in human glaucoma (Johnson *et* al., 1996; Johnson *et al.*, 2000).

The most recent glaucoma model in the rat consists of chronically developing inherited glaucoma. Royal College of Surgeons rats have been bred to produce the only high incidence rat strain with genetically elevated IOP and other glaucoma symptoms (Thanos and Naskar, 2004). As POAG has the highest incidence of all the glaucomas, models of this form of the disease are preferred to the less clinically relevant spontaneous and secondary glaucoma models.

Experimental glaucoma can also be induced in the rat by translimbal laser photocoagulation of the trabecular meshwork (Levkovitch-Verbin *et al*, 2002). Laser photocoagulation can be preceded by injection of India ink into the anterior chamber (Ueda *et al.*, 1998). This is often performed on albino rats, whose RGC survival following injury may be compromised through lack of melanin (LaVail and Gorrin, 1987). Despite drawbacks in terms of expense, this model is useful for the production of ocular hypertension-induced RGC death, and produces a measurable functional deficit (Grozdanic *et al.*, 2004).

Injection of S-antigen into the anterior chamber of the rat eye is also used to produce a glaucoma model (Mermoud *et al.*, 1994). This model has some severe drawbacks including the invasive nature of the anterior chamber injection. The immune reaction caused by S-antigen injection and the resulting uveitis are not representative of human glaucoma. However, a sustained IOP elevation of around 75% can be maintained for up to 20 days using this method (Mermoud *et al.*, 1994).

More commonly, uniocular hypertension is produced in rats by cauterisation of limbal aqueous drainage veins (Garcia-Valenzuela *et al.*, 1995; Sawada and Neufeld, 1999). The degree of ocular hypertension is proportional to the number of veins occluded; hence single vein cautery will produce mild (1.5-fold) elevation (Neufeld, 1999), while cauterisation of two or more veins results in at least a 2-fold increase in IOP (Garcia-Valenzuela *et al.*, 1995). The ability to manipulate the magnitude of pressure increase is a desirable feature of ocular hypertension models. Also favourable are the technical simplicity and the reliable increase in IOP. However, cauterisation of the limbal veins limits venous blood return from the eye. It is likely that vascular congestion affects IOP (reviewed by Goldblum and Mittag, 2002).

Direct unilateral injection of mild sclerosants into the aqueous humor outflow pathway can be used to increase IOP in inbred Norwegian brown rats (Morrison *et al.*, 1995). Mild sclerosants collapse a single aqueous drainage vessel and impede aqueous humor outflow, resulting in IOP elevations from 7 to 20 mmHg above control eye pressure. Sclerosant injections were repeated if unsuccessful, or IOP was reduced over time. Chronic primary glaucoma was modelled by increasing IOP by 10 – 20mmHg for three weeks, or more than 20mmHg for one week. These animals exhibited degeneration throughout the optic nerve, with very few axons appearing normal. Extracellular matrix components were deposited at the optic nerve head in plaques similar to human glaucoma, and axoplasmic transport was affected (Johnson *et al.*, 1996).

This model minimises circadian flux of IOP to prevent distortion of experimental results. Normal IOP varies from 21mmHg in the light to 31mmHg in the dark in animals subjected to a normal 12:12 light:dark cycle. The peak of IOP during the dark

phase of the circadian cycle, and the compromise of aqueous drainage, would result in the greatest modulation of IOP following treatment occurring during the night. Constant light introduced for a minimum of three days in this model ensures elimination of circadian control of IOP. Consequently IOP could be reliably measured at any time.

In the glaucoma model developed by Morrison *et al.* (1995), experimental ocular hypertension can be induced with various degrees and durations of pressure elevation to emulate primary open angle glaucoma, the most common form of the human disease. Changes observed in this model correspond to degeneration observed in human glaucoma studies (Johnson *et al.*, 2000).

1.6 Biochemical and Cellular Changes During Glaucoma

1.6.1 Extracellular matrix

The lamina cribrosa is the region most studied in terms of extracellular changes during glaucoma. The lamina cribrosa undergoes considerable changes during the disease process, as well as throughout normal ageing (Albon *et al.*, 2000; Albon *et al.*,1995; May, 2003; Quigley *et al.*, 1994). The normal lamina cribrosa extracellular matrix (ECM) is structurally supportive, elastic and is thought to provide nutrients for RGCs.

During glaucoma, the collagenous composition of the cribriform plate is reduced, and fibre number is decreased. Collagens I, III, IV, VI, laminin, chondroitin and dermatan suphate proteoglycans occupy the areas left vacant by nerve fibre loss (Johnson *et al.*, 1996). Collagen type VI increases, due to glial activation (Aguayo *et al.*, 1991; Johnson *et al.*, 2000). Elastin fibres become fragmented, disorganised and form plaques of nonfibrillar elastic-like material (Quigley *et al.*, 1994). In more severe glaucoma, extensive loss of elastin fibrils is seen.

These changes alter the mechanical properties of the lamina cribrosa, and may be involved in predisposing the lamina cribrosa to pressure-related changes, or be a consequence of these changes (Burgoyne *et al.*, 2004). Structural, vascular and axonal alterations may all be related, primarily or secondarily, to glial changes (Fitch and Silver, 1997; Hernandez and Condes-Lara, 1992).

1.6.2 Glial cells

Glia are most prominent in the myelinated retrolaminar optic nerve where they may be involved in glaucomatous degeneration that is slightly different to prelaminar degeneration (Furuyoshi *et al.*, 2000). There are two major divisions among glia: the macroglia (oligodendrocytes and astrocytes) and microglia. Oligodendrocytes are present only in the retrobulbar optic nerve. Astrocytes and microglia can be found in the majority at the optic nerve head, as well as dispersed in low numbers throughout the retrobulbar nerve in glial columns between the nerve fibre fascicles (Varela and Hernandez, 1997). In cell culture of the nerve head, lamina cribrosa cells of an undetermined phenotype are also present (Hernandez *et al.*, 1988).

Changes in oligodendrocytes, increases in microglia, as well as activation of astrocytes and microglia have been described in glaucoma models (Lampert *et al.*, 1968). Glia surrounding optic nerve axons also influence the regenerative capacity of the nerve depending on the production of factors from mature oligodendrocytes, astrocytes and microglia (Aguayo *et al.*, 1991). Glial alterations are also important in other central nervous system disorders. For example, the 6-hydroxydopamine pathway involved in Parkinson's disease is modulated by astrocytes and microglia (Rodrigues *et al.* 2001). Multiple sclerosis (reviewed by Carson, 2002), Alzheimer's disease, gliomas and aquired immunodeficiency syndrome (AIDS) dementia all involve reactive gliosis.

Decreased axonal density following laser-induced chronic glaucoma in primate studies coincides with glial expansion and the stress response, indicated by increased immunoreactivity to glial fibrillary acidic protein (GFAP), vimentin and αB-crystallin. Neuronal tissue is partially replaced with non-proliferative glia (Quigley *et*

al., 1980; Quigley *et al.* 1981a), and collapsed connective tissue (Johnson *et al.*, 1996). Glial changes during glaucomatous neurodegeneration are similar to the changes seen during typical Wallerian degeneration (Furuyoshi *et al.*, 2000).

1.6.2.1 Astrocytes

Astrocytes are the major cellular component of the optic nerve head, and have an extremely important supportive role. They envelop retinal axons immediately posterior to the perikaryon (Stone *et al.*, 1995), and provide a suitable extracellular environment through maintenance of ionic balance and removal of glutamate (Waniewski and Martin, 1986; Farinelli and Nicklas 1992; Swanson, 1992; Ranson *et al.*, 1997) as well as neurotrophic support (Gross *et al.*, 1998). Astrocytes are connected through gap junctions with neurons (Cotrina *et al.*, 2001; Ramirez *et al.*, 1996; Quigley and Anderson, 1977; Quigley, 1977), which allow them to buffer extracellular calcium and potassium ions to maintain extracellular conditions (Lee *et al.*, 1994).

At the choroidal lamina, astrocytic processes form tubes through which axons of RGCs can pass (Trivino *et al.*, 1996). Astrocytes have a role in maintaining structural elements of the mature optic nerve head (Trivino *et al.*, 1996). Laminar beams are juxtaposed to astrocytes, which produce the core collagen and elastin of the beams (Hernandez and Ye, 1993). Astrocytes have the capacity to remodel the laminar region and consequently affect axonal function. The role of the astrocyte in glaucoma may stem from sensitivity to mechanical or ischaemic injury combined with resistance to degeneration from these insults (Trivino *et al.*, 1996).

Type 1 astrocytes can be subdivided into two types. Type 1B astrocytes express both GFAP (Figure 1.5) and neural cell adhesion molecule (N-CAM), and are the predominant astrocyte at the optic nerve head, where they function as a physiological intermediate between connective and vascular elements (Ye and Hernandez, 1995). Type 1A astrocytes do not express N-CAM, but are GFAP-positive (Ye *et al.*, 1995), their role is predominantly as a supportive structure (Ye and Hernandez, 1995).

Astrocytes are joined at the optic nerve head by GFAP-negative lamina cribrosa cells, which are thought to have a similar supportive role (Hernandez *et al.*, 1988).

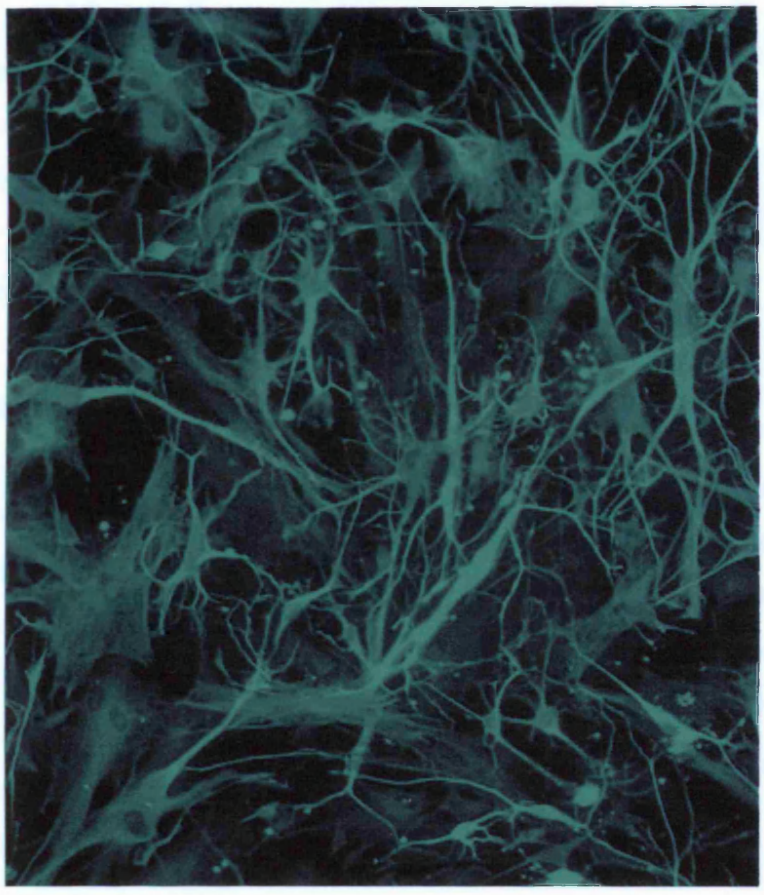

Figure 1.5 ***Astrocytes labelled for GFAP*** *Astrocytes are stellate shaped cells with multiple dendritic processes. All astrocytes express GFAP, which has been used here to label them with a green fluorescent signal (Image taken from Giuliani* et al., *2003).*

During glaucoma, activated astrocytes exhibit a denser GFAP distribution (Furuyoshi *et* al., 2000; Trivino *et al.* 1996; Varela and Hernandez, 1997; Wang *et al.*, 2002) and form a glial scar (Yucel *et al.*, 1999). Type 1A astrocytes cannot be found in the glaucomatous optic nerve head (Varela and Hernandez, 1997). GFAP elevation may be associated with both neuroprotective and neurodegenerative mechanisms (Lam *et al.* 2003[2]; Privat, 2003). For example, synthesis of neuroprotective small heat-shock proteins (Tezel *et al.*, 2000; Salvador-Silva *et al.* 2001; reviewed by Tezel *et al.*, 2004[1]) and increased transforming growth factor (TGF) as well as β cytokine production, which may contribute to microglial activation. The glial scar however,

forms a physical barrier to neuroregeneration. Activated astrocytes are antigen-presenting cells, the implications of which are not fully understood for glaucoma (Yang *et al.*, 2001[2]).

Changes in optic nerve astrocyte activity can be altered in models of glaucoma to prevent RGC death (Neufeld, 1999), for example, by decreasing the production of cytotoxic microglial activation molecules. The astrocyte-axon relationship is currently being studied to understand the initiation of RGC death, and could be modulated to prevent RGC death in glaucoma.

1.6.2.2 Microglia

Microglia are residents of the central nervous system, which migrate and mature in nervous tissue during development. The normal optic nerve is scattered with a population of OX42-positive quiescent dendritic microglia (Lam *et al.*, 2003[2]). Following injury, the immune response of the central nervous system is mediated by activated microglial cells. Infiltrating blood monocytes are also involved depending on the nature and strength of the insult (Graeber *et al.* 1998; Kreutzberg, 1996; Mueller *et* al., 2003; Streit *et al.* 1988).

Normally microglia are quiescent, but rapidly become activated following insults, such as presentation with bacterial lipopolysaccharide (LPS) and interferon-γ (IF-γ) (Bouscein *et al.* 2000). Activation of microglia involves morphological alterations (Figure 1.6), migration, proliferation and changes in cell surface markers, including MHCII and CD45 (Neufeld, 1999), as well as OX41 (Rao *et al*, 2003). However, OX42 expression is preserved in both quiescent and active optic nerve microglia (Lam *et al.*, 2003[2]). Changes during activation render resident phagocytic microglia almost indistinguishable from infiltrating macrophages (Raibon *et al.* 2002; Rao *et al*, 2003). It is therefore extremely difficult to determine the role of central and / or peripheral immune systems during neurodegeneration (reviewed by Guillemin and Brew, 2004).

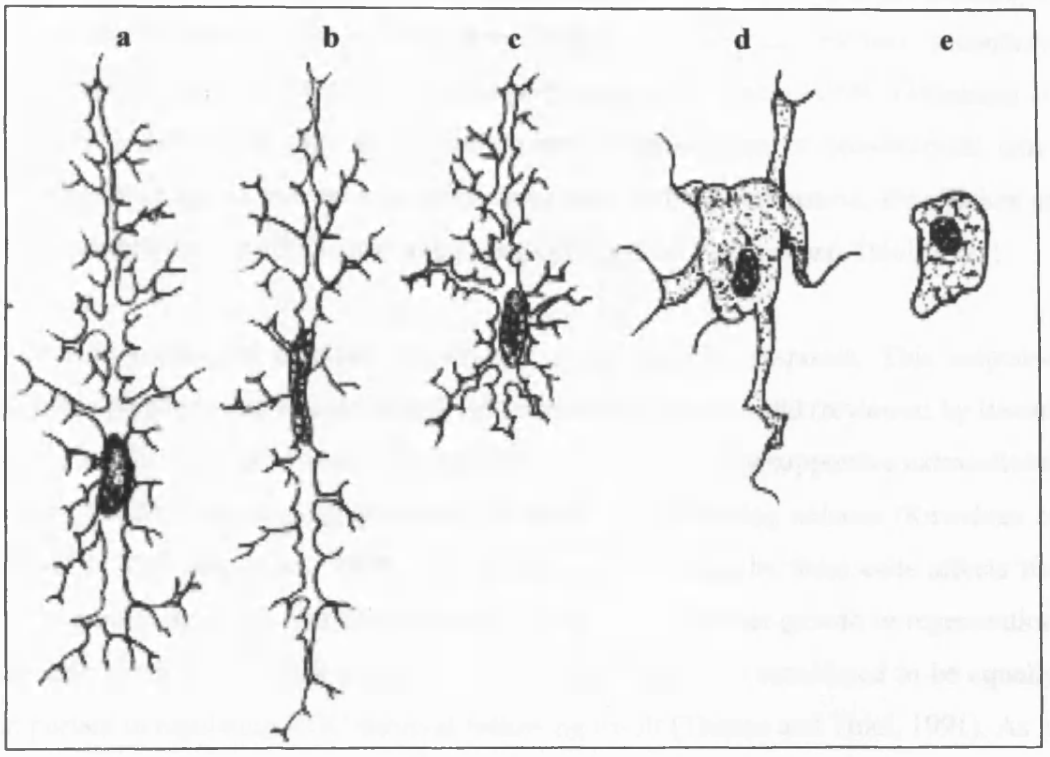

Figure 1.6 ***Microglial morphology*** *Resting microglia are dendritic cells (a). Following activation signals microglia can become elongated in preparation for migration (b). Activation continues with reduction in dendritic field (c) followed by thickening of processes (d). Eventually activated microglia become amoeboid and phagocytic (e, after Streit* et al., *1999).*

Activated microglia are present in the glaucomatous retina and optic nerve head following the initiation of apoptosis (Naskar *et al.*, 2002). Chronic activation of microglia as a result of glaucoma has been reported in the retina (Naskar *et al.*, 2002). Following clinical glaucoma, microglia are present in the optic nerve head in areas of peripapilliary chorioretinal atrophy (Neufeld, 1999). However, studies of the optic nerve head in experimental glaucoma only extend to 14 days post-induction of ocular hypertension (Lam *et al.*, 2003b).

The role of microglia during glaucoma is uncertain. There is evidence to suggest that they perform a scavenger function by engulfing axonal debris, but are not involved during the initiation of disease (Garcia-Valenzuela and Sharma, 1999; Naskar *et al.*,

2002; Schuetz and Thanos, 2004). However, once activated, microglia are capable of producing neurotoxic and inflammatory factors, which could mediate secondary neurodegeneration, or "bystander" damage (Banati and Graeber, 1994; Gehrmann *et al.*, 1995). Microglial protease inhibition and administration of non-steroidal anti-inflammatory agents prevent microglial activation, and in combination, are efficient at neuroprotection of the RGC and improving cell survival (Thanos and Thiel, 1991).

Activated microglial cells are capable of a full immune response. This response includes phagocytosis and production of neurotoxins, such as NO (reviewed by Banati *et al.*, 1993). Microglial toxins are released into the normally supportive extracellular matrix (ECM), encouraging apoptotic cell death of surrounding neurons (Kawahara *et al.* 2001; Takeuchi *et al.*, 1998). The production of toxins by these cells affects the ECM during glaucoma and development to negatively regulate growth or regeneration of optic nerve axons. Deprivation of neurotrophic factors is considered to be equally important in regulating RGC survival following insult (Thanos and Thiel, 1991). As is disruption of oligodendrocyte-mediated myelination of the optic nerve proper.

1.6.3 Neuroglial interactions

Unsurprisingly, due to the anatomical proximity of glia and axon at the optic nerve head, during glaucoma it is possible that neuroglial interactions become disturbed. This may be through loss of neurons or activation of glia. There are many neuroglial signalling pathways that are known to be disrupted during chronic neurodegenerative diseases. These include CD45 interactions in multiple sclerosis, and the CD200 axis during retinal inflammation (Dick *et al.*, 2003).

1.6.3.1 The CD200 axis

CD200 (OX2) is a 41 to 47 kd membrane-bound immunoglobulin found on neurons, activated T cells, B cells, follicular dendritic cells and endothelium (Dick *et al.*, 2001; Wright *et al.*, 2001). Retinal CD200 is localised to neurons and vascular endothelium. The CD200 receptor is found only on myeloid cells, including microglia, and has a similar structure to CD200 with a more extensive intracellular signalling domain

(Preston *et al.*, 1997; Wright *et al.*, 2000). The distribution of CD200 and the CD200 receptor are similar across species (Wright *et al.*, 2001).

CD200 down-regulates myeloid cell activation through its receptor (CD200R). This potentially involves interactions between microglial cells and neurons (Gorczynski *et al.*, 2001). The CD200:CD200R interaction regulates microglial activation in the murine retina (Broderick *et al.*, 2002) and can prevent damaging autoimmunity during retinal inflammation (Dick *et al.*, 2003). However, CD200 knockout mice show normal myeloid cell morphology, increased microglial numbers, and increased inducible nitric oxide synthase (NOS2) immunoreactivity (Broderick *et al.*, 2002; Dick *et al.*, 2003). CD200 interactions are shown in Figure 1.7.

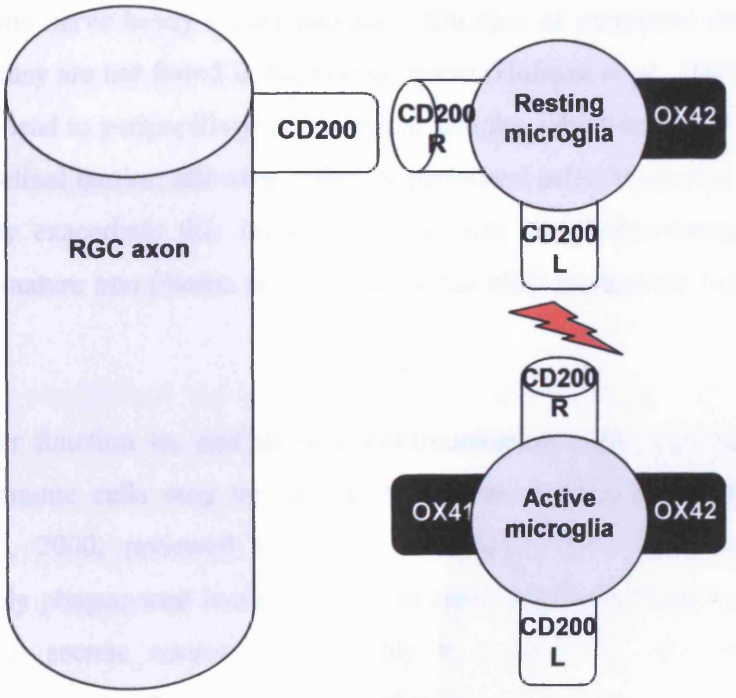

Figure 1.7 ***The CD200 axis*** *The CD200 axis involves interaction between neurons and microglia, as well as microglia:microglia interactions. Disruption of the CD200 axis involves dissociation of the CD200 receptor from the non-signalling ligand. The receptor is then free to signal, resulting in microglial activation.*

1.6.4 Immune cell reaction

Evidence suggests that the immune system is more active in glaucoma patients than the normal population (Cartwright *et al.*, 1992; Nagasubramanian *et al.*, 1978; Yang *et al.*, 2001a). Due to the indistinguishable phenotypes of active microglia and peripheral macrophages, it is difficult to determine the exact roles of these cell types during glaucomatous pathophysiology.

Active microglia in the glaucomatous optic nerve are frequently joined by infiltrating peripheral T-cells, which exacerbate the immune response (Mo *et al.*, 2003). Microglia are involved in antigen presentation to these T cells (Matsubara *et al.*, 1999). Normally tight junctions in the vascular endothelia (excluding that of the prelaminar optic nerve head) would prevent infiltration of peripheral immune cells, consequently they are not found in the normal nerve (Hofman *et al.*, 2001). However, glaucoma can lead to peripapillary chorioretinal atrophy, which involves compromise of the blood-retinal barrier, allowing influx of peripheral cells. Microglial recruitment signalling may exacerbate this influx. It is possible that B-lymphocytes are also recruited and mature into plasma secreting cells that elicit an immune response in the optic nerve.

With a similar function to, and through communication with activated microglia, infiltrating immune cells may be neuroprotective or destructive during glaucoma (Aloisi *et al.*, 2000, reviewed by Tezel and Wax, 2004). Immune cells may indiscriminately phagocytose healthy RGCs to exacerbate neurodegeneration. These cells may also secrete neurotoxins possibly as a result of aberrant microglial signalling to the infiltrating cells, or lack of tolerance to nervous system antigens. While depletion of macrophages reduces peripheral nerve degeneration (Liu *et al*, 2000), compromise of the immune system elevates neurodegeneration in experimental glaucoma. Similarly, immune enhanced rats are more resistant to RGC loss (Bakalash *et al.*, 2002). This indicates that the peripheral immune system may have a neuroprotective role in glaucoma.

1.7 Action of Nitric Oxide Synthase: Generic and in the Eye

1.7.1 Nitric oxide synthase

There are 3 major isoforms of the nitric oxide synthase (NOS) enzyme, ranging from 919 to 1400 amino acids long, and with molecular weights of between 250 to 320 kD (Bredt *et* al., 1991; Nunokawa *et al.*, 1993). NOS functions as a homodimer with a wide distribution in diverse organs, from the eye to the heart. NOS catalyses the production of nitric oxide (NO) from L-arginine and oxygen in a NADPH-dependent reaction. NOS acts on arginine with NADPH and oxygen to produce N-ω-hydroxyarginine and $NADP^+$. NO is produced in a subsequent reaction, with citrulline formed as a by-product. Each NOS subunit contains cofactors that are thought to assist in donating 5 electrons to arginine in the formation of NO. These cofactors include one each of flavin mononucleotide (FMN), flavin adenine dinucleotide (FAD), tetrahydobiopterin, and Fe(III)-heme per NOS subunit. These reactions are summarised in Figure 1.8.

1.7.2 Nitric oxide

NO is a highly reactive and toxic free radical gas produced by NOS. NO has a very short half-life of 5 – 10 seconds, before conversion to nitrites and nitrates in the extracellular space by oxygen and water (Kotikoski *et al.*, 2002). NO can diffuse no further than 200μm from its site of synthesis due to its highly reactive nature (Lancaster, 1997). However, the properties of NO mean that it acts as a novel transient autocrine or paracrine signalling molecule in several transduction pathways, despite its toxicity (Dimmler and Zeiher, 1997).

Following production, NO traverses the lipid bilayer membrane of the cell via rapid diffusion by virtue of its small size, and can pass easily into neighbouring target cells (Garthwaite and Boulton, 1995). The main target of NO is guanylyl cyclase (GC). NO interacts with the heme prosthetic group in the active site of GC to produce nitrosoheme which increases the enzymatic activity of GC 50-fold, probably through a conformational change (Stamler, 1994). GC then rapidly degrades GTP to produce

the intracellular second messanger 3',5'-cyclic GMP (cGMP). Following the rapid production of cGMP, it is speedily degraded to GMP by a phosphodiesterase, resulting in NO having a rapid (within seconds) effect on the cell. These effects depend upon the isoforms of NOS, which has been activated to produce NO.

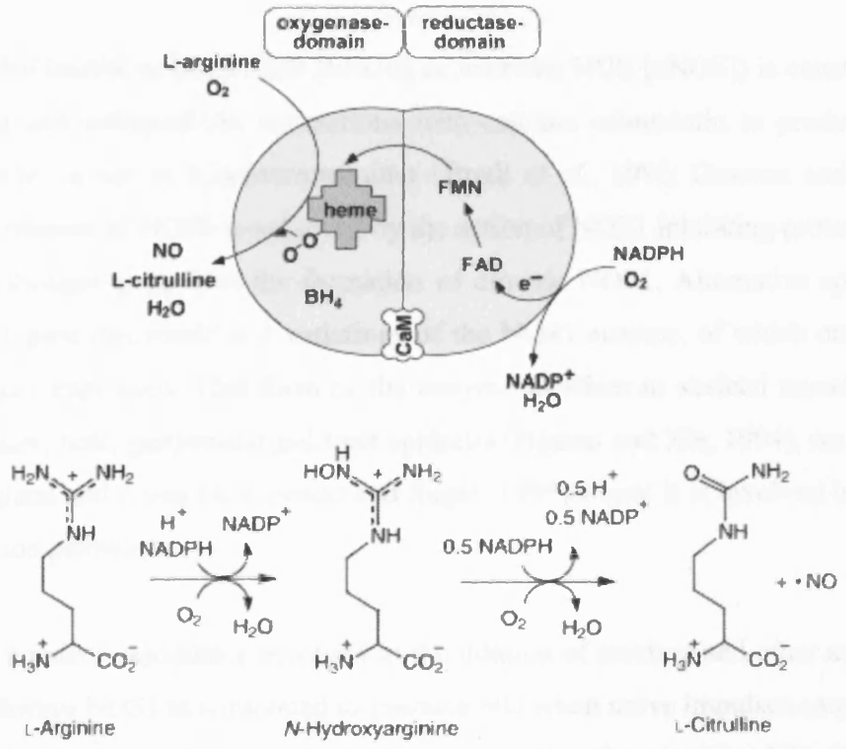

Figure 1.8 ***The structure and reactions of nitric oxide synthase*** *NOS is shown above with the reactions it catalyses, essential co-factors for NO synthesis and the amino acid L-arginine (for details of these see text). Calcium ions and calmodulin (CaM) are shown to represent the activation of the inducible NOS isoform (NOS2). The NOS enzyme is a homodimer each monomer consists of a reductase and an oxygenase domain. The enzyme catalyses the conversion of L-arginine into L-citrulline and NO (After Boger, 2005; Groves and Wang, 2000).*

1.7.3 The isoforms of NOS

Three isoforms of NOS have been isolated and cloned.

1.7.3.1 NOS-1

NOS1 (also known as brain NOS [bNOS] or neuronal NOS [nNOS]) is constitutively expressed and activated via interactions with calcium calmodulin to produce nitric oxide (NO) for use as a neurotransmitter (Bredt *et al.*, 1991; Dawson and Snyder, 1994). Inhibition of NOS1 is achieved by the action of NOS1 inhibiting protein (PIN), which is thought to prevent the formation of dimeric NOS1. Alternative splicing of the NOS1 gene can result in 4 variations of the NOS1 enzyme, of which only one is ubiquitously expressed. This form of the enzyme localises to skeletal muscle, testis, lung, kidney, heat, gastrointestinal tract epithelia (Nathan and Xie, 1994), neutrophils, adrenal gland and retina (Koistinado and Sagar, 1995) where it is involved in various transduction pathways.

NOS1 is a potent vasodilator involved in the dilation of cerebral and other arteries. In these pathways NOS1 is stimulated to produce NO when nerve impulses cause a local increase in calcium concentration at nerve terminals. The resulting NO diffuses to smooth muscle cells and acts on GC as previously described. cGMP then stimulates protein phosphorylation via cGMP-dependent protein kinases within the cell, to mediate endothelium-independent neuronal stimulation of smooth muscle relaxation. NOS1 has many diverse roles other than vasodilation, such as the reinforcement of synaptic strength during the long-term potentiation involved in memory formation (Carter and Murphy, 1999).

1.7.3.2 NOS2

NOS2 (or inducible NOS [iNOS]) is only found in cells during abnormal conditions, once its production is transcriptionally activated (Lamas *et al.*, 1992). This form of the enzyme produces extremely high amounts of NO, which exhibits paracrine toxicity

during inflammation and degeneration (Lyons *et al.*, 1992). Under these conditions NOS1 and NOS3 can also be induced (Dawson and Snyder, 1994).

NOS2 has a role in the immune response, and localises to macrophages and neutrophils. NOS2 inhibitors prevent the response of macrophages to immune challenge. If these cells are challenged with cytokines or endotoxins such as lipopolysaccharide, after a few hours extremely high, sustained levels of NO are found during the immune response. These active immune cells can also produce the superoxide radical O_2^-, which reacts with NO to form considerably toxic peroxynitrite ($OONO^-$). This decomposes rapidly into a hydroxide radical that the cells use in their attack on invading "non-self" substances.

1.7.3.3 NOS3

NOS3 (or endothelial NOS [eNOS]) is localised to the cellular endothelial lining of blood vessel walls, as well as nonvascular tissues (Lamas *et al.*, 1992) where it is constitutively expressed. NOS3 is similar to NOS1 in terms of sequence homology (about 55%) as well as in activation by calcium calmodulin. The actions of certain vasodilatory hormones result in increased free intracellular calcium concentration in endothelial cells via the phosphinositide signalling pathway. This activates NOS3 resulting in NO production. The main function of this NO is to act as a physiological regulator of blood pressure by acting on smooth muscle cells, via a similar transduction pathway to NOS1.

1.7.4 NOS and toxicity

NO released from all forms of NOS can be toxic to cells. Animal models of neurodegenerative diseases such as Parkinson's disease (Santiago *et al.*, 1994), Alzheimer's disease (Resnick *et al.*, 1995) and multiple sclerosis (Bo *et al.*, 1994) have suggested a role for NOS in the disease process. During Parkinson's disease the main brain area affected is the substantia nigra, where NOS2 expression is induced in reactive glia, resulting in increased NO and degeneration of dopaminergic neurons. Endotoxic shock for example, following lipopolysaccharide administration, can be

mediated by a sustained release of NO following production by NOS2. Similarly, inflammation mediated by NO can result in tissue damage. In animal models of stroke, NO-producing active NOS1 can damage neurons in the prenumbra, which have not been damaged by the stroke itself. Also, experimentally, in NOS1 knockout mice ischaemia results in a reduced central nervous system lesion as compared to normal mice (Huang *et al.*, 1994), indicating a role for NOS1 in ischaemic nerve damage. Glutamate neurotoxicity is also thought to be mediated through NO (Dawson *et al.*, 1991).

NO may induce toxicity through anti-apoptotic or pro-apoptotic effects. The anti-apoptotic effects of NO production are potentially important in autoimmune disease. Prevention of apoptosis may exacerbate the immune response through increased numbers of lymphocytes or microglia. It is unknown how NO prevents apoptosis. Interactions with transcription factors (Hausladen *et al.*, 1996; Peng *et al.*, 1995; Zeiher *et al.*, 1995), heme proteins and enzymes containing iron-sulphur clusters (Stamler, 1994) or oxygen radicals (Moncada and Higgs) may all induce the anti-apoptotic effects of NO.

NO can induce both necrosis and apoptosis (Figure 1.9). The precise mechanism of NO toxicity is not clear, but is likely to be independent of guanylyl cyclase (Brune *et* al., 1996). It is not clear whether NO or peroxynitrite is responsible for apoptotic effects on the cell. NO may induce apoptosis through direct DNA damage (Nguyen *et al.*, 1992) leading to accumulation of the tumour suppressor protein p53 (Messmer *et al.*, 1994). Consequently, poly(ADP-ribose) polymerase cleavage indicates that caspase activation occurs (Messmer *et al.*, 1996). However, it is also likely that NO is involved in a p53-dependent pathway (Messmer and Brune, 1996).

Most importantly, increased levels of NOS in the optic nerve head have been associated with the occurrence of primary open-angle glaucoma (Neufeld *et* al., 1997; Quigley and Addicks, 1981). The degeneration of RGC axons in glaucoma can be associated with excessive NO production due to elevated NOS. NOS upregulation can therefore be held directly responsible for some of the neurodegeneration typical of the disease.

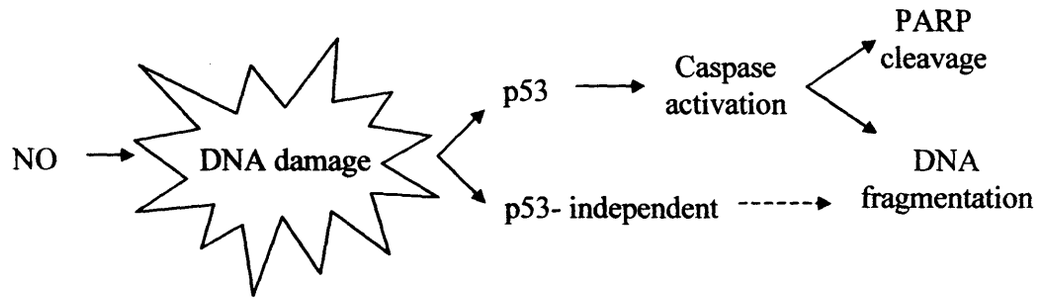

Figure 1.9 ***The mechanisms by which NO induces toxicity*** *NO induced toxicity is likely to involve p53 and caspase cleavage. However, p53-independent mechanisms may also be involved. NO can directly produce DNA damage, which is exacerbated through these proapoptotic cascades (adapted from Dimmler and Zeiher, 1997).*

1.7.5 NOS in the normal optic nerve

NOS1 is found cytoplasmically in a low number of astrocytes at the prelaminar and lamina optic nerve head (Neufeld *et al.*, 1997). This constitutive distribution among certain glia means that the NO produced by NOS1 might act as a local mediator between these cells, and between glia and neurons. NOS2 cannot be found in normal tissue (Neufeld *et al.*, 1997; Shareef *et al.*, 1999). It is expressed only when induced by certain physiological challenges. NOS3 is localized to blood vessel walls in the prelaminar optic nerve head, where it is found only in the vascular endothelium (Neufeld *et al.*, 1997). NOS3 produces NO, which functions as a vasodilator in the optic nerve head.

1.7.6 NOS in glaucoma

In the human glaucomatous optic nerve head, all isoforms of NOS are upregulated (Neufeld *et al.*, 1997) and localised to RGC axons, as well as the extracellular matrix. However, only NOS2 appears to be upregulated in experimental glaucoma (Shareef *et* al., 1999). The evidence to date points to NOS1 and NOS2 upregulation in astrocytes during human glaucoma (Neufeld *et al.*, 1997). Evidence suggests that the role of upregulated NOS2 in other central systems is part of a microglial healing response that removes damaged nerves and re-wires remaining fibres (Takeuchi *et al.*, 1998).

NOS3 is believed to be mainly neuroprotective, acting as a vasodilator, thereby preventing the tissue from undergoing glaucomatous damage by increasing blood flow. This has been proven in NOS3 knock-out mice with ischaemic cerebral infarction (Huang *et al.*, 1996).

During human glaucoma, NOS1 expression is upregulated in astrocytes, and this is thought to cause the increased toxic levels of NO resulting in neurodegeneration. Neufeld (1999) discovered that NOS1 was found in almost all astrocytes in the optic nerve head of glaucomatous human eyes. Increases in NOS1 and NOS2 may contribute to excessive NO production, which then combines with superoxide to form peroxynitrite (Lipton *et al.*, 1993). This is supported by evidence, which shows the accumulation of mitochondria in these astrocytes (Hollander *et al.*, 1995). Peroxynitrite is extremely neurotoxic and could contribute to axonal degeneration.

Therefore, it is reasonable to conclude that NOS1- and NOS2-specific inhibitors may have a role in the future treatment of glaucoma. For example, by inhibiting the action of NOS2 using a specific inhibitor, aminoguanidine, neuroprotection has been achieved in rodent ocular hypertension (Neufeld, 1999).

1.8 Strategies for neuroprotection of retinal ganglion cell death

1.8.1 Neuroprotection

Therapies that prevent pathogenesis in neurological disease are considered neuroprotective. Neuroprotection involves prevention of the processes involved in cell death during disease such as ischaemia (Cheon *et al.*, 2002; Osborne, 1999; Tezel *et al*, 2004[1]), excitotoxicity (Cakzada *et al*, 2002; Tezel *et al.*, 2004[1]), oxidative stress, free radical production (Yoshioka *et al.*, 2002), and plaque formation (Zhang *et al.*, 2004). Normally neuroprotection will be applied to a population of neurons that have already suffered a primary insult in order to prevent further damage.

Many new glaucoma treatments attempt to decrease neuronal atrophy through direct neuroprotection, regardless of effects on IOP (Schlore *et al*, 2001; Schwarz and

Yoles, 2000). These novel therapies involve pharmaceuticals, manipulation of endogenous proteins and gene therapy. In combination with neuroregeneration techniques, neuroprotection may be potentially useful in the restoration of visual function during glaucoma.

As more about the mechanisms of cell death in glaucoma become understood, and the particular pathways involved are elucidated, it will become clearer how best to protect neurons from degeneration. Many neuroprotective strategies for the optic nerve are under investigation, but the application of these remains questionable.

1.8.2 Growth factors

Growth factors (GFs) can influence various cellular pathways to induce neuroprotection or neurodestruction. GFs can reduce apoptosis, but increase necrosis by free radical (for example, NO) induced damage (Haefliger *et al.*, 2000; Klocker *et* al., 1998). Most growth factors produce similar results due to a similar mechanism of action, which also causes oxidative stress. However, BDNF, ciliary neurotrophic factor and basic fibroblast growth factor have all been shown to have an overall positive effect on neuronal survival in RGC cultures and *in vivo* (Chew and Ritch, 1997; Rabacchi *et al.*, 1994).

1.8.3 Calcium channel blockers

Calcium channel blockers, normally used in cardiac conditions, can alleviate vasospasm particularly in normotensive glaucoma (Flammer and Orgul, 1998; Rojanapongpun *et al.*, 1993). These blockers may decrease visual field loss and optic nerve degeneration (Netland *et al.*, 1993).

Nifedipine alleviates symptoms of some normotensive patients, but not others (Kitazawa *et al.*, 1989; Lumme *et al*, 1991). Flunarizine enhances RGC survival, possibly through a trophic factor mechanism. Betaxolol is a common β-blocker that is thought to function by blocking calcium channels to promote vasodilation and neuroprotection.

The neuroprotective effects of calcium channel blockers may be induced by the inhibition of vasospasm (Gasser and Flammer, 1987) or excitotoxicity (Greenberg *et al.*, 1990). However, reduction of blood pressure by these agents may decrease optic nerve perfusion resulting in ischaemia and axonal damage.

1.8.4 NMDA receptor antagonists

NMDA receptors (NMDAR) are usually activated by glutamate and are thought to be involved in RGC death through the enhancement of excitotoxicity (Dreyer *et al.*, 1996). However, some evidence suggests that vitreal glutamate levels remain normal and are therefore not excitotoxic during glaucoma (Carter-Dawson *et al.*, 2002). However supporting evidence for glutamate excitotoxicity in glaucoma has recently been demonstrated in a rodent model (Moreno *et* al., 2005).

A putative mechanism for excitotoxicity is glutamate-stimulated NOS activity, resulting in toxic NO levels (Kashiwagi *et al.*, 2001). Therefore, NMDAR antagonists can decrease excitotoxic and hypoxic damage. Memantine is a commonly used non-competitive NMDAR antagonist used to prevent Parkinsonian neurodegeneration of the substantia nigra (Chen *et al.*, 1992), which also reduces RGC death through the prevention of NMDAR activation (Osborne, 1999).

Other neuronal systems can be inhibited to reduce excitotoxic RGC death, for example, serotonin receptor antagonism (Inoue-Matsuhisa *et al.*, 2003). Neuroprotection using systemic neurotransmitter receptor antagonism is undesirable due to the wide distribution of most neurotransmitters in the nervous system and the potential effects on multiple systems.

1.8.5 NOS inhibitors

RGC neuroprotection during glaucoma and ischaemia can be achieved by preventing the production of NO from NOS using *N*-nitro-L-arginine and *N*-methyl-L-arginine. Indeed, specific inhibition of NOS2 has been investigated during chronic (6 months) experimental glaucoma induced via episcleral vessel cautery (Neufeld, 1999).

Aminoguanidine-induced inhibition of NOS2 reduced neuronal loss from 36% to 10%. Clearly blocking the action of NOS2 is neuroprotective in the cautery model of glaucoma (Neufeld, 1999). However, the induction of NOS expression, as well as neuroprotection through NOS inhibition, may be a side effect of vein cautery. It is yet to be established whether blocking the other NOS isoforms produces similar effects.

Selective inhibition of NOS isoforms may be more desirable for neuroprotection, because though NOS1 and NOS2 products are regarded as neurodegenerative, NOS3 produces vasodilatory NO, which may help prevent vasospastic glaucoma.

1.8.6 Nitrates

Nitrates such as nitroglycerin release NO, which increases intracellular cGMP levels and vasodilation, and are therefore used to treat vascular dysfunction, as well as glaucoma (Wizemann and Wizemann, 1980).

Nitrates may increase retinal or optic nerve head (ONH) perfusion and prevent ischaemia (Grunwald *et al.*, 1997), or directly inhibit NMDARs through S-nitrosylation of thiol groups at the modulatory sites of the receptor. However, increased levels of NO can be neurodestructive through nitrosylation and fragmentation of DNA.

1.8.7 Antioxidants

Antioxidants such as trilazad mesylate, a 21 amino acid steroid, can be used to neutralise toxic substances in the prevention of apoptosis. Trilazad mesylate acts on lipid peroxidation to inhibit apoptosis (Neufeld, 1999). Neutralisation may be incomplete, but other compounds can be used as free radical scavengers to enhance neuroprotection, including catalase, superoxide dismutase, vitamin C and vitamin E.

Combining the effects of neuroprotection offered by NOS inhibition and free radical scavenging enhances the effects of growth factor-mediated protection, suggesting that

combination therapies are more efficient in neuroprotection of RGCs (Netland *et al*, 1993).

1.8.8 Gene therapy

Apoptosis is particularly targeted in potential gene therapies for glaucoma. The proteins and genes that inhibit the process are being assessed for possible neuroprotective effects in glaucoma.

The Bcl-2 gene is an apoptotic inhibitor, with a potential neuroprotective capacity. Bcl-2 expression in rat neurons produces a 50% increase in RGC numbers, and overexpression in transgenic mice results in a reduced stroke size. Bcl-2 mRNA inserted, via a herpes simplex virus vector, into the murine brain protects cells from delayed death following focal ischaemia.

Other compounds that may be neuroprotective through the inhibition of apoptosis include deprenyl, a monoamine oxidase inhibitor used in Parkinson's disease (Leret *et al*, 2002; Maruyama and Naoi, 1999), as well as flumarizene and aurintricardoxylic acid.

1.8.9 Immune system modulation

1.8.9.1 Microglia

Due to the uncertain role of microglia in RGC death, the inhibition of microglial activity has been tentatively investigated as a neuroprotective strategy in glaucoma treatment. Initial studies are contradictory (reviewed by Schwartz, 2003). In some cases, inhibition of microglial activation is neuroprotective, whereas in others it exacerbates degeneration.

Early microglial activation during central nervous system injury correlates with T-cell mediated neuroprotection, suggesting a role in neuroprotective autoimmunity for both (Shaked *et al.*, 2004). However, minocycline, a tetracyclic antibiotic can be used to inhibit microglial proliferation and activation during many neurodegenerative

conditions including stroke (Wang *et al.*, 2003), (Arvin *et al*, 2002), and excitotoxicity (Tikka and Koistinaho, 2001). Minocycline is thought to be neuroprotective, although the effects it has on RGC survival are unknown.

1.8.9.2 Immuno-protective vaccination

Immune-mediated neuroprotection can be achieved using vaccination with antigens that predominate at the site of injury (reviewed by Schwartz, 2004). Copolymer-1 and interphotoreceptor retinoid binding proteins can protect RGCs from degeneration following glaucoma (Bakalash *et al*, 2003). Clinical trials are already underway to test immuno-protective vaccination of Alzheimer's disease (reviewed by Vickers, 2002). A careful balance needs to be achieved between protective autoimmunity and autoimmune disease.

1.8.10 Neuroregeneration

Neuroregeneration can be applied in combination with neuroprotection, when neuroprotection alone fails to restore function (reviewed by Schwartz, 2003). Neuroregeneration involves using trophic factors to promote the regeneration of injured neurons. Until recently this was considered impossible in the central nervous system. Now evidence suggests that regeneration is possible following central nervous system injury, as damaged axons can generate growth cones (Dickson *et al.*, 2000). RGC axons have been regenerated *in vitro* (Negishi *et al.*, 2001).

Nerve growth cone proliferation can be induced through BDNF application to the transected optic nerve (Chew and Ritch, 1997). Cell survival and axon regrowth can be enhanced by the grafting of a neurolemmal sheath into transected optic nerve (Martinou *et al.*, 1994). Neuroregeneration can result in functional synapses (Aguayo *et al.*, 1990; Keirstead *et al.*, 1989; Villegas-Perez *et al.*, 1988), with the potential to complete the circuits lost during RGC death. Neuroregeneration can also be achieved through the introduction of hNT neuronal cells (derived from N-tetra-2 teratocarcinoma cells) as a retinal graft (Konobu *et al.*, 1998).

Neuroregeneration following glaucoma may be a very difficult task. The optic nerve microenvironment may be adjusted to prevent repair and regeneration of axons through changes such as microglial activation during disease. A physical barrier to regeneration in the form of the glial scar also exists after disease. Therefore regenerative factors will need to be applied to the nerve together with other agents, which optimise or promote healing of the nerve.

1.9 Summary of research plan

In order to investigate the effects of IOP elevation on the optic nerve and further elucidate the mechanisms that cause RGC cell death, the aims of this project were to:

1) develop the episcleral vessel sclerosis rodent model of glaucoma (Morrison *et al.*, 1995)

2) relate IOP elevation to RGC degeneration and death in a rodent model of experimental ocular hypertension. Due to the lack of a definitive, practical quantification method for assessing neurodegeneration in glaucoma, various methods will be established, including some novel approaches.

3) determine the potential roles of glia in glaucoma. Astrocyte and microglial changes will be related to IOP elevation and the degree of RGC cell death. In particular, the role of microglia will be clarified.

4) clarify the controversial role of NOS in glaucomatous RGC degeneration.

Chapter II
General Method Development

2.1 Development of methods used in the animal model

2.1.1 Introduction to animal techniques

All procedures carried out on animals conformed to current Home Office regulations concerning the Animals (Scientific procedures) Act, 1986. Experiments were performed according to personal license number 30/5874, and under project license number 30/1756. The animal model used was developed was based on the episcleral drainage vessel sclerosis rodent model of glaucoma (Jia *et al.*, 2000; Johnson *et al.*, 1996; Morrison *et al.*, 1997; Morrison *et al.*, 1998).

250-450g 5 to 8 month old male ex-breeder brown Norway rats (*Rattus Norwegicus*) were housed at 21°C and provided with standard laboratory diet and water *ad libitum* (n=75). Animals were maintained on 24 hour 40-90lux light for a minimum of three days before experimentation commenced. Rats were handled daily and their weights were recorded weekly as an index of health.

2.1.2 Intraocular pressure readings

Intraocular pressure (IOP) was calculated from experimental and control eyes, using a factory calibrated Mentor® Tono-Pen™ XL, by taking the mean of 10 readings. A sanitised Ocu-film® tip cover was used to shield the tonometer probe from damage. Alternatively, a non-static film with a smaller diameter than the Ocu-film® tip cover was fixed over the tonometer probe, or the unshielded probe was used in an attempt to reduce standard error. 10 readings were taken from each of 3 animals on 3 separate occasions using these alternative shields. Eyes were locally anaesthetised using 0.5% w/v Benoxinate (Oxybuprocaine) hydrochloride (Chauvin Pharmaceuticals, UK) prior to pressure readings.

Interobserver variation was determined by comparing repeated IOP measurements taken by two investigators, between 9am and 6pm, on alternate days (n=66). On no occasion were these readings recorded on the same day. On alternate days, one set of IOP measurements were taken from both eyes between 7 and 9am or pm. Once it was established that circadian changes had been eliminated, readings were taken between 9am and 6pm. In order to detect any improvements in tonometry with practice of the technique, animals were separated into 9 temporal groups dependant upon arrival date. IOP readings from these groups were compared.

2.1.2.1 Statistical analysis

All statistical analyses were performed using Microsoft Excel (UK). Average animal weight, standard deviation, and standard error were calculated using the Excel formulae. Pre-surgical tonometry readings were analysed for statistically significant differences between contralateral and ipsilateral eyes. These analyses were performed using a two-tailed T-test to generate a P value, as calculated by Excel formula. A P-value of <0.05 was taken as statistically significant. The coefficient of variation, standard deviation and error were calculated for 9 temporal animal groups in order to assess whether tonometry became more reliable with practice. Agreement between observers using a standard tonopen cover was tested using Bland and Altman plots and also compared via a T-test. A repeated measures test (ANOVA) was used to compare alternative tonopen shields as well as alterations in circadian variation of IOP.

2.1.3 Principles of ocular surgery

Following initial IOP measurements, animals accustomed to human handling underwent surgery under general anaesthetic involving an episcleral microinjection of hypertonic saline (1.75 M NaCl, see Appendix 1) into an aqueous vein (n=58). Approximately 50 µl 1.75 M NaCl was injected into the episcleral venous system of the ipsilateral (left) eye. The contralateral eye (control, right) was not injected.

2.1.3.1 Microneedle assembly

Disposable microneedles were made from 10 µl borosilicate glass pipettes (Sigma-Aldrich, UK) pulled using a pipette puller (David Kopf Instruments, USA). The rough microneedle tips were bevelled to avoid excessive tissue damage during injection; the needle was lowered onto a flat rotating (14000 rpm) surface attached to an industrial rotator and covered with diamond lapping film (World Precision Instruments, UK). An example of a bevelled needle is shown in Figure 2.1. Microneedle diameter was measured using a DMRA2 microscope (Leica, UK) and Leica QWin image analysis software. Initially during the optimisation process all needles, with outer diameters from approximately 3 to 70 µm, were cut with a glasscutter under a light microscope yielding a length of approximately 6mm. Following optimisation, only microneedles with an outer diameter of 10-40 µm were used.

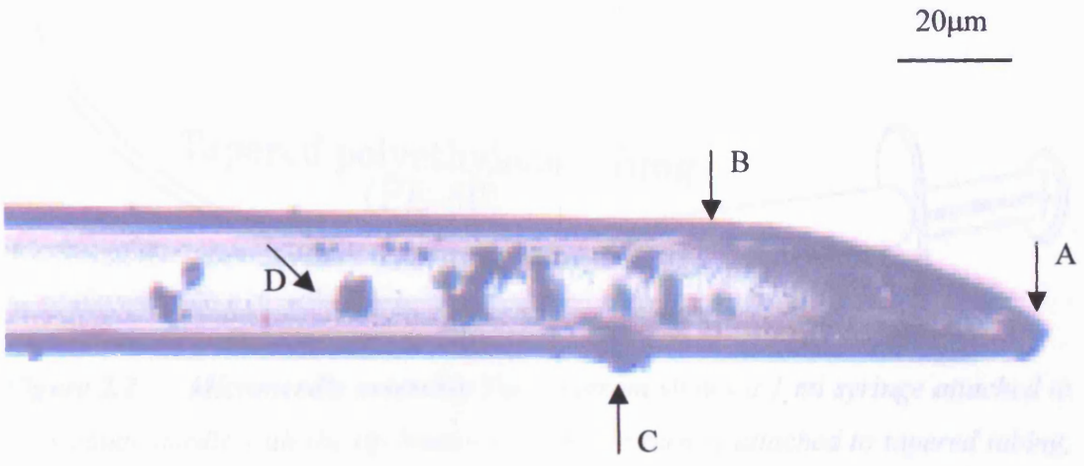

Figure 2.1 A bevelled borosilicate glass microneedle tip *The proximal tip (A) was derived from bevelling as described in section 2.1.3.1. Arrow B indicates the point at which bevel starts. Arrows C and D indicate diamond lapping film deposits.*

Approximately 3 mm of the rough (cut) end of the microneedle was inserted into a 50 cm length of polyurethane tubing (Sandown Scientific, UK) with an outer diameter of 0.038 inches or 0.048 inches, which had previously been tapered by heating and stretching by hand over a Bunsen flame. A 23 or 19-gauge needle with the tip broken off was inserted into the distal end of the tubing, and all junctions sealed with

Superglue, UHU, or Araldite over-laid with high viscosity Superglue. In some cases, these junctions were additionally sealed with heat-shrink tubing. A small plastic tab was positioned along the tubing and held with high viscosity Superglue to mark the bevel of the microneedle. This apparatus is depicted in Figure 2.2. After assembly, microneedles were stored in either a dry or moist sealed chamber and then sterilised before use by applying 100% ethanol to the bevelled tip followed by air-drying.

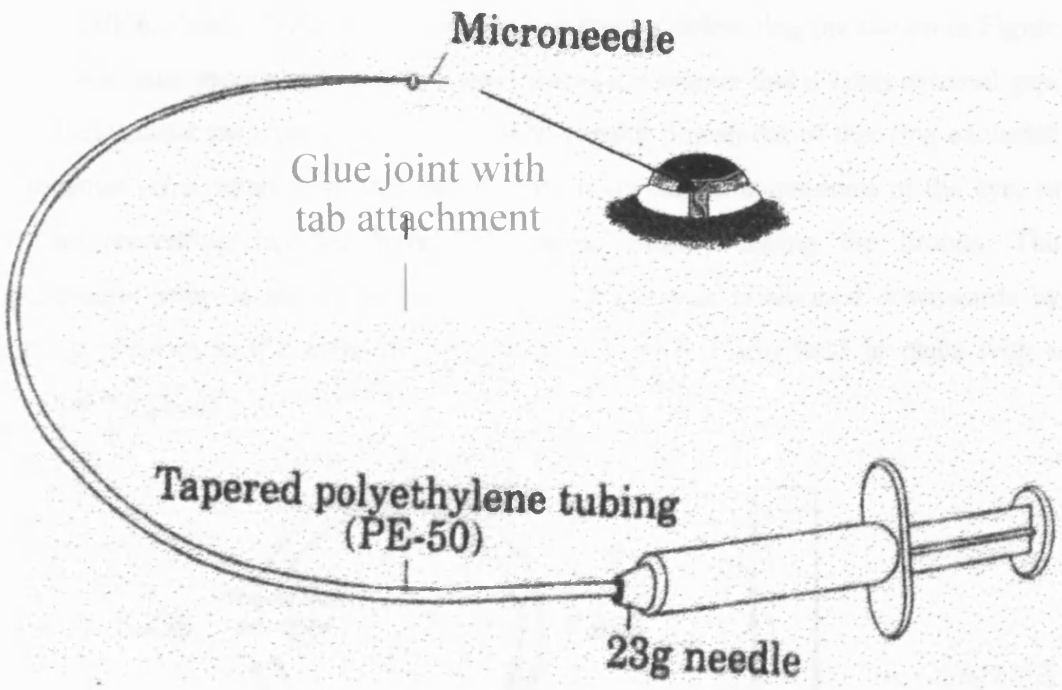

Figure 2.2 ***Microneedle assembly*** *This diagram shows a 1 ml syringe attached to a 23 gauge needle with the tip broken off. This in turn is attached to tapered tubing, which has a microneedle inserted into the narrow end. This microneedle can be used to inject a single vessel (shown in red and indicated by the arrow), which has been isolated from the vessels blocked by the plastic ring around the eye by the narrow slit in the ring (adapted from Morrison et al., 1997). The arrow indicates the vessel.*

2.1.3.2 Anaesthesia

Before microinjection, rats were anaesthetised via inhalation of 4% isoflurane with oxygen in a chamber. For the surgical procedure, they were transferred to a respirator consisting of the modified sleeve of a 10 ml syringe connected to a 3% supply of oxygenated isoflurane. Animals were monitored throughout the surgery to assess the

degree of anaesthesia, and the supply of isoflurane adjusted appropriately. The operated eye was moistened throughout surgery with drops of 0.9% sterile saline (see Appendix 1).

2.1.3.3 Surgical procedure

The conjunctiva was incised under a surgical light microscope (25x to 40x magnification, Zeiss, USA). A 5.5 mm inner diameter delrin ring (as shown in Figure 2.3) with a 1mm groove cut into its central internal diameter and a 1mm external gap, was fitted around the equator of the eye. The careful placement of this ring excluded all aqueous veins, apart from one radial vein in the superior quadrant of the eye, as well as preventing injected hypertonic saline from escaping the limbus. The experimental setup is shown in Figure 2.4. The eye was positioned downwards by applying pressure to the inferior globe using a modified arm held in place with a magnetic footplate.

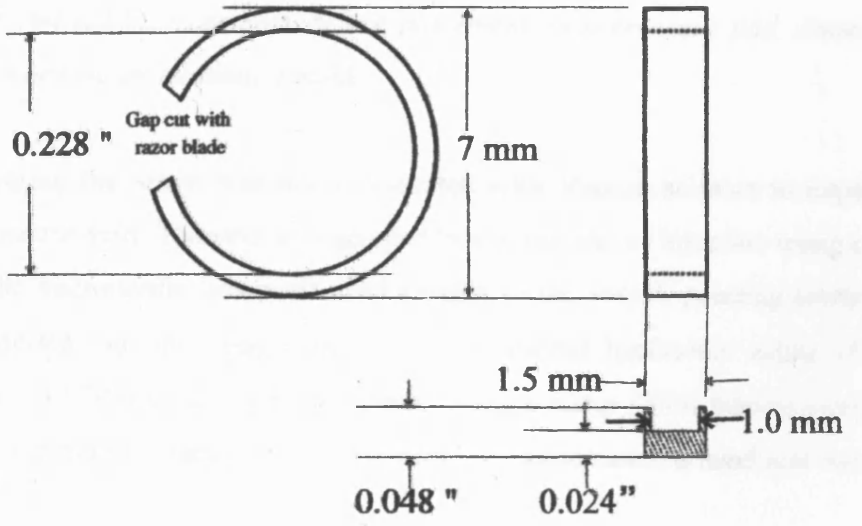

Figure 2.3 ***A polypropylene ring*** *A ring of these dimensions was fitted around the equator of the eye during surgery to prevent excessive damage to non-target blood vessels during the microinjection of a mild sclerosing agent (1.75 M NaCl) into the episcleral drainage vessel system.*

Figure 2.4 Surgical set-up used during the microinjection procedure *Animals were anaesthetised in a chamber before placement on a recovery pad. Anaesthesia was maintained via an inhalation mask.*

Sclera covering the vessel was micro-dissected with Vannas scissors to expose the isolated aqueous vein. The vein was gripped below the site of injection using cupped forceps. The microneedle was positioned parallel to the vessel, pointing towards the limbus, inserted into the vessel, and 50 µl of filtered hypertonic saline (1.75M) injected over 10-30 seconds using a "Genie" syringe pump (Wolf laboratories). This force was sufficient to blanch the limbal artery. In some cases, a hand rest was used for support.

The plastic ring was removed, and the conjunctiva closed with 8-0 vicryl-rapide® absorbable sutures, with a 6 mm micro-point® spatula needle (Johnson and Johnson International, UK). Injected eyes were then anaesthetised with benoxinate before recovery from the procedure. A drop of 0.5% chloramphenicol (Chauvin Pharmaceuticals Ltd, UK) antibiotic was administered, as well as Predsol® (Medeva, UK) as a non-steroidal anti-inflammatory. Post-injection intraocular pressure

measurements were attempted, before consciousness was regained. The same procedure, excluding injection of hypertonic saline was performed on sham-operated animals (n=8 in total).

2.1.3.4 Post-operative intraocular pressure readings

Following microinjection, IOP was measured (one set of 10 readings per eye) by one of two investigators on alternate days and analysed for statistically significant differences as described in Section 2.1.2.1. Experimental and control eyes were compared. If no significant pressure change ($P>0.05$) was recorded before day 14 post injection, animals were re-injected. IOP was measured for various durations.

2.1.3.5 Methods of euthanasia and tissue harvesting

Animals were sacrificed at appropriate time points from 0 to 65 days post-induction of elevated IOP (n=66). Critical changes occur during experimental glaucoma within 1 to 14 days post-induction, with few optic nerve changes occurring after 14 days of hypertension (Johnson *et al.*, 1997). Tissues were therefore collected from 1 day up to 14 days post pressure elevation, at frequent end-points. After 14 days of experimental hypertension, animals were sacrificed at fewer, more discrete time intervals.

Some animals were euthanised using CO_2 overdose in a chamber (n=19). All others received a lethal dose of sodium pentobarbital (40mg/kg body weight); in some cases this was followed by transcardial perfusion (n=10). The animal's chest was opened to expose the heart and the left ventricle was cannulated with a 19 gauge needle clamped into place using an artery clip, and connected to a Cole Parmer (USA) perfusion pump. Blood was flushed out using 200 ml of phosphate buffered saline (PBS, see Appendix 1) (pH 7.0), followed by fixation with 200 ml of 2% paraformaldehyde (PFA) in PBS, both pumped through the system at approximately 120 mmHg. 2% PFA was obtained by diluting an 8% frozen stock solution (see Appendix 1). Alternatively transcardial perfusion was performed using only 200 ml PBS, eliminating the use of fixative. Eyes were removed for analysis, dissected and stored

in the perfusion fixative or snap frozen in Tissue Tek (Sakura, The Netherlands), using liquid nitrogen chilled isopentane, prior to storage at -20°C.

Pre-enucleation eyes were orientated so that an 8-0 silk suture (Ethicon, UK) through the sclera marked the superior quadrant. Post enucleation, retrobulbar optic nerves were similarly orientated so that a suture distal to the globe marked the superior nerve. A scalpel blade was used to incise the sclera, just posterior to the limbus, and the anterior and posterior globes were separated with fine Vannas scissors. The superior quadrant of the posterior segment was marked using an incision through to the optic nerve. The optic nerve head and adjoining sclera were removed through a continuation of this incision around the nerve head. The retrobulbar optic nerve was separated from the remainder of the nerve using a scalpel.

2.1.3.6 Evaluation of elevated intraocular pressure

Animals (n=58) with unilateral ocular hypertension were assigned to 5 groups based on IOP data. In order to determine the effect of duration of IOP elevation on the optic nerve, the number of days that IOP elevation was statistically significant until the date of euthanasia ("T") was calculated. Following the first significant pressure elevation the difference in area under the pressure curve (mmHg plotted against days post-microinjection, "A"), and standard deviation (SD, "S") of pressure elevation, between the ipsilateral and contralateral eyes were calculated. The values for T, A and S were used to create indexes to show how optic nerve changes are dependent upon different aspects of pressure elevation. These criteria were compared for correlations using Pearson's correlation coefficient (r). Sham-operated animals were excluded (n=8).

2.2 Histology

2.2.1 Source of tissue

Brown Norway rat eyes were obtained from the animal model detailed in previous sections. Culled normal Wistar rats from University stock were also used. Hypertensive rats were euthanised using the methods detailed in Section 2.1.3.5, while normal animals received a CO_2 overdose. At all times tissue orientation was

preserved, using either an appropriately placed suture or scalpel cut. The Corneal Transplantation Service provided all human eye tissue samples from donors, for which lack of objection for research use had been specifically established. Fresh human eyes were processed within 48 hours of cadaver time.

2.2.2 Tissue processing

Rodent ocular tissues were preserved in the perfusion fixative post-enucleation, where appropriate, before at least overnight fixation in 10% neutral buffered formalin (NBF, see Appendix 4). Tissues from non-perfused animals were fixed immediately in 10% NBF following dissection. Human optic nerves were dissected immediately upon receiving the eye, using precautions appropriate to the handling of human tissue, and preserved in 10% NBF.

2.2.3 Paraffin-Wax Embedding

Fixed human optic nerves and rodent optic nerve head, retrobulbar optic nerve and eyecups or posterior segments (both containing whole retinae) were dehydrated through increasing concentrations of industrial methylated spirit (IMS, Fisher Scientific, UK) diluted in distilled water, and then chloroform in alcohol. The initial dehydration step was a 30 minute incubation in 50% IMS, followed by 60 minutes in 70% IMS. Incubation in 90% IMS was carried out for either one hour or overnight. Further dehydration was via a 60 minute incubation in 100% IMS. Tissue was prepared for paraffin-wax embedding using a 50:50 chloroform:IMS incubation for 30 minutes, followed by two 30 minute incubations in 100% chloroform. 10 minutes into the last chloroform step, samples were warmed above a 56°C oven. All steps involving chloroform were performed under a fume hood. Samples were blotted dry on filter paper (Whatman) and incubated at 56°C in molten wax for 60 minutes, and then fresh wax for 30 minutes.

Superior and inferior retinae were dissected and embedded using a more gentle method. Fixed retinae were orientated on filter paper, and then passed through increasing concentrations of ethanol (25%, 33%, 50%, 63%) for 15 minutes each.

Subsequent washes in more concentrated ethanol were for 30 minutes each (70%, 80%, 90%). Samples were washed through ethanol containing increasing concentrations of chloroform (25% chloroform: 75% ethanol, 33% chloroform: 67% ethanol, 50% chloroform: 50% ethanol, 100% chloroform, 100% chloroform) for 15 minutes each.

A plastic mould was filled to a depth of about 3 mm with molten wax, and partially set on a -12°C cold plate. The well was then filled with wax and the sample immersed in either a transverse or longitudinal orientation. Wax blocks were cooled on the cold plate for 30 minutes and stored at 4°C overnight, or until use.

2.2.3.1 Paraffin-wax sectioning

Wax ribbons, 7 μm thick, were cut from samples using a Microm microtome, and individual sections were mounted onto slides. Eye-cup or posterior segment sections were taken to include both inferior and superior retinal axes. Sections were floated out in a de-gassed water bath at room temperature, then transferred on an uncoated slide to a 45°C water bath containing Meyer's albumin (BDH, UK). Sections were mounted on an-remove Histobond slides (Sigma-Aldrich, UK) and incubated for 30 minutes on a hot plate at 80°C. Slides were transferred to an oven at 56°C overnight for use the next day.

2.2.4 Cryoprocessing of tissue

Fresh rat optic nerve head and human tissue were used for cryoprocessing. The sample was snap frozen by immersion in liquid nitrogen chilled isopentane (Sigma-Aldrich, UK) for about 30 seconds. Frozen samples were orientated appropriately in a foil container containing Tissue-tek (Sakura, the Netherlands), then immersed in isopentane until frozen, and stored at -20°C until use.

2.2.4.1 Cryosectioning

Sections, 7 μm thick, were cut from frozen samples using a cryostat (Leica, UK) and mounted onto electrostatically charged Superfrost Plus slides (Surgipath, UK). Sections were air dried overnight and used on the subsequent day.

2.2.5 Masson's trichrome green staining

Masson's trichrome green stain was used to show connective tissue elements of the optic nerve. Wax sections prepared as in section 2.2.3.1 were washed in xylene (Fisher Scientific, UK) for ten minutes twice, then rehydrated through graded concentrations of IMS (100%;100%;90%;70%;50%) for one minute each. Sections from frozen samples (Section 2.2.4.1) were defrosted and then washed in PBS for ten minutes before use.

Wax and frozen sections were stained with Harris' or Meyer's haematoxylin, respectively, for 5 minutes. Staining was developed using a 5 minute wash in tap water. Sections were rinsed in 1.3% picric acid for 3 minutes, then washed in tap water. Beibrich scarlet solution (1% weight/volume in water) was applied for 2 minutes. Excess stain was removed under running tap water. Samples were immersed in a 1:1 solution of phosphotungstic acid (5% weight/volume in water) and phosphomolybdic acid (5% weight/volume in water) for 2 minutes. Fast green solution (2g fast green, 100ml distilled water, 2ml glacial acetic acid) was used to stain the tissue over 5 minutes and excess stain removed with tap water.

Wax sections were dehydrated through increasing concentrations of alcohol (Section 2.2.3), infiltrated with xylene in two 10 minute washes, then mounted in Histomount (BDH, UK). Frozen sections were mounted in Hydromount (BDH, UK).

2.2.5.1 Light microscopy image capture

Sections were examined using a Leica DMRA2 light microscope at various magnifications using 1.6x-100x objectives. Oil immersion was required with 63x and 100x objectives. Where appropriate, images were recorded using Leica QWin image analysis software.

2.2.5.2 Areas of interest in the optic nerve

For structural staining of the optic nerve, images were captured of the optic nerve head and retrobulbar optic nerve, or optic nerve proper from longitudinal optic nerve sections. From transverse sections, images of the entire optic nerve were captured. Higher magnification images of transversely orientated optic nerves were captured from the centre of the nerve, near the retinal vessels.

2.2.6 Haematoxylin and eosin staining

Staining was performed on human and rat optic nerve heads as a morphological and structural reference. Wax sections were rehydrated as in Section 2.2.5. Paraffin-wax and frozen sections were stained for 5 minutes in Harris' Haematoxylin (BDH, UK) and Meyer's Haematoxylin respectively. Excess stain was removed with a 10 minute wash in tap water. Slides were immersed in eosin for 2 minutes and excess stain removed as before. Wax and frozen sections were then mounted as described for Masson's trichrome green staining in Section 2.2.5, and images recorded as appropriate using Leica QWin software (see Sections 2.2.5.1 and 2.2.5.2 for details).

2.2.7 Toluidine blue staining

Staining with toluidine blue was carried out as a structural reference similar to haematoxylin and eosin staining. Wax sections were brought to water as for haematoxylin and eosin staining (Section 2.2.5). Wax and frozen sections were stained in 1% toluidine blue (TAAB, UK) for 2 minutes, washed in running tap water

for 10 minutes, dehydrated and mounted as in Section 2.2.5. Image capture was as for Sections 2.2.5.1 and 2.2.5.2.

2.3 Electron Microscopy

2.3.1 Tissue fixation

Fixation was used to preserve cellular components and structural details for clarity in electron micrographs. Cells were preserved with minimum alteration from the living state and in order to protect them from subsequent treatments. All electron microscopy reagents were of electron microscopy grade, and purchased from TAAB (UK) unless stated otherwise.

Pairs of perfusion-fixed retrobulbar optic nerve samples with a superior orientating suture distal to the eye were stored in 2% (n=10) or 4% (n=2) paraformaldehyde (PFA) (perfusion and orientation were as described in Section 2.1.1.5). Fresh eyes (n=2) and pairs of retrobulbar optic nerves (n=4) were stored in 2.5% glutaraldehyde in 0.1 M phosphate buffer overnight. During each step throughout embedding samples were agitated at room temperature unless stated otherwise. All PFA was removed from fixed samples using a fine-tipped pipette and then samples were fixed for a minimum period of two hours at room temperature using 2.5% glutaraldehyde in 0.1 M phosphate buffer. The glutaraldehyde solution was removed from samples using a fine-tipped pipette, and the samples were washed twice for 15 minutes with 0.1 M phosphate buffer at room temperature. Samples were post-fixed for one hour in 1% osmium tetroxide (diluted from a 2% stock in distilled water). Traces of fix were removed using three washes of 15 minutes each in distilled water.

2.3.2 Post-fixation tissue processing and embedding

Samples were dehydrated through increasing concentrations of ethanol (50%;70%;90%;100%;100%) for 15 minutes each. A 1:1 ratio of Spurrs medium viscosity Epoxy resin (TAAB, UK) and 100% ethanol was added to the sample and then incubated for 8 hours. Three 8 hour incubations in increasing concentrations of Spurrs medium viscosity Epoxy resin in alcohol (1:1, 1:2, 1:3) followed. Samples

were then orientated and polymerised in moulds containing 100% resin in an oven at 70°C for 8 hours.

2.3.3 Semi-thin sectioning and toluidine blue staining

Semi-thin 1 μm transverse optic nerve sections were cut with a glass knife using an ultramicrotome. Sections were stained using 1% toludine blue to assess axonal damage. Tissue was examined using a Leica DMRA2 microscope under 20x to100x objectives. Images containing areas of interest were recorded for superior, inferior, nasal and temporal nerve quadrants using Leica QWin software (Section 2.2.5.1), as well as for the areas described in Section 2.2.5.2 for transverse sections.

2.3.4 Ultra-thin sectioning and labelling for protein

Ultra-thin sections (75 nm) were cut from the same samples using a glass or diamond knife and mounted onto the copper side of a grid (TAAB). Three to four samples were mounted per grid, and grids stored on filter paper in a parafilm-sealed petri dish until use. Samples were stained using 2% aqueous uranyl acetate and lead citrate (consisting of 80mM lead nitrate, 120mM sodium citrate, and 160mM sodium hydroxide in distilled water). Grids were floated on filtered uranyl acetate, sample-size down for 15 minutes. Samples were washed five times in distilled water and then dried by gentle dabbing of the grids (sample side up) on filter paper. Lead citrate was pippetted onto parafilm, and the samples stained for 10 minutes, before five washes in distilled water as previously. Samples were stored on grids in a parafilm-sealed petri dish. Nerve sections were examined using a JEOL 1010 transmission electron microscope (JEOL Ltd., Japan), and images were recorded of areas of interest.

2.4 Silver staining

Frozen 7 μm retrobulbar optic nerve sections (see Sections 2.2.4 and 2.2.4.1 for details) were probed for retinal ganglion cell (RGC) degeneration using a Neurosilver staining kit (FD Neurotechnologies, USA). Representative samples of a range of IOP elevations were used (n=10). Degenerating nerves can be distinguished by an ability

to aggregate silver ions. Consequently the agrophylic propensity of degenerating nerves was used to assess the degree of neurodegeneration. Staining was performed in accordance with kit instructions. In brief, images were captured as described in sections 2.2.5.1 and 2.2.5.2, using a Leica DMRA2 microscope and Leica QWin software to record images obtained with 1.6x to 100x objectives.

2.5 Neuronal class III β-tubulin immunolabelling

RGC neurodegeneration was detected immunohistochemically as an inverse measure of using neuronal class III β-tubulin (TUJ1) labelling, since TUJ1 specifically labels neurons (Pearson *et al.*, 2002; Sergent-Tanguy *et al*, 2003). Both 7 μm paraffin-wax embedded (as in section 2.2.3) and frozen sections (see Sections 2.2.4 and 2.2.4.1) of retina (n=5) and retrobulbar optic nerve (n=5) were used, respectively.

Wax sections were brought to water (as described in Section 2.2.5), and frozen sections defrosted. Initially the same protocol as developed for immunolabelling of the optic nerve with other primary antibodies was used (see Section 2.6.2.2 and Figure 2.5) on both the retrobulbar optic nerve (n=2) and retinal sections (n=2).

Subsequently the protocol developed by Cui *et al.*, (2004) was used (n=3 each for both retinae and optic nerve). Sections were incubated for three 10 minute washes in PBS, and then treated with 10% normal goat serum (NGS, Dako, UK), 1% bovine serum albumin (BSA, Fisher Scientific, UK) and 0.2% Triton X-100 (Sigma-Aldrich, UK) in PBS for 1 hour. A 1:500 dilution of monoclonal neuronal TUJ1 antibody (Cambridge Biotechnologies, UK) in PBS containing 10% NGS, 1% BSA and 1.2% Triton X-100 was used to treat sections overnight. Traces of unbound antibody were removed by three washes in PBS as before. Alexafluor 594 (donkey anti-mouse) secondary antibody (Molecular Probes, UK) was administered at a 1:1000 concentration in PBS with 0.002mg/ml bisbenzimide (Sigma-Aldrich, UK) as a nuclear counterstain, and reacted for 1 hour. Sections were rinsed in three 10 minute PBS washes, mounted in gelvatol (see Appendix 1), and then cover-slipped.

2.5.1 Control sections

Throughout all immunolabelling experiments, omission of primary antibody application to sections was used as a negative control. PBS was added to replace the primary antibody. Positive control tissues as recommended by the primary antibody manufacturer (for example spleen) were harvested from Norwegian brown rats.

2.5.2 Fluorescent image capture

Representative immunofluorescent images were captured using a Leica DMRA2 microscope and Leica QFluoro software. Only the 10x, 20x and 40x objectives were used. Fluorescence was difficult to distinguish using lower power objectives. Higher magnifications were not used, as they did not provide any additional information.

Alexafluor 594 absorbs 522 nm wavelength light and emits red fluorescence at 552 nm. Bisbenzimide contains a Hoechst fluorochrome, with an excitation wavelength of 360 nm, producing a colour shift to the blue part of the spectrum at 470 nm. Single colour fluorescent images, made up of 264872 pixels, were captured using the appropriate Leica fluorescent filters, and composite images were created using Leica QFluoro software.

2.5.3 Areas of interest in the retina

Images were recorded of representative areas of retinal labelling. All retinal layers were included in every image. Both the orientation and location of all images were recorded.

2.6 Detection of retinal ganglion cell apoptosis

2.6.1 Tissue and preparation

Duplicate 7 μm thick frozen retrobulbar optic nerve sections were mounted onto electrostatically charged slides (section 2.2.4.1), and posterior segment (PS) or retinal paraffin-wax embedded sections (section 2.2.3.1) onto Histobond slides for each animal (n=25). All sections were then processed for both terminal deoxynucleotidyl transferase-mediated deoxyuridine triphosphate nick end labelling (TUNEL) and active Caspase 3 labelling. Sections of retina contained both inferior and superior portions. Positive control slides, consisting of paraffin-wax embedded rat mammary gland (Chemicon International, UK), were used as a reference.

2.6.2 TUNEL labelling

TUNEL labelling was performed using the Apoptag® Peroxidase *In Situ* Apoptosis Detection Kit (Chemicon International, UK). All reagents used were included in this kit (unless stated otherwise). Paraffin-wax sections were prepared by rehydration using three 5 minute washes in xylene, two 5 minute washes in ethanol, then a 3 minute wash in 95% ethanol, a 3 minute wash in 70% ethanol and a 5 minute wash in PBS. Tissue was permeabilised using a 15 minute wash in 20 μg/ml proteinase K (PK), and then washed in distilled water twice for 2 minutes each.

Frozen transverse retrobulbar optic nerve sections were fixed in 1% PFA in PBS for 10 minutes, followed by two 5 minute washes in PBS. Pre-cooled ethanol:acetic acid at 4°C was used to further fix the tissue for 10 minutes.

From this point onwards, frozen and paraffin-wax sections were treated similarly. 3% hydrogen peroxide obtained via dilution of a 33% stock (Sigma-Aldrich, UK) in PBS was used to quench endogenous peroxidase activity. Two 5 minute washes in PBS were used to remove residual hydrogen peroxide. Slides were then dried using Kim wipes (Fisher Scientific, UK), and sections encircled using a PAP pen (Dako, UK).

Equilibration buffer (10 µl) was pipetted onto each section, and allowed to react for a minimum of 10 seconds. 10µl of TdT enzyme was added to each sample, while negative control slides received the same volume of PBS. Slides were covered with a plastic hybrislip (Chemicon International, UK) and incubated in moist chambers at 37°C for 1 hour. Hybrislips were gently removed, and working strength stop-wash buffer was applied to the sections to prevent further reaction. Three washes in PBS were followed by application of 10 µl per section of antiperoxidase conjugate. After 30 minutes, unreacted conjugate was removed with four 2 minute washes in PBS. Working strength peroxidase substrate, diaminobenzoate (DAB) in the form of Fast DAB (Sigma-Aldrich, UK) was applied to each section for 6 minutes. Excess reagent was removed by three 1 minute, and then one 5 minute wash in distilled water.

Subsequently, nuclei in the tissue sections were counter-stained with methyl green for 10 minutes. Excess stain was removed by five 1 second washes in each of two distilled water baths, followed by a 30 second wash. Staining was fixed using acetone, by washing in two acetone baths (for five 1 second washes each) followed by a 30 second wash. Sections were dehydrated in two 2 minute washes of xylene and mounted in Histomount.

2.6.1.1 Quantification of TUNEL positivity

TUNEL positivity was assessed by cell counts undertaken in a masked fashion. All TUNEL positive and methyl green positive nuclei (i.e. all cells) in the ganglion cell layer of the retina were counted for two sections per eye (n=50) by a masked observer. The number of TUNEL positive cells was expressed as a percentage of total cell number in Microsoft Excel. Average percentage TUNEL positivity was calculated for each eye and for each animal group (for group details see Chapter 3, Section 2.3.1.6) using a Microsoft Excel formula.

Statistical comparisons were made between ipsilateral hypertensive and contralateral normotensive TUNEL positivity at the nasal, superior and overall retina for different IOP groups. These comparisons were made using two-tailed T-tests and ANOVA, as described in Section 2.1.2.1.

2.6.3 Active Caspase 3 immunolabelling

Active caspase 3 immunolabelling was performed on the same set of retinae as TUNEL labelling (Sections 2.6.1 and 2.6.2) in order to confirm apoptosis in support of TUNEL results.

Sections were brought to water as described in Section 2.2.5, then rinsed three times for 10 minutes each in PBS and fixed for 10 minutes in acetone. Sections were incubated in 0.2% Triton X-100 for 20 minutes, followed by PBS washes as before. 20 μg/ml PK was applied, and sections incubated for 20 minutes, 40 minutes or 1 hour in order to optimise labelling conditions. Three PBS washes were performed as before. Monoclonal active caspase 3 donkey anti-rabbit primary antibody (Abcam, UK) was applied to the sections at a 1:10 dilution in PBS. Two hours later, primary antibody was removed via three 10 minute PBS washes. Alexafluor 594 donkey anti-mouse secondary antibody conjugate at a 1:1000 dilution in PBS was used to fluorescently label active caspase 3 tissue antigen. Excess secondary antibody was removed by washing three times for 10 minutes each in PBS. Sections were mounted in gelvatol (see Section 2.5.2 and Appendix 1). Images were captured as described in Sections 2.5.3 and 2.5.4.

2.7 Immunohistochemical staining for NOS, glia and microglial cell markers

2.7.1 Primary and secondary antibodies

Antigens in tissue sections were localised using the primary antibodies described in Table 2.1. Initially, single immunolabelling was used in order to optimise techniques and to clearly show the tissue localisation of each antigen.

Secondary antibodies were fluorescent Alexafluor 488 donkey anti-rabbit and/or Alexafluor 594 donkey anti-mouse.

Table 2.1 ***Primary antibodies used in optic nerve immunolablling***

Antigen	Origin	Clonality	Supplier
Anti-rat CD200L	Mouse	Monoclonal	Harlan-Sera lab, UK
Anti-rat CD200R	Mouse	Monoclonal	Harlan-Sera lab, UK
Anti-rat CD45	Mouse	Monoclonal	Harlan-Sera lab, UK
Anti-cow GFAP	Rabbit	Polyclonal	Dako, UK
Anti-rat MHCII	Mouse	Monoclonal	Immunologicals direct, UK
Anti-human NOS1	Rabbit	Polyclonal	Autogen Bioclear, UK
Anti-human NOS2	Rabbit	Polyclonal	Autogen Bioclear, UK
Anti-human NOS3	Rabbit	Polyclonal	Autogen Bioclear, UK
Anti-rat OX33	Mouse	Monoclonal	Harlan-Sera lab, UK
Anti-rat OX41	Mouse	Monoclonal	Harlan-Sera lab, UK
Anti-rat OX42	Mouse	Monoclonal	Harlan-Sera lab, UK

2.7.2 Immunohistochemical techniques

2.7.2.1 Optimisation of paraffin-wax section immunolabelling

Preparation for immunolablling of paraffin-wax sections

Wistar rat eye wax sections (7 μm) on Histobond coated slides were rehydrated by passing through xylene, decreasing concentrations of alcohol (as described in Section 2.2.5), then fixed for 10 minutes in acetone. Between all subsequent steps, three 10 minute washes in PBS were used to remove residual reagents.

Antigen unmasking steps

Slides were treated with 20 μg/ml PK in PBS for 20 minutes to aid antibody entry into the tissue. Then a 10 minute wash in a 0.2% solution of Triton X-100 in PBS was used to permeabilise cell membranes. Subsequently, as PK did not adequately unmask antigens, PK was replaced by 0.1% pepsin in 0.01N HCl administered to the sections for 15 minutes. 0.5% normal donkey serum (NDS, Abcam, UK) in PBS was

substituted for PBS throughout experiments where pepsin was used, to reduce non-specific binding.

Application of antibodies

Anti-glial fibrillary acidic protein (GFAP) primary antibody was administered to the sections at the following dilutions: 1:100, 1:200, 1:300, 1:400, 1:500, and reacted for 2 hours at room temperature. Alexafluor 488 secondary antibody diluted to 1:1000 in PBS containing 0.002mg/ml bisbenzimide was applied to sections for 1 hour.

2.7.2.2 Development of an immunolabelling protocol for frozen sections

Preperation for immunolabelling

Fresh and PFA-fixed 7 μm frozen optic nerve sections on Superfrost Plus slides (see Section 2.2.4.1 for details) were brought to room temperature for 20 minutes, then washed for 30 minutes in PBS. Labelling was improved by removing the PBS wash and replacing with an overnight incubation in 30% sucrose at 4°C.

Tissue fixation

Following sucrose treatment, further improvements included fixation in 100% methanol for 10 minutes at room temperature. Methanol was substituted with acetone for clearer labelling.

Pre-antibody application antigen unmasking and blocking procedures

Following these initial treatments, the same protocol, as used for wax sections, was implemented using PK to unmask tissue antigens (Section 2.7.2.1). Due to excessive labelling, and in order to further develop this technique, experiments were run where PK and/or Triton X-100 were omitted. Incorporation of a one hour blocking step using 5% NDS in PBS did not improve immunolabelling sufficiently. However, further optimisation revealed that non-specific tissue antigenicity was eliminated by treatment with a 30 minute wash in PBS containing 2% BSA and 0.1% Triton X-100 (Wash Buffer 1).

Primary antibody application

Initially primary antibody was added, appropriately diluted (according to manufacturers guidelines) in PBS. The addition of 2% BSA and/or 0.1% Triton X-100 to the primary antibody dilution did not improve labelling. However, by primary antibody dilution in PBS containing 0.1% Tween-20 (polyoxyethylenesorbitan monolaurate, Sigma-Aldrich, UK), and further by the addition of 0.5% NDS (Wash Buffer 2) conditions were optimised. Sections were incubated with primary antibody at room temperature for 2 hours or overnight at 4°C.

Removal of excess primary antibody

Initially excess primary antibody was removed by three 10 minute washes in PBS. Washing in Wash Buffer 1 as opposed to PBS improved clarity of results.

Secondary antibody application

The appropriate Alexafluor secondary antibody diluted to 1:1000 in PBS containing 0.002 μg/ml bisbenzimide was applied to the sections for one hour at room temperature. Secondary antibody application was optimised as for the primary antibody, using Wash Buffer 2. Traces of antibody were then rinsed away using three 10 minute PBS washes.

Substitution of PBS with Tris-buffered saline (TBS), pH 7.5 (see Appendix 1) did not appear to improve immunolabelling, consequently PBS was used in the optimised immunolabelling protocol. The final immunohistochemical experimental protocol is summarised in Figure 2.5.

2.7.2.3 Control tissue and sections

Control sections were used as described in Section 2.5.1. Two control sections were used for each eye. Positive control tissues, as recommended by the primary antibody manufacturer, were harvested from Norwegian brown rats.

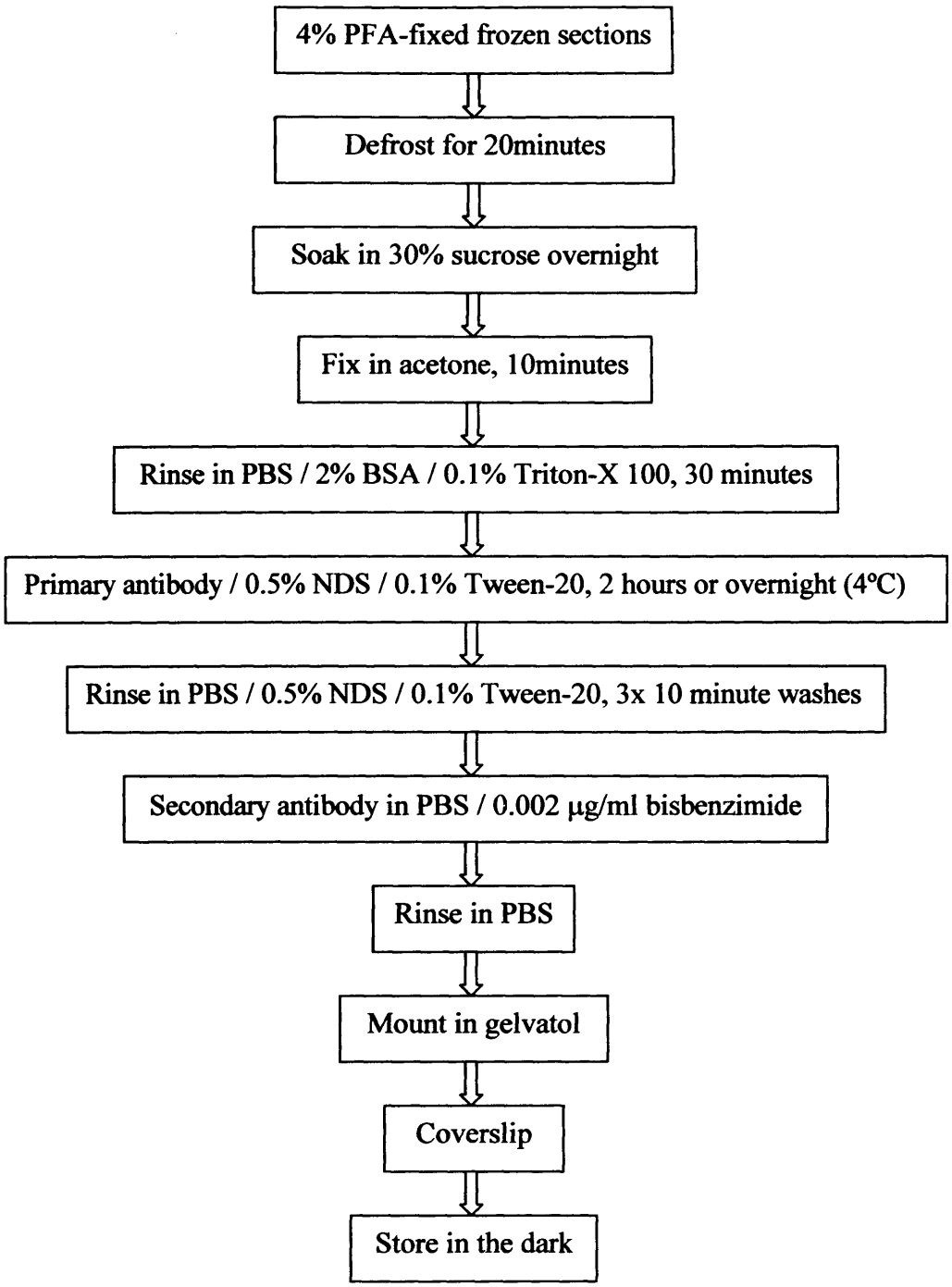

Figure 2.5 ***Summary flow chart of immunohistochemical protocol*** *Following optimisation of immunolabelling the same protocol was used consistently on all tissue sections. This method is detailed in the flow chart.*

Positive control tissues were brain for GFAP and all nitric oxide synthase (NOS) antibodies, as well as lymph and spleen for all macrophage, lymphocyte and microglial markers. Additional positive control tissues for NOS-2 and NOS-3 were penis and heart, respectively.

2.7.2.3 Non-fluorescent immunohistochemical mountants

During the optimisation procedure, samples were mounted in Hydromount, glycerol or gelvatol (see Appendix 1 for details).

2.7.2.4 Primary antibody combinations

Initially, single immunolabelling was used to optimise the protocol for each primary antibody in parafin wax and frozen tissue sections. Subsequently, dual labelling was performed on two fresh frozen sections from hypertensive (n=25) and normotensive (n=25) Norwegian brown rat eyes using combinations of primary and secondary antibodies. Dual labelling was required to colocalise NOS antigenicity with astrocyte, microglial and immune cell markers. This should provide information on the cell types responsible for any alterations in NOS immunolabelling following experimental glaucoma. As a general immune and microglial cell marker, major histocompatability complex II (MHCII) primary antibody was used in conjunction with each NOS isoform primary antibody. MHCII was also used together with GFAP in order to ensure there was no colocalisation of microglia or peripheral immune cells with astrocytes.

All other cell markers were used in conjunction with NOS2 in order to ascertain where potentially neurotoxic nitric oxide (NO) may originate from following ocular hypertension. CD200R and CD200L were also used in dual labelling with GFAP. Very little is known about the distribution or cellular localisation of CD200 and its receptor in the optic nerve, particularly during glaucoma. During dual labelling, tissue was incubated in a solution containing both Alexafluor secondary antibodies and 0.002 μg/ml bisbenzimide (see Figure 2.5).

2.7.2.5 Image capture

The orientation and location of fluorescent images captured for each region of interest is shown in Figure 2.6. Fluorescent red and blue immunolabelling were examined using appropriate fluorescent filters, magnifications and software as described in sections 2.5.3. Labelling using the secondary antibody, Alexafluor 488 was visualised by excitation at 495nm wavelength light, with green fluorescence emission at 525 nm.

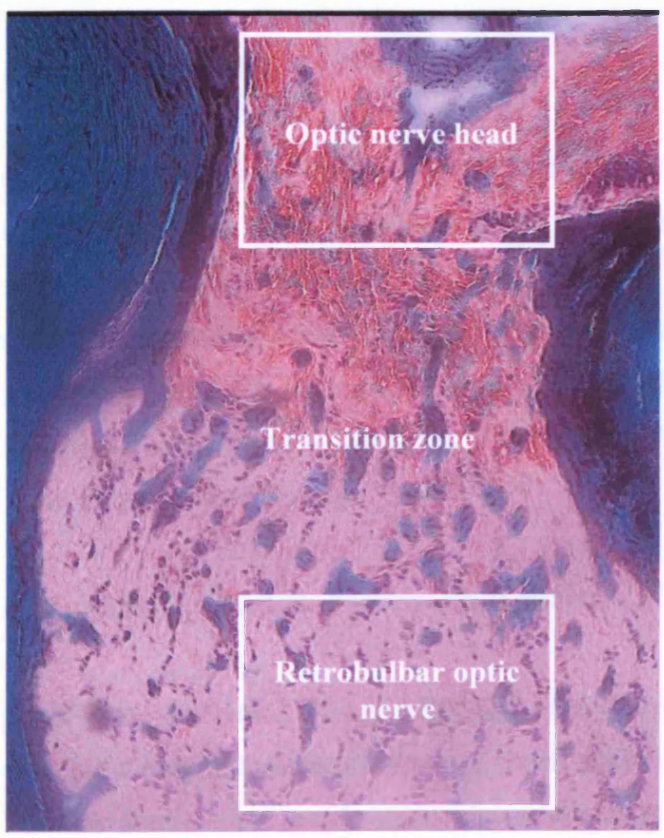

Figure 2.6 Locations in the rat optic nerve of captured immunofluorescent images *The rat optic nerve is shown in longitudinal section stained with Masson's trichrome green (x20 magnification). Images were consistently recorded from the same locations in the optic nerve following labelling for glial markers and NOS. For each optic nerve used, two images were recorded from each region of interest, namely the optic nerve head and optic nerve. The white boxes in the diagram above indicate the areas that were imaged.*

All images consisted of 264872 pixels each and were captured using Leica Qfluoro software. One optic nerve head and one retrobulbar optic nerve composite image were captured per longitudinal section. Each composite image consisted of one each of green, red and blue images overlaid. The 40x objective was used, as this enabled image capture of the entire optic nerve head width. Optic nerve head images were taken from the point of convergence of retinal nerve fibres into the optic cup, while retrobulbar optic nerve images were taken from the centre of the nerve immediately post-transition zone.

2.7.2.6 Quantification of immunofluorescence

Immunofluorescence was quantified in optic nerve head and retrobulbar optic nerve images. Leica QWin software was used to convert single colour red or green (depending on the secondary antibody used) fluorescent images to grey scale. These single colour images contained 264872 pixels. For each grey scale image, the intensity of every individual pixel was measured. Each pixel was therefore assigned an intensity value on a scale from 0 (black) to 255 (white). Pixel intensities were recorded and input into Microsoft Excel.

2.7.2.7 Statistical analysis of quantified immunofluorescence

All data analysis was performed using Microsoft Excel (n=25). Formulae and calculations were input manually unless otherwise stated. Results were separated into three animal groups (containing n=25 each) characterised by IOP elevation (see section 2.3.1.6). Each of these three groups contained five sub-groups with increasing severity of IOP elevation. Each sub-group contained two sets of results for each of five animals (n=10 each). Results were normalised by measuring background red or green fluorescence from two control (without primary antibody) sections and subtracting this from either red or green labelling of the equivalent experimental sections from each control and ocular hypertensive eye. Normalisation was performed independently for each eye in order to account for variations between eyes. Mean numbers of pixels at each intensity (from 0 to 255) were calculated separately for each

region of interest in contralateral and ipsilateral in each sub-group for every antibody used.

Two-sample, two-tailed T-tests were also used to compare the differences in immuno-related fluorescence data in contralateral and ipsilateral eyes. The total value, equal to the sum of (xy), where x=intensity of a given pixel, and y=the number of pixels at a given intensity, was calculated for each intensity. Ipsilateral and contralateral (xy) values were compared using a two-tailed T-test. The mean differences were also compared for significance between IOP groups, eg T1 and T2, T2 and T3, and so on.

Chapter III
Development of a Rodent Glaucoma Model

3.1 Introduction

Histological similarities between the rodent and human optic nerve have led to the development of experimental glaucoma models in the rat. Ultrastructural studies of the optic nerve head, Schlemm's canal (van der Zypen, 1977), and the episcleral drainage vessels (Morrison *et al.*, 1995) reveal important similarities between the rat and human. The rat is therefore potentially useful for modelling glaucoma.

Glaucoma can be modelled in retinal ganglion cell (RGC) culture or co-cultures with glia to illustrate pressure-induced cellular alterations at a biochemical level (Hernandez *et al.*, 2000; Liu and Neufeld, 2001). However, in glaucoma the entire optic nerve head structure and dynamic is altered, involving mechanisms likely to affect RGC survival which are still not fully understood. Pressure-induced alterations in cell culture can only provide a fraction of the information required for understanding the pathogenesis of glaucoma.

Many glaucoma models are available in various experimental animals with conditions as diverse as the human disease. Inducible glaucoma models most frequently involve manipulation of intraocular pressure (IOP), as IOP elevation is a major risk factor for the human disease (Davanger *et al.*, 1991). Experimental animal models of pressure – independent glaucoma are available, for example the DBA/2J mouse model of pigment dispersion glaucoma (John *et al.*, 1999). During this form of glaucoma, the iris pigment disperses and clogs the trabecular meshwork. Hypertension can be induced via reduction of aqueous outflow through laser treatment of the trabecular meshwork, cauterisation of episcleral drainage vessels, and most recently a spontaneously occurring glaucoma model has been discovered (Thanos and Naskar, 2004).

The most common form of human glaucoma, primary open angle glaucoma (POAG), can be closely emulated in some forms of experimental glaucoma. Glaucomatous changes homologous to primary open angle glaucoma (POAG) can be induced in the Norwegian brown rat by a direct injection of a mild sclerosant into the episcleral drainage system (Johnson *et al.*, 1995). By virtue of direct links between the episcleral venous system, and Schlemm's canal (Morrison *et al.*, 1995), aqueous drainage vessel sclerosis directly results in elevation of IOP. Variation in technique, such as amount, concentration and injection rate of sclerosant can produce different degrees of IOP elevation sustainable over chronic periods.

IOP should be monitored on a regular basis during experimental glaucoma. Accurate assessment of IOP elevation can allow direct correlation between IOP and optic nerve changes. Daily tonometry causes artefactual reduction of IOP, therefore less frequent readings are more accurate (Moore *et al.*, 1995). IOP measurements are highly sensitive and can be affected by many variables including ocular rigidity and pathology (Damji *et al.*, 2003). General anaesthesia can reduce IOP up to 60% (Jia *et al.*, 2000). Therefore, measurement is best obtained via awake tonometry using a local anaesthetic. Indications are that the hand-held Mentor® tonopen can be used on small rodents to obtain reliable IOP readings (Danias *et al.*, 2003; Moore *et al.*, 1995).

IOP shows circadian variation under the control of suprachiasmatic nucleus (SCN) oscillator neurons (Quintero *et al.*, 2003). Human IOP peaks during the day, with a trough during the night (Asrani *et* al., 2000; Pointer, 1997). However, most rodents are nocturnal, and therefore experience peak ocular tension during the night (Krishna *et* al., 1995; Nii *et al.*, 2001). Maintenance on a 12:12 light:dark cycle results in a two hour peak or trough in IOP one hour into the dark or light cycle, respectively (Jia *et al.*, 2000). In order to avoid the effects of circadian control on IOP animals can be exposed to constant low levels of non-neurotoxic 60 – 90 lux light.

Many fundamental characteristics of IOP elevation via episcleral drainage vessel sclerosis in the rat render this model and species the most convenient for experimental glaucoma studies. Similarly, due to our current understanding of IOP (including the

effects of anaesthesia and circadian control), glaucoma can now be reliably induced by the experimental elevation of IOP.

The aim of this chapter was to develop a reliable animal model of pressure-dependent glaucoma similar to that developed by Morrison *et al.*, 1995. Analysis of aspects of hypertension in order to relate these to other glaucomatous pathological changes was also essential.

3.2 Methods used to develop experimental glaucoma

All methods used in the development of an experimental glaucoma model are described in Chapter II, Section 2.1 inclusive. Objectives included determination of an accurate method to measure IOP (including the minimisation and control of circadian IOP), as well as optimisation of surgical techniques of IOP elevation.

Adult male Norwegian brown rats were used (n=75), animal heath was measured as an index of health throughout experimentation. IOP was measured using 10 readings taken from both eyes using a Mentor Tonopen ® tonometer.

Tonometric techniques were developed pre-surgery by the use of alternative probe shields. Two observers took all tonometry readings, and interobserver analysis was used to ensure consistency. Low lighting levels (60 to 90 lux) were used to minimise circadian variation in IOP. These methods were developed to ensure that multiple investigators could perform the most accurate method of tonometry, and reliable IOP readings could be recorded at any time.

Surgical elevation of IOP involved ipsilateral retrograde microinjection of a single episcleral drainage vessel with 1.75M hypertonic saline. Contralateral eyes were used as controls. Optimisation of surgical methods involved may fine adjustments to published technique (Morrison *et al.*, 1995). In particular, the structure of the microneedle used to inject hypertonic saline was adapted to improve success rate of IOP elevation.

Following surgery to elevate ocular pressure, IOP was measured consecutively for the first five days. Tonometry was then performed on alternate days until euthanasia. Duration of IOP elevation (T), area under the pressure curve (A) and standard deviation of pressure elevation (S) were calculated for all animals with a significant pressure elevation ($P<0.05$) in ipsilateral versus contralateral eye. Five groups were created within each of T, A and S, to represent the wide variation in aspects of IOP, and to allow pathological alterations of the optic nerve to be ascribed to the different aspects of pressure elevation. Correlation between these groups were assessed using Pearson's correlation coefficient.

3.3 Results

3.3.1 Animal health during experimentation

Mean animal weight increased from 383 g on initiation of licensed procedure to 395 g at euthanasia (Figure 3.1). All animals appeared healthy and infection, irritation or inflammation of the operated area was not observed. 10.9% of animals experienced bladder infections both pre and post-procedure and were treated with veterinary prescribed systemic antibiotics. One animal suffered from a skin irritation treated by daily swabbing with dilute Betadine. Irreversible weight loss was recorded from 2 animals due to circumstances unrelated to husbandry or procedure.

3.3.2 Development of tonometric techniques

Initial pre-surgical tonometry readings from the first group of experimental animals suffered from high variability due to experimenter inexperience. For all animal groups other than the first, standard deviation was low and sustained. Over time standard deviations became significantly reduced for both experimenters, in both eyes. More reliable tonometry readings were obtained with practice of the technique (Figure 3.2).

Standard deviation of tonometric techniques were not significantly reduced by use of alternative tonopen probe shields ($P>0.05$). The naked probe produced the minimum

standard deviation (7.11), which increased with the thickness of the shield (i.e. 7.74 with non-static film and 8.42 with a Mentor Ocu-film cover).

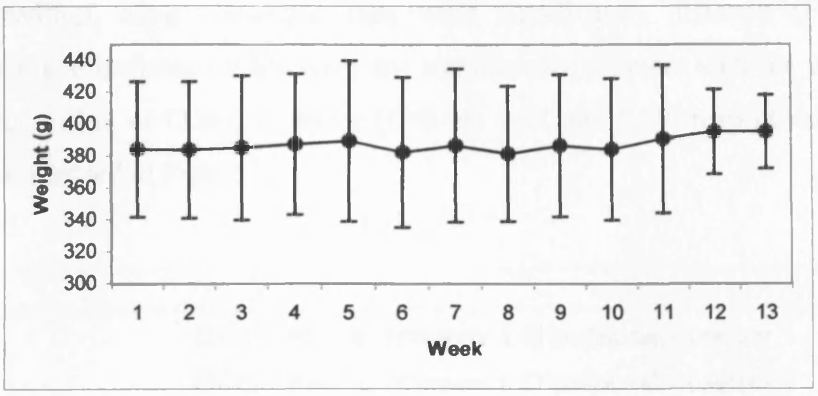

Figure 3.1 Animal weight as an index of health (n=75) *Weekly animal weight is shown post-microinjection. Animal number reduced over time due to euthanasia. Mean animal weight did not reduce as a result of the microinjection procedure. Microinjection appears to have no adverse effects on animal health. Standard deviation (bars) indicates a high variability of animal weight.*

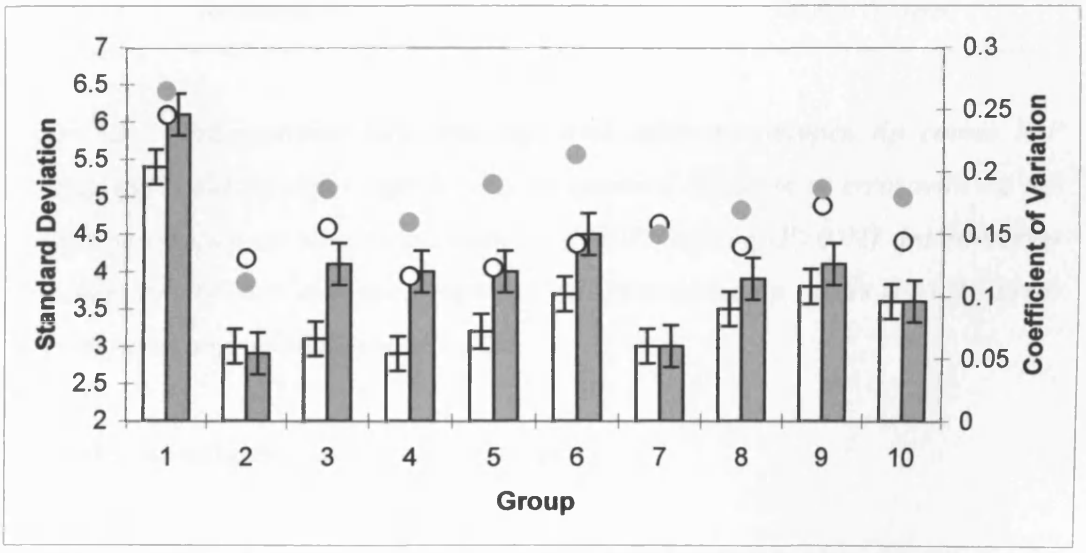

Figure 3.2 Increased reliability in IOP reading over time *IOP readings from animals (n=75), grouped depending on the start date of IOP measurements proved that initial (group 1) measurements of IOP suffered from high deviation (columns), standard error (bars) and coefficient of variation (dots). White represents contralateral measurements, while ipsilateral measurements are shown in grey. In subsequent groups, deviation, variation and error decreased.*

On comparison, interobserver variation was not significantly different with the unshielded probe (P=0.62) or the Ocu-film cover (P=0.35). However, interobserver tonopen readings using non-static film were significantly different (P=0.0059). Contralateral and ipsilateral IOPs were not significantly different with the unshielded tip, non-static film, or Ocu-film cover (P=0.95, 0.72 and 0.99, respectively). These data are summarised in Figure 3.3.

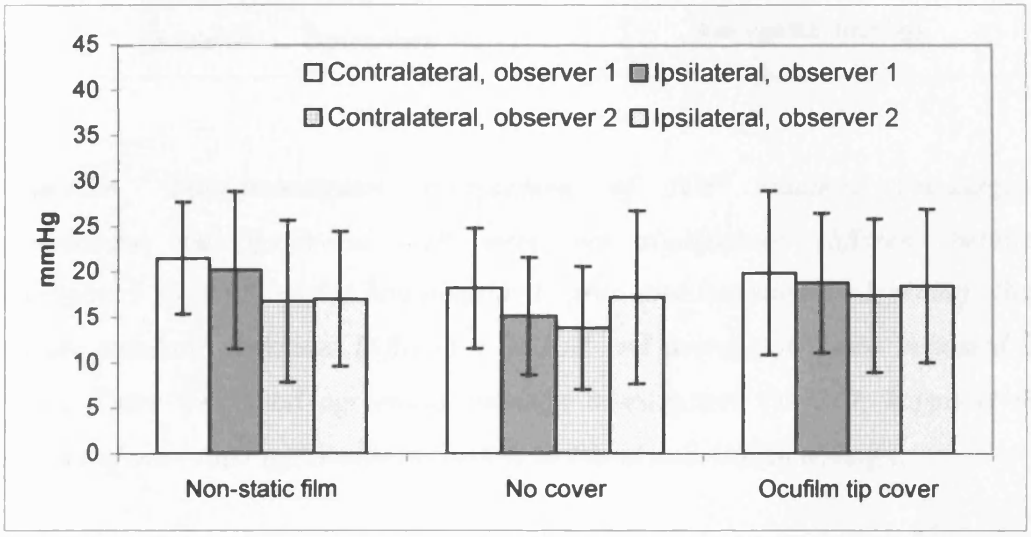

Figure 3.3 Pre-operative IOP readings with different tonopen tip covers *IOP readings (n=3) did not differ significantly in standard deviation or error with the use of different tonopen tip covers according to ANOVA testing (P>0.01). Interobserver differences in IOP were also not significant with alternative tip covers (P>0.1). Error bars show the range of standard deviation.*

3.3.3 Inter-investigator tonometry readings

Inter-investigator variations in pre-surgical tonometry readings were not statistically significant for contralateral (P=0.32) or ipsilateral (P=0.41) eyes. Mean contralateral pre-surgery readings for investigator 1 and 2 were 25.42 mmHg and 24.99 mmHg, respectively (figure 3.4). Investigator 1 obtained a mean ipsilateral IOP of 26.36 mmHg, while investigator 2 obtained an ipsilateral IOP of 24.77 mmHg (Figure 3.4).

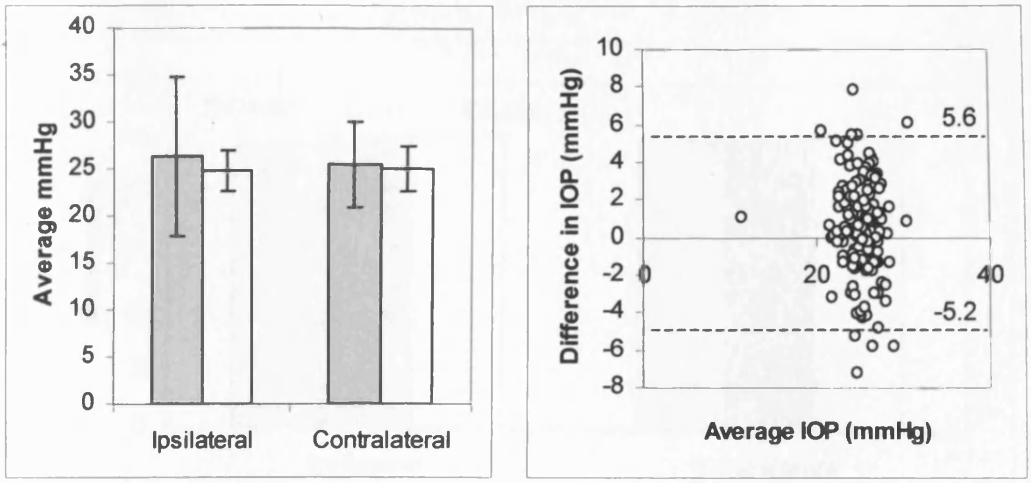

Figure 3.4 Inter-investigator comparison of IOP readings *Pre-surgical contralateral and ipsilateral IOP were not significantly different between investigators ($p>0.05$, $n=75$, Investigator 1, grey and Investigator 2, white). Bars indicate standard deviation. Difference in IOP and average IOP are indicated by circles. There was good agreement between investigators ($\kappa=0.61$, kappa is the measure of inter-rater agreement according to Bland and Altman testing).*

3.3.4 Minimisation of circadic control of IOP

Circadian peaks and troughs in aqueous outflow and secretion were eliminated by 72 hour exposure to low levels of constant light. Under normal lighting conditions, a peak during the dark phase (7-9pm) and a trough during the light phase (7-9am) of the light cycle would be expected. Comparison of readings, taken during these time points, with readings taken during the day, demonstrated that circadian control of IOP had been eliminated by exposure to constant lighting (Figure 3.5).

Mean contralateral IOP was 25.16 mmHg during "day" readings. A reduction of only 0.11 mmHg was observed with readings taken during the "dark" phase of the light cycle, when IOP mean was 24.31 mmHg. A slight IOP increase of 0.35 mmHg was observed during the "light" phase, with a mean IOP of 25.36 mmHg. Similar discoveries were made using the ipsilateral IOP, which increased by 0.83 mmHg and reduced by 0.4 mmHg during the "dark" and "light" phases respectively. Day ipsilateral IOP was recorded as 25.10 mmHg.

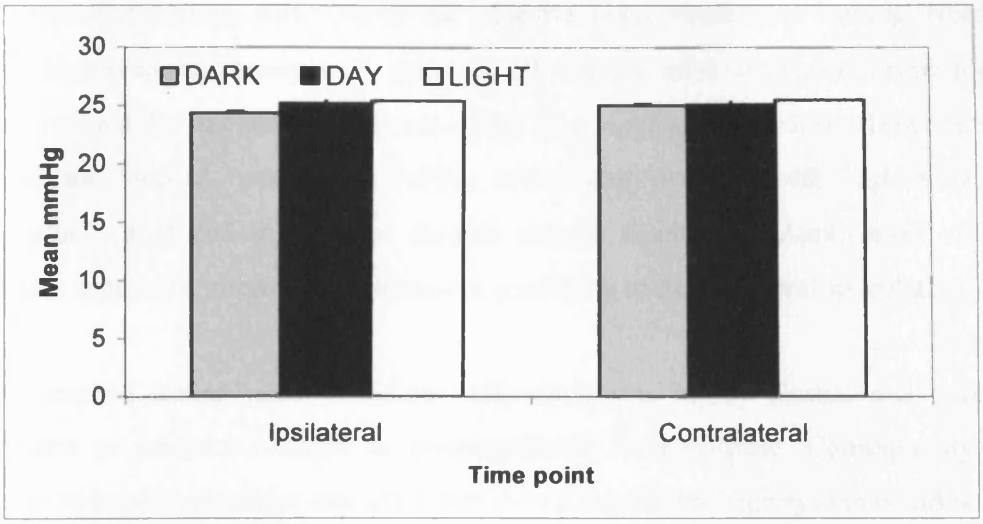

Figure 3.5 Exposure to constant light eliminated the circadian control of IOP

IOP recorded at time points with circadian relevance were not significantly different according to ANOVA testing (n=75, P>0.1). Light readings were performed during the circadian trough, while dark readings were taken during the peak in aqueous outflow. Day readings were recorded at any time point between these peaks and troughs. Therefore reliable tonometry readings can be recorded at any time over a 24-hour period.

Slight IOP differences were recorded from each eye at all time points. Ipsilateral IOP was higher than contralateral IOP both during the "dark" (0.68 mmHg) and "light" (0.09 mmHg) phases. However, during the day, contralateral IOP was slightly above ipsilateral by 0.06 mmHg. None of these differences were significant (P>0.1). These changes are opposite to those produced by circadian flux. Constant lighting eliminated the circadian control of IOP. Therefore, IOP measured at any point would not be artificially elevated or reduced.

3.3.5 Microneedle adaption

Some adhesive agents were highly electrostatic and attracted dust particles in the form of a white deposit. Capillary action allowed entry of adhesive into the needle due to low viscosity. Successful microinjection was not achieved using these needles due to blocked fluid outflow. Storage in a moist chamber prevented successful

microinjection through softening of the adhesive bond resulting in leaking. Needles where high viscosity Superglue™, dried for 10 minutes before application were found to be optimal for successful IOP elevation. The application of heat shrink tubing around the blunted needle and tubing attachment overlaid with high viscosity Superglue™ produced even more durable needle assemblies. Application of this tubing to secure the microneedle limited accessibility to the episcleral vasculature.

Heat-stretched tubing used to deliver sclerosant was highly elastic, and reduced resistance to pressure resulted in uncontrollable fluid outflow. Consequently the volume of hypertonic saline delivered into the episcleral drainage system could not be measured. Slightly tapered small (0.038 inch OD) diameter tubing was found to be far more accurate and safe for episcleral fluid delivery.

Initial surgeries using 50 μm diameter microneedles, supplied by the Morrison laboratory were unsuccessful. The superior episcleral drainage vessels were too small for successful cannulation with a needle of this diameter. Significant pressure fluctuations were recorded from the 10 animals microinjected with these needles, relating to either IOP reduction (Figure 3.6) or unsustained elevation (Figure 3.7). Microneedle diameters of less than 15 μm often blocked with dust particles. Increased resistance to fluid outflow due to a small inner diameter resulted in leakage from the adhesive joints and lack of fluid delivery. Microneedles of between 20 and 30 μm outer diameter were optimal for cannulation. Insertion of approximately 2 mm of the needle length was sufficient to occlude the vessel, produce a successful microinjection and elevated IOP (Figure 3.8).

3.3.6 Development of surgical techniques

Ergonomics of surgery were an issue, as it necessary to insert then maintain a microneedle in a small aqueous drainage vessel for almost a minute. The hand rest designed specifically for this purpose assisted in successful microinjections. After some time it was found that this rest interfered with accessibility to the tissue, and that practice had increased hand stability sufficiently for rest-free microinjections.

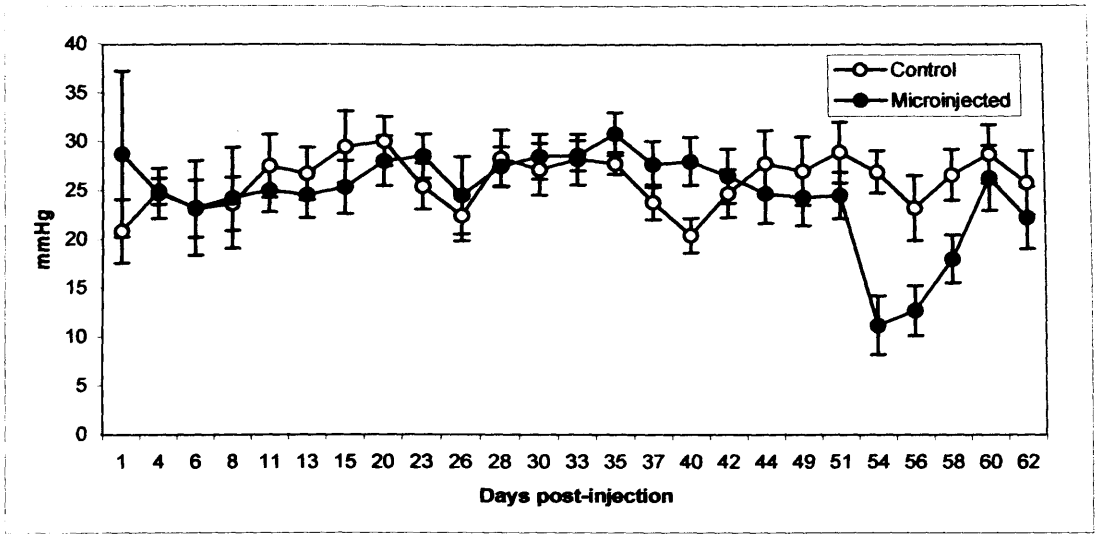

Figure 3.6 ***An example of IOP reduction*** *Reduction of IOP during optimisation of microinjection is shown (n=1). IOP elevated only at day 1 post-microinjection. IOP returned to normal by day 3, and no further elevations were recorded up to 62 days post-microinjection. Bars indicate standard deviation.*

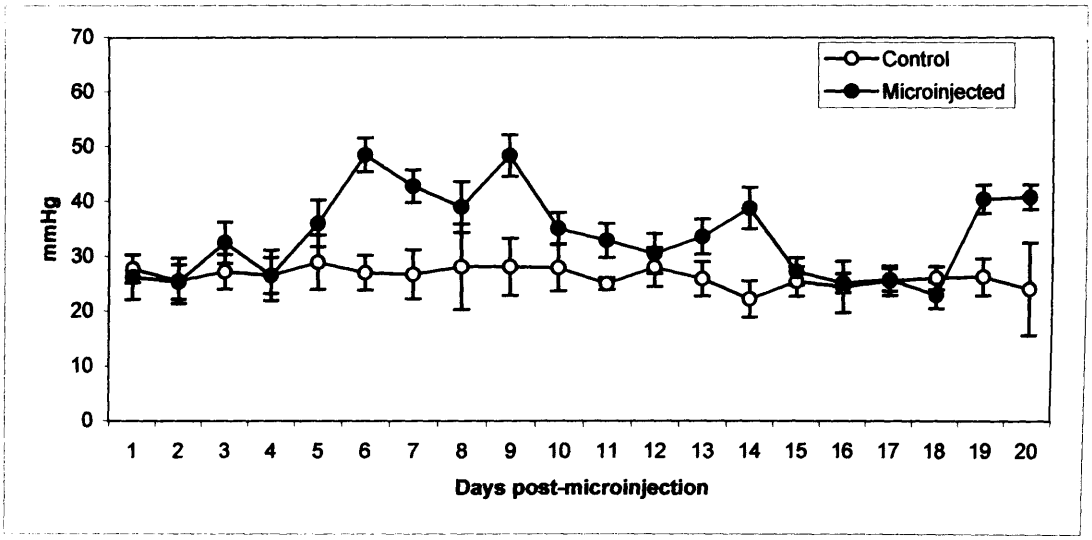

Figure 3.7 ***Fluctuation of experimental eye pressure*** *In some cases fluctuation of experimental eye pressure was recorded, as shown above (n=1). This deviation can be accounted for by optimisation of the microinjection procedure, and the variability between individual animals. Bars indicate standard deviation.*

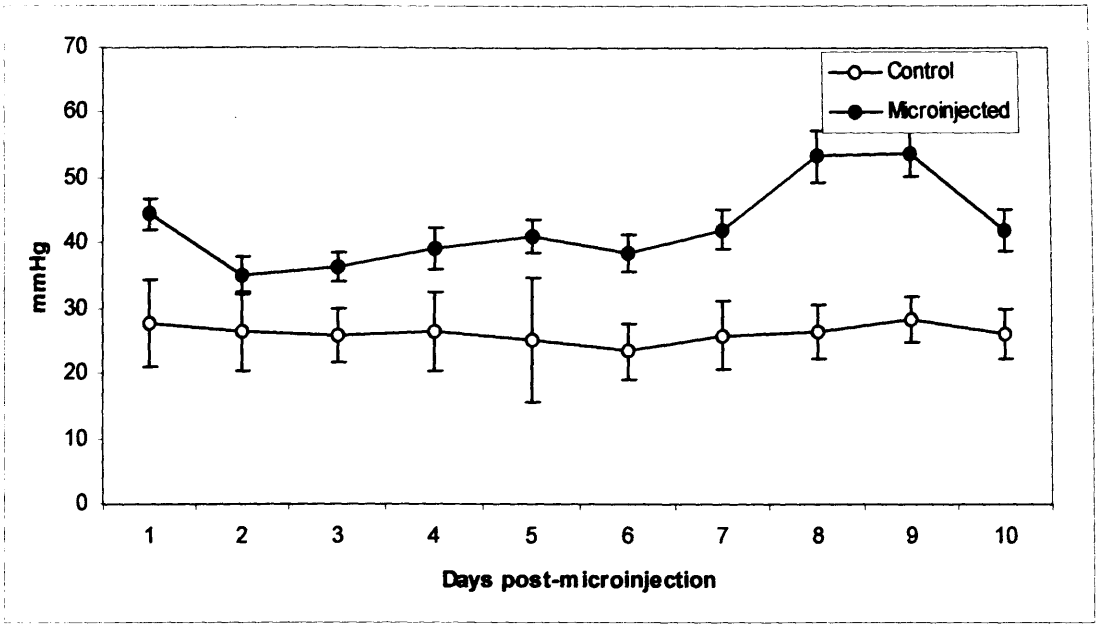

Figure 3.8 ***Consistent IOP elevation*** *Following optimisation of the microinjection technique it was possible to secure a consistent IOP elevation. However, this elevation could become unstable, producing extremely high pressure as shown (n=1). In the majority it was possible to avoid this pressure response by reducing the force of hypertonic saline injection. Bars indicate standard deviation.*

3.3.7 IOP elevation

IOP elevation was successfully sustained in the majority of animals (n=57). Post-surgical mean contralateral IOP was 25.34 mmHg, while ipsilateral was 31.25 mmHg, an increase of 5.89 mmHg. Sham-operated animals (n=8) did not experience a sustained significant pressure elevation under any circumstances.

Mean daily ipsilateral IOP elevation for all animals was 6.55 mmHg. IOP was elevated for between 1 and 65 days. Standard deviation of elevated IOP ranged from 1.05 to 13.56 depending on whether the IOP elevation was sustained, or fluctuated. The average standard deviation of all readings was 3.76. Sham-operated animals (n=8) did not experience a sustained significant pressure elevation under any circumstances. Ocular hypertensive animals were separated into groups with increasing pressure duration, area under the pressure curve or standard deviation. The

table shown in Figure 3.9 illustrates the boundaries of these IOP sub-groups. Group boundaries were set based upon the available range of animals, post-mortem. Figures 3.10 to 3.12 show the full range of duration of pressure elevation (T1 to T5), area under the IOP curve (A1 to A5) and standard deviation of elevated pressure (S1 to S5). These groups can be used to correlate pathological optic nerve changes with changes in IOP.

Level	**GROUP "T"** Duration of IOP elevation (days)	**GROUP "A"** Area under the pressure curve (mmHg)	**GROUP "S"** Standard deviation
1	**1 – 7** (n=10)	**0.9 – 22.7** (n=8)	**0 - 1.511** (n=6)
2	**11 – 19** (n=19)	**24.3 – 96.8** (n=16)	**1.52 - 2.96** (n=13)
3	**20 - 27** (n=11)	**97.2 – 151.1** (n=15)	**3.20 - 3.75** (n=9)
4	**33 – 46** (n=10)	**165.3 – 256.1** (n=8)	**3.81 - 5.57** (n=16)
5	**47 - 65** (n=7)	**271.9 – 469.3** (n=10)	**6.02 - 12.76** (n=12)

Figure 3.9 Attributes of IOP used to categorise experimental IOP elevation *Animals (n=57) falling between the values shown for each variable were assigned to the relevant group. The number of animals within each group is shown.*

Area under the IOP curve is equal to IOP multiplied by number of days of pressure. Area under the IOP curve and duration of pressure elevation covary, with a correlation coefficient (r) of 0.602 ($p<0.001$). There is a trend towards an increase in both factors. This correlation would increase if all pressure elevations were similar. There is variation in the magnitude of pressure elevation, which is independent of the duration of IOP elevation in some cases. However, in the majority longer durations of pressure elevation produce a higher area under the curve (Figure 3.10). Standard deviation of IOP elevation correlated negatively with the duration of pressure elevation at $r = -0.0784$ ($p<0.001$, Figure 3.11). Longer pressure durations resulted in the lowest standard deviations. IOP may stabilise at longer durations or as familiarity with and tameness of the animal increase. Area under the pressure curve and standard deviation of pressure elevation elevated together and correlated with a coefficient of $r = 0.17$ ($p<0.001$, Figure 3.12).

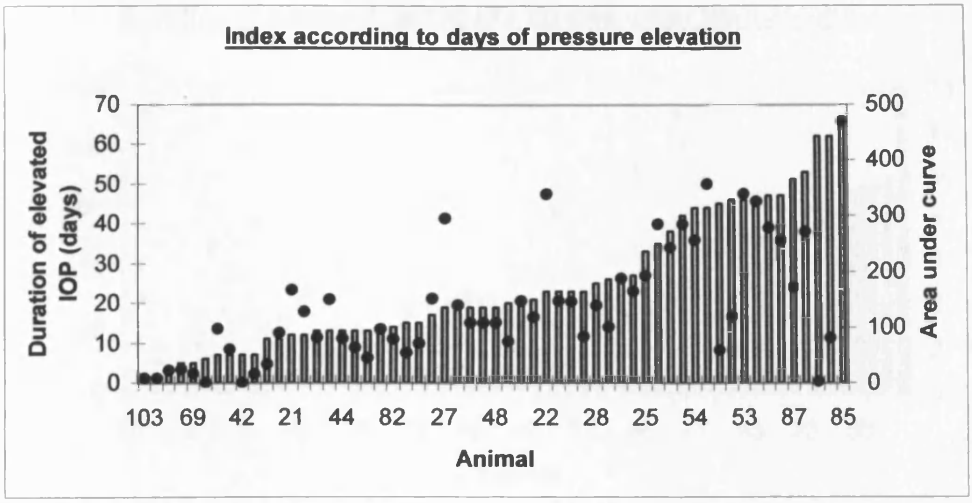

Figure 3.10 Duration of IOP elevation and area under the IOP curve *Duration of IOP elevation (shown as bars) was over a wide range from 1 to 65 days (n=58). Duration of elevated pressure increased with area under the pressure curve (r = 0.602). Outliers indicate generation of very low or very high-pressure elevations in combination with particularly short or long durations of elevated pressure.*

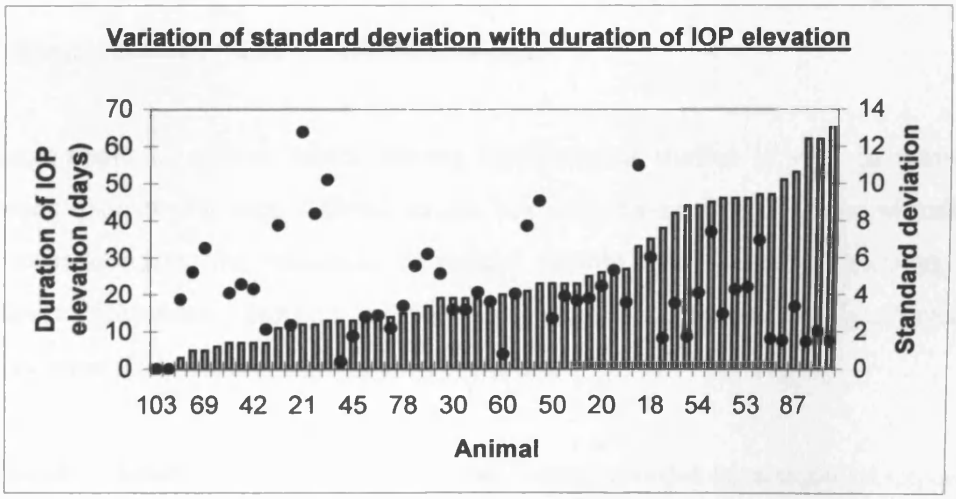

Figure 3.11 Standard deviation of IOP elevation with duration of elevation *Overall standard deviations of IOP elevation (black points) covaried with duration of IOP elevation (grey bars) for individual animals (n=58). There was a low correlation between these sets of values (r = -0.0784).*

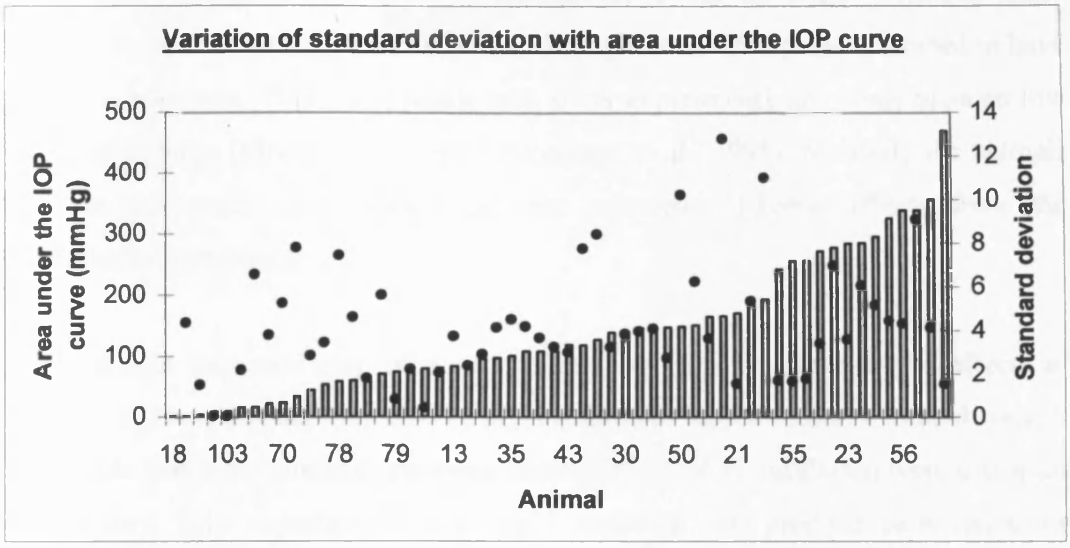

Figure 3.12 Standard deviation of IOP elevation with area under the curve *Standard deviation of IOP elevation (black points) correlates at a low level with area under the IOP curve (grey bars, r = 0.17). As area under the curve increases, there is a slight trend for standard deviation to elevate (n=58).*

3.4 Discussion

3.4.1 Animal health and constant illumination

The assessment of animal health during experimental studies is vital in terms of producing good quality data. Animal weight is the most convenient method of making such measurements. No reduction in animal weight was recorded following the initiation of procedure. Therefore it is unlikely that animals were adversely affected in any way other than that intended by the procedure.

The few anomalous cases of weight loss and illness recorded here might be expected in any normal population of animals. However, failure to thrive may be the consequence of a number of experimental variables, including infection, anxiety, or procedural side effects. Many studies have investigated the effects of constant light, which may have a profound effect on ability to thrive. Constant lighting was included in these experiments in order to minimise the circadian control of IOP fluctuation.

The evidence suggests that circadian fluctuation of IOP no longer occurred under constant light. IOP was relatively constant throughout all time points expected to have circadian relevance. This corresponds with other experiments involving constant low levels of lighting (Moore *et al.*, 1995; Morrison *et al.*, 1995). Similarly the animals used in this study (and others) did not experience adverse effects from the experimental conditions.

Slight weight increases may be a consequence of growth, however the effects of constant light on feeding may also be shown through the elevation of animal weight. It possible that other circadic processes controlled by SCN oscillation were disrupted by constant light exposure. Visible light exposure can produce neuroendocrine alterations leading to changes in hormone levels, which contribute to immune response and feeding (reviewed by Roberts, 2000). In particular, the hypothalamo-pituitary-adrenal (HPA) axis, normally involved in maintaining homeostasis during chronic inflammation though adrenal glucocorticoid release can be disrupted by exposure to constant light (reviewed by Harbuz, 1999). Therefore animals exposed for long periods to constant light would be more likely to develop autoimmune disease.

The elimination of circadian control may result in more reliable tonometry readings (Moore *et al.*, 1995; Morrison *et al.*,1995), however, the effects may be more far reaching. For example, through compromise of the immune system which may affect neurodegeneration in glaucoma (Bakalash *et al.*, 2002).

3.4.2 Validity of tonometric techniques

Tonometry was used to identify experimental glaucoma via elevation of IOP. IOP readings are most commonly recorded from experimental animals via a hand-held Tonopen. This is an extremely reliable method, and is much more convenient for studies on small animals than other methods such as Goldmann which may require general anaesthesia.

Many studies use an unshielded tonopen to measure IOP in experimental glaucoma. The use of Mentor Ocu-film tip covers, non-static film, or the absence of a cover does not improve tonometry readings. It is therefore best practice to use the manufacturers recommended method, as this is not significantly worse than other methods. This also avoids unnecessary damage to the tonopen, and voiding of the warranty. This small study suggests that use of an unshielded tonopen may be an unnecessary precaution.

3.4.3 The elevation of IOP

In order to successfully elevate IOP it was necessary to make various improvements and adjustments including a reduction in microneedle diameter and taper of microneedle tubing. The techniques used by Morrison *et al.* (1995) were found to be inappropriate due to the small sized aqueous drainage vessels of our animals. Inaccuracies in hypertonic saline delivery resulting from the use of tapered microneedle tubing were also eliminated by our study. These alterations should improve success rate and ease of the microinjection procedure during future studies.

Several problems were encountered during the development of the glaucoma model. During optimisation of the microinjection procedure, surgery sometimes resulted in reduction of IOP. Hypertonic saline injection causes reduction in the size of the ciliary body, which may account for this low IOP (Chanis *et al.*, 2003). It is also possible that fitting a constrictive equatorial band around the eye during surgery in order to limit vessel sclerosis may affect IOP. The pressure from this band may have forced aqueous to exit the eye resulting in IOP reduction. There is also no evidence to suggest that this band did not have adverse effects on RGC survival through physical damage of the retina. However, lack of IOP elevation or adverse effects of surgery in sham-operated animals indicated that surgical techniques other than hypertonic saline delivery were unlikely to cause IOP fluctuations that induce RGC damage.

3.4.3.1 Elevation of IOP in other rat models

Many laboratories have reported difficulties in developing the episcleral drainage vessel sclerosis glaucoma model identified by Morrison *et al.* (1995). These groups

often resort to either the episcleral drainage vessel cautery model (Garcia-Valenzuela *et al.*, 1995; Sawada and Neufeld, 1999), or translimbal laser photocoagulation of the trabecular meshwork (Levkovitch-Verbin *et al.*, 2002). Episcleral vessel cautery disrupts blood flow, and it is unknown whether optic nerve alterations are produced by reduction of aqueous drainage, or from congestion of ocular blood flow. Similarly, the effects of laser treatment on the ocular system may not be localised to just the trabecular meshwork. Damage to other ocular tissues may result from laser treatment, for example the iris or the cornea may become damaged.

These alternative models may be representative of secondary or vasospastic glaucoma. However, they do not convincingly represent POAG, the most common form of the human disease. The elevation of IOP via sclerosis of an aqueous drainage vessel is more representative of the human condition. The changes suggested here to the techniques used by Morrison *et al.* (1995) may improve the success rate of this model in other laboratories.

3.4.3.2 Comparisons between basal and elevated IOP

IOP has been used to define many glaucoma models, and is a major diagnostic factor in the human disease. As a result there is a wealth of information available regarding IOP elevation during glaucoma.

In comparison with data collected by Johnson *et al.* (2000) from the same breed and strain of rat, mean control IOP used in the present study is relatively high. Johnson *et al.*, (2000) found mean control IOP was 19.5 mmHg, as compared to our value of 25.34 mmHg. Norwegian brown rats have been shown to exhibit a control IOP of 25.1 mmHg (Grozdanic *et al.*, 2003) similar to IOP values achieved in this study. The high number of readings recorded, and the use of two separate investigators limits the possibility of tonometric error produced from experimental technique. It is possible that similar to discrepancies in vasculature of the episcleral drainage vessels, there are discrepancies in IOP between the rats used in this study, and those used by Johnson *et al.* (2000).

Other glaucoma models use different breeds of rat. Both the vein cautery (Garcia-Valenzuela *et al*, 1995; Sawada and Neufeld, 1999) and the laser photocoagulation (Lekovitch-Verbin *et al.*, 2002) models involve Wistar rats. While the spontaneously glaucoma model recently discovered by Thanos and Naskar (2004) occurs in Royal Collage of Surgeons rats. Unfortunately the use of different breeds and frequent aneasthesia before tonometry means it is difficult to draw comparisons between the ocular pressures in these and the present study. The control IOP levels of these animals appears to be much lower than the Norwegian brown, with reports of 11.6 mmHg (Garcia-Valenzuela *et al*, 1995; Sawada and Neufeld, 1999), 19 mmHg (Lekovitch-Verbin *et al.*, 2002) and 15.1 mmHg (Thanos and Naskar, 2004[3]). It is likely that these differences are due to breed of rat and anaesthesia.

As in the human population, the IOP of the rat will vary. The majority of studies indicate that control IOP of the rat is lower than that of the human. However, in this study the Norwegian brown IOP is higher than the human upper limit of 21 mmHg. This is not relevant to the present study as it is impossible to draw interspecies comparisons due to the effects of ocular rigidity, corneal surface and corneal thickness on IOP readings. Not all ocular hypertensive patients will develop glaucoma, and some glaucoma patients have IOP within the normal range. Therefore the important factor in the development of glaucoma is degree of pressure elevation and not the actual pressure. Therefore, despite a higher than expected control IOP (as compared to other rat studies), the model used here provides a reliable mild pressure elevation.

Episcleral vessel sclerosis can result in much higher pressure elevations than the 5.6 mmHg with average pressure of 31.24 mmHg produced here. Pressure was elevated by 19.5 mmHg to 36 mmHg by Johnson *et al.* (2000) despite use of the same techniques. However vein cautery in the Norwegian brown can result in a milder pressure elevation of 9 mmHg (Grozdanic *et al.*, 2003) while in Wistar rats cautery elevates pressure by 10.6 mmHg to a value of 22 mmHg (Garcia-Valenzuela *et al*, 1995; Sawada and Neufeld, 1999). Laser photocoagulation of the trabecular meshwork produces IOP elevations of 25.5 to 49 mmHg in Wistar rats depending on experimental conditions and duration of elevation (Lekovitch-Verbin *et al.*, 2002). In

the spontaneously hypertensive rat model IOP elevates unilaterally to 35 mmHg (Thanos and Naskar, 2004[3]), an increase of 19.9 mmHg.

Severe IOP elevations are normally induced in experimental glaucoma. Mild pressure elevation such as that achieved in the present study may be more representative of human glaucoma. Degeneration typical of very high pressures, which appears as a porous appearance of the optic nerve, is rarely seen in human glaucoma, and has only been documented in the most serious conditions (Quigley *et al.*, 1981). This degeneration is often found in experimental glaucoma.

3.4.3.3 Attributes of IOP elevation

No other published studies have examined the attributes of raised IOP in experimental glaucoma in the detail described here. Other studies calculate average daily IOP elevation, together with the duration of this increase. Peak IOP as well as average IOP elevation have also been measured (Levkovitch-Verbin, *et al.*, 2002). Daily IOP elevation and average IOP are not representative of the overall IOP elevation. An average or peak IOP may be maintained over a wide range of time points or may vary considerably throughout. As glaucoma is a progressive disease, during which IOP can vary the most informative method of describing IOP should combine both duration and magnitude of elevation. Standard deviation of IOP elevation may also be useful. Therefore the direct effects of duration of pressure elevation, area under the pressure curve and standard deviation of pressure elevation on RGC survival can be measured.

Standard deviation varied considerably during different cases of experimental glaucoma. Long durations of pressure elevation can be sustained at consistent pressures, while higher pressures are less consistently maintained. Duration of IOP elevation and degree of pressure elevation are both crucial attributes of the area under the pressure curve. Area under the curve will enable the association of a combination of IOP elevation and duration of elevation with any alterations following experimental glaucoma. Future results can now be correlated with specific and relevant aspects of the pressure curve.

3.4.4 Conclusions

In order to develop a representative glaucoma model, IOP was manipulated and measured as accurately as possible. Attributes of IOP elevation during experimental glaucoma that have never previously been examined were assessed and compared during this study. These investigations should improve understanding of the IOP changes involved during experimental glaucoma. These IOP changes can then be related specifically to biochemical, cellular and pathological disease alterations.

Chapter IV

Comparative Optic Nerve Histology and Neurodegeneration

4.1 Introduction

In order for an animal model to be a good glaucoma model, optic nerve tissue morphology should be similar to that of the human. Glaucomatous structural and cellular optic nerve alterations, which are likely to play a role in retinal ganglion cell (RGC) death (Lam *et al.*, 2003b; Naskar *et al.*, 2002; Varela and Hernandez, 1997; Quigley and Addicks, 1981; Wang *et al.*, 2002b), should also be comparable.

Following glaucoma, detectable morphological alterations such as excessive optic cup excavation, bowing of the lamina cribrosa and reduction in nerve fibre bundle density occur. These can be used to identify successful elevation of IOP and the induction of experimental glaucoma. Alterations in the content of optic nerve connective tissue (Johnson *et al.*, 1996) and cellular changes have also been reported (Ahmed *et al.*, 2004; Naskar *et al.*, 2002; Neufeld, 1999; Quigley *et al.*, 1981; Varela and Hernandez, 1997; Wang *et al.*, 2002b; Yucel *et al.*, 1999).

It is essential to correlate degree of RGC death and degeneration with IOP in glaucoma models. Glaucomatous RGC degeneration begins at the site of injury, where axons traverse the lamina cribrosa (Quigley *et al.*, 1981) and frequently results in axonal loss (Shou *et al*, 2003; Weber *et al.*, 1998). Therefore, glaucomatous neurodegeneration can be reliably quantified using optic nerve proper axon counts (Ogden and Miller, 1966; Potts *et al.*, 1972; Levkovitch-Verbin *et al.*, 2002). However, these are impractical due to the technique's labour-intensive nature and expense. Unfortunately, retrograde labelling used in many glaucoma studies is inaccurate due to the effects of glaucoma on retrograde transport. Grading axonal degeneration on a scale following histological staining is possible as large pores or vacuoles remaining following axon loss (Johnson *et al.*, 2000). While of limited

quantitative use, this technique can be used to reproducibly classify the degree of damage in a qualitative approach.

Distinctive morphological alterations are displayed by degenerating RGC axons. These include dilation, inclusion of large intracellular vesicles and Wallerian degeneration (Marques *et al.*, 2003; Quigley *et al.*, 1981). However, the changes that occur during rodent experimental glaucoma have not been explored at this level of detail. This information would enhance the knowledge of the degeneration process during ocular hypertension.

Axonal degeneration is known to enhance the accumulation of silver ions. Silver staining methods have been relied upon in the study of nervous system anatomy and pathology for some time (Grimelius, 2004). Silver staining has not been investigated for the assay of glaucomatous neurodegeneration, and may prove to be a novel, practical and accurate method for assessing neuronal degeneration.

Initial degeneration of the RGC axon spreads retrogradely to the soma, possibly, through loss of neurotrophic support amongst other factors. Subsequently, RGC bodies die mainly through the process of apoptosis and rarely via necrosis (Garcia-Valenzuela *et al.*, 1995) at a rate of around 4% per week (Laquis *et al.*, 1998).

A popular method for quantifying RGC apoptotic death is cell counts of TUNEL positivity in the retinal RGC layer, reinforced with detection of apoptosis-associated enzymes such as active caspase 3. However, these studies are limited by the transient nature of apoptosis and restriction to the RGC body in the retina. Consequently the quantification of axonal degeneration, together with that of RGC apoptosis counts, may be more reliable.

In this chapter, morphological aspects of the normal and glaucoma optic nerve will be examined from a superficial histological level, through to the high-resolution electron microscopy level. Rat optic nerve head morphology will be compared to that of the human. New techniques for quantitative and qualitative assessment of

neurodegeneration will be developed and compared with existing standards. The effects of IOP elevation on cell death and degeneration will be investigated.

4.2 Methods

Various methods were used to compare optic nerve structure and illustrate glaucomatous cell death and neurodegeneration. These included some novel techniques as well as established methods.

Normotensive human (n=2) and rat eyes (n=6) were compared histologically for similarities. See Chapter II, Section 2.2 for the histological methods, including haemotoxylin and eosin, Masson's trichrome green, and toluidine blue staining, developed and used during this chapter.

Following the induction of unilateral experimental ocular hypertension, contralateral control (n=6) and ipsilateral hypertensive rat eyes (n=6) were also compared using the histological techniques described above in order to show glaucomatous degeneneration of the optic nerve at various levels of pressure elevation.

Details of all techniques used to detect neurodegeneration can be found in Chapter II, Sections 2.3, 2.4 and 2.5. These included electron and light microscopy, used to investigate nerve fibre loss in retrobulbar optic nerve samples (n=5). Silver staining was used to detect degenerating neurons in the retrobulbar nerve by virtue of the agrophillic propensity of degenerating nerves. Two samples were taken from each group of duration of IOP elevation (T1 to T5, n=10). TUJ-1 immunofluorescence labelling of neurofilament protein in the retinal ganglion cell layer of the retina was also used to detect neurodegeneration (n=3) during intermediate durations of ocular hypertension (T3).

Cell death was detected using TUNEL positivity and immunolabelling for active caspase 3, as described in Chapter II, Section 2.6. These methods were used to label the apoptosing retinal ganglion cell body in the retina (n=25), as well as any glial cell

death occurring in the optic nerve head (n=5). Retinae used were representative of the 15 different groups of IOP elevation created by dividing the retinae depending on duration of IOP elevation (T1 to T5), area under the IOP curve (A1 to A5), and standard deviation of IOP elevation (S1 to S5). The number of TUNEL positive cells per retina were counted twice each in a total of 5 pairs (contralateral control and ipsilateral hypertensive) of retinae per group and groups compared using ANOVA followed by T-testing. Consequently, RGC degeneration as a function of IOP variables (T, A and S) were monitored to assess the effect of IOP on optic nerve degeneration over time.

Table 4.1 Experimental animal groupings according to pressure elevations

Level	**GROUP "T"** Duration of IOP elevation (days)	**GROUP "A"** Area under the pressure curve (mmHg)	**GROUP "S"** Standard deviation
1	**1 – 7** (n=10)	**0.9 – 22.7** (n=8)	**0 - 1.511** (n=6)
2	**11 – 19** (n=19)	**24.3 – 96.8** (n=16)	**1.52 - 2.96** (n=13)
3	**20 - 27** (n=11)	**97.2 – 151.1** (n=15)	**3.20 - 3.75** (n=9)
4	**33 – 46** (n=10)	**165.3 – 256.1** (n=8)	**3.81 - 5.57** (n=16)
5	**47 - 65** (n=7)	**271.9 – 469.3** (n=10)	**6.02 - 12.76** (n=12)

4.2 Results

4.2.1 Histology of the human and rat optic nerves

4.2.1.1 Histology of the human optic nerve

Human optic nerve histology was similar to that described in the literature (Figure 4.1 and 4.2). As the RGC axons leave the retina they become grouped into nerve fascicles, separated by cells, in the prelaminar region. At this level the optic nerve nerve head is narrow. Connective tissue elements first appear in the underlying lamina

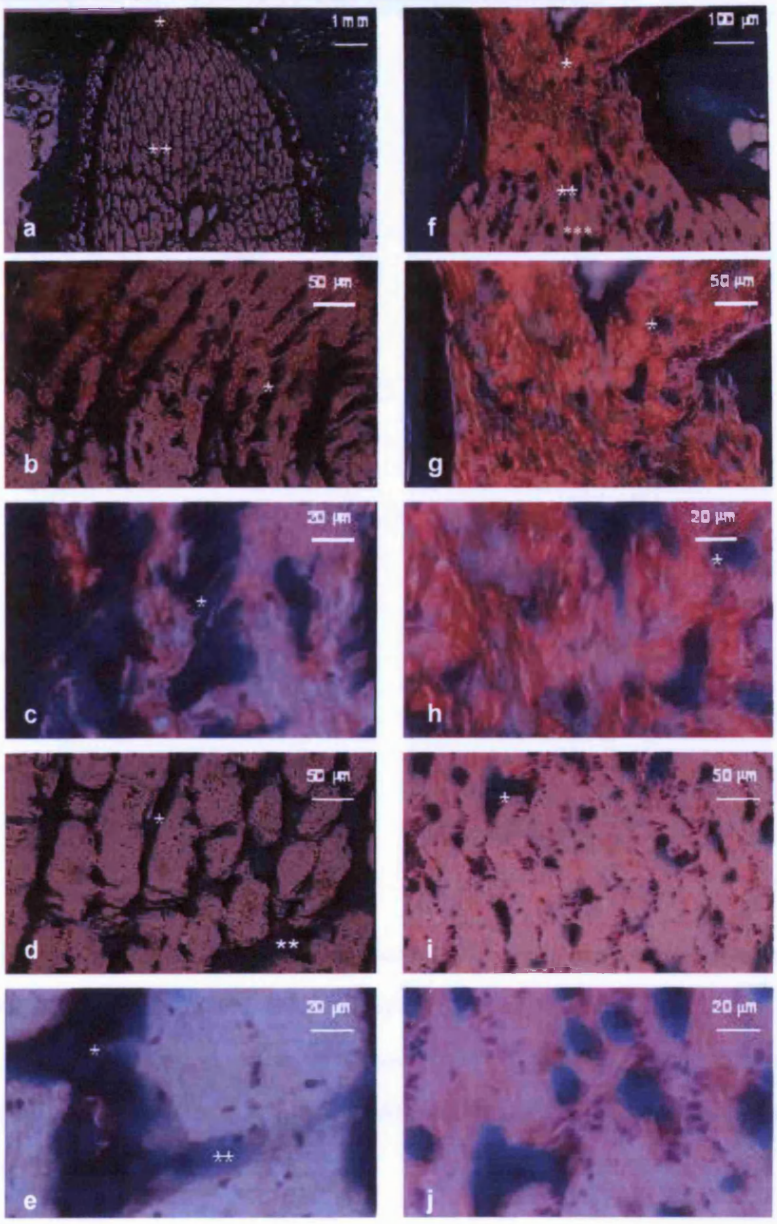

Figure 4.1 Histology of the normal human and rat optic nerve in longitudinal section *Images show Masson's trichrome green staining of the normotensive human (a-e) and rat (f- j) optic nerve. Areas of green staining represent connective tissue elements. Cytoplasmic elements are stained pink, while cell nuclei are blue-black. Low magnification longitudinal images (a-e) show details of structure from the nerve head to the retrobulbar or postlaminar optic nerve. The human optic nerve head and lamina cribrosa are shown at higher magnifications in images b and c, with the equivalent areas for the rat in g and h. The postlaminar human optic nerve is shown at higher magnification in images d and e, and the rat retrobulbar optic nerve in images i and j. *, **, *** denote areas discussed in text.*

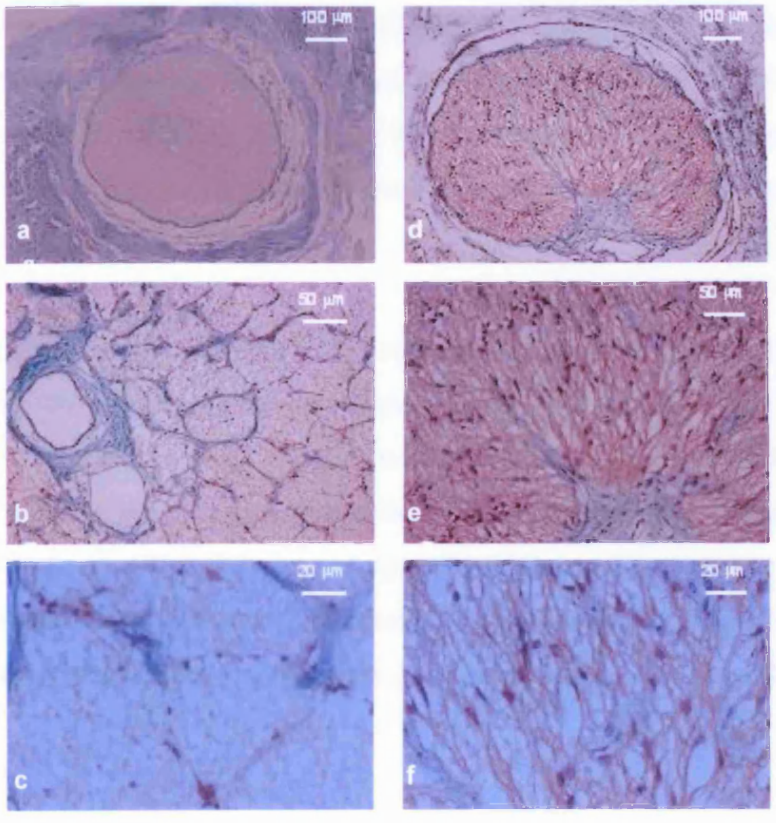

Figure 4.2 Histology of the normal human and rat optic nerve in transverse section *Masson's trichrome green stained images of the normotensive human (a-c) and rat (d-f) optic nerve in transverse section are shown. Colours represent tissue components as described for Figure 4.1. Magnification increases from images a-d for the human nerve, and d- f for the rat.*

cribrosa at the level of the sclera (Figure 4.1 a, *). Then in the postlaminar region, the nerve diameter widens into the optic nerve proper (Figure 4.1 a, **).

Connective tissue beams were found throughout the human optic nerve (Figure 4.1 a to e, * and **). These elements have a dense well-organised horizontal distribution at the nerve head (Figure 4.1 a, b and c). Beams were interspersed with pores containing axons fascicles. A few cell nuclei were detectable within the nerve head fascicles (Figure 4.1 b and c), but were packed around the collagenous beams (Figure 4.1 c). Connective tissue elements were also present throughout the optic nerve proper (Figure 4.1 a, d and e). These elements stained less intensely than those of the lamina cribrosa, and were not of uniform organisation or orientation. Vertical septae were

joined occasionally by horizontal septae (Figure 4.1 d and e, **), the latter occuring with more frequency along the course of the nerve (Figure 4.1 d and e, *). More nuclei were visible than in the nerve head, localised around connective tissue elements (Figure 4.1 d), with some dispersed among the nerve fibre bundles (Figure 4.1 e).

The human optic nerve was round in cross section and surrounded by connective tissue sheaths (the meningeal sheaths, Figure 4.2 a). The central retinal vessels were surrounded by connective tissue sheaths in the optic nerve head. Nerve fibre fascicles were surrounded by green connective tissue in transverse section of the optic nerve (Figure 4.2 b and c). Glial nuclei were again proximal to these columns. Transverse sections revealed some glia that appeared to be separating the nerve into fascicles independently of connective tissue. Other glial nuclei were observed within the nerve bundle.

4.2.1.2 Histology of the rat optic nerve

In comparison with the human, the rat optic nerve reveals a much simpler structure overall. The rat optic nerve begins at the narrow optic nerve head (Figure 4.1 f, Figure 4.3 a and f, *), followed by a slightly wider transition zone (Figures 4.1 f, **), which widens further into the retrobulbar nerve (Figure 4.1 f, ***).

The connective tissue beams of the human lamina cribrosa were replaced in the rat by sparse connective tissue islands with horizontally orientated septa. Septae were located throughout the nerve head and transition zone (Figure 4.1 h and i, *). Optic nerve head connective tissue stained less densely. Transition zone septae appeared more densely stained and fewer in number. The rat nerve head and transition zone appeared to contain less connective tissue with opposite orientation than the human equivalents. Similar to the human, this connective tissue is surrounded by few glial nuclei (Figure 4.1 h and i, 4.3 a, b, c, f, g and h), between which, the nerve axons appeared in fascicles (Figure 4.1 h and i, Figure 4.3 b, c, g and h).

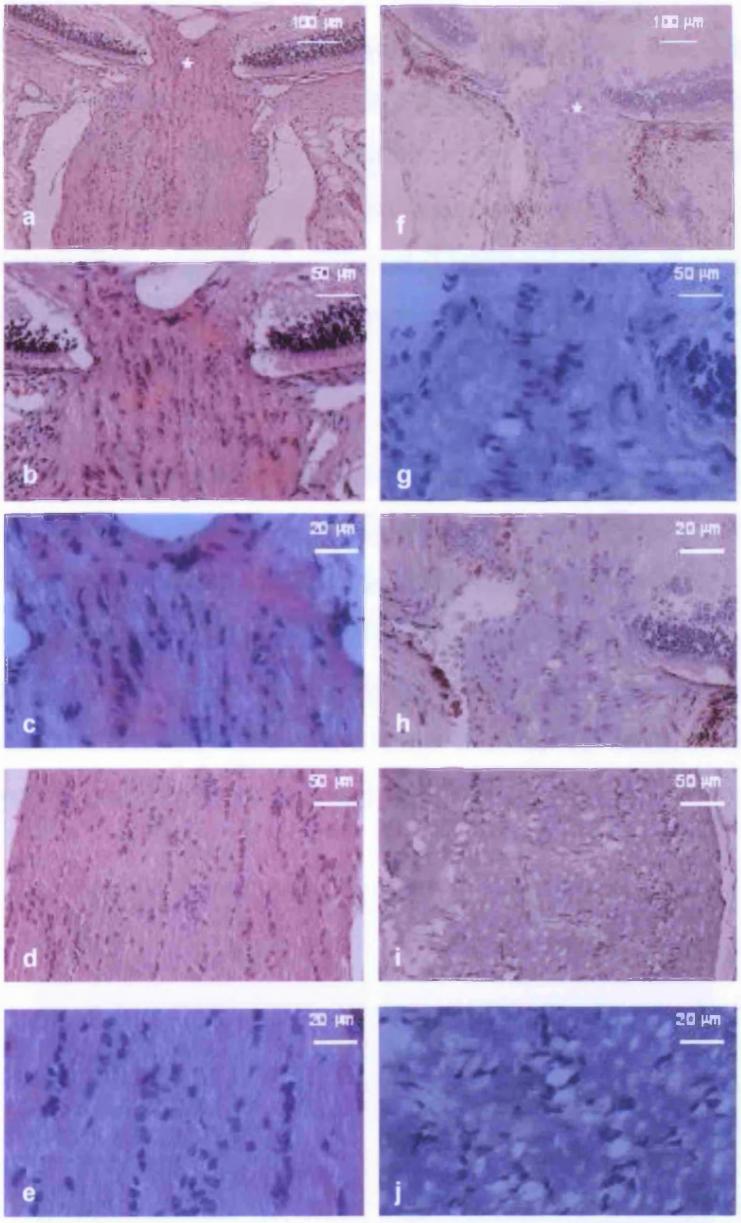

Figure 4.3 Haematoxylin & Eosin and Toluidine blue stained normal rat optic nerve in longitudinal section *Longitudinal rat optic nerve sections were stained with haematoxylin and eosin to produce images a-e. Nuclei were stained blue-black, and all other tissue elements were stained pink by this method. Images f-j are the equivalent sections stained with toluidine blue. In f to j nuclei are stained blue. Images a- e and f- j show from the optic nerve head through to the retrobulbar optic nerve. Images b, c, g and h show the nerve head in more detail. The retrobulbar optic nerve is shown in more detail in images d, e, i and j.*

The connective tissue of the rat retrobulbar optic nerve is also less, compared to the postlaminar human optic nerve (Figure 4.1 f, g and h, *). Retrobulbar connective tissue elements appear to maintain the orientation of those in the transition zone (Figure 4.1 i * and j,). Compared to the human optic nerve there were far more glial nuclei in the retrobulbar optic nerve of the rat (Figure 4.1 i and j, Figure 4.3 d, e, i and j). These nuclei form glial columns, which are more prominent than connective tissue in this area of the nerve (Figure 4.1 i).

The rat optic nerve proper appeared horizontally oval in transverse section (Figure 4.1 n, Figure 4.4 a and d), in contrast to the human nerve. Meningeal sheaths surrounded the rat nerve. The nerve fibres and glial nuclei did not appear organised into or around regularly arranged fascicles when viewed in cross section (Figure 4.2 a-f), Figure 4.4 a-f). The central retinal vessels of the rat optic nerve were not clearly identifiable. However transverse sections contained a large element of connective tissue in the central inferior portion (Figure 4.2 d and e) likely to mark the equivalent of these vessels.

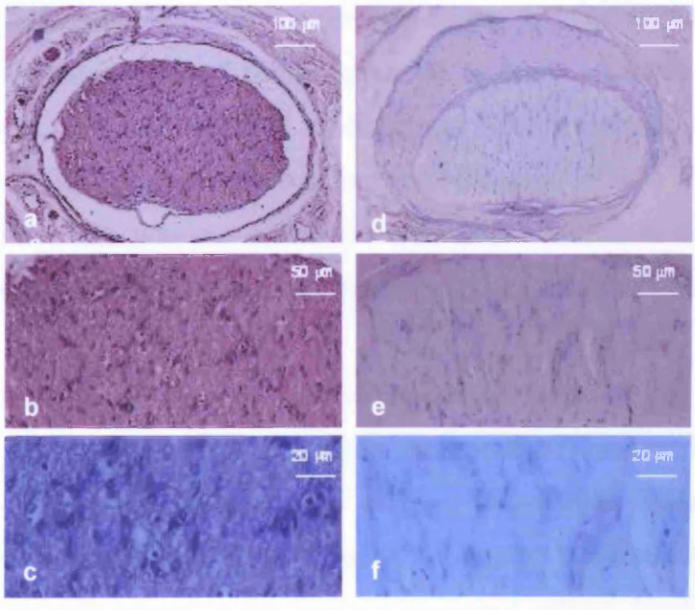

Figure 4.4 Haematoxylin & Eosin and Toluidine blue stained normal rat optic nerve in transverse section *Transverse sections of optic nerve are shown at increasing levels of detail following haematoxylin and eosin staining in images a to c, and for toluidine blue staining in images d to f. Colours represent tissues as described in Figure 4.3.*

4.2.2 Histological alteration of the optic nerve following glaucoma

The rat optic nerve following ocular hypertension is shown in Figures 4.5a-j. The nerve shown is of T5 pressure duration. The most notable alteration in the nerve was excessive retrograde bowing of the nerve head (Figures 4.5a, d and g, *) to produce a large physiological cup. The entire optic nerve head region was retrogradely displaced. The optic cup extended to the transition zone and terminated were the nerve widens. The retrobulbar nerve appeared much wider than controls perhaps through retrodisplacement of nerve tissue rather than fibre myelination.

Islands of connective tissue were sparse in the hypertensive optic nerve. Very few lightly stained beams of connective tissue with no detectable organisation can be observed in Figure 5.4b. No retrobulbar connective tissue was identified following glaucoma (Figure 4.5c). Connective tissue appeared to decrease throughout the optic nerve following experimental glaucoma.

Staining of cytoplasmic elements, including nerve fasicles appeared less dense following hypertension. Loss of tissue appeared as large vacuoles or holes in the nerve. These holes were mostly round in shape and were prominent in the nerve head becoming less evident in retrobulbar regions (Figures 4.5a-i) with no regular arrangement. Tissue loss was not associated with glial columns or connective tissue, but was preferentially located in the optic nerve head or transition zone.

The nuclear elements of the optic nerve appeared to have lost their columnar organisation at the nerve head and transition zone probably due to retrodisplacement of nerve tissue (Figures 4.5a, b, d, e, f and g). Retrobulbar nuclei retained their columnar organisation (Figures 4.5c, f and i). However, these columns were not as uniform or parallel in arrangement as those of control nerves. Nuclei also appeared enlarged, indicating aggregation of cells, or glial hypertrophy.

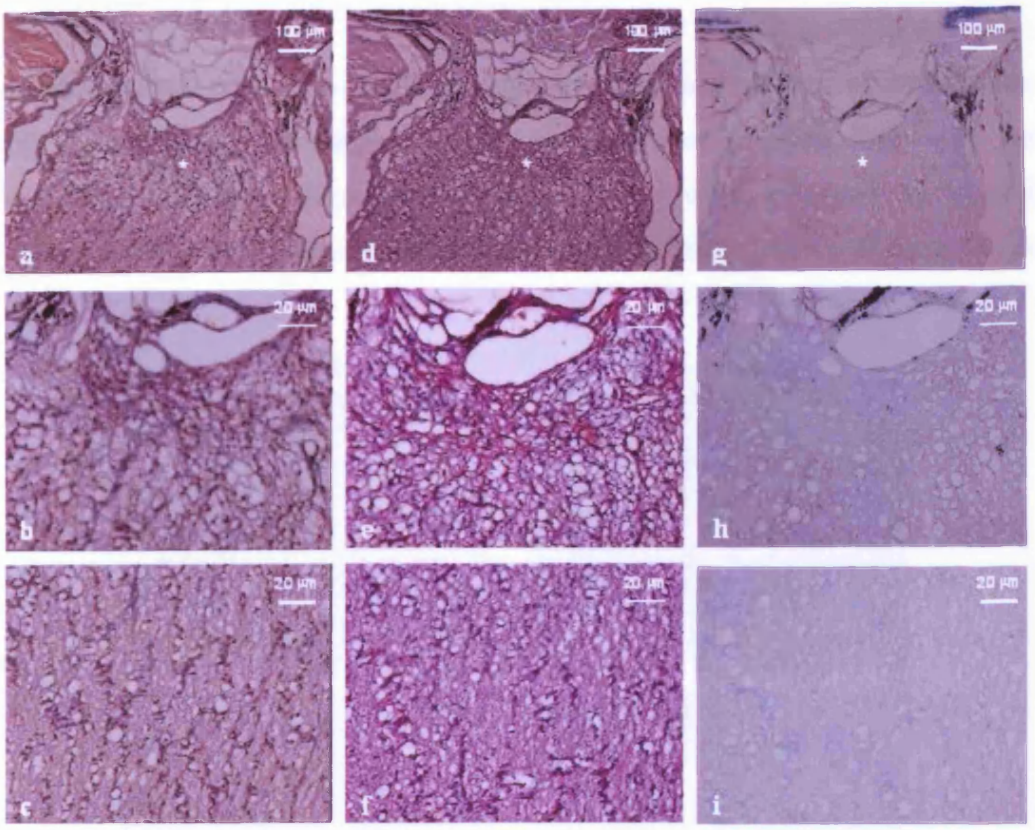

Figure 4.5 ***Ocular hypertensive rat optic nerve histology*** *Longitudinal sections of the rat optic nerve were stained with Masson's trichrome green (a-c), haematoxylin and eosin (d-f) and toluidine blue (g-i) following experimental glaucoma. Images a, f and k show the optic nerve head and retrobulbar regions following glaucoma. The optic nerve head is shown at higher magnifications for the three stains in image b (Masson's trichrome green), e (haematoxylin and eosin) and g (toluidine blue). Higher magnification retrobulbar optic nerve is shown in images c (Masson's trichrome green) f (haematoxylin and eosin) and i (toluidine blue). * denotes retrograding bowing of the optic nerve head.*

Many important alterations induced by IOP elevation were observed by simple optic nerve histology. Alterations in connective tissue, nerve fibre density, and nuclear elements as well as the shape of the optic nerve head were observed.

4.2.3 Semi-thin sections of the rat optic nerve

Untreated control eyes and dissected retrobulbar optic nerves, fixed post-dissection in 2.5% glutaraldehyde overnight at 4°C, revealed normal retrobulbar optic nerve morphology. Minimal degenerative characteristics were observed by semi-thin sectioning, followed by toluidine blue staining and light microscopy (Figure 4.6 a and b).

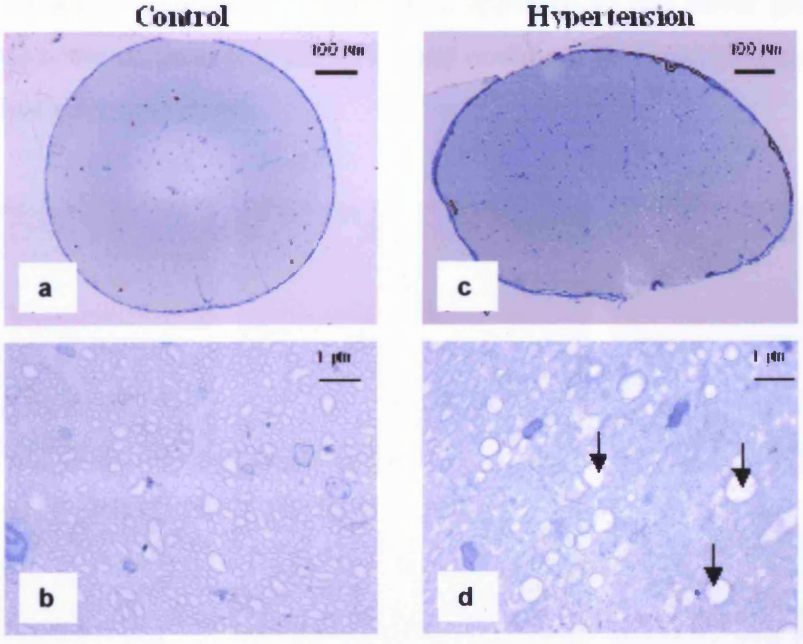

Figure 4.6 Toluidine blue stained semi-thin sections of rat retrobulbar optic nerves *following a mild degree of pressure elevation over a relatively short period of time. Control images (a and b) show a normal optic nerve morphology, while images following hypertension (c and d) contain alterations typical of neurodegeneration. This includes the appearance of vacuoles in the optic nerve (d, arrows). Dark patches of staining indicate macroglia, most likely to be oligodendrocyte cell bodies (b and d).*

The quality of sectioning was superior to thick sections, cut for histological processing, resulting in the observation of very clear differences in contralaral control and ipsilateral hypertensive retrobulbar optic nerve.

Normal nerves were structurally dense with few irregular shaped vesicles (Figures 4.6a and b). Oligodendrocytes were identifiable throughout the nerve. Ocular

hypertension reduced nerve density, and predominantly rounded vesicles appeared increased in number and size (Figures 4.6c and d). Glial elements were as described for control nerve.

4.2.4 Silver staining of optic nerve axon neurodegeneration

Silver staining of control retrobulbar optic nerve did not produce any detectable indication of neurodegeneration. Background appeared as tiny silver grains, even in control optic nerve sections (Figure 4.7a), and could not be removed due to the use of electrostatically charged slides.

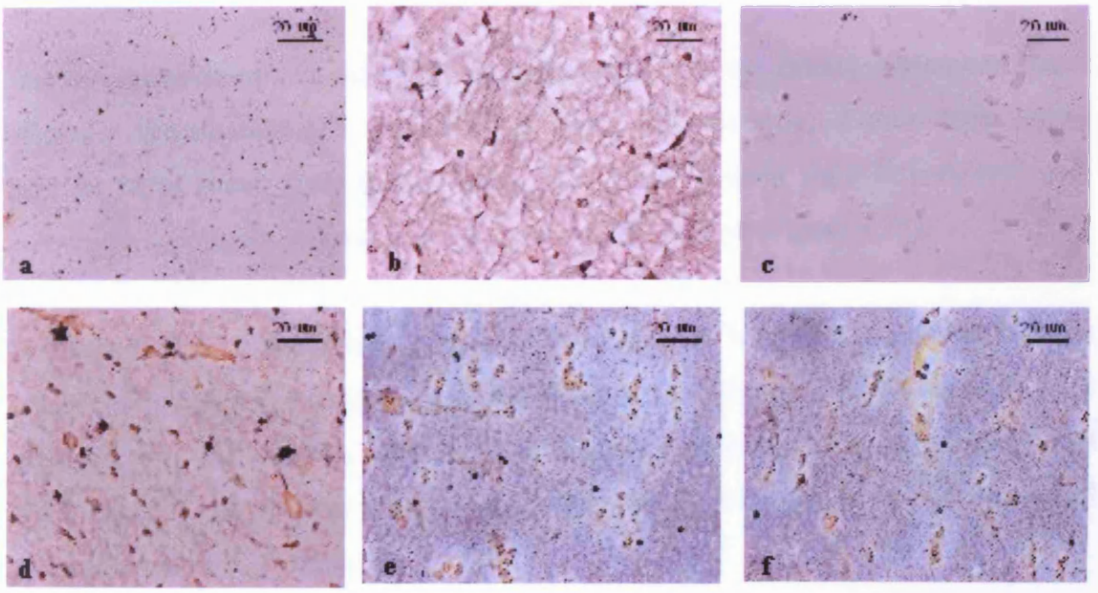

Figure 4.7 Silver staining of rat optic nerve *Control retrobulbar optic nerve revealed no signs of neurodegeneration (a). As duration of hypertension increased through images b to f, (T1-T5), signs of neurodegeneration also became greater. Dark brown silver aggregates were first visible (b). These were then replaced by more diffuse aggregates (c). Dark brown aggregates were again visible in d with a less ramified morphology, together with gold coloured patches. In images e and f dark brown aggregates were replaced by discrete black aggregates, while gold-coloured patches were still evident.*

Initially, at short durations of hypertension (3 days, T1, Figure 4.7b) silver labelling of degenerating axons was detectable using light microscopy. Accumulation of silver grains appeared as discrete dark brown patches within the optic nerve. Staining appeared as rounded areas, as well as more elongated shapes (Figure 4.7b).

Following 14 days (T2, Figure 4.7c) of ocular hypertension, silver labelling did not identify neurodegeneration as clearly as in earlier time points. Silver accumulation appeared discrete, but not as dense due to the lighter colour of labelling (Figure 4.7c). This indicated that following an initial wave of neurodegeneration and axonal damage, there was an intermediate period where this damage was alleviated or delayed. Damage was barely detectable at the 14 day time point.

The accumulation of dark silver grains appeared to increase during subsequent stages of ocular hypertension (T3, Figure 4.7d). Many discrete areas of stain were visible here as fairly round dark brown areas. The nerve stained light brown, and gold coloured irregular-shaped patches were present throughout (Figure 4.7d).

In more severe cases of hypertension (T4, Figure 4.7e) silver accumulation was present as rounded black deposits with a reduced size (Figure 4.7). Some fairly large granules were still evident, however, the majority of staining appeared as very small black deposits. These areas were present within the light brown stained nerve, as well as in gold-coloured patches.

A further lean toward this trend for smaller accumulations of silver was seen in staining of T5 (Figure 4.7f) nerves. It was not possible to distinguish by eye whether there was more or less staining between groups T4 and T5.

4.2.5 Electron microscopy of the rat optic nerve

Electron micrographs revealed normal retrobulbar optic nerve morphology including a regular round/oval closely packed axonal arrangement, minimal myelin degeneration and slightly granular ordered cytoplasm (Figures 4.8a-d). Optic nerve

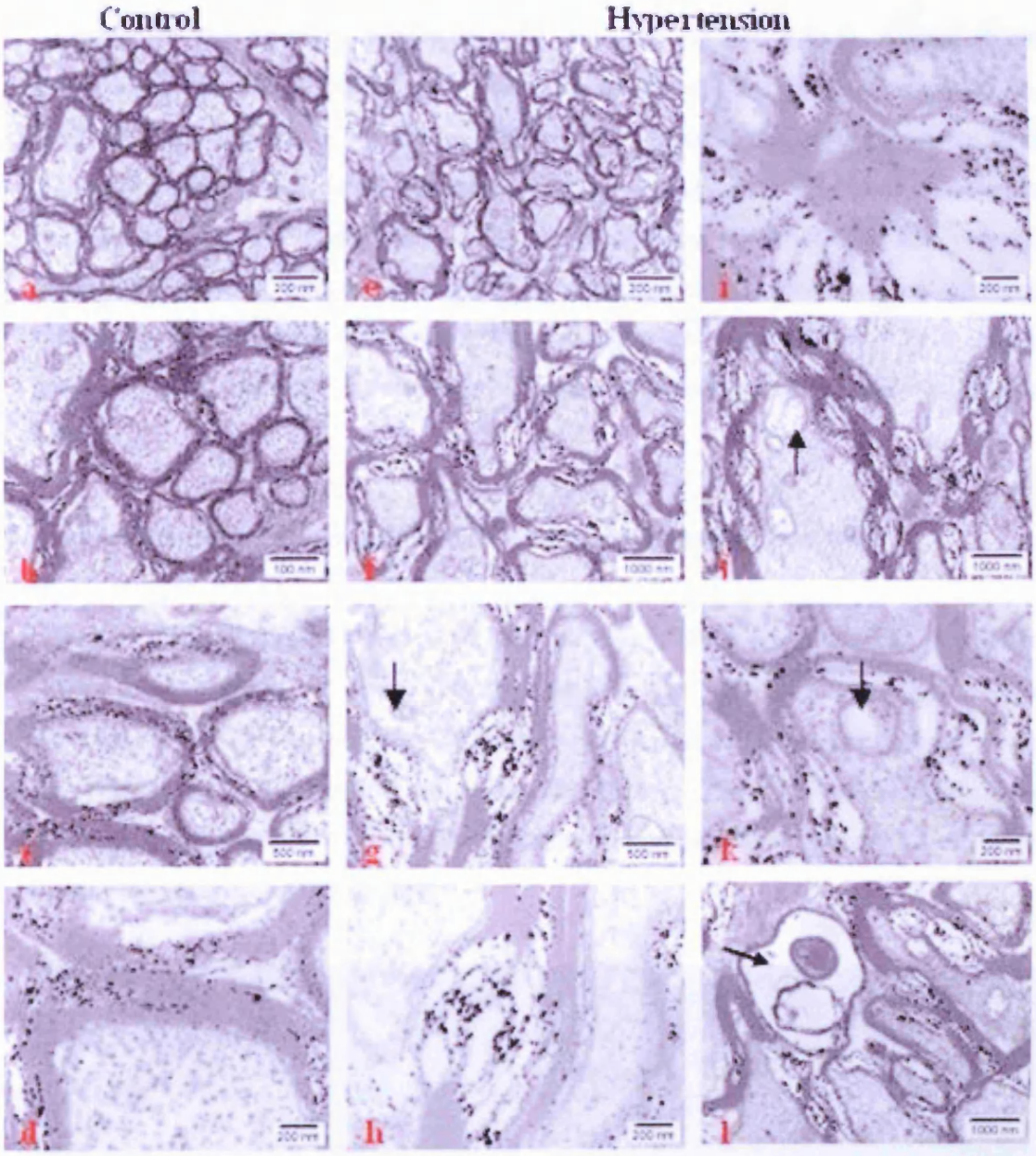

Figure 4.8 Electron micrographs of control and hypertensive retrobulbar optic nerves *High magnification electron microscopy shows the effect of IOP on the retrobulbar optic nerve. The control optic nerve (a to d) showed normal morphology, whereas the hypertensive optic nerve (e to l) showed signs of degeneration. Major morphological changes included irregular axonal arrangement (e and f), organelle accumulation (g, arrow), damaged myelin sheaths and debris (h and i), large intracellular vesicles (j and k, arrows), and watery degeneration (l, arrow).*

degeneration was revealed following IOP elevation (Figure 4.8e-l). Axonal shape altered to an appearance typical of "watery" degeneration (described by Narciso *et al.*, 2001; Marques *et al.*, 2003; Sefton and Lam, 1984), cytoplasmic shrinkage away from the myelin sheath, as well as inclusion of large intracellular vesicles were evident. Dark cytoplasmic inclusions likely to be organelle accumulations were also present. Myelin damage and fragmented debris were widespread, evident as dark granules throughout the sheath as well as an "unravelled" appearance (Figure 4.8e-l). Some axons appeared qualitatively enlarged (Figure 4.8j) compared to controls (Figure 4.8b).

4.2.6 Alterations in neurofilaments following experimental glaucoma

Neuronal class III β-tubulin (TUJ-1) was present in the retinal ganglion cell layer (GCL) of the normal rat retina (Figure 4.9a). Bright red labelling of RGCs was observed. These cells appeared to be fairly dendritic and were regularly spaced along the GCL. A few TUJ-1 positive cells were also found in the other retinal layers. This is likely to be due to cross-reactivity with neurofilament components of other neuronal or glial cells in these layers.

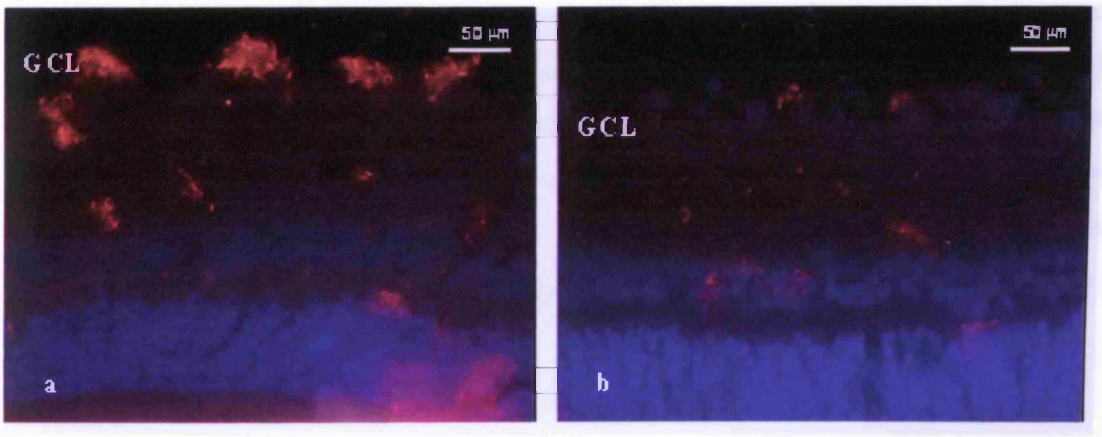

Figure 4.9 TUJ-1 immunolabelling of the retinal ganglion cell layer *(a) Red TUJ-1 immunolabelling appeared mainly to be localised to the retinal ganglion cell layer (GCL). Some TUJ-1 positivity was observed in other layers. (b) TUJ-1 immunoreactivity was reduced following experimental ocular hypertension. Blue labelling denotes Hoechst stained nuclei.*

Following hypertension, the intensity of TUJ-1 labelling appeared to be reduced (Figure 4.9b). Fewer cells were labelled in the GCL, with less intense labelling also in the other retinal layers. TUJ-1 labelled cells were irregularly spaced and occurred less frequently. TUJ-1 positive RGCs also appeared less dendritic following ocular hypertension.

4.2.7 Retinal ganglion cell apoptosis

Labelling of apoptotic RGC bodies in the retina increased following hypertension (Figure 4.10c-e). Qualitative observations of active Caspase 3 immunoreactivity revealed similar results (Figure 4.11c-e).

In the control retinae (Figure 4.10c and Figure 4.11b) and retrobulbar optic nerve sections (Figure 4.10f and Figure 4.11a), no TUNEL or active caspase 3 immunoreactivity was observed. Results of TUNEL positive RGC counts are detailed in the following sections in relation to ocular hypertension (see Chapter III, Figure 3.9 for details of IOP groups).

Overall significant elevations in superior, inferior and total number of apoptotic RGCs ($P<0.001$, $n=25$) were found following hypertension. The mean percentage of apoptotic RGCs following hypertension was 3.47%, while control levels were 0.70% ($n=25$). Similar apoptotic percentages were found between superior and inferior retinal portions ($n=25$). Mean superior apoptosis was 3.25%, while inferior was 3.70% following hypertension. The equivalent control values were 0.85% (superior) and 0.70% (inferior).

4.2.7.1 The effects of duration of pressure elevation on RGC apoptosis

Figure 4.12 shows how duration of hypertension affects retinal TUNEL positivity. Low durations of hypertension (T1) did not significantly elevate RGC apoptosis ($P>0.05$). T1 apoptosis was slightly increased in superior (1.46%), inferior (2.62%) and overall retina (2.04%) as compared to controls.

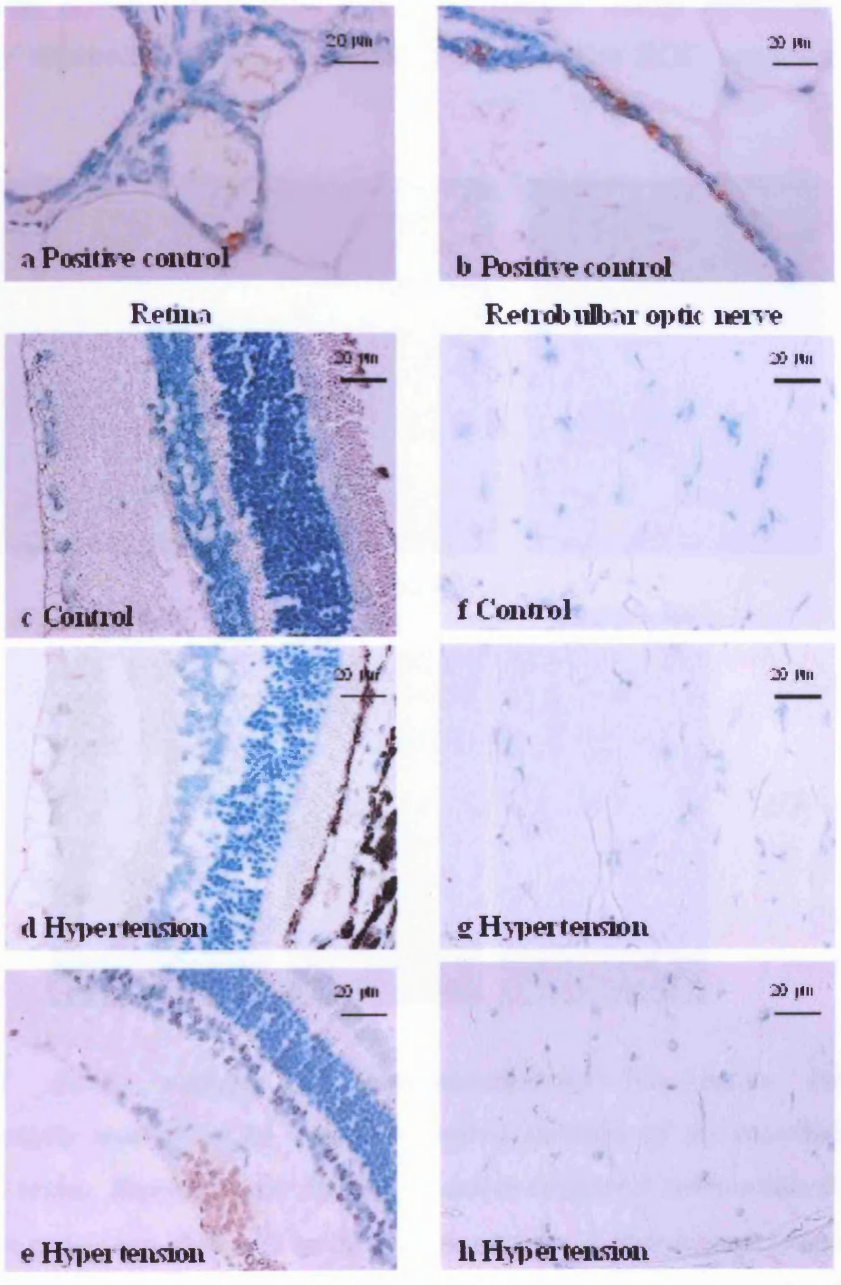

Figure 4.10 TUNEL staining in the rat retina and optic nerve *TUNEL positivity is shown as brown-stained areas in the retina, nuclei were counterstained using methyl green (n=25). Images a and b show positive control (rat mammary gland) with clear brown TUNEL positive cells. Negative controls of contralateral retina (c) infrequently contained TUNEL positive cells, while retrobulbar optic nerve sections (f-h) did not show any TUNEL positivity (c). At relatively short durations of hypertension few TUNEL positive cells were present in the RGC layer (d). Longer durations resulted in an elevation of TUNEL positivity (e).*

Significant elevation of apoptosis was initiated at T2 durations of hypertension in the inferior retina ($P<0.05$) at a rate of 2.06%. Overall retinal apoptosis was also significantly elevated ($P<0.05$) at 1.89%, while superior RGC apoptosis was not ($P>0.05$).

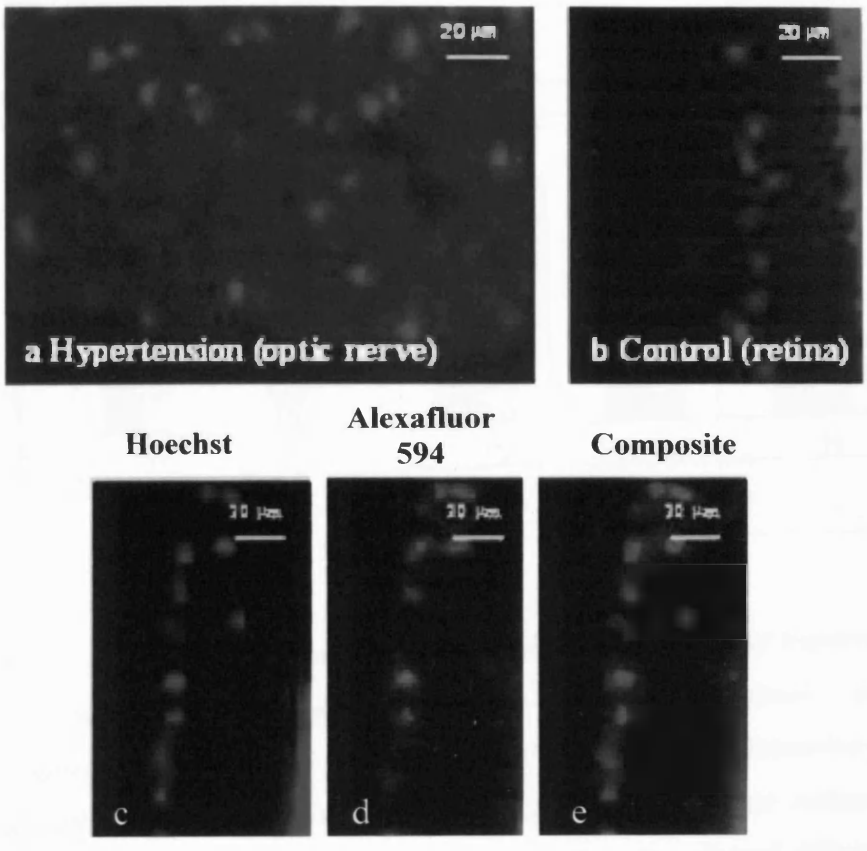

Figure 4.11 Active caspase 3 immunoreactivity *No active caspase 3 immunoreactivity was found in negative control sections of (a) retrobulbar optic nerve or (b) retina. Representative images of active caspase 3 immunoreactivity in the hypertensive retina are shown (c to d). Active caspase 3 immunoreactivity appeared as discrete red nuclear labelling in the ganglion cell layer (d), that colocalised with Hoechst stained blue nuclear labelling (e).These images confirmed retinal ganglion cell death via apoptosis following ocular hypertension.*

Significant elevations extended to both superior and inferior retinal axes, as well as in the overall retina, in longer duration groups T3 and T4 ($P<0.05$). Apoptotic rates for T3 durations were 5.29%, 5.47% and 5.38% for the superior, inferior and overall retina respectively. T4 values were slightly reduced at 3.38%, 5.56% and 4.47%

respectively. The slightly higher apoptotic rates in the inferior retinal portion were not significant for T3 or T4 ($P>0.05$). Following the longest durations of ocular hypertension (T5), a more diffuse significant level of apoptosis at 1.46% was found throughout the ipsilateral retina ($P<0.05$), while neither superior ($P>0.1$) nor inferior ($P>0.05$) axes appeared to be specifically affected.

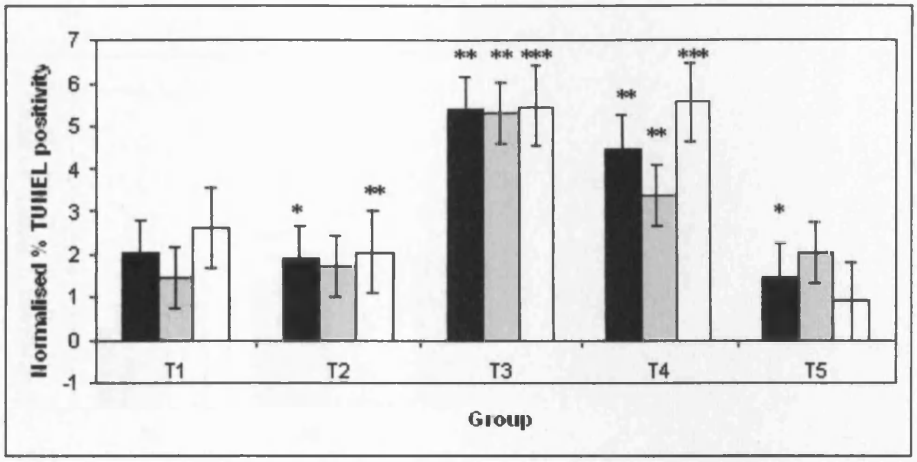

Figure 4.12 RGC TUNEL positivity as a function of duration of hypertension.
*% TUNEL positivity increased in all ocular hypertensive retinae, compared to normal controls. The difference between control and ocular hypertensive percentage apoptotic cells is shown for the retina overall (black), superior retina (grey and inferior retina (white). TUNEL positivity significantly altered between groups ($p<0.01$, ANOVA testing) and significantly increased for groups T2, T3 and T4 (T-testing, $n=25$). Bars show standard deviation. */**/*** indicate increasing levels of significance.*

4.2.7.2 RGC apoptosis with area under the IOP curve

RGC apoptosis appeared to consistently increase with area under the pressure curve (A), (Figure 4.13). For group A1, diffuse (not localised to a particular area of retina) RGC death was indicated through significant elevation ($P<0.05$) of overall RGC apoptosis by 1.71%. In A2, significant elevation of superior ($P<0.05$), inferior ($P<0.05$) and overall retinal ($P<0.001$) apoptosis to 2.29%, 3.27% and 2.78% respectively resulted. Apoptosis significantly increased in A3 retinae overall

(P<0.001) at 3.27%, as well as in inferior regions (P<0.05) at 3.45%. Overall RGC apoptosis significantly increased to 3.75% by A4 (P<0.05), this was localised to the inferior retina (P<0.01). In highest area under the pressure curve group (A5), RGC apoptosis elevated to 4.65% in the overall retina (P<0.001). Superior and inferior axes were also significantly affected with increases of 3.75% and 5.56% respectively (P<0.01).

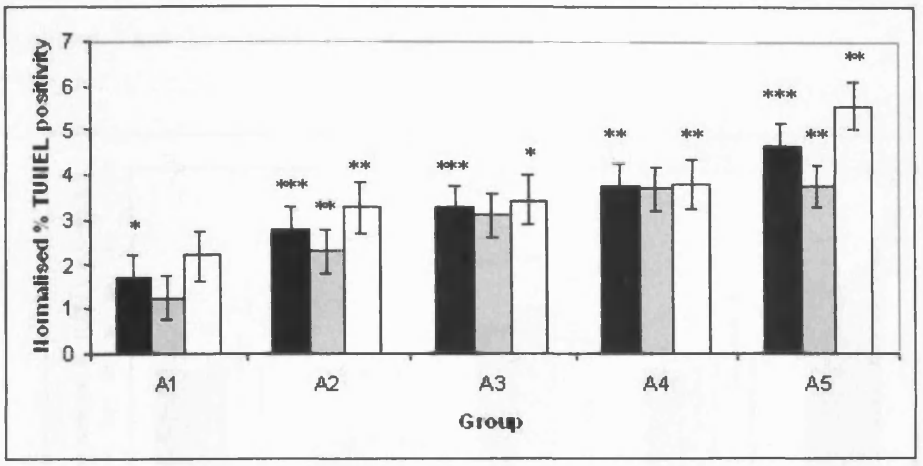

Figure 4.13 RGC TUNEL positivity as a function of area under IOP curve.

*% TUNEL positivity increased with increasing area under the IOP curve in groups A1 to A5 (n=25) these changes were significantly different according to ANOVA testing (p<0.01). Normalised percentage apoptotic RGCs following hypertension are shown for the retina overall (black), superior retina (grey and inferior retina (white). Increasing levels of significance according to T-testing (p<0.05, p<0.01, p<0.001) are indicated by *, ** and ***.*

4.2.7.3 RGC apoptosis with standard deviation of IOP elevation

Pressure elevation resulted in increased RGC apoptosis in the overall retina in all groups of standard deviation. Elevation of apoptosis was very significant for groups S1 to S4 (P<0.001) with a slight reduction in S5 (P<0.05). Percentage apoptosis fluctuated with increasing standard deviation from between 1.48% to 5.28%.

Even at low levels of standard deviation of pressure elevation (S1) significant increase of apoptosis was found in the superior (3.11% $P<0.05$) and inferior (3.20% $P<0.01$) retina. Apoptotic rates significantly increased to 1.51% and 1.45% in superior and inferior S2 retina ($P<0.05$). These rates significantly increased further to 4.57% and 3.91% in S3 ($P<0.05$). S4 conditions significantly elevated the number of apoptotic RGCs in inferior ($P<0.05$) retina by 3.59%. Under S5 conditions significant elevation of inferior and superior RGC apoptosis was found ($P<0.05$) at 4.20% and 6.36%. These changes are shown in Figure 4.14.

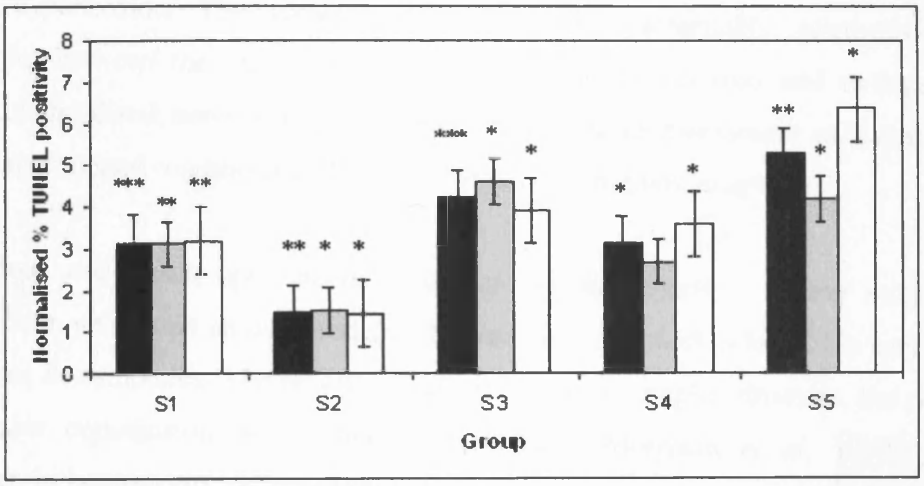

Figure 4.14 RGC TUNEL positivity as a function of standard deviation of IOP. *The effect of increasing standard deviation of pressure elevation throughout groups S1 to S5 (n=25) are shown on RGC apoptosis in the retina overall (black), superior retina (grey) and inferior retina (white). The difference in % TUNEL positivity in all ipsilateral hypertensive retinae as compared to contralateral controls was plotted. Overall TUNEL positivity significantly increased for all groups of standard deviation of pressure elevation ($p<0.05$, ANOVA). * ($p<0.05$), ** ($p<0.01$) and ***($p<0.001$) denote increasing levels of statistical according to T-testing.*

4.4 Discussion

The detection of neurodegeneration and changes in optic nerve structure are a vital indication of both experimental glaucoma and the human disease. Excessive optic cup

excavation, as well RGC axonal loss, is crucial in the detection of clinical glaucoma. Optic nerve head alterations can contribute to degeneration of the retinal RGC body and axon in the optic nerve. Many new exciting techniques, in addition to more tried and tested methods, are available for the detection of neurodegeneration.

4.4.1 Histology of the normal optic nerve

General histology of the rat and human optic nerves demonstrated the structural features and organisation of the nerves as well as alterations following experimental ocular hypertension. The presence of cell nuclei, presumably microglial and astrocytic, between the cribriform layers of the lamina cribrosa and collagenous beams in the distal nerve was particularly important, as assessment of these cells under experimental conditions will be determined out in future chapters.

The human and rodent optic nerve head were found to have a similar structural organisation, vital in an animal model of human disease, which affects this very area to produce its symptoms. The rat optic nerve has a much simpler structure, but of the same basic organisation as the human equivalent (Morrison *et al*, 1997). The difference in lamina cribrosa structure between species should be taken into account when relating experimental glaucoma to the human equivalent. The less pronounced connective tissue organisation of the rodent optic nerve head is important in experimental glaucoma studies. Increased ocular tension can result in pressure-dependent glaucoma whereby laminar beams are weakened through genetic mutation or disease (Gonzalez *et al*, 2000). The rat optic nerve head inherently contains less structural support, but may be more suited to studies of this type of human disease than other animal models that do not have a lamina cribrosa, as this tissue plays such a crucial role in protecting the human optic nerve from pressure within the eye.

The rat optic nerve head compares more favourably to the human, in terms of morphology, than the murine optic nerve. Some glaucoma models use the murine eye in which to develop disease despite a complete absence of lamina cribrosa in the mouse. Layers of elongated astrocytes and an external ring of collagenous material replace the lamina cribrosa (May and Lutjen-Drecoll, 2002). Therefore essential

alterations in the optic nerve head that arise in glaucoma cannot be investigated in murine models.

Correlation in density and distribution between glial nuclei in the human and rat optic nerve head indicate that these elements may react similarly to ocular hypertension across species. The prominence of glial columns in the rat retrobulbar nerve may indicate that astroglial columns rather than connective tissue beams support this area in the rat. It is not known what effect this may have on initial or chronic nerve damage. Prominent glial columns may also accentuate any glial alterations following hypertension beyond their significance in human glaucoma.

It is important to recognise the limitations of using the rat optic nerve. The structure of the rat optic nerve is far simpler than the primate. However, in terms of connective tissue elements and glial organisation, the rat is far more similar to the human than many other mammals. Other advantages of studying the rat nerve include potentially high animal numbers and a quick tissue turnover, meaning fast generation of many experimental results.

4.4.2 Optic nerve histology in experimental glaucoma

The rat optic nerve head appears to react to IOP elevation with significant retrograde displacement, similar to human glaucoma. However, the lack of connective tissue observed in the rat optic nerve following glaucoma does not correspond with other human or animal data. Speculatively, it more likely that this reduction may have occurred due to phagocytosis or changes in active astrocyte secretion profiles, and may indicate that the severity of induced hypertension was excessive. Histological staining, carried out in this study, to identify structural components of the optic nerve was superficial. Other studies using immunolabelling (Johnson *et al*, 1996), western blotting (Hernandez *et al.*, 2000) and electron microscopy techniques (Quigley *et al.*, 1981; Quigley, Dorman-Pease and Brown, 1991) have closely examined these components in disease (reviewed by Morrison 2005). It is possible that the histological stains used here do not show the dynamic effects of ocular hypertension on structural components of the optic nerve.

Histological loss of axonal material following experimental glaucoma is supported by electron microscopy studies (Quigley and Addicks, 1981). The presence of large pores replacing axoplasmic material is only recorded from post-mortem glaucoma eyes in the most severe disease cases. The time-course of glaucoma is artificially accelerated in experimental animals. Changes that would normally occur over several years are induced to occur over weeks in the laboratory. These pores may therefore indicate that experimental glaucoma induced in this study is representative of only the most severe human conditions, or that the disease is indeed experimentally accelerated.

Temporal alterations following experimental glaucoma can be used to determine how human glaucoma might progress, for example by using the duration of hypertension (T) groups created in this study. T1 is representative of human glaucoma before the onset of symptoms. T2 shows the initial stages of disease when a glaucoma sufferer may begin to loose the peripheral visual field. The condition then progresses from T3 to T5, where chronic glaucoma is represented in the animal model. This indicates that our model may cover the full time-course of disease. However, this hypothesis has severe limitations due to the presence of a porous nerve even at T2 durations of ocular hypertension, indicating a far more advanced disease state than should occur after only 10 days of hypertension. This then raises the question as to the state of a truly chronic rat glaucoma nerve.

We do not know how the rat optic nerve would appear after a more chronic disease situation, perhaps one year of hypertension using our model. However, it is likely that disease would be far more advanced than for a relative time in a human study. This data strongly suggests that correlation of specific time points between experimental and human glaucoma is not practical. However, in examining the initiation and maintenance of a human disease it is necessary to ascribe the human disease stages to the animal equivalent, which is not necessarily exactly the same. Certainly in this study, there would be nothing gained by developing rats with severe ocular hypertension of months duration, as the chronic human disease is represented by T5.

It appears as though in experimental glaucoma, as is common in the human disease, the number of glial nuclei increase. It is not known whether glia are proliferating or migrating in an effort to neuroprotect the axons, or whether this effect is deleterious to the nerve.

Not all optic nerve alterations following experimental glaucoma were as described in the literature. A loss of connective tissue may be important in the overall reaction of the optic nerve to ocular hypertension. Alterations in glia are of particular interest in this study, therefore conservation of their reaction to hypertension between human and rat is essential. Excessive excavation of the optic disc (Rahman *et al*, 2002; Spaeth *et al.*, 2002), a paucity of optic nerve axons (Chauhan *et al.*, 2002; Johnson *et* al., 2000; Levkovitch-Verbin, 2002) and proliferation of glial nuclei (reviewed by Neufeld and Liu, 2003) are widely documented. Axonal or RGC loss is a major attribute of glaucoma and is essential in order to quantify nerve damage in experimental glaucoma.

4.4.3 Neurodegeneration of the RGC axon

Neurodegeneration was identified via optic nerve and axon morphology, as well as the accumulation of silver ions. Ultrastructural studies of nerve morphology were particularly informative with regard to the specifics of degeneration i.e. myelin damage and organelle accumulation. Due to the time consuming nature of electron microscopy and the qualitative nature of morphologically grading damage, new more quantitative measures are required. Silver staining is a useful and reliable technique used extensively throughout neuroscience to identify degeneration. This study showed that silver staining can be used to identify neurodegeneration following glaucoma. Due to the nature of the silver stain (black dots in the tissue), further method development is required to develop an accurate quantitative measure of the degenerating axon count, perhaps through computer assisted counting of stained areas.

In order to detect the extent of neurodegeneration semi-thin sections of optic nerve can be compared for integrity. This idea was introduced in the first automated fibre

counts of axon number in the primate optic nerve (Ogden and Miller, 1966; Potts *et al.*, 1972). Subsequently reliable quantitative optical density measurements of stained optic nerve and qualitative grading scales of axonal damage have been developed. Qualitative comparisons of semi-thin optic nerve sections were used to reveal typical signs of axonal loss following ocular hypertension in the present study. Other similar studies have shown cell shrinkage or selective loss of large diameter axons through reduction in axonal size during early stages of experimental glaucoma (Levkovitch-Verbin *et al.*, 2002).

This type of experiment has been used extensively to ascertain the number of optic nerve fibres in normal experimental animals, and following disease. Levkovitch-Verbin *et al.* (2002) used such a system to show the axon count of Wistar rats at around 87,318 axons. Progressive axonal loss was recorded up to 9 weeks of ocular hypertension, where 51.6% of axons remained. However, axon counts can be prone to sampling errors, are time consuming and require extensive resources. Due to variability in the number of axons counted, other methods may be more informative in quantification of degeneration. In current assessment of experimental glaucoma the arbitrary classification of semi-thin sections on a damage grading scale by masked observers is generally accepted as an accurate method. Alternatively counts of apoptotic RGCs are a more quantitative widely accepted method of assaying damage.

However, studies on the axonal size and distribution, such as those performed by Bennis *et al.* (2001), Levkovitch-Verbin *et* al. (2002), Ogden and Miller (1966) as well as Potts *et al.* (1972[2]) require sampling and quantification techniques similar to axon counts. No other techniques can currently quantify all these aspects of degeneration or compare the extent of axonal loss with changes in axonal size and distribution. However, qualitative assessment of nerve damage via electron microscopy can be useful in determining the attributes and time-course of axonal damage. For example, electron microscopy of the optic nerve has revealed demyelination, axonal swelling, and peripheral immune cell infiltration following experimental optic neuritis (Guy *et al.*, 1992).

Studies of ocular hypertension generated through episcleral vessel sclerosis have shown axonal swelling and myelin debris (Johnson *et al.*, 2000). We can now confirm that myelin debris takes on the form of granular deposits, as well as an unravelled disorganised appearance of the sheaths. These are changes typical of the human disease (Quigley *et al.*, 1981), and are normally combined with an accumulation of intracellular organelles associated with a reduction in retrograde transport (Tsukita and Ishikawa, 1980). Unlike normal optic nerves with uniformly distributed axonal contents (Forrester and Peters, 1967), granular intracellular deposits thought to be organelle accumulations were found following hypertension in this study. These results demonstrate for the first time that axonal transport may be disrupted following episcleral vessel sclerosis.

Silver staining of the retrobulbar optic nerve has not previously been used to qualify experimental glaucoma. This study demonstrates that silver staining can show a pressure-dependent pattern and increase in glaucomatous neurodegeneration. This type of labelling is ideal for the development of a qualitative damage grading scale, or indeed computerised quantification. Hopefully in the future this technique will be used to quantify RGC axon degeneration.

This study confirms loss of optic nerve material and degeneration of RGC axons following experimental glaucoma using both light and electron microscopy. Pores remained in the nerve in regions of axonal loss. Optic nerve degeneration involved many morphological alterations some of which can be related to functional deficits. Degeneration of the RGC axon would be expected to result in reduced neurotrophin supply to the RGC body in the retina, and consequently cell death. These studies do not confirm whether this degeneration leads to RGC loss in the retina.

4.4.4 RGC degeneration in the retina

The use of labelling neurofilament components of the axon has long been examined as a method for quantification of RGC loss, not only degeneration. The neurofilament proteins represent a potential target for the assessment of neurodegeneration as well as regeneration. In general, loss of neurofilament protein is indicative of disease or

degeneration. Rather than a measure of cell death, these studies are more indicative of RGC stress which does not necessarily lead to death (Schlamp *et al.*, 2001). Loss of TUJ-1 can be used to indicate glaucomatous RGC damage in the cell soma, or ganglion cell layer of the retina. Other neurofilaments are also thought to decrease before the onset of cell loss in glaucoma (Schlamp *et al.*, 2001).

Since Cui *et al.* (2003) demonstrated that TUJ-1 selectively labels RGC in the GCL, TUJ-1 could be used to monitor RGC counts. This study is the first to successfully label normal and ocular hypertensive RGCs with TUJ-1. Similar to other cytoskeletal components of the axon, TUJ-1 did appear decreased following ocular hypertension.

TUJ-1 studies of the retina indicated that experimental glaucoma affects the RGC body as well as the axon. Reduction of neuron-specific tubulin labelling implicates loss of postmitotic RGCs (Lee *et al.*, 1990) in ocular hypertension. Immunolabelling of purified astrocytes identifies a low percentage of TUJ-1 positive cells despite the high specificity of TUJ-1 immunopositivity to differentiated neurons (Mellough *et* al., 2004; Pimental *et* al., 2000; Sergent-Tanguy *et al.*, 2003; Snow and Robson, 1994; Watanabe *et al.*, 1991). This slight overlap in immunoreactivitiy is supported in this study where other non-GCL cells are TUJ-1 immunopositive. It is likely therefore that these cells are astrocytes with TUJ-1 immunoreactivity.

Identification of RGC degeneration at the level of the retina benefit from an independence from retrograde transport elements. Therefore quantification of damage should be far more accurate with these techniques than retrograde labelling. Cell morphology can also be examined for a better understanding of neurodegeneration in the retina. Immunolabelling studies of neurofilament proteins are particularly amenable to this. Initial studies using these new methods have far reaching implications, not just for the study of glaucoma but also, for investigations into other forms of neurodegeneration.

Despite the suitability of TUJ-1 immunoreactivity for the assessment of nerve damage, there are some drawbacks. Immunoreactivity for TUJ-1 is very specific for post-mitotic neurons (Sergent-Tanguy *et al.*, 2003). However, a small proportion of

cultured astrocytes are also TUJ-1 immunopositive (Sergent-Tanguy *et al.*, 2003). These cells may express TUJ-1 as a result of neuro-glial interactions. Therefore some astrocytes can be expected with TUJ-1 positivity in retinal tissue sections. This is supported by the present study where TUJ-1 immunoreactivity was found to be present in the retinal ganglion cell layer, as well as in other layers of the retina. Therefore TUJ-1 immunoreactivity may also be present in retinal glia. Co-localisation studies, for example using GFAP and OX42, may be used for the future investigation of TUJ-1 retinal cell specificity.

TUJ-1 immunolablling clearly identifies morphology of RGC soma and processes (Mellough *et al.*, 2004). TUJ-1 studies of the glaucoma retina have the potential to elucidate size and shape alterations in the RGC dendritic field, following these initial investigations. TUJ-1 studies have been used to co-localise RGCs with calcium signalling in the retina (Pearson *et al.*, 2002). Tuj-1 has also been used to quantify cell survival in retinal whole-mounts after axotomy (Cui *et al.*, 2003). However, TUJ-1 labelling has not been used with the episcleral vessel sclerosis model of glaucoma before. These findings indicate that loss of TUJ-1 immunoreactivity may provide a new quantification method for the assessment of neurodegeneration and nerve loss in the RGC layer. RGC loss was also examined by quantification of apoptosis in the RGC layer.

4.4.5 RGC apoptosis

Upregulation of apoptotic retinal cell death and degeneration in glaucoma occurs throughout all retinal layers (Wang *et al.*, 2002). The number of apoptotic RGCs occurring in the retina is commonly used as a quantitative measure neurodegeneration. RGC numbers also decrease with severity of pressure elevation in experimental glaucoma (Hanninen *et al.*, 2002).

Apoptosis occurs at a low rate in the normal retina in order to sustain cellular turnover (Hanninen *et al.*, 2002). Low levels of apoptosis in control retinae were indicated in the present study by TUNEL positivity, and confirmed by active caspase 3 immunoreactivity.

4.4.5.1 Caspases

Apoptosis can be indicated by caspase activation. Activation of caspase 3 indicates that effector caspases are activated following episcleral drainage vessel sclerosis, consistent with limbal vessel sclerosis (McKinnon *et al.*, 2002). Episcleral vessel sclerosis also activates caspase 9 and the intrinsic caspase pathway regulated by intracellular or mitochondrial signals (Hanninen *et al.*, 2002). Laser photocoagulation of the trabecular meshwork similarly activates retinal effector caspases (caspase 3) as well as the extrinsic (caspase 8) pathway (McKinnon *et al.*, 2002). The extrinsic caspase pathway (caspase 8) regulated by cell surface receptor-ligand binding is therefore involved in glaucoma, and is followed by activation of effector caspases (caspase 3) and apoptosis. The present study indicated effector caspase activation following experimental ocular hypertension. Therefore it is likely that extrinsic and/or intrinsic caspases are also upregulated. These data support a role for apoptosis in RGC death.

Caspase activation is a useful method of determining the extent of nerve damage, as well as a potential point for therapeutic intervention. The application of caspase inhibitors may reduce RGC death during glaucoma (Kermer *et al.*, 1998; Kugler *et al*, 1999). Ocular development studies show that macrophages can induce target cell apoptosis (Lang *et al.*, 1994). It is possible that activated macrophagic microglia are involved during RGC apoptosis, and may exacerbate neuronal loss. This however is yet to be determined.

4.5.5.2 TUNEL

Apoptosis measured by TUNEL positivity increases with duration and magnitude of IOP elevation (Garcia-Valenzuela *et al.*, 1995). Apoptosis is thought to initiate at 4 days post-initial injury (Hanninen *et al.*, 2002). The present study confirmed that ocular hypertension does not induce apoptosis in the first 4 days following RGC insult, and extends this to 7 days under conditions of mild pressure elevation. Significant elevation of RGC apoptosis was not recorded until 11 days post-induction of hypertension, where low levels of RGC death were localised to the inferior retina.

In the present study, initially very low levels of apoptosis were recorded; this increased between days 20 to 46, and then began to reduce after day 47 of ocular hypertension. Mild pressure elevation appeared to produce a peak in apoptosis during intermediate disease time points, with a lag during initiation, and late disease stages. Apoptosis appeared to follow a different course over time with more severe pressure elevation. Apoptosis progressed at around 5 to 8% per week up to 6 weeks following the doubling of IOP via episcleral vein cauterisation (Garcia-Valenzuela *et al.*, 1995). Increasing the magnitude of pressure elevation 4 to 6 times resulted in 20% RGCs becoming apoptotic after only 7 days. Lower IOP elevations are therefore expected to produce a smaller effect on RGC apoptosis. However, episcleral vessel sclerosis produced apoptotic levels as low as 0.14% including high pressures and long durations of pressure (Johnson *et al.*, 2000), and may therefore affect RGC death in a different manner than other glaucoma models.

Elevation of area under the IOP curve produced a consistent increase in the number of apoptotic RGCs. Indicating that a combination of magnitude and duration of IOP elevation and RGC death show a positive correlation. These factors are important therefore in inducing and maintaining conditions of cell death.

The effects of standard deviation of IOP elevation were not as clear. Small pressure fluctuations in the lower standard deviation groups did not seem to have a direct effect on cell death, indicating that lower levels of standard deviation are not important in inducing death. However, high levels of standard deviation (S5) produced the highest levels of apoptosis seen in any group. This indicates that the consistency of elevated IOP is an important factor in the amount of cell death. Therefore a combination of duration and magnitude of pressure elevation is likely to affect cell death, while only the highest level pressure deviation will produce a definite increase in apoptosis. It is likely that other studies would produce similar results, however, these attributes of the IOP curve have remained uninvestigated until now.

Neurotrophin studies indicate that loss of neurotrophic factors initially localises to the superior retina, which may therefore be worse affected in experimental glaucoma (Johnson *et al.*, 2000). In contrast the present study indicated that RGC death was

initiated in the inferior retina. Localised deprivation of neurotrophins occurs when IOP is doubled for only one week (Johnson *et al.*, 2000), a much higher IOP elevation than achieved here. However, at the longest durations of pressure elevation, RGCs in the present study preferentially apoptosed in the superior retina. This indicates that the localisation of neurotrophic deprivation and cell death to the superior retina only occurs under severe IOP elevations or long durations of elevation. The implications of these findings are twofold. Firstly, moderate pressure elevations may not follow the same pattern of apoptosis in the retina as more severe elevations. Secondly, at lower pressures neurotrophin deprivation may not be involved in the initiation of RGC death.

TUNEL positivity correlates with RGC number following hypertension (Garcia-Valenzuela *et al.*, 1995) and is therefore likely to provide a good measure of cell loss. Although identification of apoptotic RGCs is useful in determining the degree of IOP induced damage, there are drawbacks to this technique. The main failure is the short time that fragmented cellular DNA is free to bind exogenous TdT. This may only be a few hours, and as a result measurements of apoptosis may underestimate neuronal damage (Wyllie *et al.*, 1980; Darzynkiwicz *et al.*, 1992; Garcia-Valenzuela *et al.*, 1995). RGCs are not the only cell type present in the ganglion cell layer of the retina. Supportive glia in the form of Muller cells may also become affected by elevated IOP, and respond through apoptosis or proliferation. These cells are difficult to distinguish from neurons in the type of study presented here, and may therefore affect results.

4.5.6 Conclusions

Neurodegeneration following ocular hypertension can be qualified and quantified in many ways. All of these methods have various drawbacks. However, as in this study a combination of techniques can used successfully to show RGC degeneration and death following hypertension. Generally, identification of apoptotic RGCs was used, in combination with axonal counts and qualitative retrobulbar optic nerve grading, in the assessment of nerve damage in glaucoma. This study supports others which have indicated that RGC death by apoptosis occurs with ocular hypertension. Cell death occurs at a lower rate at more moderate pressure elevations. Data regarding apoptosis

was supported by retrobulbar optic nerve studies, which indicated extensive axonal degeneration following the induction of elevated IOP. Techniques measuring apoptotic RGC death were valuable in the assessment of disease progression. Apoptotic cell counts appear relatively quick and non-subjective as compared to axonal counts and nerve grading respectively.

Morphological alterations, analogous to that in human glaucoma, were shown from the level of the optic nerve tissue, through to the degeneration of single axons as a result of experimental ocular hypertension. All of the findings presented here should enhance the understanding of RGC death in experimental glaucoma, and draw further parallels with the human disease.

In conclusion, the rat is a good model for the evaluation of the effects of ocular hypertension on the expression of glia and microglia. These will be described in future chapters.

Chapter V

Glial Activation Following IOP-Induced RGC Death

5.1 Introduction

Primary open angle glaucoma (POAG) usually initiates when elevated intraocular pressure (IOP) causes retrodisplacement of the lamina cribrosa associated with reduced retrograde neurotrophic support and pathological cellular changes (Quigley and Addicks, 1981). Retinal ganglion cell (RGC) loss continues after reduction of IOP to normal levels, indicating attenuated secondary neurodegeneration during which microglia activate and proliferate (Bakalash *et al.*, 2002).

There is considerable evidence that macroglia, particulary optic nerve head astrocytes, are involved in initiation and maintenance of cell death (Wang *et al.* 2002). The role of microglia is less clear, despite their potential influence over damage (Tezel and Wax, 2004). The temporal response of retinal microglia to ocular hypertension is known (Lam *et al.*, 2003b; Wang *et al.*, 2000), however, chronic optic nerve responses have yet to be elucidated. Clarification is also needed on the neuroprotective and/or destructive role of microglia during glaucoma (reviewed by Schwartz, 2003; Tezel and Wax, 2004).

Microglial activation influences RGC survival (Raibon *et al.*, 2002). Production of toxins including nitric oxide (NO), implicate activated microglia in neurodegeneration (Chao *et al.*, 1992; Neufeld *et al.*, 1997; Siu *et al.*, 2002). Th-1 type cytokine (IL-2 and IFN-γ) stimulation of microglia can generate chronic neurodestructive immune response (Abbas *et al.*, 1996; Matsubara *et al.*, 1999; Mosmann and Sad, 1996) during disorders such as stroke and multiple sclerosis.

The temporal relationship between neuroretinal cell death and microglial activation suggests a scavenger function for microglia (Naskar *et al.*, 2002; Schuetz and Thanos, 2004). Evidence also suggests a neuroprotective function for microglia and T-cells via secretion of potent anti-inflammatory factors, which limit damaging autoimmunity (Bakalash *et al.*, 2002; Morris *et al.*, 1997; Parra *et al.*, 1997).

Microglia may mediate neuroprotection only when in contact with neurons (Zeitlow *et al.*, 1999). Neuroglial contact or communication may become compromised during glaucoma similarly to conditions of axotomy (Schuetz and Thanos, 2004) or stress, where the retinal CD200/CD200L axis is disrupted (Broderick *et al.*, 2002). Microglial CD200R interacts with myeloid and RGC CD200 (Dick *et al.*, 2001) to downregulate retinal microglial-induced autoimmunity and may have similar effects in the optic nerve (Dick *et al.*, 2003).

Determining the temporal relationship between immune response and chronic RGC death in the glaucoma optic nerve will help elucidate the microglial role in pathophysiology. The relationship of neuroglial signalling with microglial activation may uncover mechanisms of secondary degeneration with possible relevance to other neurodegenerative diseases. Consequently astrocyte, microglial and immune cells as well as neuroglial interactions via the CD200 axis were measured from the initiation of experimental glaucoma through to more chronic time points.

5.2 Methods

Methods developed and used in the chapter are described in full in Chapter II, Section 2.7. The final immunolabelling protocol summarised in Chapter II, Section 2.7, Figure 2.5 produced acceptable results for all primary antibodies in dual labelling and was used to produce all results for quantification.

Experimental ocular hypertension was induced in Norwegian Brown rats, using episcleral drainage vessel sclerosis. Ocular hypertension was maintained as described in Table 5.1, to various durations, area under the IOP elevation/duration curve and

standard deviation of IOP elevation. These aspects of ocular hypertension were then examined for astroglial and microglial alterations.

Table 5.1 Experimental animal groupings according to pressure elevations

Level	GROUP "T" Duration of IOP elevation (days)	GROUP "A" Area under the pressure curve (mmHg)	GROUP "S" Standard deviation
1	1 – 7 (n=10)	0.9 – 22.7 (n=8)	0 - 1.511 (n=6)
2	11 – 19 (n=19)	24.3 – 96.8 (n=16)	1.52 - 2.96 (n=13)
3	20 - 27 (n=11)	97.2 – 151.1 (n=15)	3.20 - 3.75 (n=9)
4	33 – 46 (n=10)	165.3 – 256.1 (n=8)	3.81 - 5.57 (n=16)
5	47 - 65 (n=7)	271.9 – 469.3 (n=10)	6.02 - 12.76 (n=12)

Quantification involved subtraction of control immunofluorescence (without the addition of primary antibody) from contralateral (control, normotensive) and ipsilateral (hypertensive) optic nerves. The number of pixels at each intensity were measured on a brightness scale of 0 to 255. Each intensity was multiplied by the number of pixels at that intensity to give a value, the pixel (xy). This value was used in T-tests to test for significant differences between contralateral and ipsilateral eyes.

Immunolabelling was used to detect alterations in astrocytes (GFAP) and haematopoetically derived peripheral cells and/or microglia (CD45 and MHCII). The pan-microglial cell marker OX42 was used to label all optic nerve microglia, regardless of activation state, while the macrophage marker, OX41, was used to identify activated (and therefore macrophagic) microglia.

Due to inseparable differences between the microglia of the CNS and cells of the peripheral immune system, it was necessary to use an additional marker, OX33. This marker was used to identify infiltrating peripheral lymphocytes, the presence of which would indicate compromise of the blood-brain-barrier (BBB), and therefore the possible infiltration of peripheral immune cells. Due to the nature and similarities between both the central and peripheral immune response, and the role of recruitment signalling it was necessary to use this panel of markers to clarify the cell types involved in the reaction to hypertension at the optic nerve head.

5.3 Results

5.3.1 Quantification of immunofluorescence

Immunofluorescence quantification graphs for peaks in pixel number and intensity results were improved through subtraction of control immunofluorescence (Figure 5.1). Control immunofluorescence, present in the absence of primary antibody, can be regarded as "noise" or "background fluorescence", and is commonly subtracted from fluorescence results in terms of both data analysis, as in the present study, and images.

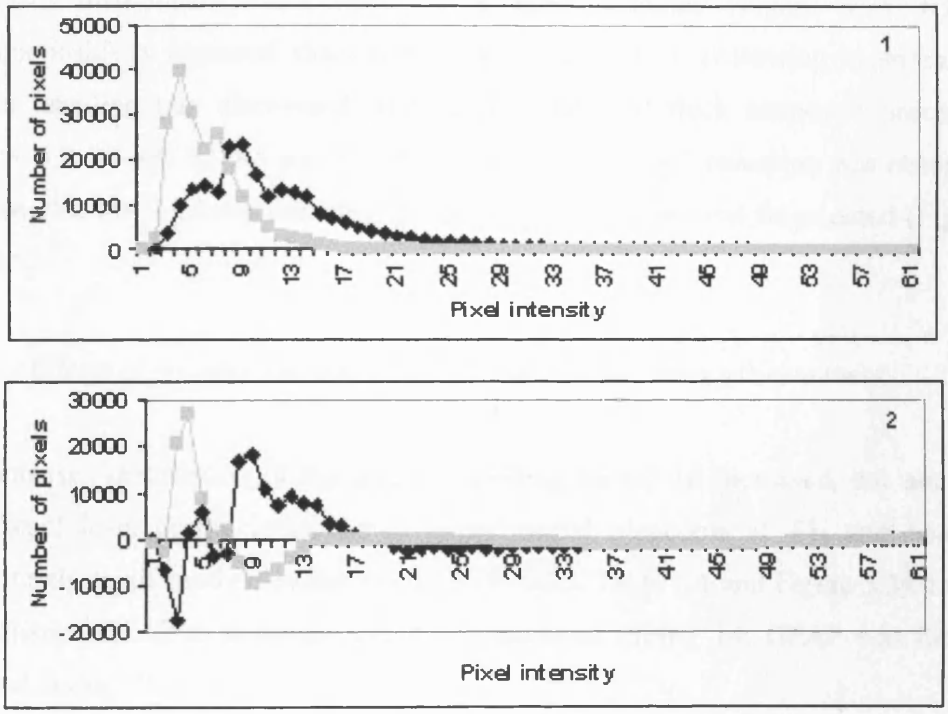

Figure 5.1 Quantification of immunolabelled pixel intensity *Quantification of T4 duration CD200 ligand immunolabelling pixel intensity are shown at the optic nerve head (n=5). Black plots represent pixel intensity following hypertension (ipsilateral eye), while grey plots represent control (contralateral eye) pixel intensity. Raw data is shown in graph 1. Clearly changes in results were produced by subtraction of control immunofluoresence (2).*

5.3.1 Astrocytic reactivity

5.3.1.1 GFAP distribution in the normal and hypertensive optic nerve

A summary of astroglial changes as aspects of IOP elevation increase during experimental glaucoma is shown in Table 5.2 and Figure 5.1. Alterations in GFAP are also shown with respect to area under the pressure curve and the standard deviation of IOP (Table 5.2). These figures also show summaries of the relevant data for all other markers probed.

GFAP was distributed throughout normal optic nerve head astrocytic processes in a transverse orientation. Columns of astrocytes could be identified, with dense processes distributed within optic nerve head columns (Figure 5.2). GFAP immunopositivity appeared sharp throughout (Figure 5.2). Following hypertension denser labelling was discovered with brightly labelled thick astrocytic processes (Figure 5.2, T1-T4, A1-A5 and S1-S5). Alternatively GFAP reduction was observed as disrupted low intensity labelling, processes were thinner and fragmented (Figure 5.2, T5).

5.3.1.2 Effects of pressure elevation on optic nerve head astrocyte reactivity

The intensity distribution of fluorescent labelling for GFAP increased, but not to a significant level during initiation of experimental glaucoma at T1, and became consistently significantly elevated until T3 ($P<0.05$, Table 5.1 and Figure 5.3). Later, reduction of GFAP to normotensive levels occurred during T4. GFAP was further reduced during T5.

Area under the IOP curve and standard deviation affected the distribution of GFAP fluorescence intensity in a similar manner. In groups A1 to A5 and S1 to S5 there was not significant change in GFAP immunofluorescence excluding A3 and S3. Intermediate area under the IOP curve and standard deviation were most likely to produce a significant GFAP elevation. Both low and high area under the IOP curve and standard deviation did not result in significant GFAP elevation.

Marker	Duration of pressure elevation					Area under IOP curve					Standard deviation of pressure elevation				
	T1	T2	T3	T4	T5	A1	A2	A3	A4	A5	S1	S2	S3	S4	S5
CD200L	+++				---	+			-						
CD200R	---		+++			-		+							
CD45	+	+		+++	+++	+++			+	++	+	+++	+		
MHCII															
OX33										+					
OX41			+++	++	-										
OX42		++	+++	++				+++					+	+	+
GFAP		+	+++					+++					+		
CD200L		---			---										
CD200R		+++		--				++						+	
CD45				+											
MHCII															
OX33				+	+++										
OX41															
OX42		+++	+++	---	---		+++	++	++			++			
GFAP				---					-			+			

Table 5.1 **Quantification of immunolabelled pixel intensity** This table summarises how duration of elevated IOP (T1 to T5), area under the IOP curve (A1 to A5) and standard deviation of pressure elevation (S1 to S5) can affect optic nerve head cell markers (n=25). Significant increases in fluorescence distributions following hypertension were found by comparing average pixel (xy) between and within T, A and S groups following T-testing at significance levels of $P<0.05$ (+), $P<0.01$ (++) and $P<0.001$ (+++).

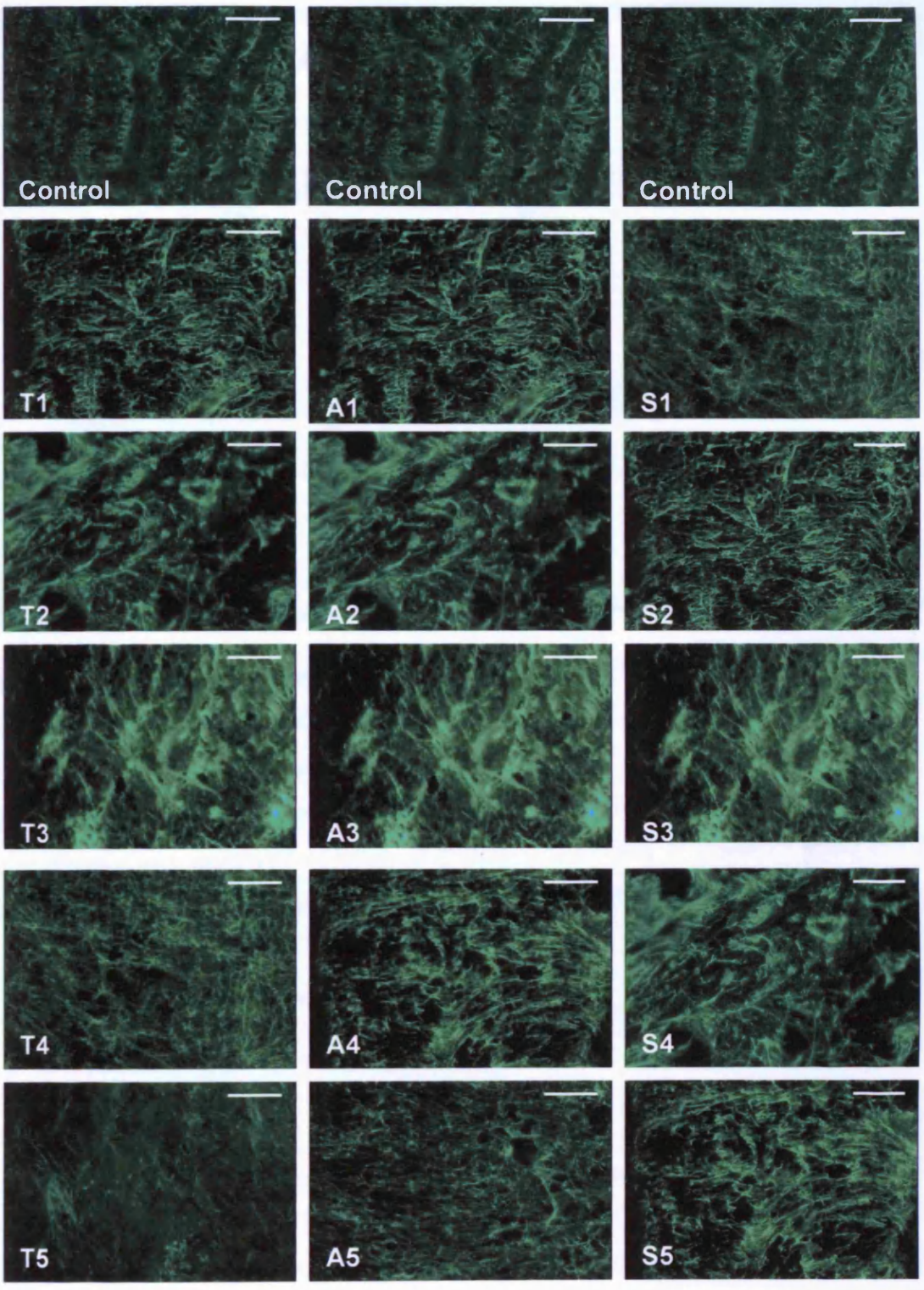

Figure 5.2 GFAP immunolabelling at the optic nerve head *Control GFAP immunolabelling (green) was highly organised into astroglial columns. Elevated immunolabelling at the optic nerve head is shown in T1-T4, A1-A4 and S1-S5. Reduction of GFAP immunolabelling following hypertension is shown in T5 and A5. White bar represents 50μm.*

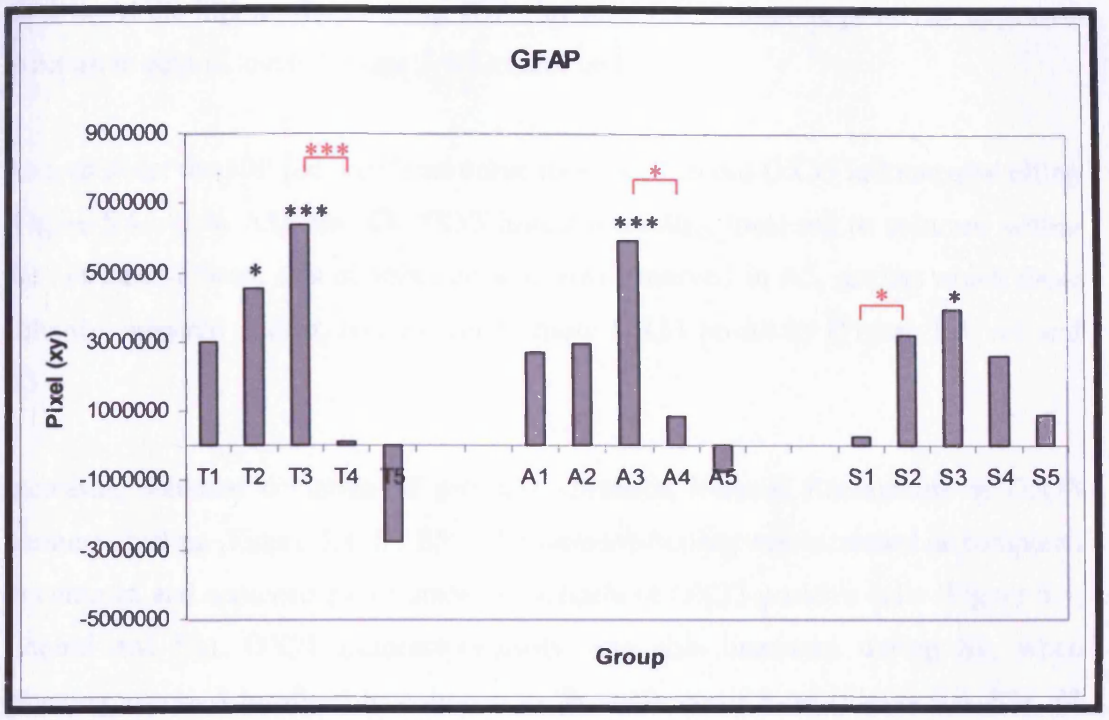

Figure 5.3 Effects of pressure elevation on optic nerve head GFAP *Groups T1 to T5, A1 to A5 and S1 to S5 inclusive are shown (n=25). The difference in overall distribution as calculated by multiplying the number of pixels at each intensity and subtracting contralateral controls from ipsilateral hypertensives is shown in grey. Significance was measured at levels of P<0.05 (*), P<0.01 (**) and P<0.001 (***) using a T-test. Significant inter-group differences are indicated by over-plot bars.*

5.3.2 Infiltration of peripheral lymphocytes

5.3.2.1 Distribution of OX33 immunolabelling

Contralateral control optic nerve heads did not show any OX33 immunopositivty (Figure 5.4, Control). Sharply labelled OX33 positive cells appeared to infiltrate the nerve under hypertensive conditions (Figure 5.4, T1-T4, A1-A5, S1-S3 and S5). OX33 used to identify infiltrating peripheral lymphocytes localised to large amoeboid cells, occasionally in astroglial columns, usually just within the nerve border at the level of the optic nerve head (Figure 5.4 T1-T4, A1-A5, S1-S3 and S5).

As duration of ocular hypertension increased from T1 to T4, OX33 immunopositivity also increased, and appeared organised into a columnar distribution by T4 (Figure 5.4,

T1-T4). At the highest durations of IOP elevation OX33 immunopositivity appeared to return to control levels (Figure 5.4, Control and T5).

As area under the IOP pressure/time curve increased, so did OX33 immunoallabelling (Figure 5.4, A1 to A5). By A4 OX33 immunolabelling localised to columns within the optic nerve head, this distribution was also observed in A5, during which these columns appeared thicker, and contained more OX33 positivity (Figure 5.4, A4 and A5).

Increasing standard deviation of pressure elevation induced fluctuations in OX33 immunolabelling (Figure 5.4, S1-S5). S1 immunolabelling was increased as compared to controls, and appeared as a number of amoeboid OX33 positive cells (Figure 5.4, Control and S1). OX33 immunopositivity was also increased during S2, when labelling appeared localised to columns in the optic nerve head (Figure 5.4, S2). S3 immunolabelling was similar to S1 (Figure 5.4, S1 and S3), while S4 immunolabelling appeared to return to control levels (Figure 5.4, Control and S4). OX33 positivity had returned to elevated levels by S5, and regained a columnar distribution (Figure 5.4, S5).

5.3.2.2 Changes in optic nerve head OX33 immunolabelling with elevated pressure

OX33 labelling for B lymphocytes although increased during all durations of pressure elevation (T1 to T5) did not achieve statistical significance as compared to controls via T-testing (Table 5.1 and Figure 5.5). However, on inter-group comparison, a small significant increase in OX33 positivity was found between groups T3 and T4 ($P<0.05$). Subsequently OX33 immunopositivity was significantly reduced between T4 and T5 ($P<0.001$).

In both area under the IOP curve and standard deviation of IOP elevation groups, only following high area under the IOP curve in group A5 were OX33 immunolabelling levels increased significantly ($P<0.05$) as compared to controls. Elevation of area under the IOP curve, and standard deviation did not produce a consistent effect on OX33 immunolabelling.

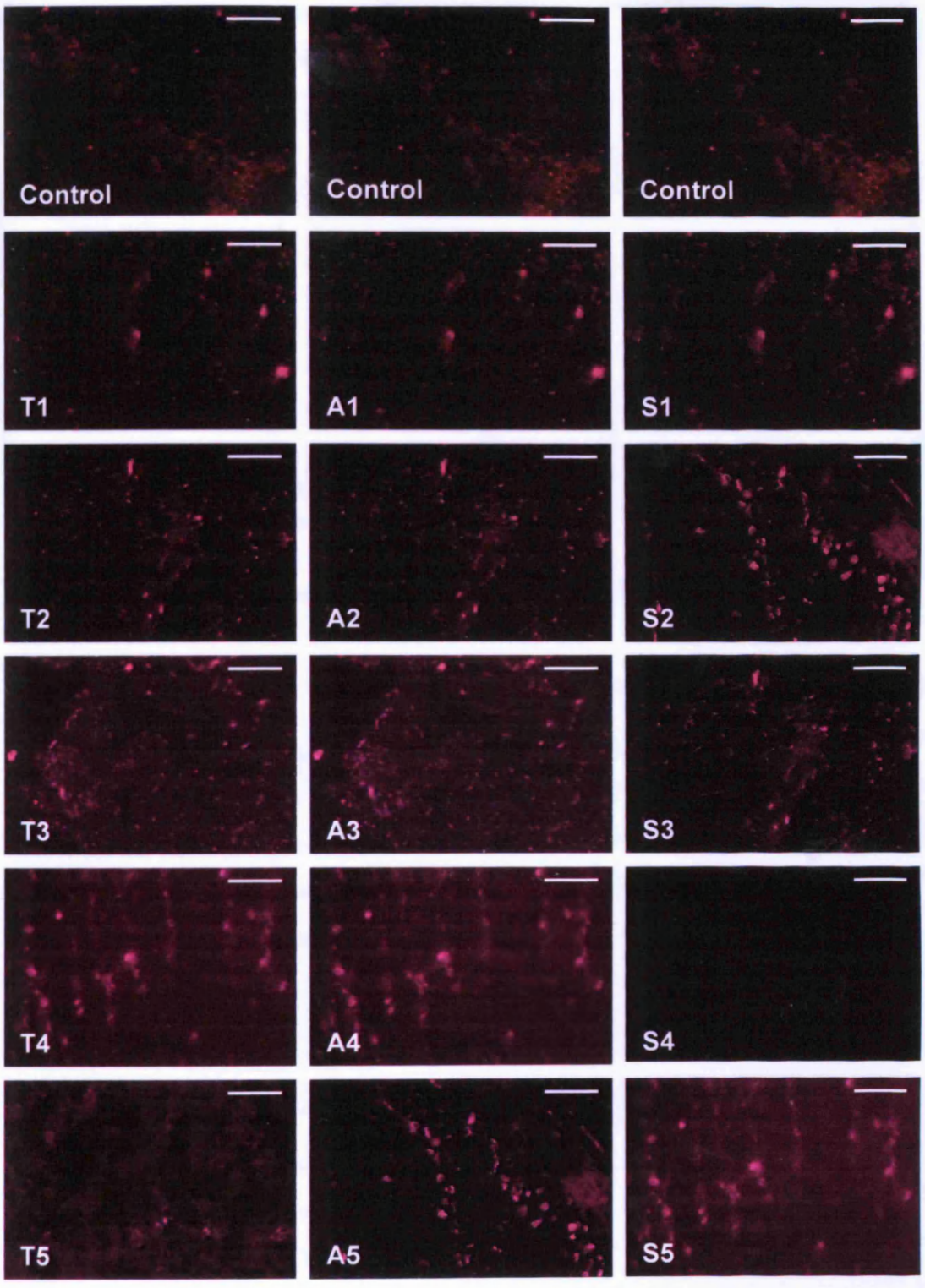

Figure 5.4 OX33 immunolabelling at the optic nerve head *Representative images of optic nerve head immunolabelling from control and all hypertensive groups T1-S5 are shown. Red labelling indicates OX33 immunoreactivity, which appeared localised mainly to rounded amoeboid cells (C), and occasionally elevated following induction of ocular hypertesion (T4, A4, A5, S2 and S5). White bar represents 50μm.*

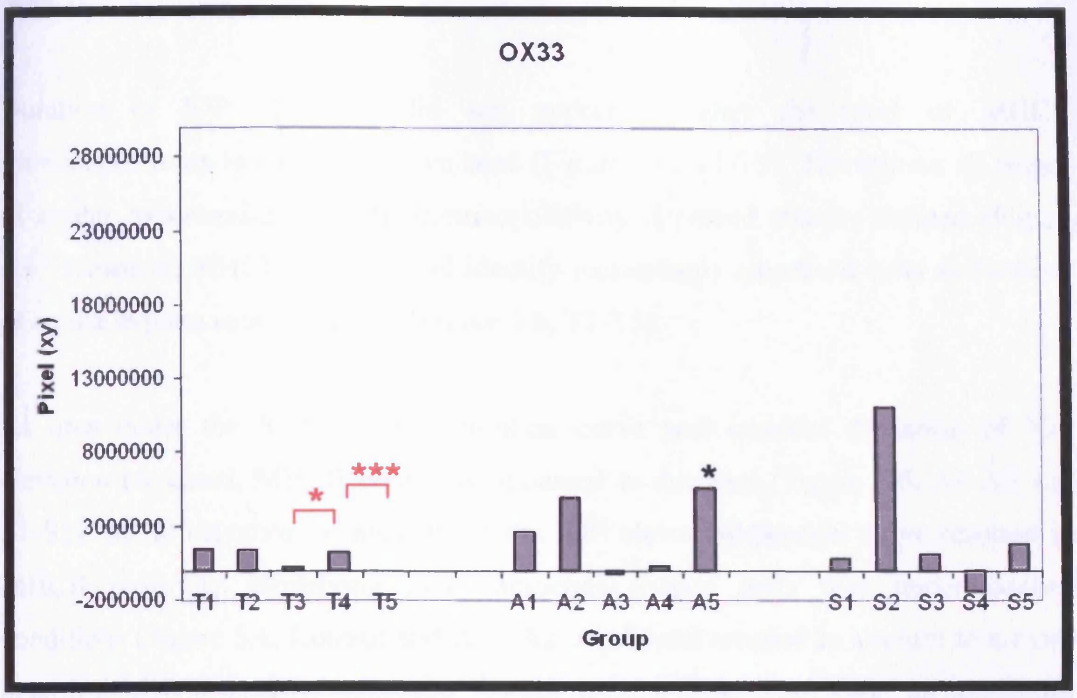

Figure 5.5 Effects of pressure elevation on optic nerve head OX33 *Quantified optic nerve head OX33 varied depending on pressure elevation on statistical comparison. The difference between ocular hypertension and control pixel (xy) is shown. Intra-group comparisons are shown in black, inter-groups comparisons are in red. Significance was measured at levels of P<0.05 (*), P<0.01 (**) and P<0.001 (***) using two sample, two tailed T-testing.*

5.3.3 Microglial changes

5.3.3.1 Qualitative observations of microglial activation

Few MHCII and CD45 positive dendritic cells were found in control optic nerve, indicating a lack of microglia and haematopoetically derived peripheral cells under normal ocular pressures (Figures 5.6 and 5.7). Following ocular hypertension few alterations in MHCII were found, while CD45 labelled cells with both amoeboid and dendritic morphologies (Figures 5.6 and 5.7) at the nerve head.

MHCII

Duration of IOP elevation did not appear to alter the level of MHCII immunopositivity in the optic nerve head (Figure 5.6, T1-T5). Throughout all stages of ocular hypertension MHCII immunopositivity appeared sharply defined (Figure 5.6). However, MHCII labelling did identify increasingly amoeboid cells as duration of ocular hypertension increased (Figure 5.6, T1-T5).

As area under the IOP elevation/duration curve and standard deviation of IOP elevation increased, MHCII positivity appeared to decrease (Figure 5.6, A1-A5 and S1-S5). Initial elevation of area under the IOP elevation/duration curve resulted in MHCII positivity identifying more amoeboid-shaped cells than under control conditions (Figure 5.6, Control and A1). A2 conditions resulted in a return to a more dendritic MHCII positive labelling pattern (Figure 5.6, A2), while an amoeboid distribution was regained by A3 (Figure 5.6, A3). Both A4 and A5 MHCII immunopositivity appeared amoeboid in distribution, but was reduced as compared to controls (Figure 5.6, Control, A4 and A5).

Groups S1 and S2 were similar in MHCII positivity to A1 and A2. Intermediate standard deviation of IOP elevation (S3) resulted in an amoeboid CD45 labelling pattern which identified very few cells (Figure 5.6, S3). CD45 immunolabelling returned to increased levels by S4, when positivity appeared fragmented (Figure (5.6, S4). At the highest conditions of standard deviation of IOP elevation (S5) CD45 immunopositivity again became reduced, and appeared less than control levels (Figure 5.6, Control and S5).

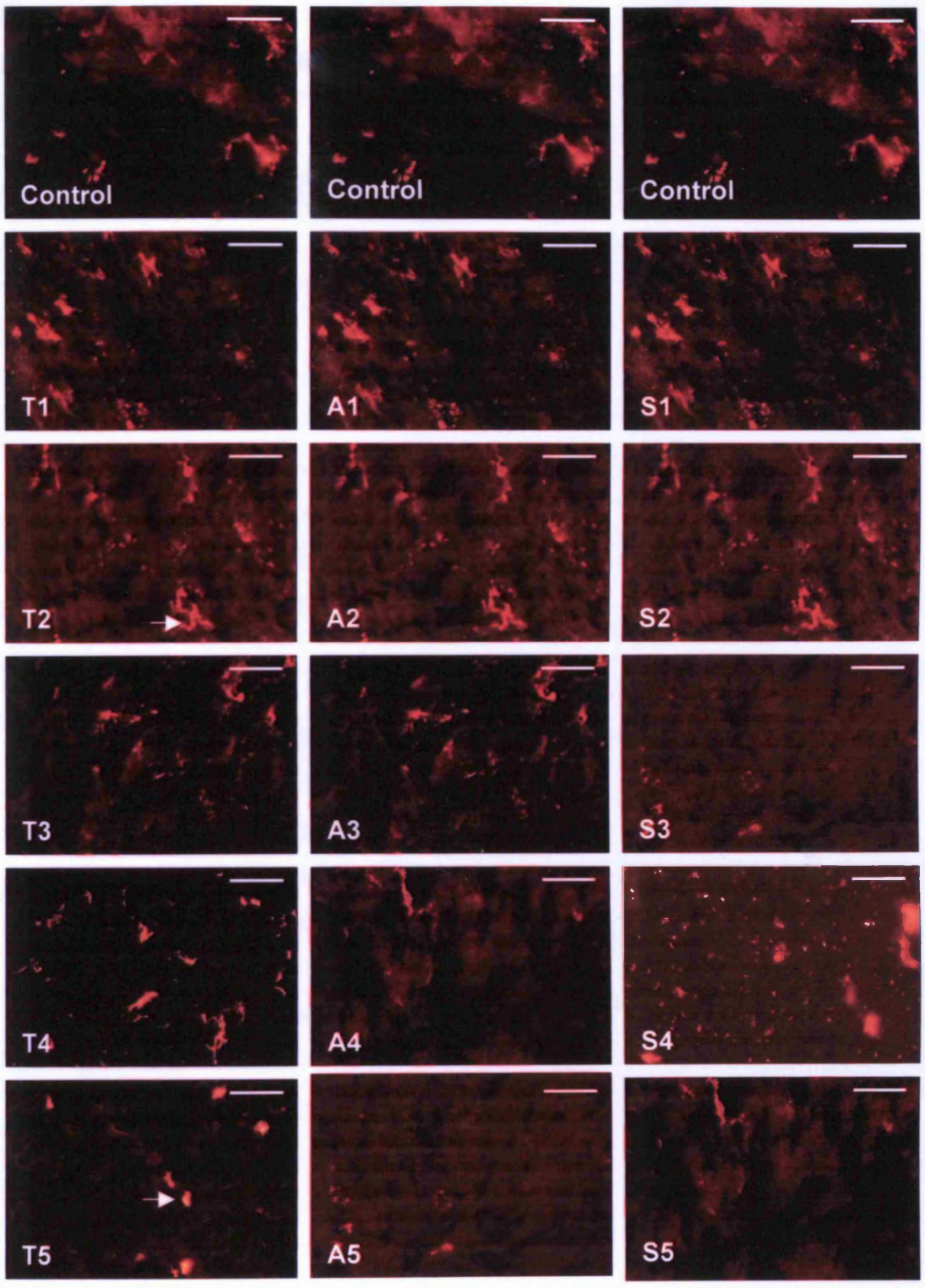

Figure 5.6 MHCII immunolabelling at the optic nerve head *MHCII immunolabelling was used to identify optic nerve myeloid cells including dendritic microglial cells (arrow, T2, A2 and S2) as well as amoeboid peripheral infiltrating myeloid lineage cells (arrow, T5). Labelling appeared to fluctuate following ocular hypertension (T1 to T5, A1 to A5 and S1 to S5). White bar represents 50μm.*

CD45

Under control conditions CD45 sharply labelled few fairly amoeboid cells (Figure 5.7, Control). CD45 positivity was increased at all stages of duration of IOP elevation (Figure 5.7, T1-T5).

Elevated duration of ocular hypertension appeared to increase the number of amoeboid, sharply-labelled CD45 positive cells (Figure 5.7, T1). CD45 immunopositivity identified larger cells at T2 (Figure 5.7, T2), while by T3, cells appeared even larger (Figure 5.7, T3).

CD45 immunlabelling appeared more diffuse at T4, labelling appeared localised to both large and small cells (Figure 5.7, T4). Increased diffusion of label was observed by T5, possible indicating localisation of label to cell of a more dendritic morphology (Figure 5.7, T5).

Throughout increase of area under the IOP elevation/duration curve increased CD45 immunoreactivity appeared localised to sharply-labelled large amoeboid cells (Figure 5.7, A1 to A5). At A2 and A5 labelling appeared more fragmented, and may have loclalised to smaller cells (Figure 5.7, A2 and A5). By A5, CD45 positivity appeared slightly more dendritic than at other stages of hypertension (Figure 5.7, A5).

Similarly, CD45 imunolabelling appeared elevated and localised to large amoeboid cells in all standard deviation of IOP elevation groups (Figure 5.7, S1-S5). S3 and S5 labelling also appeared more fragmented, and similarly to A2 and A5 (Figure 5.7, A2, A5, S3 and S5).

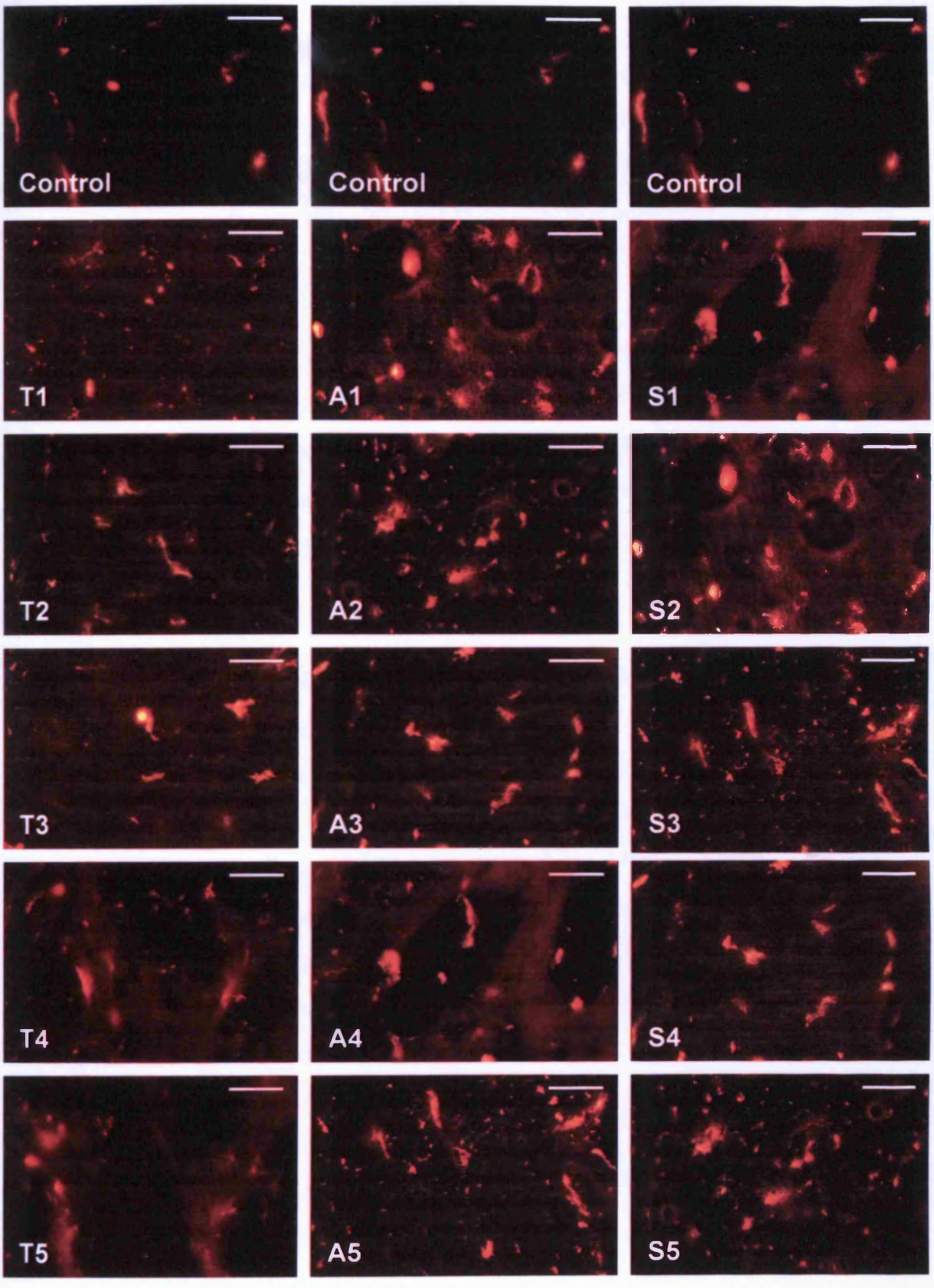

Figure 5.7 CD45 immunolabelling at the optic nerve head *CD45 immunolabelling (red), was used to identify all leukocytes as well as microglia in the optic nerve head. More optic nerve cells appeared CD45 positive in relation to MHCII positivity. Following induction of ocular hypertension CD45 immunolabelling appeared elevated in the optic nerve head (T1-S5). White bar represents 50μm.*

OX42

In control nerve head and retrobulbar regions, many cells sharply labelled with OX42. In the majority these cells had diffuse dendritic fields (Figure 5.8, Control). Ocular hypertension was associated with elevated OX42 positive cell number, as well as labelling intensity (Figure 5.8). These OX42 positive cells appeared less dendritic with fewer, thicker processes.

Initially ocular hypertension induced brighter, sharper labelling of less dendritic cells (Figure 5.8, T1, A1 and S1). The number of cells labelled did not appear to differ from controls during the initial stages of hypertension (Figure 5.8, Control, T1, A1 and S1). T2, A2 and S2 labelling appeared similar to T1, A1 and S1, however, labelled cells were of an elongated morphology (Figure 5.8, T1, T2, A1, A2, S1 and S2).

The third group of duration of ocular hypertension, area under the IOP elevation/duration curve and standard deviation of IOP elevation indicated a peak in OX42 immunoreactivity (Figure 5.8, T3, A3 and S3). In these third stage groups many OX42 positive cells were sharply labelled, all appeared completely amoeboid in morphology (Figure 5.8, T3, A3 and S3). OX42 immunoreactivity was subsequently reduced in more severe hypertensive groups, appearing as sharply labelled, bright, but few amoeboid cells (Figure 5.8, T4, T5, A4, A5, S4 and S5). In summary the effects of severity of IOP variables investigated here produced similar effects on OX42 pan-microglial labelling.

In general the myeloid cell markers CD45, MHCII and OX42 appeared to change in distribution and density following ocular hypertension.

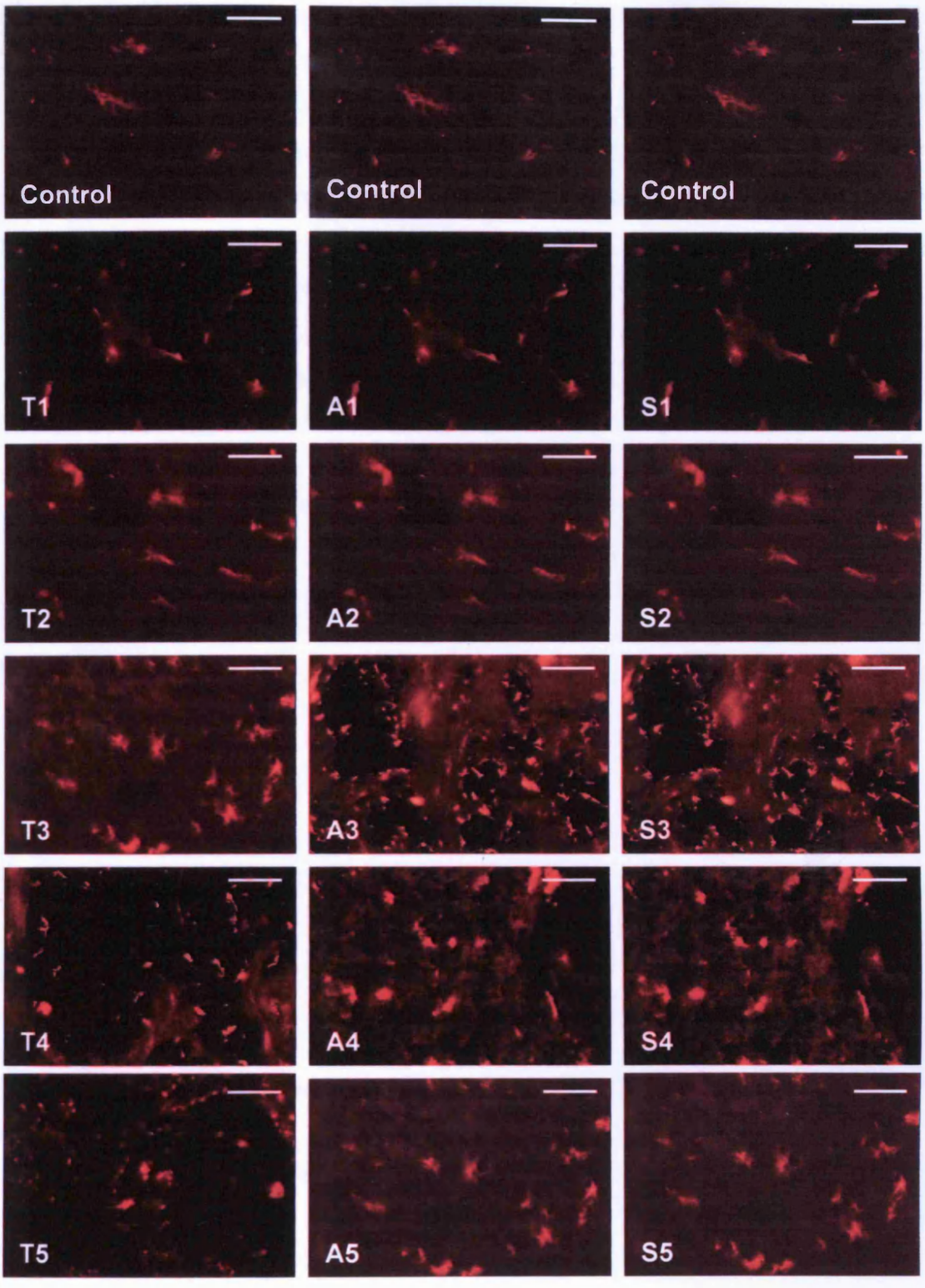

Figure 5.8 OX42 immunolabelling at the optic nerve head *OX42 immunolabelling identified dendritic microglial cells at the optic nerve head in controls. OX42 immunoreactivity is shown in red. OX42 immunolabelling appeared to elevate as a consequence of ocular hypertension (T1-S5 inclusive). Many optic nerve head cells were OX42 positive in all images. White bar represents 50μm.*

5.3.3.2 Quantification of optic nerve head MHCII at different pressure elevations

No significant changes in distribution of MHCII fluorescence intensity were found following hypertension when examining duration of pressure elevation or area under the IOP curve (Table 5.1 and Figure 5.9). Therefore MHCII positive myeloid cells including resident microglia and possibly peripheral immune cells were not affected by increasing duration of IOP elevation or area under the IOP curve. One significant elevation was found between groups T3 and T4, where MHCII immunoreactivity significantly elevated ($P<0.05$). High standard deviation of pressure elevation induced a mildly significant MHCII elevation between groups T4 and T5.

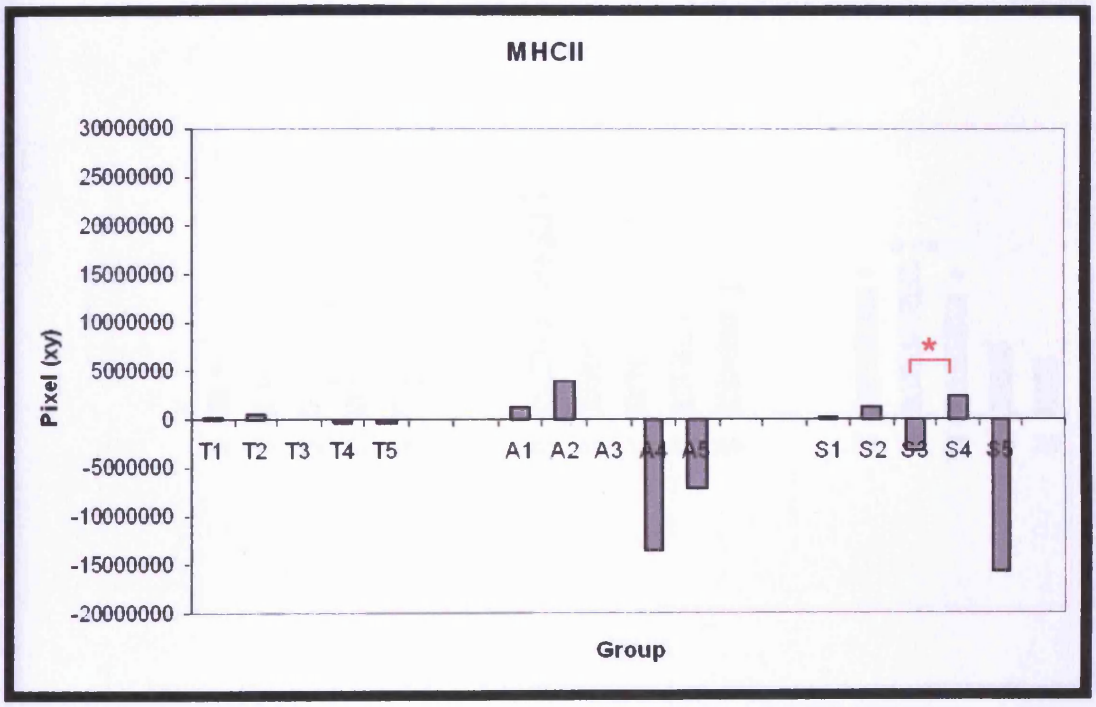

Figure 5.9 Effects of pressure elevation on optic nerve head MHCII *A two sample t-test was used to compare MHCII optic nerve head immunolabelling at different pressure elevations (n=25). The differences between these data values are represented by a grey bar for duration, area under the curve and standard deviation of pressure elevation. Significant differences between groups are shown in red (P<0.05).*

5.3.3.3 CD45 immunolabelling with increasing elevated pressure

During initial (T1 and T2, P<0.001) and chronic (T4 and T5, P<0.001) durations of pressure elevation CD45 fluorescence distribution and pixel (xy) significantly increased as compared to controls. Pixel (xy) was also significantly elevated between groups T3 and T4 (P<0.05). Similarly significant elevation of optic nerve head CD45 immunoreactivity occurred in groups of high (A4, P<0.05 and A5, P<0.01) as well as low (A1, P<0.001) area under the IOP curve (Table 5.1 and Figure 5.10). CD45 immunoreactivity was also significantly elevated when standard deviation was low in groups S1 (P<0.05), S2 (P<0.001), and S3 (P<0.05).

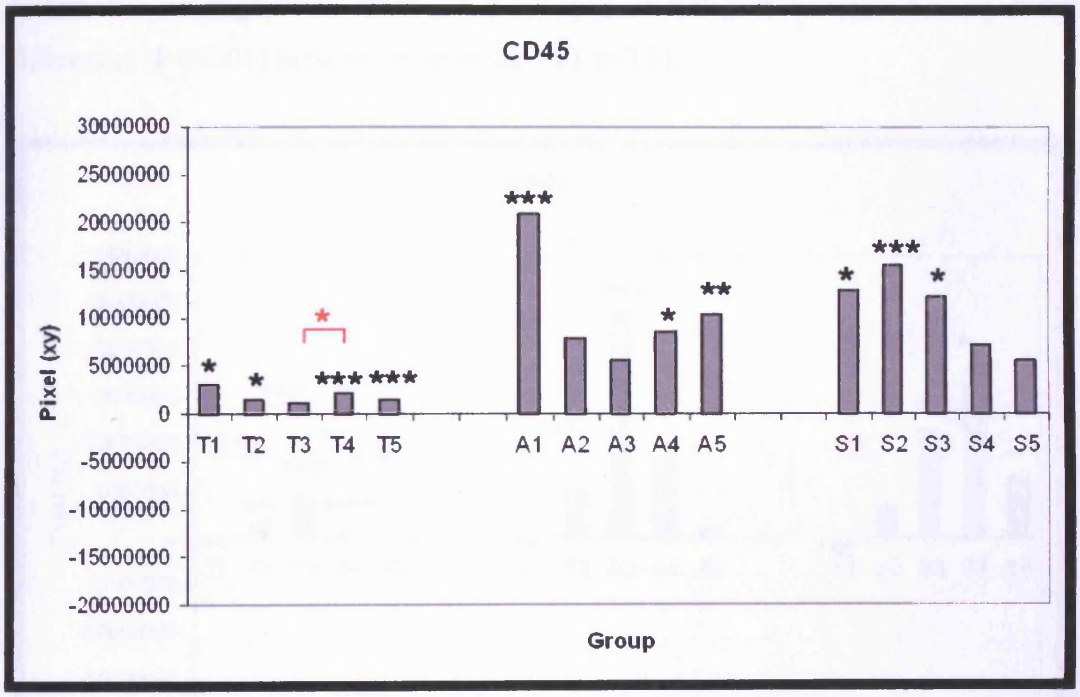

Figure 5.10 Effects of pressure elevation on optic nerve head CD45 *Optic nerve head CD45 immunofluorescence was quantified and compared following ocular hypertension using a two sample t-test (n=25). The difference between data sets are shown in grey. Significant differences between control and hypertensive nerves are shown by the black stars (P<0.05, P<0.01, P<0.001). Differences between groups are shown in red (P<0.05).*

Statistical comparisons indicated that CD45 levels were most likely to elevate at chronic IOP elevations with low area under the curve and standard deviation. However, initial disease stages, or higher area under the IOP curves were also likely to elevated CD45 levels. CD45 upregulation did not appear to correlate directly with elevation of any other markers described in this chapter.

5.3.3.4 OX42 positive microglial alterations with elevation of IOP

The intensity distribution of labelling for OX42 significantly elevated during T2 ($P<0.05$), T3 ($P<0.001$) and T4 ($P<0.01$, Table 5.1 and Figure 5.11). Pan-microglial elevation indicated, during T2 to T4, that microglial cells were increased due to proliferation or migration. Inter-group analysis revealed that there were significant differences ($P<0.001$) between each group (T1 to T5).

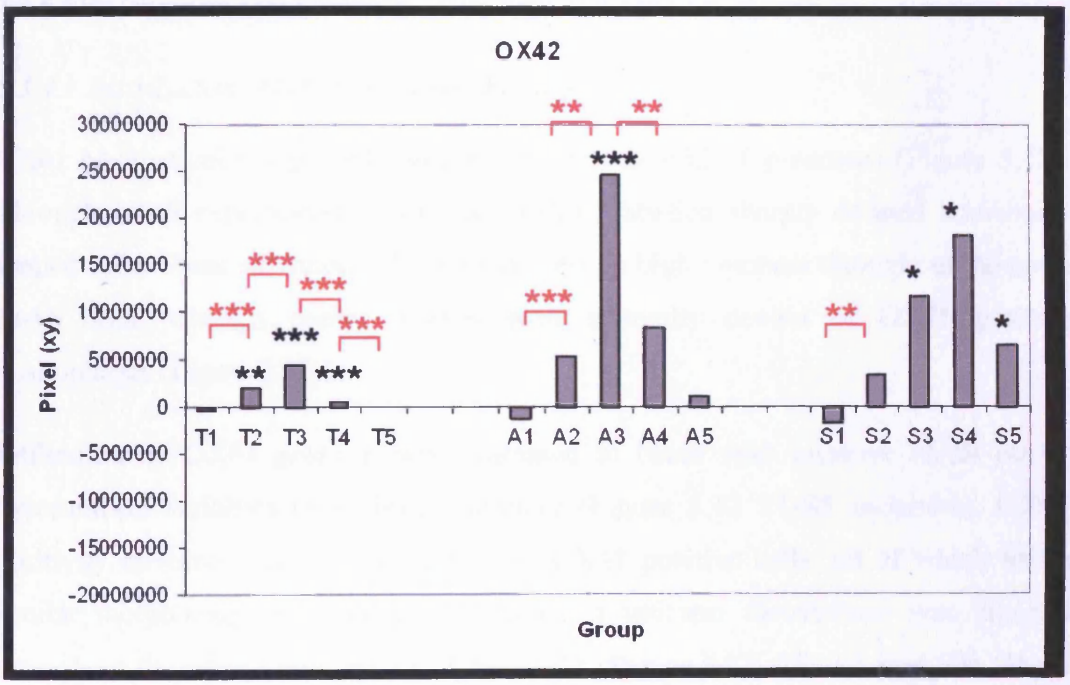

Figure 5.11 Effects of pressure elevation on optic nerve head OX42 *All hypertensive groups are shown (n=25). Grey bars indicate overall differences in distribution (pixel xy). Significance was measured at levels of P<0.05 (*), P<0.01 (**) and P<0.001 (***) using a T-test. Red over plot bars indicate significant inter-group differences.*

By examining area under the IOP curve it was possible to determine specifically that A3 area under the pressure curve was more likely to produce OX42 upregulation ($P<0.001$) than any other. OX42 significantly elevated during the high standard deviation of pressure elevation achieved in groups S3 ($P<0.05$), S4 ($P<0.05$) and S5 ($P<0.05$).

Elevation of microglia corresponded with increase of CD45 positive myeloid cells. Both OX42 and CD45 were significantly elevated ($P<0.05$) from S2 to S4 inclusive. Increased microglial labelling also corresponded with elevation of the macrophage marker, OX41, at T4, A3 and S4. This will be described and discussed in more detail later (Chapter V, Section 5.3.4.2). Briefly, the elevation of microglial markers appeared to occur before microglial activation.

5.3.4 Macrophagic cell changes

5.3.4.1 Distribution of OX41 immunolabelling

OX41 positive cells appeared rounded, but not devoid of processes (Figure 5.12). Throughout all experimental conditions OX41 labelled sharply defined amoeboid-shaped cells. These activated cells were present in high numbers throughout the optic nerve head, whereas control nerves were normally devoid of OX41 positive macrophages (Figure 5.12).

Infiltration by OX41 positive cells appeared to occur with increase of all ocular hypertension variables in a similar manner (Figure 5.12 T1-S5 inclusive). OX41 positivity increased via greater number of OX41 positive cells, all of which had a similar morphology throughout. Eventually a uniform distribution was reached throughout the optic nerve by T3, A3 and S4 (Figure 5.12, T3, A3 and S4). These peaks in OX41 positive cell number were followed by a reduction in labelling (Figure 5.12, T4, T5, A4, A5 and S5). Overall, OX41 positive macrophages appeared to be present in increased numbers following experimental glaucoma.

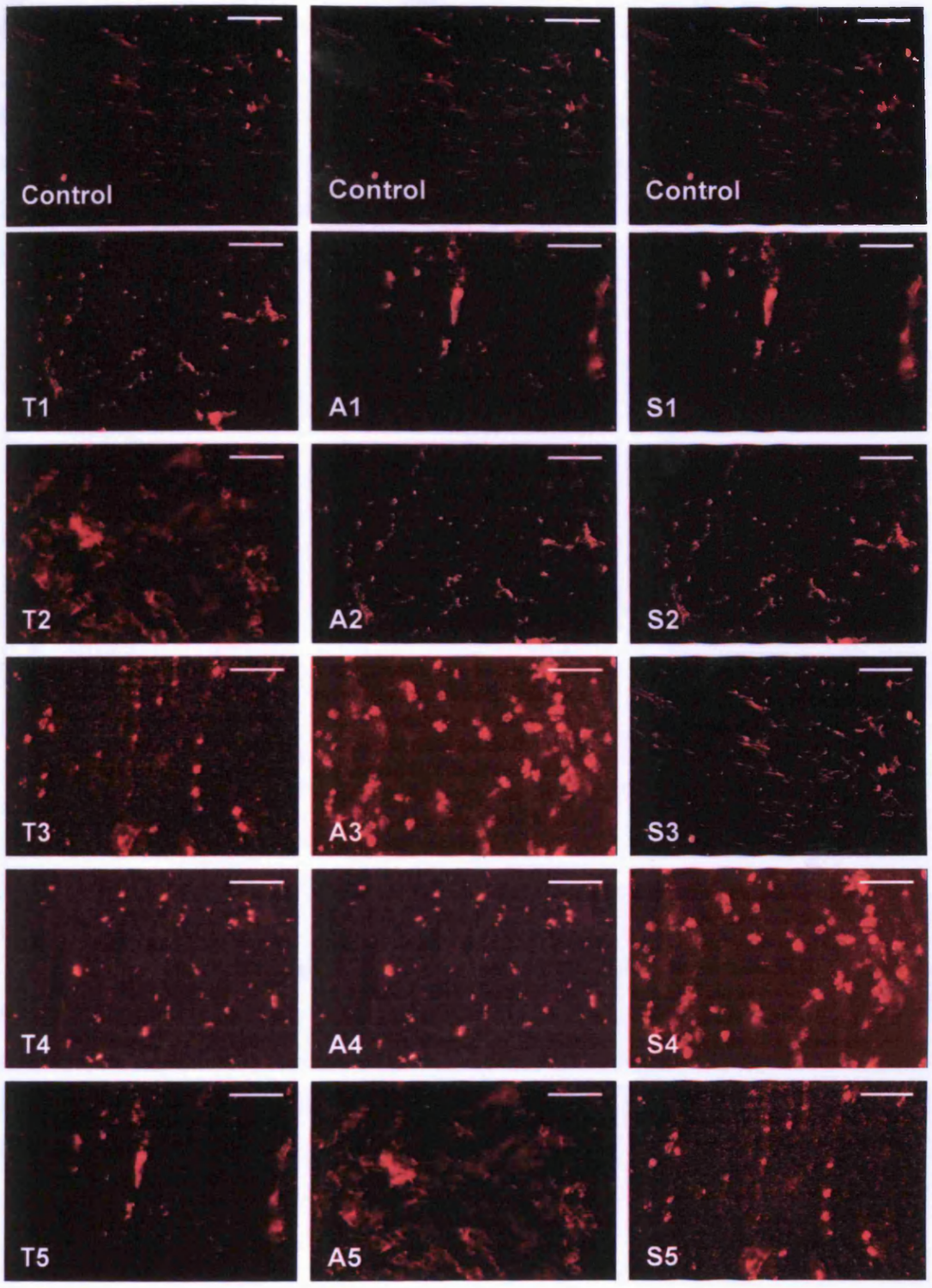

Figure 5.12 OX41 immunolabelling at the optic nerve head *Control optic nerves were virtually devoid of macrophage positivity (Control, red). Ocular hypertension induced elevation of optic nerve head OX41 immunoreactivity, (T1-S5 inclusive) Peaks in macrophage activity are shown in images T3, A3 and S4. White bar represents 50μm.*

5.3.4.2 Changes in optic nerve head OX41 with pressure elevation

Increased immunofluorescence distribution of optic nerve head OX41 positive macrophages was recorded at T3 (P<0.001) and T4 (P<0.01, Table 5.1 and Figure 5.13). These elevations were also consistently significantly different between ipsilateral experimental eye groups.

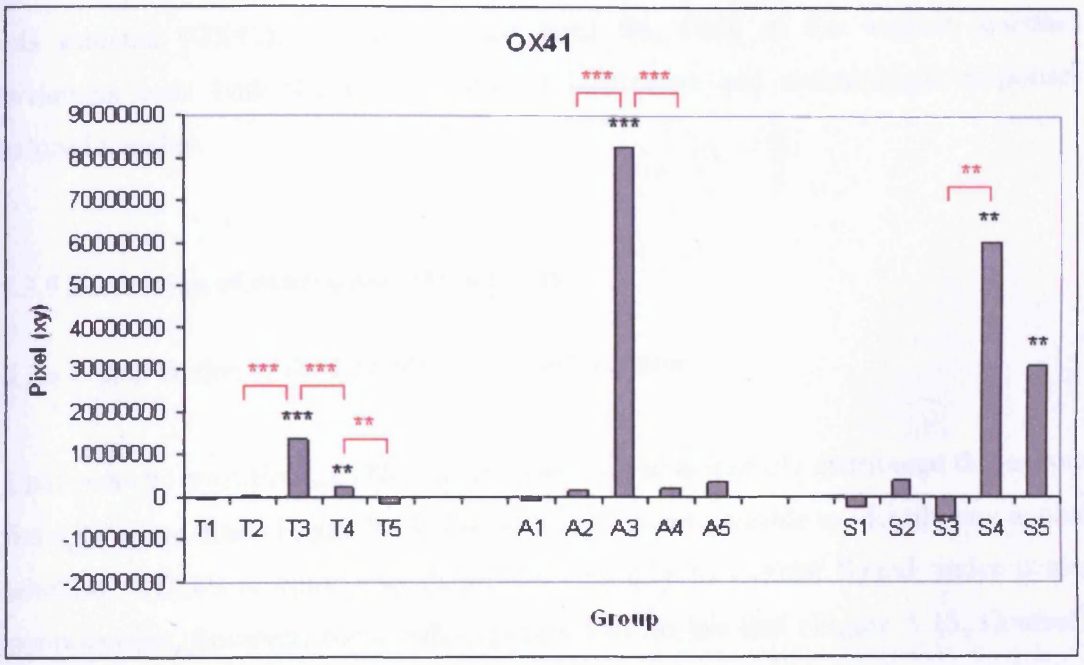

Figure 5.13 Effects of pressure elevation on optic nerve head OX41 *Optic nerve head OX41 immunolabelling at different durations of pressure elevation (n=25) were compared using a two sample t-test, the difference in distribution of pixel intensity (xy) is shown in grey. Significant differences within (black stars) and between groups (red bars and stars) were found at levels of P<0.05 (*), P<0.01 (**), and P<0.001 (***).*

Intermediate are under the pressure curve induced significantly increased OX41 positivity (A3, P<0.01) which was also significant elevated as compared to other hypertensive ipsilateral optic nerves (P<0.001). High standard deviation of pressure elevation induced OX41 upregulation in groups S4 (P<0.05) and S5 (<0.05). S4 OX41 was also significantly elevated as compared to S3 levels. As no labelling of peripheral cells was found (OX33), it can be assumed that any immune cell markers

in the optic nerve are those of resident microglial. OX41 upregulation occurred following increase of microglial (OX42) labelling according to duration of pressure elevation groups. Data indicates that microglial proliferation or infiltration preceded microglial activation. Proliferation / infiltration occurred throughout T2 to T4, with activation occurring later at T3 and sustaining until T5.

Activation (OX41) and proliferation / infiltration also coincided at A3 (intermediate) are under the pressure curve. At low standard deviations (S2) the microglial response was initiated (OX42), and maintained until S4. Only at the highest standard deviations were both the proliferative / infiltrative and macrophagic responses induced together.

5.3.5 Disruption of neuroglial interactions

5.3.5.1 Distribution of the CD200 ligand and receptor

Under control conditions, CD200 ligand labelling was sparsely distributed throughout the optic nerve head (Figure 5.14, Control). It was not possible to identify any axonal labelling. CD200 receptor was dispersed similarly to CD200 ligand under ocular normotension, however, more cells appeared to be labelled (Figure 5.15, Control). Following ocular hypertension elevations in both receptor and ligand were evident as increased labelling intensity of a greater number of cells.

CD200 Ligand

As duration of ocular hypertension increased, many amoeboid-shaped areas of sharp CD200 ligand immunopositivity appeared in the optic nerve head (Figure 5.14, T1). This labelling pattern progressed into fewer, brightly-labelled sharp CD200 ligand positive areas (Figure 5.14, T2). Labelling was similar to T2 at T3 and T4, with fewer areas of CD200 ligand positivity (Figure 5.14, T2-T4). At the highest durations of ocular hypertension (T5) labelling distribution was similar to previous groups, but very few areas of positivity were identified (Figure 5.14, T1-T5).

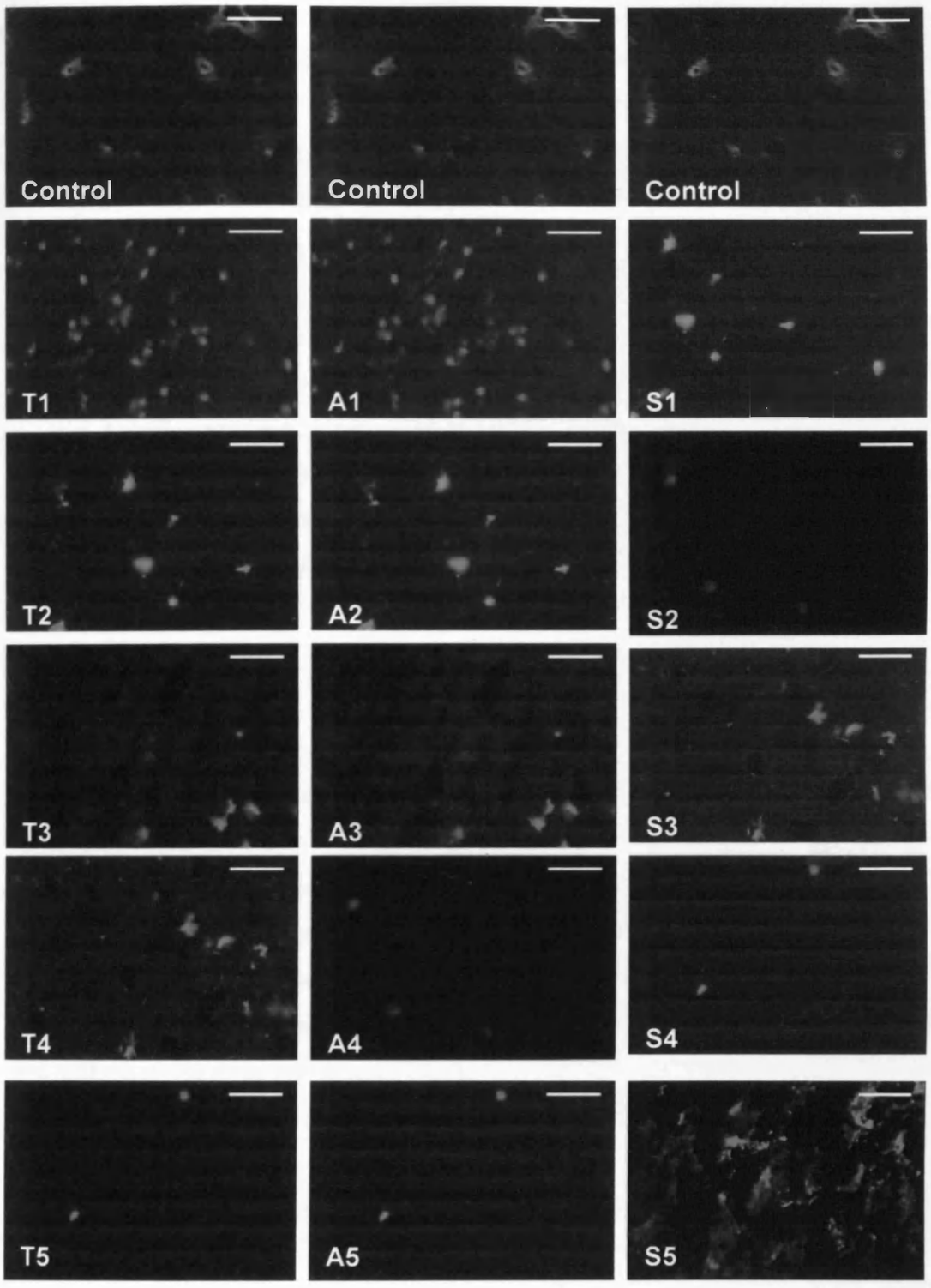

Figure 5.14 CD200 ligand immunolabelling at the optic nerve head *CD200 ligand (red labelling) identified very few cells. In the majority labelled cells were of an amoeboid morphology. Elevated labelling following ocular hypertension appeared in the majority as brighter labelling of a greater number of cells with amoeboid morphology (T1, T2, A1, A2, S1 and S5). White bar represents 50μm.* S4).

Initially, increased area under the IOP duration/elevation curve (Figure 5.14, A1-A3) had similar effects to increasing duration of ocular hypertension (Figure 5.14, T1-T3). The highest areas under the IOP duration/elevation curve (A4 and A5) resulted in reduced CD200 ligand positivity to bellow control levels (Figure 5.14, Control, A4 and A5). Throughout increased area under the IOP curve, labelling appeared sharp and amoeboid in distribution (Figure 5.14, A1-A5).

Increased standard deviation of IOP elevation resulted in sharp, brighter labelling of a similar number of areas as controls (Figure 5.14, Control, S1). Further elevation of standard deviation resulted in reduction of CD200 ligand labelling very few areas of positivity (Figure 5.14, S2). CD200 ligand labelling under S3 and S4 conditions identified few, amoeboid sharp and bright areas of positivity (Figure 5.14, S3 and S5 conditions produced many areas of more diffuse, dendritic labelling (Figure 5.14, S5).

CD200 Receptor

The labelling pattern produced by CD200 receptor immunopositivity did not change throughout experimental conditions. Immunopositivity appeared as discrete, sharp labelling in an amoeboid distribution. (Figure 5.15). Elevation of ocular hypertension induced a reduction in the number of CD200 receptor-positive labelled areas (Figure 5.15, T1). Further elevation resulted in increased labelling, appearing as more discrete and amoeboid areas of CD200 receptor labelling (Figure 5.15, T2 and T3). The highest levels of hypertension (T4 and T5) resulted in a return of CD200 receptor similar to control labelling (Figure 5.15, Control, T4 and T5).

A1 and A2 area under the IOP elevation/duration curve reduced CD200 receptor immunopositivity in the optic nerve head, as compared to controls (Figure 5.15, Control, A1 and A2). Immunopositivity increased to the highest level during intermediate area under the IOP curve (A3), this increase, sustained throughout to the highest levels of area under the IOP curve (A4 and A5), appeared as a higher number of CD200 receptor positive areas in the optic nerve head (Figure 5.15, A4 and A5). Standard deviation of IOP elevation produced the same alterations in optic nerve head

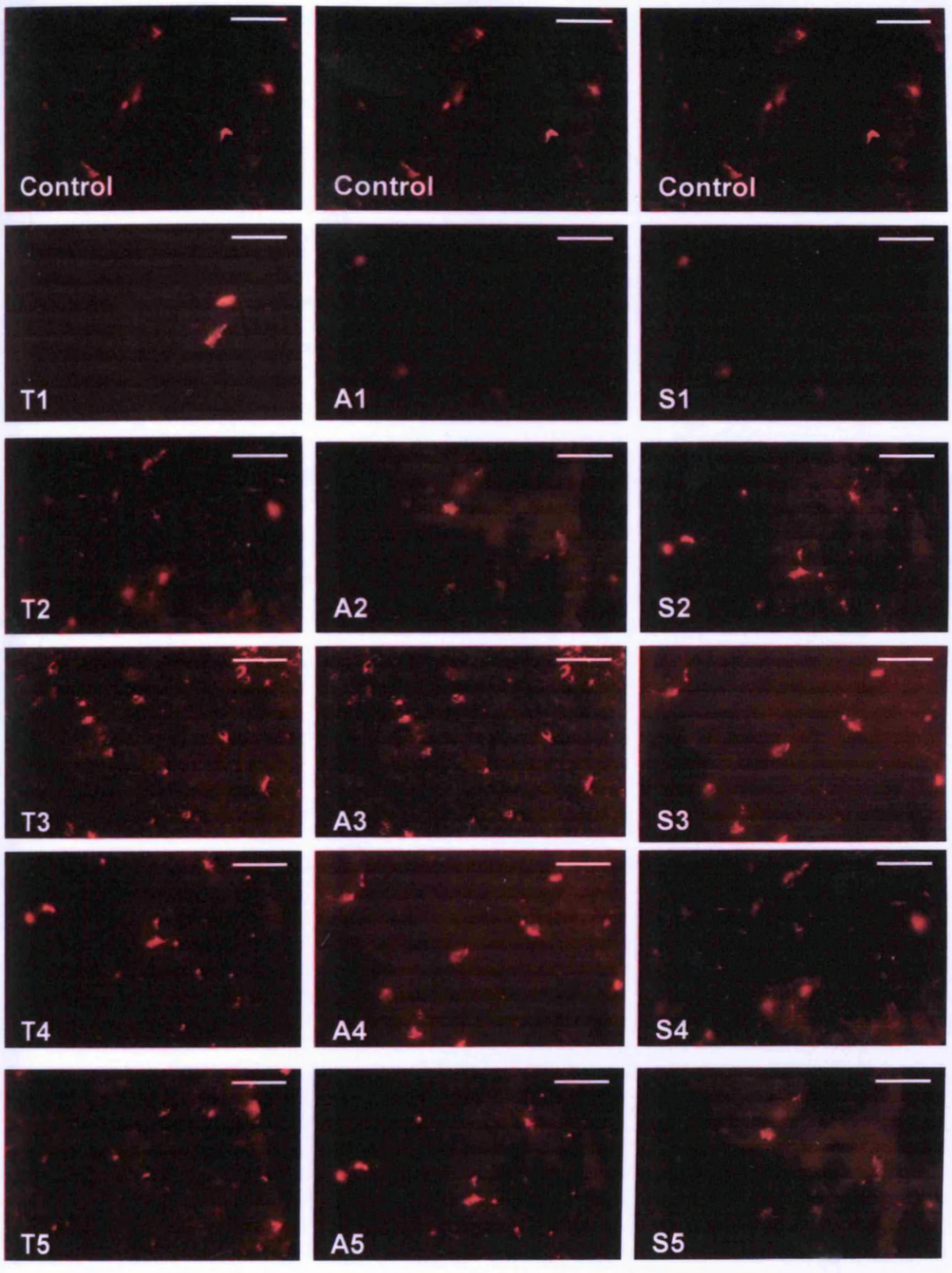

Figure 5.15 CD200 receptor immunolabelling at the optic nerve head *CD200 receptor immunolabelling (red) distribution was similar to the CD200 ligand. A representative example of optic nerve head labelling is shown in control images. Hypertension induced mild elevation of CD200 receptor labelling (T3 and A3). Increased immunoreactivity appeared as brighter labelling of amoeboid cells exemplified in images T3 and A3. White bar represents 50μm.*

CD200 receptor labelling as area under the IOP elevation/duration curve (Figure 5.15, S1 to S5).

5.3.5.2 Correlation of nerve head CD200 ligand and receptor with IOP elevation

CD200 ligand significantly elevated at T1 levels of ocular hypertension ($P<0.001$) (Table 5.1, Figures 5.16 and 5.17). However, CD200 receptor was significantly reduced ($P<0.001$) at this time point. These changes are supported by inter-group comparisons ($P<0.001$).

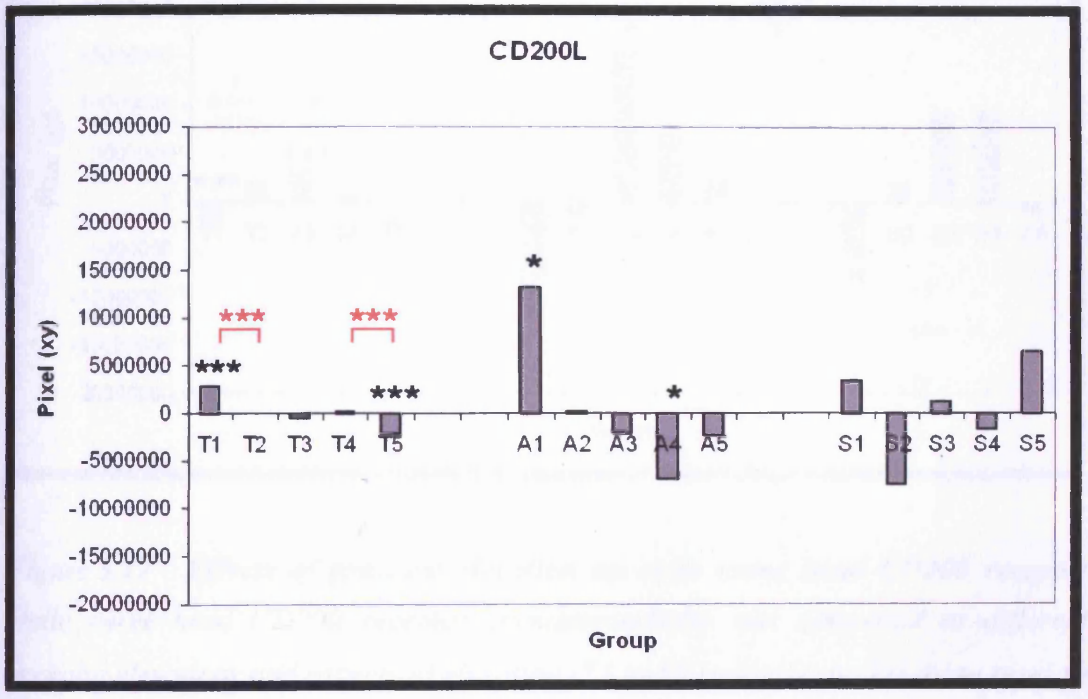

Figure 5.16 Effects of pressure elevation on optic nerve head CD200 ligand *Immunofluorescence varied with each group of elevated IOP (T1 to S5 inclusive, n=25). Differences shown via two sample T-testing between hypertensive and control are indicated by grey bars. Inter-group differences are shown in red. Significance was measured to a level of $P<0.01$ (*) and $P<0.001$ (***).*

Significant ($P<0.001$) upregulation of CD200 receptor also occurred transiently during T3, this was a significant elevation as compared to ipsilateral T4 data ($P<0.01$). At T5 significant reduction of CD200 ligand occurred. CD200 axis

alterations according to area under the IOP curve mirrored those of duration of pressure elevation. During A1, CD200 ligand was significantly elevated ($P<0.05$) as compared to controls, while the receptor was significantly reduced ($P<0.05$). Later, at T3 CD200 receptor became significantly increased, subsequently at higher area under the pressure curve (A4) the ligand became significantly reduced ($P<0.05$).

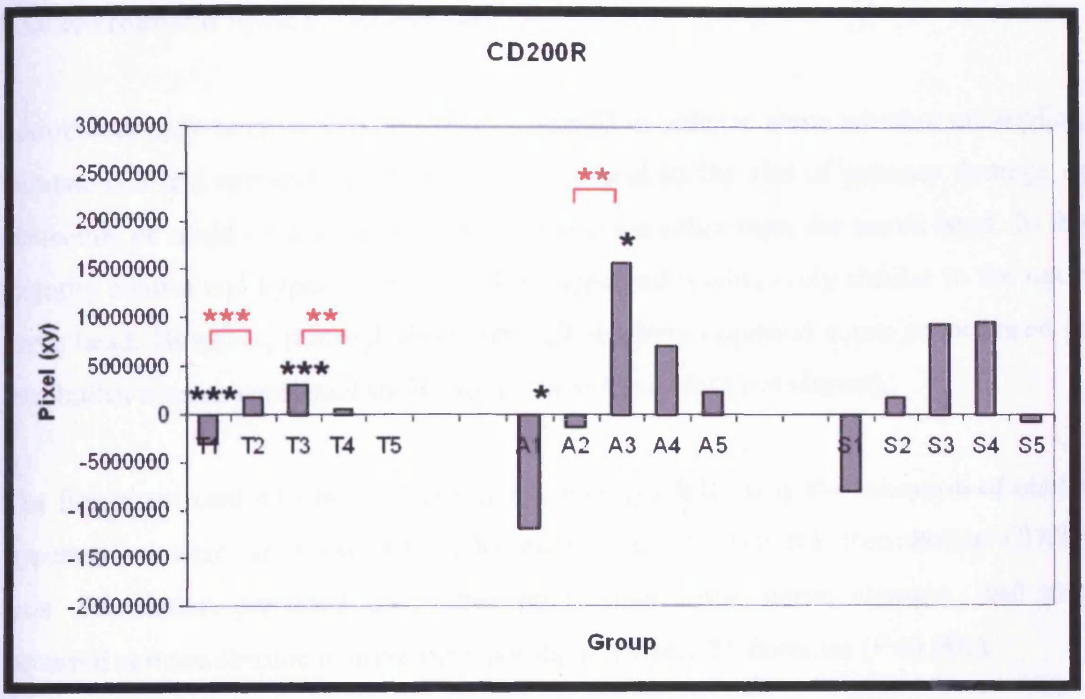

Figure 5.17 Effects of pressure elevation on optic nerve head CD200 receptor *Optic nerve head CD200 receptor immunoreactivity was compared at different pressure elevations and aspects of elevation (T1 to S5 inclusive, n=25) using pixel xy values (grey) generated by two-sample T-testing. Inter-group differences are shown in red. Significance was measured to a level of P<0.01 (*), P<0.05 (**), and P<0.001 (***).*

Grouping of hypertensive changes by level of standard deviation indicated that CD200 axis alterations were not specific to any particular range of standard deviation of IOP elevation produced in this study.

Significant alterations in the CD200 axis did not appear to correspond well with changes in the other markers used. Changes of CD200 ligand at T1 occurred while

CD45 positivity / myeloid cells were also elevated. At T3 CD200 receptor upregulation coincided with pan microglial (OX42) and macrophage (OX41) marker elevation. These associations were similar during area under the IOP curve associated CD200 axis changes. As CD200 axis alterations occur before microglial changes, the axis is implicated in the microglial response to injury.

5.3.6 Retrobulbar optic nerve changes

Retrobulbar optic nerve alterations were assessed in order to show whether microglial, immune cell and astrocyte alterations were typical to the site of primary damage in glaucoma, or could be extended to include regions other than the nerve head. In the majority control and hypertensive labelling appeared qualitatively similar to the optic nerve head. However, microglial/myloid cell markers appeared more pronounced in retrobulbar sites as compared to the optic nerve head (data not shown).

The first significant retrobulbar optic nerve changes following the initiation of ocular hypertension were elevation of CD200 receptor at T1 ($P<0.01$). Retrobulbar CD200 axis dissociation preceded any other retrobulbar optic nerve changes, and also occurred at more chronic disease time points of T4 and T5 duration ($P<0.001$).

MHCII and OX42 positive myeloid cells and microglia responded to ocular hypertension at the same time in retrobulbar and nerve head regions. Significant elevations of OX42 initiated at T2 ($P<0.01$), with lack of MHCII elevation. The retrobulbar OX42 response was maintained until T3 ($P<0.01$) indicating an attenuated microglial response similar to the optic nerve head. In the retrobulbar nerve OX41 positive macrophages significantly elevated in advance of the optic nerve head reaction with significant elevation at T2 and T3 ($P<0.001$).

OX33 positive B lymphocyte labelling was similar to the optic nerve head, without significant elevation. Retrobulbar CD45 did not correspond with optic nerve head labelling, indicating a lack of CD45 positivity throughout disease. GFAP was also not elevated at retrobulbar sites.

5.3.7 Co-localisation studies

Dual immunolabelling studies revealed little correlation between the cell markers probed. GFAP immunoreactivity identified cells within astroglial columns, similar to MHCII immunopositivity. However, the distribution patterns of these two markers were very different aside from this similar origin in the optic nerve head astroglial columns. GFAP labelling was far more widespread throughout the nerve, while MHCII was localised around cell nuclei. Lack of cross-reactivity was observed between GFAP and MHCII positive cells (Figure 5.18). This positive control indicates therefore that astrocytes and microglia are spatially and morphologically distinct in all regions of the optic nerve.

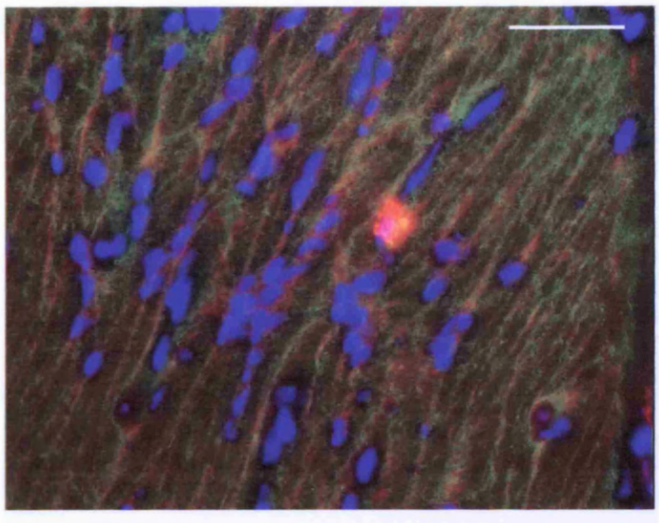

Figure 5.18 GFAP and MHCII colocalisation *Immunohistochemistry did not identify colocalisation of GFAP (green) and MHCII (red) in the optic nerve head. These two markers are clearly separated in distribution. Nuclei are labelled blue. White bar represents 50μm.*

Dual labelling studies of GFAP and CD200 ligand and receptor revealed lack of colocalisation of these markers (Figure 5.19). CD200 ligand and receptor did not appear to be expressed on astrocytes at the optic nerve head (Figure 5.19 and 5.20) or retrobulbar regions (not shown). It can be assumed therefore that the CD200 axis involves neuroglial optic nerve interactions that are microglia-neuron in nature.

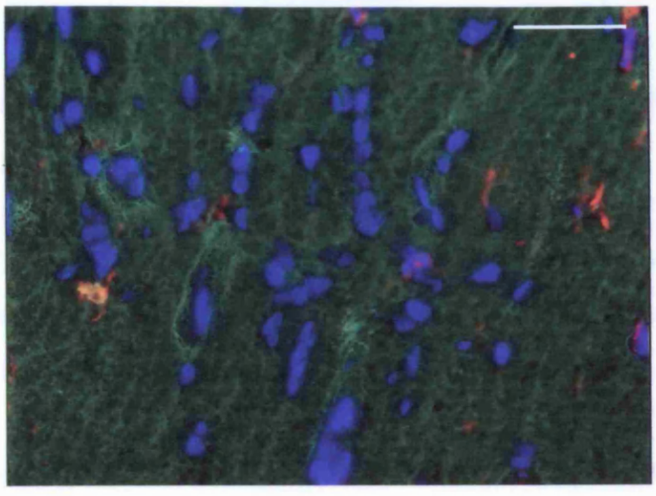

Figure 5.19 GFAP and CD200 Ligand colocalisation *CD200 ligand did not exhibit a similar labelling pattern to GFAP at the optic nerve head. Green labelling indicates GFAP, CD200 ligand is shown in red, while nuclei are labelled blue. White bar represents 50μm.*

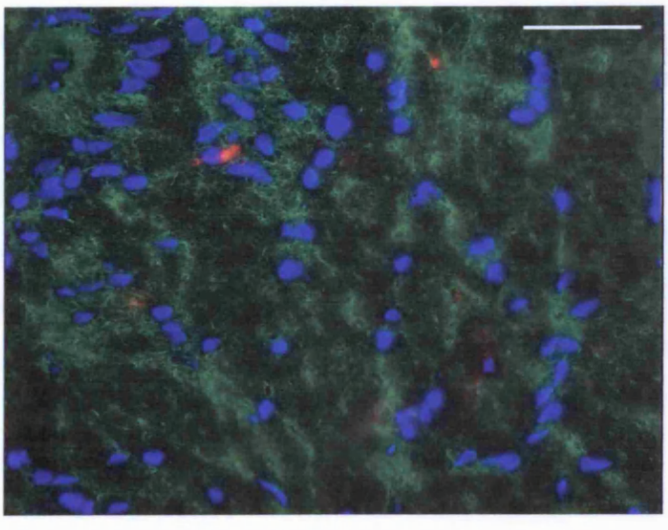

Figure 5.20 GFAP and CD200 Receptor colocalisation *CD200 receptor is shown in red, while a clearly different labelling pattern shown in green represents GFAP immunopositivity. Nuclei are labelled blue. White bar represents 50μm*

5.4 Discussion

Neuroglial interactions and regulation of the central immune response are critical in many neurodegenerative central nervous system disorders such as Alzheimer's and Parkinsons disease as well as glaucoma (Vickers *et al.*, 1995[1]; Vickers, 1997). Although glaucoma is not generally regarded as an inflammatory disease, it is becoming increasingly clear that immunomodulatory mechansisms are involved in the pathophysiology of retinal ganglion cell death.

Microglial activation has been reported in both human and experimental glaucoma but only the relationship of optic nerve head microglial activation to initiation of damage has been previously reported (Lam *et al.*, 2003[2]). The present report confirms the role of microglial activation in chronic experimental glaucoma.

5.4.1 Development of a method for immunolablling quantification

Quantification of immunolabelling using QWin to measure pixel intensity produced results that were difficult to interpret. Partially this was caused by the spread of fluorescence across 256 pixel intensities. Had this number of pixel intensities been reduced, perhaps by using a positive control to create a measurement scale, results would have been more precise and clearer. In current literature there is a deficit in clear fluorescence quantification methods, as well as the statistics used on fluorescent data. This study shows that Leica QWin can be used to measure raw fluorescence from images, however, the techniques developed could be refined further for clarity of results.

Parametric two-sample t-testing used the sum value generated by multiplying pixel number at each intensity by total pixel numbers, which were then compared for significance. This is particularly conservative in comparison with other techniques, such as non-parametric Kolmogorov-Smirnov testing, and therefore suitable to analyse data which can vary according to distribution in terms of pixel number and intensity. A large peak in pixel number at low intensity was normally present in the contralateral plot, while peaks in ipsilateral pixel number were much smaller, but at higher intensities. This means that the consistency of the data may have affected the

results using other tests. Subtraction of background fluorescence was a vital step and is commonly used to enhance clarity of results in fluorescence analysis.

5.4.2 Correlation of cellular marker upregulation with apoptosis data

In order to ascertain the importance of upregulation of cellular markers in the optic nerve head, it is necessary to compare immunofluorescence data with data on retinal ganglion cell apoptosis following ocular hypertension. Correlation of optic nerve markers with apoptotic rates described in Chapter IV, Figures 4.12, 4.13 and 4.14 should clarify the role optic nerve head components play during glaucomatous neurodegeneration.

5.4.2.1 GFAP levels and apoptosis

Initial significant elevation of GFAP coincided with significant elevation of RGC death. Later, reduction of GFAP to normotensive levels during T4 occurred following an RGC cumulative apoptotic rate of 13.78%. GFAP was further reduced during T5, as was the apoptotic rate. Astrocyte reactivity appeared to be involved in experimental glaucoma following initiation of RGC death. Reactivity was then reduced at more severe hypertensive levels when the cumulative apoptotic rate was high. Both low and high area under the IOP curve and standard deviation did not result in significant GFAP elevation. Apoptosis in these groups was raised to an intermediate level, indicating that GFAP elevation was primarily related to aspects of pressure elevation as opposed to the resultant apoptosis

5.4.2.2 OX33 levels and apoptosis

Lack of OX33 upregulation indicates that cumulative RGC apoptosis over time did not induce significant infiltration of OX33 positive peripheral cells following ocular hypertension as compared to controls.

5.4.2.3 MHCII levels and apoptosis

The RGC damage and cumulative apoptotic rate of up to 15.24% produced in this study were not sufficient to induce elevation of MHCII positivity in ipsilateral as compared to contralateral eyes.

5.4.2.4 CD45 levels and apoptosis

CD45 elevation occurred before apoptosis was significantly increased, and was consistently elevated at all apoptotic rates excluding the highest at T3 (5.38%). Similarly, these elevations correspond with the lowest rate of apoptosis during A1 (1.71%, $P<0.05$), as well as the highest during A4 (3.75%, $P<0.05$) and A5 (4.65%, $P<0.05$). The apoptotic rate varied without consistency during CD45 elevation with standard deviation of IOP elevation from 1.48% ($P<0.05$) at S2 to 4.24% ($P<0.05$) during S3. Consequently it appears unlikely that CD45 levels are involved with RGC apoptosis. Increased CD45 levels were correlated with the highest and lowest apoptotic rates.

5.4.2.5 OX42 levels and apoptosis

Significant elevation of OX42 corresponded with the initiation of significant levels of RGC apoptosis at 1.89%, which focused at inferior retinal regions. OX42 was consistently elevated until the cumulative apoptotic rate reached 13.78%. When the apoptotic rate became reduced at T5 (1.46%, $P<0.05$), OX42 also reduced to normotensive levels. This data indicates a direct link between microglial upregulation and apoptotic rate. Cumulative apoptosis had only reached 3.27% at A3 OX42 elevation. This shows that despite a low apoptotic rate, OX42 was induced as a function of increased area under the pressure curve. Cumulative apoptotic levels were greater in groups S3-S5, co-incident with OX42 upregulation, than in lower standard deviation of pressure elevation groups, indicating as association between OX42 level and apoptotic rate.

5.4.2.6 OX41 levels and apoptosis

OX41 upregulation at both T3 and T4 were associated with the highest apoptotic rate at 5.38% and 4.47%, respectively. This suggests that macrophages may be involved in the increased apoptotic rate present in the RGC layer following the induction of chronic experimental glaucoma. A3 OX41 upregulation corresponds with a moderate cumulative apoptotic rate of 7.76%, and a significant elevation in apoptosis specific to the inferior retina ($P<0.05$). Therefore, while increased duration of pressure elevation and a high apoptotic rate were likely to produce elevation of OX41 positivity, so was an intermediate area under the pressure curve combined with a moderate apoptotic rate. S4 OX41 elevations occurred after a cumulative apoptotic rate of 8.87%, with S5 reductions after 12.00% RGC apoptosis. Significantly elevated ($P<0.05$) apoptotic rate at these time points, though were at both moderate and high levels (3.13% and 5.28%, respectively). Inducation of OX41 upregulation, or increase of macrophagic cells at both intermediate and high apoptotic rates indicates that macrophages may not have directly increased the apoptotic rate of glaucomatous RGCs.

5.4.2.7 CD200 axis levels and apoptosis

Initial upregulation of CD200 ligand occurred at T1, preceding significant increase of apoptotic rate. However, reduction of CD200 receptor at T1 indicated loss of receptor preceding significant RGC loss. Upregulation of CD200 receptor also occurred at T3 when apoptosis peaked (5.38%). Meanwhile T5 CD200 ligand down-regulation occurred with a drop in the apoptotic rate to 1.46%, and a cumulative rate of 13.78%, again this implicates the CD200 axis in glaucomatous pathophysiology. A low apoptotic rate (1.71%) at A1 occurred with significant CD200 ligand elevation ($P<0.05$). Following a cumulative apoptotic rate of 3.93% at T3, CD200 receptor became significantly elevated ($P<0.01$). CD200 ligand then became reduced at the cumulative apoptotic rate of 7.76% (A4). This data is a good indication that the CD200 axis was involved in the induction of RGC death.

5.4.3 The astroglial reaction in ocular hypertension

GFAP is a molecular marker for astrocytes which is used extensively to identify these cells (Eclancher 1996). GFAP immunoreactivity within the optic nerve shows that astrocytes and their processes make up an extensive network, around and within the nerve fibre bundles. Other research indicates that in both animal models and human glaucoma, GFAP at the optic nerve head is augmented. The astroglial stress response incorporates prolonged metabolic and morphological changes, which produce a glial scar (Norenberg, 1994). GFAP upregulation may indicate glial scarring and prevention of axonal regeneration (Fawcett and Asher, 1999), or alternatively astrocytic promotion of neuronal plasticity and repair (Goss *et al.*, 1998; Ridet *et al.*, 1997).

GFAP elevation has been detected using ELISA and RT-PCR techniques in the glaucoma rat retina following 8 and 35 days of ocular hypertension. However, immunolabelling techniques do not detect any early changes in optic nerve head GFAP expression (Johnson *et al.*, 1996; Lam *et al.*, 2003b). Our study reinforces this immunolabelling data, and localises the time frame of optic nerve head glial activity during initiation at the onset of significant cell death, as well as at some more chronic disease stages. We can also conclude that astrocytic activation is not affected by conditions of particularly mild and severe pressure elevations or standard deviation. The astroglial response is not induced in the retrobulbar optic nerve following glaucoma, indicating that it does not have a role to play in clearing RGC debris.

GFAP elevation indicates that the astrocyte response to elevated IOP may be an essential and potential target for therapeutic intervention. Neuroprotective strategies for glaucoma treatment combined with targeting the glial scar may prevent further RGC damage and promote neuronal regeneration (Fawcett and Asher, 1999). Some neurons also express GFAP due to the close coupling between neural and glial elements in the nervous system (Ling, 1989), therefore neuroglial interactions at this level may also be involved in the disease.

5.4.4 Infiltration of peripheral immune cells

The central and peripheral immune systems share inseparable similarities. Lack of correlation between optic nerve head OX33 upregulation and macrophage (OX41) upregulation means that we can rule out the possibility that we are observing infiltration of blood-borne immune cells as well as activation of resident optic nerve microglia, as B lymphocyte immunoreactivity was not recorded. A lack of correlation between B lymphocyte infiltration and the microglia/macrophage response indicates that in the retrobulbar nerve neither peripheral cell proliferation or migration occur in concordance with microglial activation. Peripheral immune cells are not elevated in the retrobulbar nerve

Lack of OX33 positive peripheral B lymphocytes indicates integrity of the blood-retina–barrier (BRB) without peripapillary atrophy during disease. Normal lamina cribrosa, retrobulbar optic nerve and brain vascular endothelia contain tight junctions (Rapaport, 1976), with blood-brain barrier (BBB) markers. However, the prelaminar optic nerve lacks these characteristics, and represents a weak point in the BRB (Hofman *et al.*, 2001). B lymphocyte optic nerve entry through the prelaminar BRB may be exacerbated by recruitment signalling. It is possible that optic nerve head astrocytes and microglia, both elevated during experimental glaucoma, produce lymphoid chemokines, which attract peripheral immune cells including B lymphocytes (Columba-Cabezas *et al.*, 2003). However, it is unlikely that B-cell recruitment occurred in this glaucoma model, and BRB integrity was maintained.

We assume that lack of OX33 signal indicates correct function of the BRB, however, a lack of B cell response may indicate that peripheral B-lymphocytes invade optic nerve sites, but do not proliferate and mature into antibody secreting cells during glaucoma. CD40 signalling has been implicated in B lymphocyte maturation and proliferation as well as T cell differentiation during Alzheimer's disease (reviewed by Town *et al.*, 2001) and CD45-mediated inhibition of microglial activation (Tan *et al.*, 2000). Following B lymphocyte infiltration, interactions with microglia via the CD40 axis including CD45 may prevent lymphocyte proliferation and maturation. Interaction with this axis may account for upregulation of CD45 positivity following ocular hypertension.

As infiltration does not occur either during or subsequent to microglial proliferation/activation and the initiation of RGC death, B lymphocytes are unlikely to influence initiation of microglial responses or neurodegeneration during glaucoma. Also, immune cell responses can be ascribed to the resident cells of the CNS, rather that infiltrating peripheral immune cells.

5.4.5 Microglial activation during ocular hypertension

The microglial response to central nervous system injury typically occurs early in disease onset, and may be neuroprotective, or destructive (Soares *et al.*, 1995). This response is characterised by an alteration in cell morphology from a dendritic phenotype to an activated amoeboid state, when microglia become motile, macrophagic and proliferative. Under conditions of prelaminar BRB compromise resident active optic nerve microglia and peripheral macrophages are virtually indistinguishable by cell surface marker expression. However, activation of microglia has been measured throughout retinal and optic nerve pathologies using OX41 and OX42 as markers (Lam *et* al., 2003[2]; Raibon *et al.*, 2002; Rao *et* al., 2003; Wang *et al.*, 2000), as well as the more general immune cell markers MHCII and CD45 (Neufeld, 1999).

Increased CD45 and OX42 positive optic nerve head microglia indicated that microglial proliferation or recruitment occurs early during glaucoma, while activation occurs later. Simultaneous activation and proliferation or recruitment occurs early in retrobulbar regions. Microglial markers are upregulated in the initial stages of disease coincident with the onset of IOP induced cell death. Macrophages are induced later and the response is sustained. Microglia therefore may exacerbate the initiation of RGC death in glaucoma.

During microglial activation RGC apoptosis peaks, followed by a trough when activation abates. This is consistent with a role for optic nerve head microglia in glaucoma pathophysiology, which may be either degenerative or reparative (Lam *et al.*, 2003[2]; Wang *et al.*, 2000). Due to increased apoptosis during activation microglial exacerbation of cell death is likely. However, reduction of apoptosis immediately following microglial activation suggests that microglial-mediated neuroprotection

may also occur. Retrobulbar microglia are likely to share a similar role to their nerve head counterparts.

Increase of optic nerve head microglia before macrophages indicates that microglia may influence macrophage recruitment during glaucoma. However, this study establishes that macrophage-mediated neurodegeneration is a result of microglial activation and not the result of recruited peripheral cells. Recruited macrophages have been shown to increase axonal degeneration following nerve injury (Liu *et al.*, 2000). Macrophages can interact with myeloid and neuronal signal-regulatory proteins to induce neurotoxic NO production (Adams *et al.*, 1998) via a CD8 (OX8) mediated mechanism (Hirji *et al.*, 1997). NO has been implicated during RGC pathophysiology, however this is controversial. It is likely that resident activated microglia serve a similar role.

Activated microglia are potent regulators of the immune response themselves. Activation involves upregulation of immune-stimulatory molecules, such as tumour necrosis factor (TNF) α and interleukin (Il) 12. These molecules signal to other microglia and infiltrating cells to regulate, for example differentiation of T cells, and maturation of B-lymphocytes. T-cell differentiation into Th-1 and Th-2 types may influence autoimmunity and neuroprotect during glaucoma (Bakalash *et al.*, 2002). Microglial restriction of the Th-1 mediated immune response may be neuroprotective in experimental glaucoma.

The evidence suggests a role for microglia during initiation of RGC death. Microglial activation is likely to occur at high levels of RGC apoptosis, and therefore may have a role to play in cell death. This study was unable to ascertain whether this role is in active initiation of cell death, or in bystander damage. However, reduction of apoptosis following the microglial response may implicate microglia in neuroprotective pathways during glaucoma.

5.4.6 Neuorglial interactions during glaucoma

Neuroglial signalling via the CD200 axis appears to be involved during initiation of ocular hypertension induced nerve damage and modulation of optic nerve head microglia. Retrobulbar optic nerve CD200 ligand and receptor also appear to be involved during the initiation of disease, as well as at more chronic time points. During early disease stages, the CD200 receptor and ligand dissociate, and may upregulate subsequent microglial activation.

The present study confirms the role of the CD200 axis during the microglial interactions of glaucoma. Glaucoma, not normally thought of as an immune disease, may involve microglial cells. Regulation of these cells may also be involved in disease via the CD200 axis. The role of this axis in other disease models makes it an ideal candidate for investigation during glaucoma. For example, CD200 has a role in immunosupression during transplant rejection (Chen *et al.*, 1997; Gorczynski *et al.*, 1999; Gorczynski *et al.*, 1998) as well as susceptibility to collagen-induced arthritis and experimental allergic encephalomyelitis (Chen *et al.*, 1997; Gorczynski *et al.*, 1998; Hoek *et al.*, 2000). Numbers of retinal microglia are elevated and tonically activated in CD200-/- mice (Broderick *et al.*, 2002).

Our data supports a role for changes in the optic nerve head CD200 axis during the initiation of retinal ganglion cell death. Disruption of this axis is found at initial stages of disease in the optic nerve, and therefore may play an important role in neurodegeneration.

It is possible that due to RGC death RGC-expressed CD200 ligand is reduced during glaucoma. The free receptor may then bind an alternative ligand to signal microglial activation. The receptor-ligand interaction normally serves to prevent receptor-mediated intracellular signalling and microglial activation. However, binding of an alternative ligand may enhance this signalling and prevent immunological detection of CD200 receptor. The evidence from other studies suggests that this in not the case, and that free receptor induces microglial activation, however no other studies have examined alternative CD200 interactions in the optic nerve. It is unlikely that reduction of the type 1 cytokines IL-2 and IFN-γ, and an elevation of type-2

cytokines, IL-10 and IL-4 due to CD200 receptor activation (Gorczynski *et al.*, 1999; Gorczynski *et al.*, 2001) are involved in glaucoma pathophysiology.

It seems likely that microglial upregulation is important during initiation of retinal ganglion cell death and that microglial activation has a role during later stages. These observations may explain why clinical glaucoma can often progress despite reduction of IOP to normal levels, as microglia may continue to support neuronal damage. Other neuroglial signalling pathways are likely to be responsible for the initiation of microglial activation during glaucoma.

5.4.7 Conclusions

This study demonstrates the involvement of microglia, B lymphocytes and astrocytes in experimental glaucoma. The data support involvement of the CD200 axis in the initiation of glaucoma and in chronic regulation of microglial activation at the primary site of damage, the optic nerve head. Temporal specificity of the microglial response suggests that the role of microglia in optic nerve injury may involve more than removal of apoptotic debris.

Chapter VI
NOS during experimental glaucoma

6.1 Introduction

Nitric oxide (NO) is a vital component of brain physiology including synaptic plasticity, learning, memory, development and immunity. Excessive NO production can cause oxidative and nitrosative stress resulting in neurodegeneration and apoptosis (Frenzel J, Richter J, Eschrich K, 2005; McKinney *et al.*, 2004). However, inhibition of NO production can be both neurodestructive and neuroprotective (Chiou, 2001; Ciani, Baldinotti and Contestabile, 2001; Mohanakumar *et al.*, 2002; Neufeld, Sawada and Becker, 1999). Controversy surrounds NO function during neurodegenerative disease.

Human neuronal nitric oxide synthase (NOS1) is located in optic nerve head astrocytes (Neufeld *et al.*, 1997) and retinal ganglion cells (RGCs) (Neufeld *et al.*, 2000). Inducible NOS (NOS2) is not present (Neufeld *et al.*, 1997), while endothelial NOS (NOS3) localises to small prelaminar blood vessel endothelia (Neufeld *et al.*, 1997). In the rat optic nerve, NOS is additionally present in pericytes (NOS1) and vascular endothelia of large vessels (NOS3, Neufeld *et al.*, 1997). NOS1 has also been identified in human and rat neutrophils (Greenberg *et al.*, 1998), while active macrophages produce NOS2. These peripheral cells may also have a role in RGC survival.

The potential effects of NOS on the optic nerve microenvironment have led to investigations into their role in glaucoma. Generally, NOS3 activity is thought to enhance blood flow and neuroprotect through reduction of vasoconstriction during glaucoma. NOS1 may serve either a neuroprotective or neurodestructive function. Once activated, NOS2 is likely to produce cytotoxic amounts of NO originating from

active microglia and macrophages to exacerbate neuronal damage following nerve injury (reviewed by Neufeld, 2004).

In human glaucoma, some studies report upregulation of all NOS isoforms (Neufeld *et al.*, 1997), while others contradict this (Pang *et al.*, 2005). NOS1 expression has reportedly been elevated in astrocytes (Neufeld *et al.*, 1997). NOS3 localisation has been found to extend to astrocytes and all blood vessel endothelia (Neufeld *et al*, 1997), while NOS2 is also found in cells at the lamina cribrosa (Neufeld *et al.*, 1997). However, other reports suggest that NOS2 is not upregulated during glaucoma (Pang *et al.*, 2005).

Similar controversy is apparent from studies of NOS in experimental glaucoma. In experimental glaucoma via episcleral vein cautery, NOS2 expression is induced in rat optic nerve astrocytes, while NOS1 and NOS3 expression remained unaffected (Shareef *et al.*, 1999). The effects of vein cautery may include ischaemic damage, and NOS2 may be a by-product of this reaction, particularly as episcleral vessel drainage vessel sclerosis induces experimental glaucoma without induction of NOS2 expression (Pang *et al.*, 2005).

Retinal NO production is also experimentally elevated following induction of experimental glaucoma via laser photocoagulation of the trabecular meshwork (Siu *et al.*, 2002). Infiltrating peripheral macrophages, as well as resident glia and/or neurons, may influence NOS levels following glaucoma. Activated macrophages express NOS2 during immune regulation. Ligation of the macrophage signal regulatory protein OX41 can induce NO production (Adams *et al.*, 1998). This signalling pathway may have a role to play during disease, particularly autoimmunity.

The neuroprotective effects of NOS2 inhibition reduced RGC loss to one third of experimental glaucoma levels following episcleral vein cautery (Neufeld *et al.*, 1999). However, did not improve neurodegeneration following episcleral vessel sclerosis (Pang *et al*, 2005). NO has a role in potentiating anoxic or excitotoxic injury of RGCs in astrocyte cocultures (Morgan *et al.*, 1999). Endogenous NO may also be involved in the control of RGC repair. Evidence suggests that NO acts on neurogenesis to

facilitate differentiation into mature neurons (Moreno-Lopez *et al.*, 2004), the manipulation of which may potentially result in neuroprotective or even regenerative effects. However, the issue of which NOS pathways can be manipulated to produce predominant neuroprotection remains unresolved, as evidence is contradictory.

The role of NOS1 and NOS3 following episcleral drainage vessel sclerosis induced glaucoma has not been investigated, while contradictory evidence exists as to the involvement of NOS2 in glaucoma (Neufeld *et al.*, 1999; Pang *et al.*, 2005). In order to determine the role of NOS in glaucomatous RGC degeneration, the aim of this chapter was to determine if NOS expression (all three isoforms) differed between normal and hypertensive optic nerves. Aspects of ocular hypertension including duration of hypertension, area under the IOP elevation/duration curve, and standard deviation of IOP elevation will also be investigate in conjunction with NOS protein levels in order to dissect the exact role of NOS2 in the episcleral drainage vessel sclerosis model of glaucoma.

6.2 Methods

Methods used in this section are described in Chapter II, Section 2.7. Immunolabelling was used to localise optic nerve NOS isoforms. Similar to the immunolabelling results in Chapter V, no clear results were obtained in labelling for any NOS isoform until the optimisation of the final immunolabelling protocol, as detailed in Chapter II, Section 2.7, Figure 2.6.

Following IOP elevation, experimental animals were grouped for NOS labelling according to IOP elevation duration (T1-T5, total n=25), standard deviation of elevated IOP (S1-S5, total n=25) and area under the IOP versus time elevation curve (A1-A5 total n=25, Table 6.1). Normal and hypertensive rat optic nerve heads (n=5 of each, for each category within each group), were subjected to immunolabelling procedures twice each for NOS1, 2, and 3.

Labelling was quantified using Leica Qfluoro software, followed by data analysis in Microsoft Excel. Qualitative observations of NOS immunofluorescence in the

normotensive and hypertensive optic nerves were identified. Statistical comparisons were made between levels of NOS-related immunofluorescence in contralateral (normotensive) and ipsilateral (hypertensive) optic nerves, following subtraction of control immunofluorescence from each. The sum of each pixel intensity multiplied by the number of pixels at that intensity (pixel xy) was calculated and compared between contralateral and ipsilateral optic nerves. Results describe the outcome of statistical comparisons using two-sample, two-way T-tests for analysis.

Table 6.1 Experimental animal groupings according to pressure elevations

Level	GROUP "T" **Duration of IOP elevation (days)**	GROUP "A" **Area under the pressure curve (mmHg)**	GROUP "S" **Standard deviation**
1	1 – 7 **(n=10)**	0.9 – 22.7 **(n=8)**	0 - 1.511 **(n=6)**
2	11 – 19 **(n=19)**	24.3 – 96.8 **(n=16)**	1.52 - 2.96 **(n=13)**
3	20 - 27 **(n=11)**	97.2 – 151.1 **(n=15)**	3.20 - 3.75 **(n=9)**
4	33 – 46 **(n=10)**	165.3 – 256.1 **(n=8)**	3.81 - 5.57 **(n=16)**
5	47 - 65 **(n=7)**	271.9 – 469.3 **(n=10)**	6.02 - 12.76 **(n=12)**

6.3 Results

6.3.1 NOS1

6.3.1.1 Distribution of NOS1 in the normal and ocular hypertensive nerve

NOS1-immunorelated fluorescence was present in control optic nerve head (Figure 6.1). In normal optic nerve heads, labelling could be found in cell processes, likely to be those of astrocytes. Retrobulbar optic nerve demonstrated similar NOS1 labelling.

After T1 durations of pressure elevation NOS1 labelling appeared brighter than controls, but did not alter in distribution (Figure 6.1, T1). Labelling became increasingly sharper at T2 and T3, also with increasing localisation to well-defined astrocytic processes (Figure 6.1, T2 and T3). Upregulation of NOS1 was demonstrated by the presence of few NOS1 weakly positive axons with intense,

widespread and sharp labelling of what appeared to be many highly organised astrocytic elements of the nerve by T4 (Figure 6.1, T4). At this stage, NOS1 labelling appeared to correlate well with the distribution and staining for GFAP (Chapter V, Section 5.3.1.1). At T5 NOS1 labelling appeared more diffuse than at any other time, and was reduced in intensity as compared to T3 and T4.

Group A1 demonstrated a less dendritic NOS1 labelling pattern than controls, while labelling intensity appeared similar (Figure 6.1, Control and A1). Sharp labelling of cellular processes was regained during A2, and intensity appeared slightly increased as compared to controls and A1 (Figure 6.1, Control, A1 and A2). NOS1 labelling intensity appeared increased throughout A3 to A5 (Figure 6.1, A3, A4 and A5). Groups A3 and A4 demonstrated sharp labelling likely to be localised to astrocytic processes (Figure 6.1, A3 and A4), while group A5 labelling was more diffuse, and similar, though more intense, to control NOS1 labelling (Figure 6.1, Control and A5).

Standard deviation of IOP elevation initially appeared to have similar effects on NOS1 positivity to area under the pressure curve (Figure 6.1, S1 and S2). Intensity increased with increasing standard deviation (Figure 6.1, S1-S4), while the highest deviations demonstrated a labelling intensity similar to controls (Figure 6.1, Control and S5). NOS1 labelling distribution also altered with increasing standard deviation of IOP elevation. S1 and S2 labelling distributions were similar to A1 and A2 (Figure 6.1, S1, S2, A1 and A2). A more diffuse labelling pattern was observed in S3 (Figure 6.1, S3), while S4 labelling was sharper than all other "S" groups (Figure 6.1, S4). During S5, labelling returned to a diffuse pattern.

Following hypertension alterations in NOS1 labelling were varied. Significant changes in NOS1 with varying duration of ocular hypertension are summarised in Table 6.1. The effects of area under the pressure curve and standard deviation of pressure elevation (Table 6.2) on all NOS isoforms are as tabulated.

Marker	Duration of pressure elevation					Area under IOP curve					Standard deviation of pressure elevation				
	T1	T2	T3	T4	T5	A1	A2	A3	A4	A5	S1	S2	S3	S4	S5
NOS1			++	+++				+	+	+				++	
NOS2	+		++	+++	+	+		+		++		+	+	+++	+
NOS3															
NOS1			++	+	---										
NOS2			+++												
NOS3			-												

Table 6.2 ***Summary of the effects of IOP elevation on NOS*** *Alterations in each of the three NOS enzymes are shown with changing duration of elevated IOP, area under the IOP curve and standard deviation of pressure elevation (n=25). Two-sample T-tests were used to compare control and ocular hypertensive nerve pixel (xy) for significant increases in fluorescence distributions. Significant elevations were tested at levels of P<0.05 (+), P<0.01 (++) and P<0.001 (+++), significant reductions in pixel (xy) are indicated by "-" (P<0.05), "—" (P<0.01), and "---" (P<0.001).*

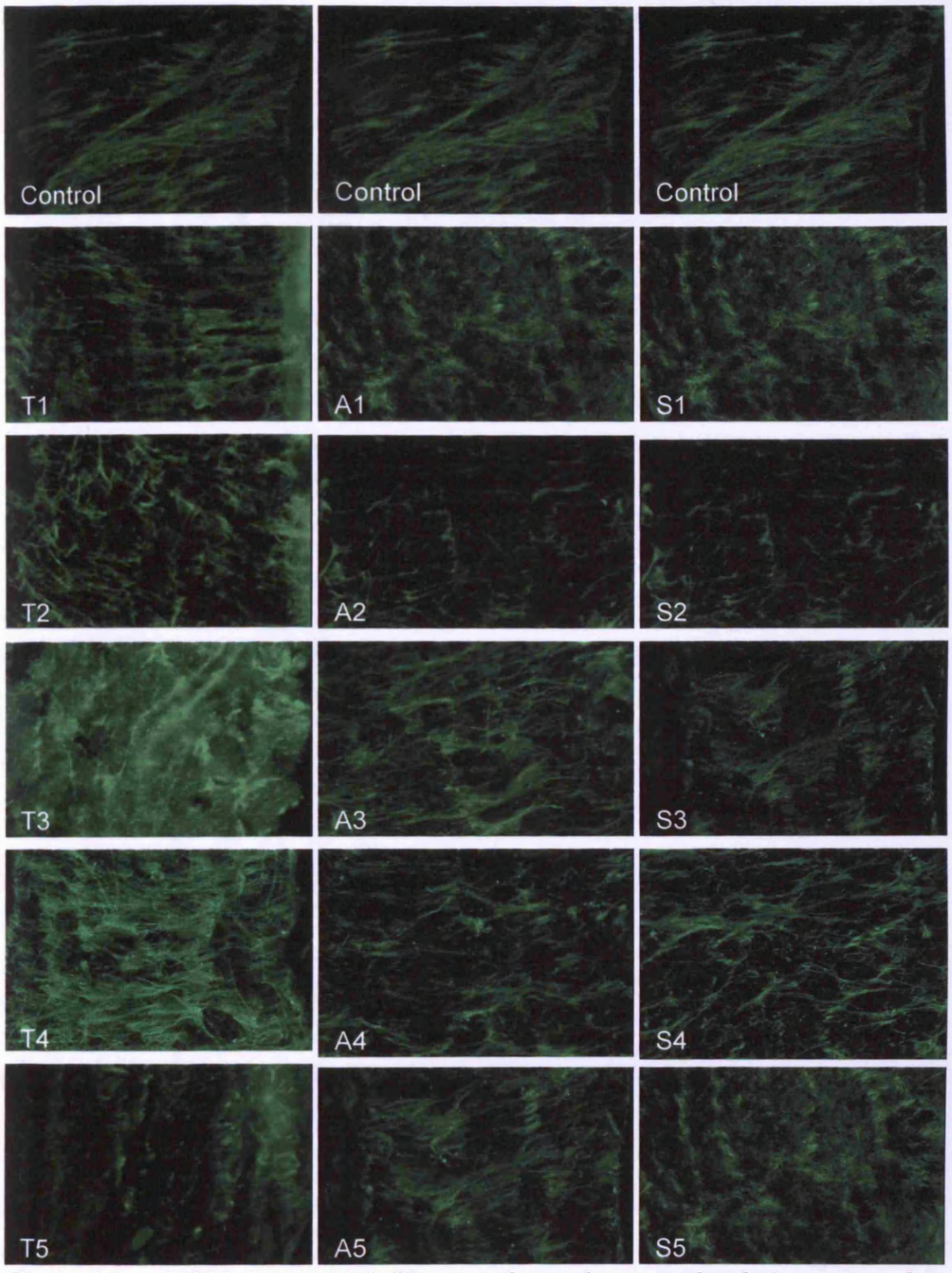

Figure 6.1 NOS1 immunolabelling at the optic nerve head *As compared to controls NOS1 immunoreactivity occasionally appeared elevated following ocular hypertension (T1 to T5, A2 to A5 and S2 to S5). NOS1 positivity occasionally appeared axonal (T4) and, similar to GFAP, labelling within and between glial columns (T4). Single colour images are shown with NOS1 labelled green, scale bar indicates 50 μm.*

6.3.1.2 Alterations in optic nerve head NOS1 pixel (xy) with elevation of IOP

Statistical analysis of pixel (xy) supported qualitative observations of NOS1 immunofluourescence labelling. Significant elevations of optic nerve head NOS1, as determined by sum of (pixel xy), were recorded at T3 ($P<0.01$) and T4 ($P<0.001$), following a minimum of 20 days IOP elevation (Table 6.1 and Figure 6.2). However, during the most chronic disease stage (T5) NOS1 labelling had reduced to a level that was not significantly different from normotensive controls.

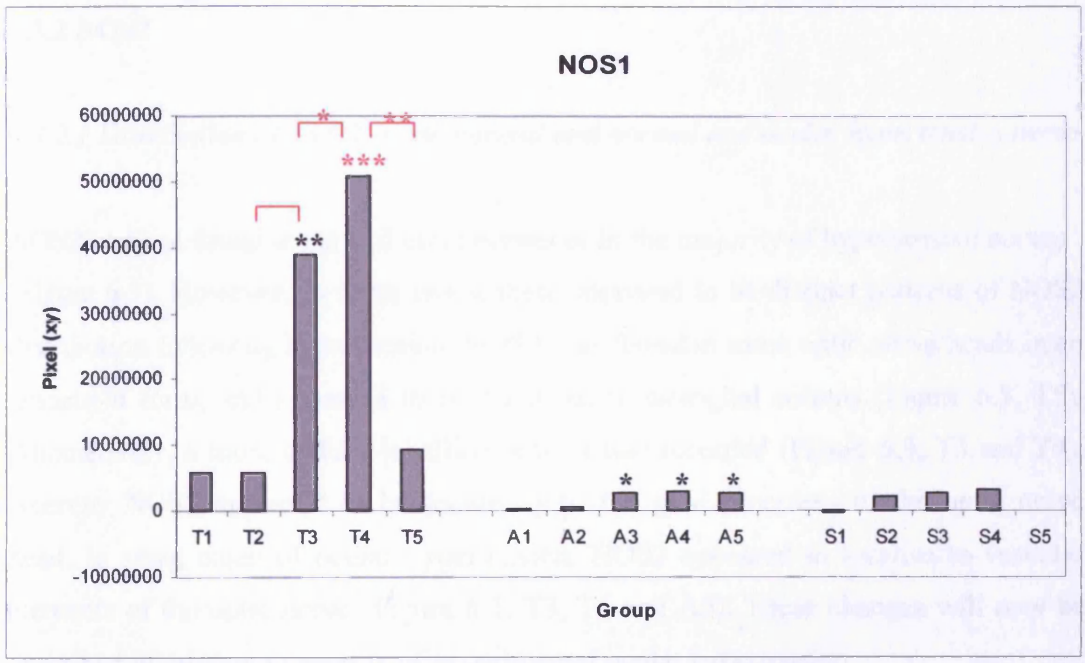

Figure 6.2 Effects of pressure elevation on optic nerve head NOS1 *Grey bars show the difference between contralateral control and ipsilateral ocular hypertensive nerve sum of pixel (xy) values, grouped according to increasing duration of ocular hypertension (T1 to T5), area under the IOP curve (A1 to A5) and standard deviation of IOP elevation (S1 to S5). Significant differences were measured to levels of $P< 0.05$ (*), $P<0.01$ (**) and $P<0.001$ (***) using a two-sample T-test. Significant differences between ocular hypertensive groups were measured similarly and are indicated by brackets above with significance levels shown as stars.*

Area under the IOP curve also produced significant elevation of NOS1 in groups A3 ($P<0.05$), A4 ($P<0.05$) and A5 ($P<0.05$, Figure 6.2). A combination of longer duration

and magnitude of elevated pressure (represented in high area under the pressure curve) was therefore more likely to induce a NOS1 response during ocular hypertension, while at low area under the pressure curve, NOS1 did not appear to be activated.

Increased standard deviation of pressure elevation produced a significant elevation of NOS1 labelling in group S4 only (Figure 6.2). Both lower and the highest standard deviations did not result in increase of NOS1 levels.

6.3.2 NOS2

6.3.2.1 Distribution of NOS2 in the normal and normal and ocular hypertensive nerve

NOS2 was not found in control optic nerves or in the majority of hypertensive nerves (Figure 6.3). However, in some cases, there appeared to be distinct patterns of NOS2 distribution following hypertension. NOS2 was found in some optic nerve heads in an amoeboid form, and appeared to be localised to astroglial colums (Figure 6.3, T5). Alternatively, a more diffuse labelling pattern was recorded (Figure 6.3, T3 and T4), whereby NOS2 appeared to be localising to the glial processes of the optic nerve head. In some cases of ocular hypertension, NOS2 appeared to localise to vascular elements of the optic nerve (Figure 6.3, T3, T4 and A5). These changes will now be described in relation to aspects of experimental ocular hypertension.

At T1, elevated IOP appeared to induce increased and diffuse NOS2 positive labelling in the optic nerve head as compared to controls (Figure 6.3, Control and T1). Labelling was less diffuse by T2, and slightly increased as compared to controls (Figure 6.3, Control and T2). The labelling pattern of NOS2 during T2 appeared to localise to around the vasculature. T3 labelling was further increased in intensity as compared to controls, T1 and T2 and appeared to be much sharper (Figure 6.3, Control, T1-T3). At this stage NOS2 positivity as akin to the distribution of the optic nerve vasculature. By T4 NOS2 reaches its brightest levels. Labelling appeared very sharp, with a similar distribution to GFAP immunopositivity (Figure 6.3, T4). Small hollow circles of labelling were also seen at T4, which may indicate NOS2 positivity

at optic nerve head microvessels (Figure 6.3, T4). By T5 a completely different labelling pattern was found. Sharply labelled NOS2 positive dots, localised in a similar manner to astroglial columns were found throughout the optic nerve head (Figure 6.3, T5).

NOS2 labelling also appeared slightly altered with area under the IOP duration/elevation curve, however, changes in labelling intensity were more subtle than for duration of IOP elevation, and alterations in intensity were not pronounced (Figure 6.3 A1 to A5). At A1, a few fairly thick sharply defined cellular processes were NOS2-positive (Figure 6.3, A1). A2 labelling was similar to A1, however, small hollow circles of NOS2 positivity could also be found (Figure 6.3, A1 and A2). NOS2 positive labelling at A3 also identified clearly defined cellular processes more numerous than A1 and A2, but with a low labelling intensity (Figure 6.3, A3). Immunopositivity also appeared to localise to RGC axons at this stage. A4 NOS2 positivity was as described for A2, while at A5 labelling was more fragmented, and in some cases appeared axonal (Figure 6.3, A5).

Standard deviation of pressure elevation also affected the labelling pattern of NOS2 (Figure 6.3, S1 to S5). At low standard deviations (Figure 6.3, S1) few thick cellular processes were identified as weakly NOS2 positive. At standard deviations represented by groups S2 and S3 NOS2 positivity similarly identified few cellular processes, and also localised to a hollow rounded pattern, which might be expected of vascular labelling (Figure 6.3, S2 and S3). More processes appeared labelled under S4 conditions, while a low labelling intensity was maintained (Figure 6.3, S4), while S5 optic nerves appeared to contain few thick NOS2 positive processes, similar to S1 labelling, as well as some NOS2 positive RGC axons (Figure 6.3, S1 and S5).

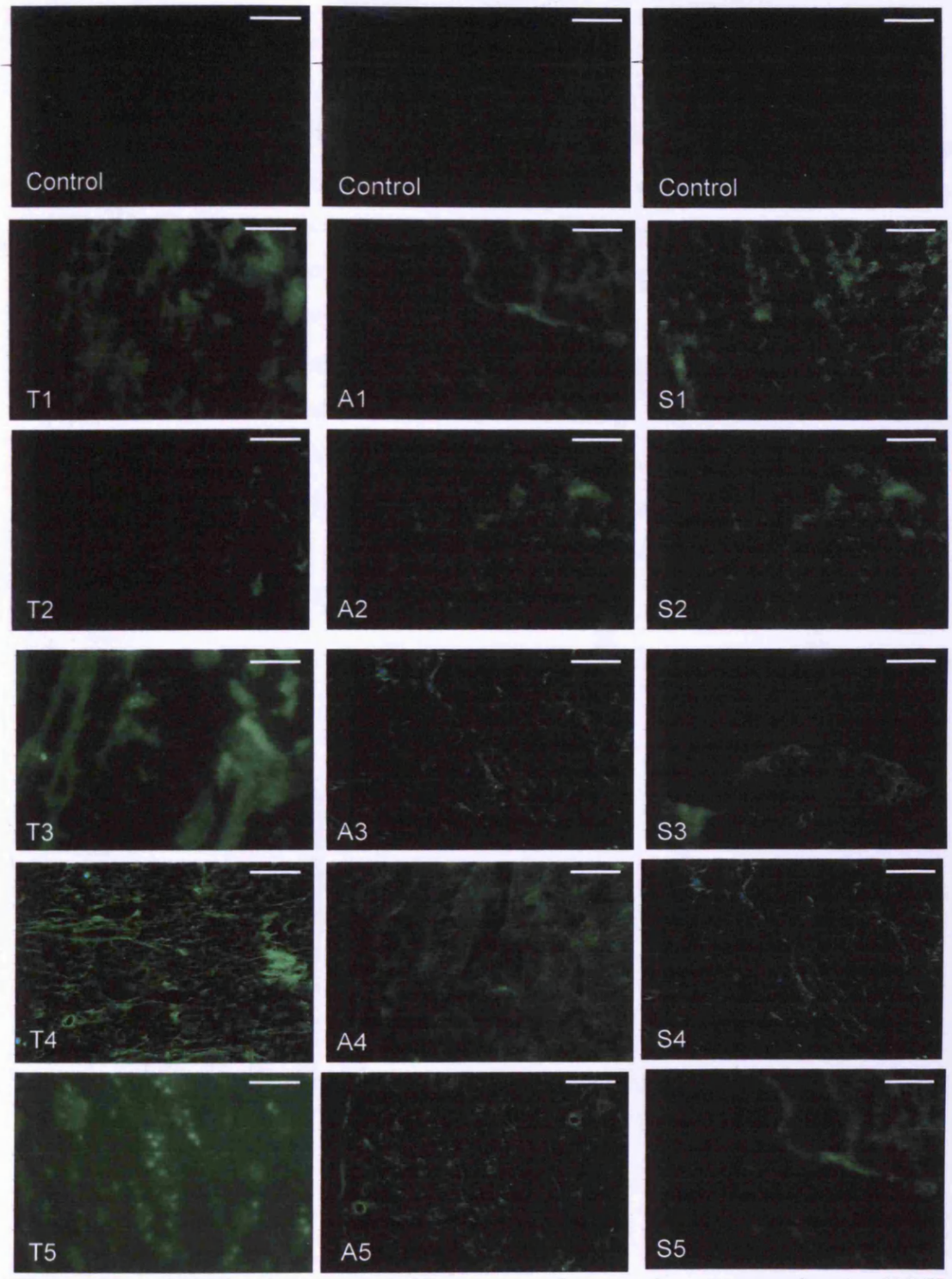

Figure 6.3 NOS2 immunolabelling at the optic nerve head *NOS2 immunoreactivity was rarely detectable in control normotensive optic nerves. Following hypertension, labelling was varied in nature and appeared localised to glial columns (T3), and/orlocalised to amoeboid-shaped cells (T5). Localisation to the processes of small microglia-shaped cells appeared under mild conditions of hypertenstion (A1, A2, S3). Single colour images are shown. White bar equals 50μm.*

6.3.2.2 Changes in optic nerve head NOS2 pixel (xy) with ocular hypertension

Significant NOS2 elevation occurred at stage T1 of ocular hypertension, during initial disease ($P<0.05$, Table 6.2 and Figure 6.4, T1). NOS2 was not significantly elevated during T2. Significant elevation of NOS2 returned during T3 ($P<0.01$) and T4 ($P<0.001$), and corresponded with significant NOS1 elevation. It is possible that NOS1 and NOS2 responses during these time points were similar. However, unlike the NOS1 response, NOS2 remained significantly ($P<0.05$) elevated during T5. NOS2 elevation at this chronic stage was not as pronounced as during T3 and T4, indicating that the NOS2 response may have been reducing or ending at more chronic disease states No significant changes in levels of NOS expression were identified between hypertension optic nerves in groups S1-S5 or A1-A5, or when compared to contralateral normotensive optic nerves.

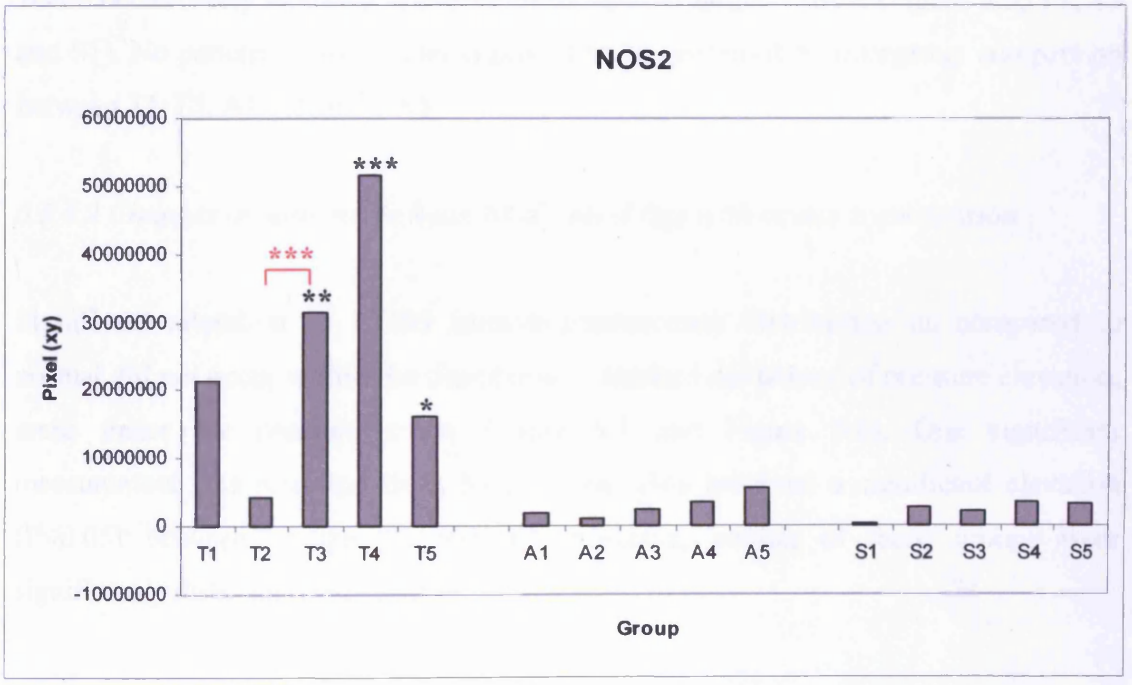

Figure 6.4 Effects of pressure elevation on optic nerve head NOS2 *The effects of elevating IOP on optic nerve head NOS expression in terms of duration (T1 to T5), area under the IOP curve (A1 to A5) and standard deviation (S1 to S5) are shown. Grey bars indicate the sum of (pixel xy). Data were compared using two-sample T-testing, at significance levels of $P<0.05$ (*), $P<0.01$ (**) and $P<0.001$ (***). Significance is shown as for Figure 6.3.*

6.3.3 NOS3

6.3.3.1 NOS3 distribution in the normal and hypertensive optic nerve

NOS3 sparsely labelled the optic nerve head (Figure 6.5). Only a low level of labelling could be distinguished (Figure 6.5, Control). This labelling appeared vascular in nature, and localised in mainly oval or rounded bands. These bands appeared to be made up from smaller bands radiating outwards from what was likely to be the vessel lumen (Figure 6.3, Control).

Following hypertension, NOS3 rarely appeared to be elevated, and a similar distribution pattern was often seen. NOS3 labelling occasionally appeared increased and/or fragmented around smaller vessels (Figure 6.5, T3, A1, A3, S1, S4 and S5). While occasionally labelling appeared to localise to larger vessels (Figure 6.5, T1, T3 and S1). No pattern of alterations appeared to be produced by intergroup comparison between T1-T5, A1-A5 or S1-S5.

6.3.3.2 Changes in optic nerve head NOS3 pixel (xy) with ocular hypertension

Significant alteration of NOS3 immunofluorescence distribution as compared to normal did not occur within the time points, standard deviations of pressure elevation, areas under the pressure curve (Table 6.1 and Figure 6.6). One significant measurement was recorded from NOS3 data. This involved a significant elevation ($P<0.05$) between groups T2 and T3; however, neither of these groups were significantly different from controls.

6.3.4 Retrobulbar NOS during ocular hypertension

In order to determine whether the upregulation of NOS is typical of the optic nerve head and therefore likely to be involved in processes other than microglial scavenging NOS, nerve head and retrobulbar regions were compared.

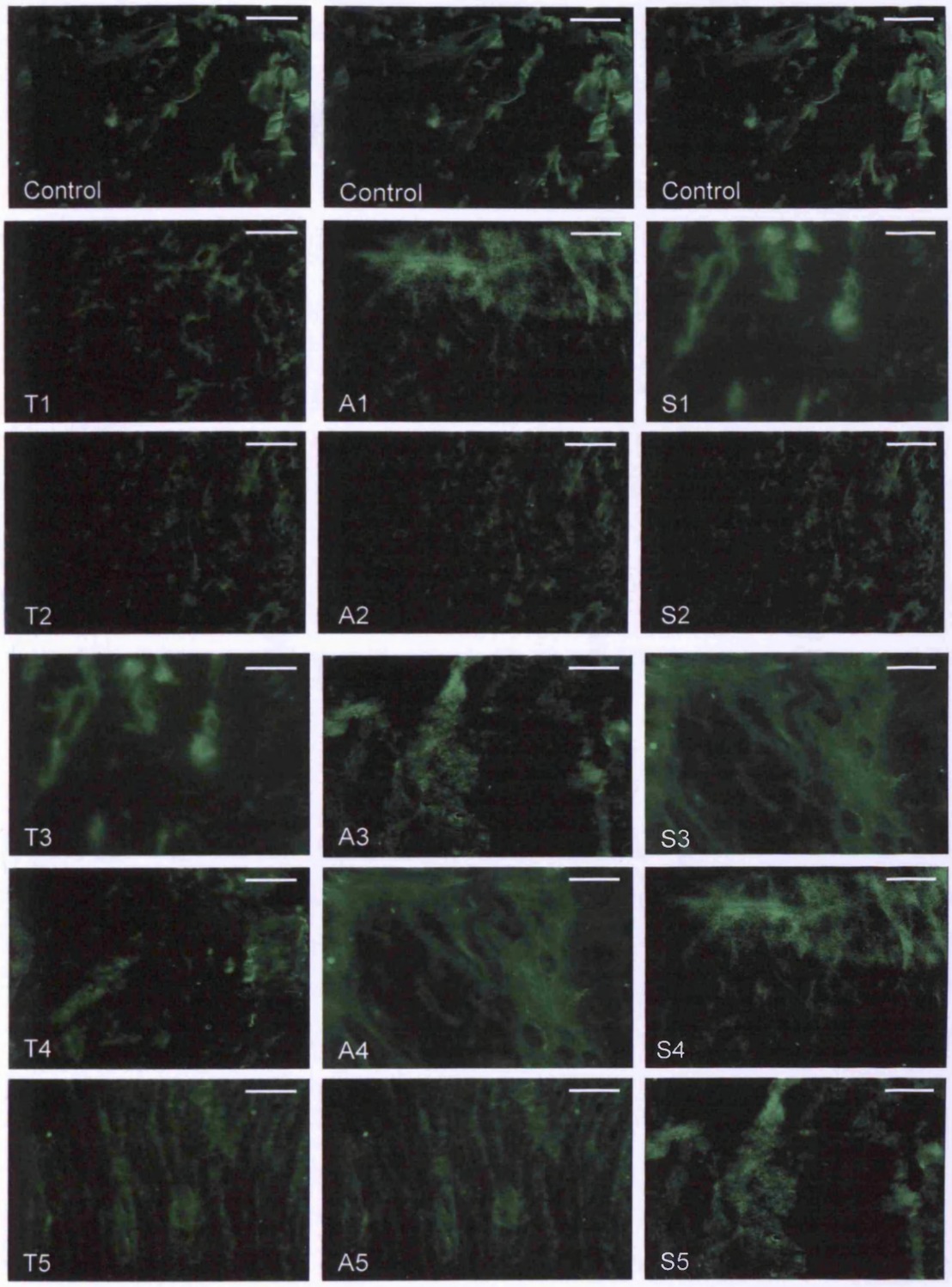

Figure 6.5 NOS3 immunolabelling at the optic nerve head *NOS3 appeared to surround vessels in the optic nerve (all images, green labelling). Following hypertension NOS3 rarely appeared upregulated (T1 to T5, A1 to A5 and S1 to S5). Upregulation appeared as brighter more fragmented labelling and elevated area of label, indicating proliferation of blood vessels as well as damage by hypertension). Bar represents 50μm.*

NOS2 was found in some retrobulbar optic nerves in a globular form. It was found that, similar to nerve head regions, NOS1 and NOS2 did significantly upregulate ($P<0.001$), while NOS3 did not ($P<0.05$). Upregulation of these NOS isoforms was only found during T4 time points (data not shown).

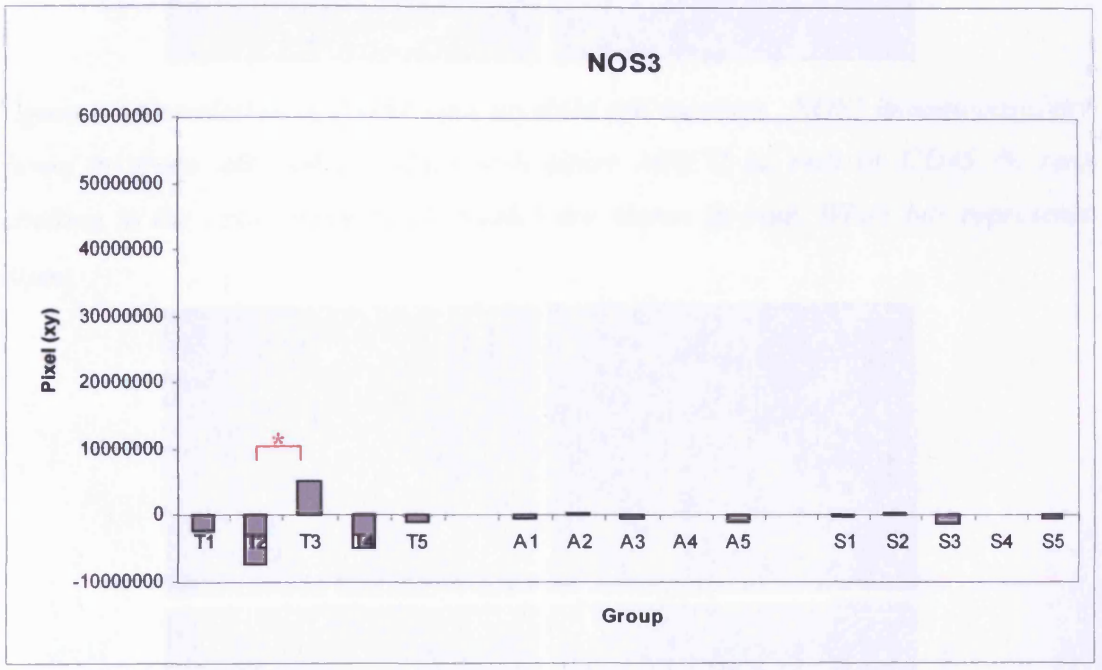

Figure 6.6 Effects of pressure elevation on optic nerve head NOS3 *The fluorescence intensity distribution of NOS3 in normal and hypertensive optic nerve heads was compared using pixel (xy) values and a two-sample T-test. Significant alteration in the level of NOS3 enzyme following hypertension as compared to control was not found ($P>0.05$). One significant elevation in sum of pixel (xy) was found when comparing between groups T2 and T3($P<0.05$).*

6.3.5 NOS isoform and cell marker co-localisation

NOS1 did not qualitatively correlate well with the myeloid cell markers MHCII and CD45 Figure 6.7 a and b). NOS2 immunolabelling corresponded to microglial and immune cell labelling better than NOS1 labelling. NOS2 was occasionally associated with CD45 and MHCII in the ipsilateral optic nerve (Figure 6.8, a and b). NOS2 also occasionally colocalised with the pan-microglial marker OX42 (Figure 6.8, d) or the components of the CD200 axis (Figure 6.8, d and e) However, NOS2 was not frequently associated with OX41 (Figure 6.8, c).

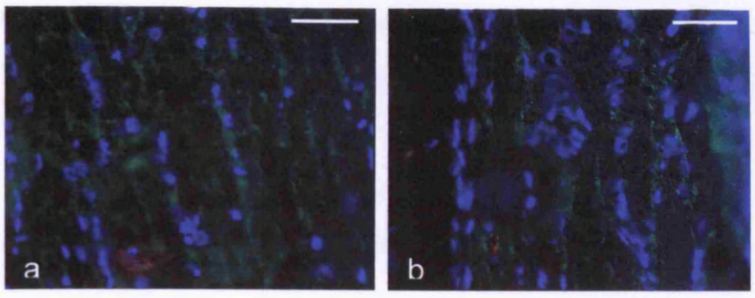

Figure 6.7 Correlation of NOS1 with myeloid cell markers *NOS1 immunopositivity shown in green, did not correlate with either MHCII (a, red) or CD45 (b, red) labelling in the optic nerve head. Nuclei are shown in blue. White bar represents 50μm.*

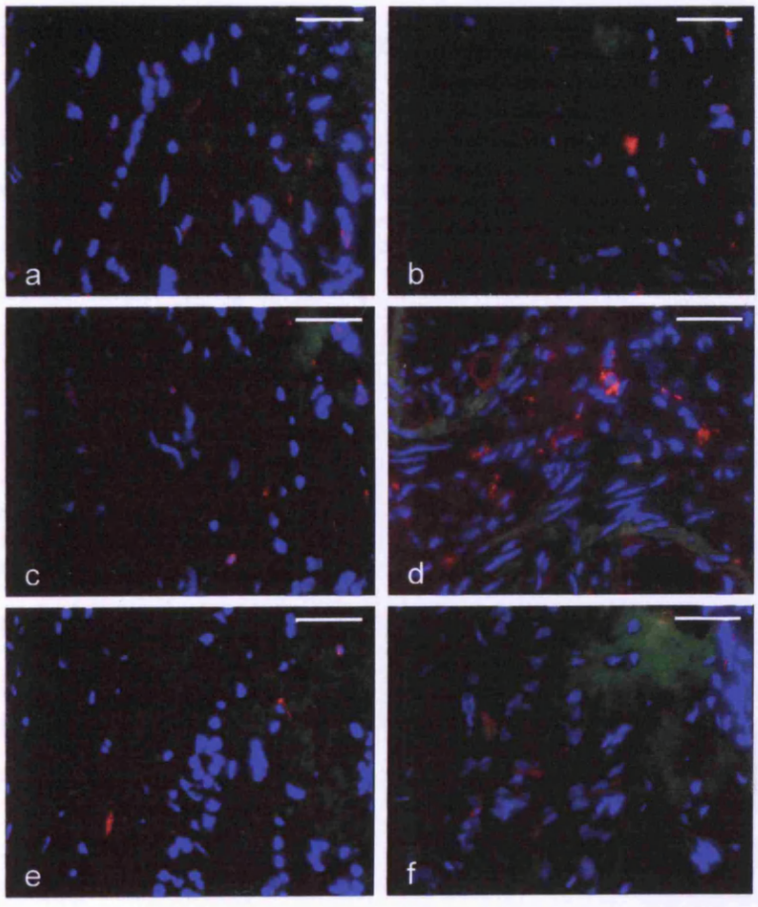

Figure 6.8 NOS2 colocalisation with microglial and immune cell markers *Hypertension induced upregulation of NOS2 immunopositivity (green, all images). NOS2 labelling correlated well with CD45 (a, red), MHCII (b, red), and OX41 (c, red). OX42 (d, red), CD200 ligand (e, red) and CD200 receptor (f, red) labelling did not correlate with NOS2 positivity. Nuclei are labelled blue, white bar represents 50μm.*

There did not appear to be any correlation between glial markers and NOS3 immunoreactivity in any optic nerve region (not shown). The labelling pattern of GFAP positivity did not resemble NOS3 immunoreactivity (not shown).

6.4 Discussion

The role of NOS in glaucoma has been controversial for some time. This study indicated that NOS2 is likely to have a role during initiation of glaucomatous optic nerve degeneration. It is possible that secondary neurodegeneration is partially mediated by NOS1 in the degenerating optic nerve. NOS3 does not appear to be involved in glaucomatous RGC death.

Previous studies have examined the extent and localisation of NOS at the optic nerve head of normal and glaucomatous rat and human tissue (Neufeld 1997; Neufeld 2000). However, no literature is available with regard to NOS alterations with duration of ocular hypertension in experimental glaucoma, including the model used in this study. The present study then confirms and extends the time frame of NOS upregulation in a reliable glaucoma model according to aspect of pressure elevation (duration of elevation and standard deviation of IOP elevation) which have not previously been investigated.

6.4.1 The distribution of optic nerve NOS isoforms

NOS distribution in the present study correlates well with the findings of others. Both human and experimental animals show a similar sparse distribution of NOS in the normal optic nerve in glia and capillaries (Shareef *et al.*, 1999). In these areas native NOS upregulates in some studies of experimental glaucoma (Shareef, *et al.*, 1999), similar to the human disease (Neufeld *et al.*, 1997). Consequently the mechanisms of NOS-induced cell death are likely to be similar in both human glaucoma and animal models of the disease.

However in contradiction to the present study, lack of NOS2 upregulation has previously been determined at 35 days duration of varying severity of ocular

hypertension in the episcleral drainage vessel sclerosis glaucoma model (Pang *et al.*, 2005). At this duration of hypertension no NOS2 activation was reported in the optic nerve, via several different techniques used to detect protein and mRNA. In contrast the present study identified NOS2 upregulation following episcleral drainage vessel sclerosis, and has both determined and extended the time scale of NOS elevation following episcleral drainage vessel sclerosis. Most importantly, the present study specifies the attributes of IOP in terms of duration, area under the IOP elevation/duration curve and standard deviation of IOP elevation that are likely to cause this NOS2 elevation.

6.4.2 Correlation of NOS with RGC death

6.4.2.1 Correlation of NOS1 labelling with apoptotic cell death

NOS1 was significantly upregulated only following the initiation of RGC death in glaucoma (at T2), and during more intermediate disease stages where apoptosis occurred at its highest rate of 5.38% (T3) and 4.47% (T4, Chapter VI, Figure 4.12 and Figure 6.2). At T5 RGC apoptosis was reduced to a rate of 1.46% above control levels. This indicates that the NOS1 response may have been transient during intermediate stages of disease, and was not involved during the crucial initiation and chronic disease states.

NOS1 elevation appeared to occur following significant elevation of RGC death, which occurred during both A1 and A2. However, NOS1 elevation did not occur until apoptotic rates reached 3.27% above normal in A3, and continued during the 3.75% and 4.65% increases found in A4 and A5, when apoptotic rates were at their highest.

For standard deviation of IOP elevation groups, NOS1 elevation did not occur before initiation of RGC death, and was present only after a cumulative increase in apoptotic rate of 8.87%.

NOS1 became elevated only following the initiation of RGC apoptosis, and therefore was not involved during initiation of RGC death. Intermediate duration of

hypertension and standard deviation of pressure elevation as well as intermediate to chronic are under the pressure curve, were therefore critical factors in elevation of NOS1 levels.

6.4.2.2 Correlation of NOS2 labelling and apoptotic cell death

Significant NOS2 elevation occurred at stage T1 of ocular hypertension ($P<0.05$, Table 6.2 and Figure 6.4, T1), before significant increase of RGC death (apoptosis was increased by only 2.04%). Significant elevation of NOS2 was also recorded from the peak of apoptotic rate with duration of pressure elevation (T3) until the experimental end-point. Low, intermediate and high levels of apoptosis in area under the IOP duration/elevation curve were associated with NOS2 upregulation (A1, A3 and A5). NOS2 elevation was associated with all levels of apoptosis with standard deviation of IOP elevation, excluding S1, as significant elevation occurred throughout groups S2 to S5.

6.4.2.3 Correlation of NOS3 labelling and apoptotic cell death

Significant alteration of NOS3 immunofluorescence distribution as compared to normal did not occur within the levels of cell death tested (Table 6.1 and Figure 6.6). Lack of an alteration in NOS3 labelling indicates that this isoform was not involved in neuroprotection, degeneration or apoptosis of the RGC under these conditions.

6.4.3 Correlation of NOS upregulation with other markers in the optic nerve

In order to determine the likely origin of NOS following experimental glaucoma it is necessary to compare and contrast the labelling of other optic nerve markers used in this study (Chapter V) with labelling of NOS. This comparison may also give some clues as to the mechanisms underlying NOS, macro, and microglial regulation following experimental glaucoma.

6.4.3.1 NOS1

Significant elevation of NOS1 as duration of IOP elevation increased corresponded with significant elevations of GFAP ($P<0.05$), CD200R ($P<0.001$), OX41 ($P<0.001$) and OX42 ($P<0.001$) at T3. This indicates that during T3, NOS1 elevation may have resulted from increased levels of resident macrophages (OX41) and/or microglia (OX42) as well as disruption of the CD200 axis (CD200R). It is also possible at this stage that NOS1 was astrocytic in origin. However, during NOS1 elevation at T4 only CD45 ($P<0.001$), MHCII ($P<0.05$) and OX41 ($P<0.01$) were significantly changed. Therefore the NOS1 response at T3 and T4 appeared to differ. The T4 response was more likely to involve activated microglia implicated most importantly by OX41 elevation. It was possible to distinguish the NOS1 response from peripheral macrophages (OX41) and macrophagic microglia (OX41) at both T3 and T4 as a consequence of lack of OX33 upregulation. These findings were supported both by statistical analysis of immunolabelled pixel intensities and qualitative observations of immunofluorescent images.

Significant elevation of NOS1 during A3 corresponded with markers as in T3. During A4 the CD200L ($P<0.05$) together with CD45 ($P<0.001$) became significantly elevated with NOS1 indicating a slight alteration in the aetiology of the response as compared to A3. During A5 NOS1 elevation corresponded with significant elevation of OX33 ($P<0.05$), as well as CD45. At A5 therefore, NOS1 may be microglial or invading peripheral cell in origin.

S4 NOS1 elevation only corresponded with elevation of microglial and macroglial markers (CD45, $P<0.05$; OX41, $P<0.05$; OX42, $P<0.05$), with no indication of peripheral cell infiltration. NOS1 produced during S4 is most likely to derive from activated optic nerve microglia.

In the majority NOS1 elevation was attributed to elevated astroglial and microglial activity. In some disease states it was not possible to determine whether NOS1 was microglial in nature, or originated from astrocytic cells.

6.4.3.2 NOS2

During significant increase of NOS2 at T1, microglia/immune cells (CD45, $P<0.05$) and components of the CD200 axis ($P<0.001$) were also significantly upregulated. It is likely therefore that T1 NOS2 upregulation occurred in microglia as either a consequence or a cause of CD200 axis disruption. Correlation of immunofluorescence data indicates that NOS2 elevations at T3 occurred as a result of microglial or astroglial activation, while at T4 NOS2 may have originated from resident microglial cells.

6.4.3.3 NOS3

As NOS3 upregulation was not recorded, it was unlikely that this isoform of NOS was involved in either the glial or vascular reaction to experimental ocular hypertension. This indicates that perivascular microglial, involved in maintaining vascular tone, did not react to increase blood flow by way of NOS3 upregulation, and consequent NO release. The vascular system does therefore not appear to be involved in glaucomatous neurodegeneration or neuroprotection.

6.4.4 The role of NOS during initiation of RG cell death

Normally NO acts as a neurotransmitter, participating in interastrocytic and astrocyte-neuron interactions (reviewed by Guix *et al.*, 2005). Microglia also express NOS once activated, as part of the immune response (reviewed by Minghetti *et al*, 2005). However, at high concentrations NO is toxic through the induction of apoptosis, and may exacerbate cell death via necrosis (Borutaite and Brown, 2003).

NOS2 is often used as a marker for active microglia due to the upregulation of this isoform during the immune response. It is this form of the enzyme that is the most likely candidate for the over expression of neurotoxic levels of NO due to the inducible nature of its activity. NOS1 and NOS3 are less likely to be involved in this type of response due to a constitutive activity maintained by calcium signalling.

However, it is also possible that these isoforms become misregulated during disease to over produce NO resulting in either a protective or degenerative response.

The evidence presented here indicates that the NOS2 isoform is involved in the initiation of retinal ganglion cell death during experimental glaucoma, in concurrence with a disruption of microglial cell response (Chapter V). Therefore RGC death during glaucoma is likely to be initiated by separate factors such as mechanical damage to axons at the level of the lamina cribrosa, as well as disruption of microglial signalling axes and NOS2 upregulation.

This is the first study to indicate a role for NOS at early stages of disease, while there are many studies that support NOS2 and microglial activation following the induction of RGC death. The role of NOS in chronic glaucoma is less secure.

NOS3 is unlikely to have a role during the initiation of cell death, due to a lack of upregulation of this isoform during experimental glaucoma. However, the fragmented pattern of NOS3 observed following ocular hypertension might indicate disruption of the vasculature, or proliferation of small vessels as a result of ocular hypertension.

6.4.5 The role of NOS during secondary degeneration

During chronic glaucoma both human and animal studies have implicated NOS upregulation as a potential mediator of continued RGC death. Upregulation of NO has also been shown following chronic glaucoma (35 days) produced via laser treatment of the trabecular meshwork (Siu *et al.*, 2002). Indications are that all NOS isoforms are upregulated in the optic nerve following similar treatment (Shareef *et al.*, 1999).

The present study confirms that at chronic IOP elevations associated with high levels of RGC apoptosis, NOS1 and NOS2 expression is upregulated at the optic nerve head. This is consistent with a role for these isoforms in RGC death, as well as in the ensuing immune response.

6.4.5.1 NOS1

NOS1 upregulation represents a point of neuroglial as well as glia-glia communication, which may become compromised during glaucoma. NOS1 upregulation in chronic glaucoma may be as a direct result of RGC stress. The source of this enzyme is likely to be RGCs, as well as astrocytes (Shareef *et al.*, 1999), although microglia and other immune cells are also implicated. Over activation of this constitutive enzyme is likely to result in excessive NO, which has a deleterious effect on RGC survival through induction of apoptosis. However, the effects of NOS1 upregulation are unlikely to be as severe as those of NOS2, as this isoform has the capacity to generate huge amounts of NO.

6.4.5.2 NOS2

NOS2 is not expressed under normal conditions. However, this inducible form of the enzyme produces high amounts of NO following activation, which is used during the immune response to destroy neighbouring cells (Lyons *et al.*, 1992). NOS2 is likely to be over expressed by microglial cells in the optic nerve both during initiation, and as part of the immune response, following elevated IOP-induced RGC degeneration. Consequently, over expression may further influence RGC apoptosis via the provision of an environment conducive to cell death.

6.4.5.3 NOS3

The present study indicates that NOS3 does not have a role to play in glaucoma pathophysiology. However it has been hypothesised that NOS3 may play a vital role in vasospasm during glaucoma. Evidence suggests that initiation of glaucomatous damage at the lamina cribrosa (Hayreh, 1979) may include vasospasm resulting in ischaemia, as well as mechanical crushing of axons and diminished neurotrophic support. Astrocytes are closely coupled to vascular elements at the nerve head; consequently it is likely that alteration of vascular NOS3 affects the function of astrocytes in glaucoma. This function may include glial proliferation and activation at the optic nerve head, increasing production of extracellular matrix (ECM) molecules,

and further affecting IOP Agapova *et al.*, 2001; Hernandez *et al.*, 2000; Hernandez *et al.*, 2002). Effects of NOS3 on RGCs may be mediated through both increase of ocular blood flow, as well as astroglial responses. However, following episcleral vein sclerosis, a NOS3 response is not elicited, indicating that neither glia nor vasulature are affected by NOS3 during glaucoma in this model.

6.4.5.4 Potential pathways of secondary neurodegeneration

NO production, by NOS isoforms, are likely to affect RGC survival via similar mechanisms. However the present study shows that only NOS1 and NOS2 produced NO are likely to influence RGC survival during glaucoma.

It is likely that following production NO exerts effects on the cell through control of transcription factors (Hausladen *et al.*, 1996; Peng *et al.*, 1995; Zeiher *et al.*, 1995), interactions with heme proteins or enzymes with iron-sulphur clusters (Stamler, 1994), as well as reacting with oxygen radicals to alter the redox balance (Chun *et al.*, 1995).

These reactions may combine to produce the high rate of cell death associated with NOS upregulation in the present study. However, due to the immediate reduction in RGC loss subsequent to NOS upregulation, it is also possible that these reactions are responsible for alleviating RGC damage and promoting survival.

6.4.6 Controversial NOS upregulation.

With many animal models available for the experimental induction of glaucoma, fundamental differences between these models are likely to influence disease pathophysiology. This is particularly apparent with regard to NOS in glaucoma. NOS upregulation remained uncorrelated with cell death (apoptosis) until the present study.

The present study showed how NOS isoforms 1 and 2, but not 3 were upregulated during chronic disease stages at high levels of RGC apoptosis. Others have reported upregulation of all NOS isoforms following vein cautery (Shareef *et al.*, 1999).

However, more recent publications suggest that NOS2 is not upregulated following 35 days of experimental glaucoma (Pang, *et al.*, 2005), while in the present study NOS upregulation was limited to 20 to 46 days, vein cautery upregulated NOS from 4 days to 3 months post-induction of ocular hypertension.

It is possible that the high levels of pressure elevation (1.6 times control pressure) in comparison to the present study were the cause of this discrepancy (Shareef *et al.*, 1999). As we have shown that NOS upregulation is dependent upon elevated pressure duration rather than degree or deviation, it is also possible that inter-model variations account for differences in NOS expression. This is supported by a lack of endothelial NOS upregulation in the present study, while following vein cautery this isoform is elevated (Shareef *et al.*, 1999). The vein cautery model of glaucoma may produce undesirable effects on the ocular blood system through lack of drainage. These effects may include elevation of NOS3.

6.4.6.1 The episcleral drainage vessel sclerosis model and NOS2 upregulation

Current published data from the episcleral drainage vessel sclerosis model indicates that NOS2 upregulation does not occur following induction of ocular hypertension (Pang *et al.*, 2005), which is contradictory to many glaucoma studies of both animals (Shareef *et al.*, 1999) and man (Neufeld *et al*, 1997). This data appears to be solid by virtue of a multitude of techniques used to verify a lack of NOS2 protein and mRNA, including immunohistochemistry, gene expression profiling and quantitative PCR (Pang *et al.*, 2005). Also, inhibition of NOS2 did not improve RGC degeneration following experimental glaucoma (Pang *et al.*, 2005). However, there are also several apparent limitations of the design of this study.

Pang *et al.* (2005) examined NOS2 only at 35 days of ocular hypertension. Despite production of a complete range of damage by this duration of ocular hypertension, actual glaucoma progression is not only dependent upon degree, but also duration of ocular hypertension. A severe oversight by Pang *et al.* (2005) is the potential fluctuation of NOS2 expression with duration of hypertension, and not solely with degree of damage (reviewed by Morrison *et al.*, 2005). The present study, however

examines NOS2 upregulation as a function of several aspects of the elevated IOP, and therefore, despite a relative lack of impressive techniques provides a better indication of the true involvement of NOS2 in experimental glaucoma.

According to the optic nerve damage scale developed by Johnson *et al.* (1997) Pang *et al.* (2005) produced optic nerves with a range of damage from those unaffected by sclerosis, to those with severe damage in all areas of the nerve. Although this scale is a good indicator of RGC damage, it does not enable correlation of NOS2 alterations with RGC death, which is essential in any model of ocular hypertension. The present study was able to ascertain actual RGC death levels, and subsequently the effects of NOS2 can be accurately associated with apoptosis, and not merely nerve damage.

6.4.6.2 Origins of hypertensive optic nerve head NOS

Data presented here indicated that the cells responsible for NOS1 and NOS2 upregulation are likely to be resident microglia and astrocytes. Astrocytic data is supported by studies using the vein cautery model of glaucoma where NOS2 induction occurs in active astrocytes of the optic nerve (Shareef *et al.*, 1999). However, no attempts have been made to correlate NOS upregulation with microglial upregulation in the vein cautery model, despite the potential importance of the immune reaction of these cells in pathophysiology.

6.4.7 Neuroprotection mediated by NOS inhibition

Immunohistochemical evidence has shown upregulation of all isoforms of the NOS enzyme, implicating NOS upregulation, and consequently NO production in RGC death during glaucoma. NOS upregulation in support astrocytes, closely associated with the nerve fibre bundles, is thought to be neurodestructive, whilst the NOS activity found in glia coupled to vascular epithelia is neuroprotective (Shareef *et al.*, 1999). Consequently, NOS inhibition should be effective in the prevention of neurodegeneration during experimental glaucoma, as well as in treatment of the human disease.

Neufeld *et al.*, (1999) have shown that RGC loss can be alleviated during glaucoma through direct inhibition of NOS2 activity via aminoguanidine, while this is contradicted by more recent studies (Pang *et al.*, 2005). However, the transient nature of NOS upregulation indicates a limited role in secondary neurodegeneration. Neuroprotection mediated by NOS inhibition may only be effective in neuroprotection under certain disease conditions or stages of progression, as the present study shows the transient nature of NOS1 and NOS2 upregulation. Therefore the efficacy of this treatment for the alleviation of RGC loss is questionable. Combining NOS inhibition with other pharmacological agents, perhaps CD200 ligand peptide or other microglial inhibitors may be more effective in reducing glaucomatous cell loss.

6.4.8 Conclusions

This study clarifies the role of NOS during glaucoma. NOS2 may have a role during the initiation of RGC death in glaucoma. Both NOS1 and NOS2 are likely to be involved in glaucomatous secondary degeneration. These isoforms are produced through immune-mediated responses of resident microglia and/or astrocytes. Specific production of cytotoxins is vital to optic nerve pathophysiology, and may assist in future development of pharmacological intervention of secondary degeneration, which in combination therapies could also alleviate IOP elevation.

Chapter VII
General discussion

7.1 Summary of findings

This study showed the progressive development, through logical manipulations, of a rodent model of ocular hypertension, based on the model used by Morrison *et al.* (1995). The model was used to generate and maintain mild experimental glaucoma representative of the human condition. Principle findings generated from this model are described in full in Table 7.1.

Novel techniques of silver staining and neurofilament labelling, normally applied to detect other systemic forms of neurodegeneration, were used for the first time to monitor glaucomatous neurodegeneration. Neurofilament labelling of RGCs appeared reduced following glaucoma, while silver staining of axonal degeneration was increased. These novel methods were used in conjunction with the more established techniques of qualitative light and electron microscopy of the optic nerve, which supported neurodegeneration following the induction of ocular hypertension.

As well as neurodegeneration, apoptotic cell death was also examined in the retina. Results of both TUNEL and active caspase 3 labelling of the retinal ganglion cell layer were used to support the hypothesis that the degeneration observed in the optic nerve occurred in conjunction with RGC death.

Fluctuation, duration and degree of IOP elevation all appeared to play a vital role in RGC cell survival. Mild intraocular pressure (IOP) elevation resulted in consistent, but moderate RGC cell death with a late onset (11 days post-induction of hypertension). Cell death was at lower levels during chronic late disease stages (day 47-65). Apoptotic cell death appeared to correlate in a linear manner with increased area under the IOP elevation/duration curve, indicating that death is dependent upon a

combination of duration and magnitude of hypertension. The effects of IOP fluctuation varied; however, the highest standard deviation of IOP elevation (6.02-12.76) produced the greatest apoptotic rate of any IOP variable. Therefore a combination of these IOP variables is likely to affect rate of cell death following elevation of IOP, with perhaps the most important of these being IOP fluctuation.

This study provided evidence that both astrocytes and microglia are involved in the pathological processes of glaucomatous neurodegeneration and RGC death. Initial glaucomatous alterations in the optic nerve head included dissociation of the CD200 axis, together with upregulation of NOS2 (suggesting microglial activation) before the onset of significant levels of apoptosis.

Disengagement of the microglial regulatory system, the CD200 axis, before initiation of RGC apoptosis indicates that microglial changes may play a part in initiating RGC apoptosis. Subsequently microglia proliferate, indicated by increased OX42 labelling at T2, coincident with the onset of IOP-induced retinal ganglion cell (RGC) apoptosis Similarly, astrocytic reactivity and proliferation occurred at the same point in disease progression as onset of RGC death.

In intermediate stages of disease (T3 and T4) NOS1 and NOS2 were both upregulated, indicating further activation of microglia, and astrocytes following the onset of cell death. These upregulations coincided with increased detection of both astrocytic, pan-microglial and macrophage markers (T3). In intermediate stages of disease (T3) when RGC death is underway, there is further signalling through the CD200 axis, while microglia increase in both number (OX42) and reactivity (OX41).

At the longest duration of hypertension, only one of these changes persist, that is NOS2 upregulation. This indicates that the microglial, but not astroglial response is sustained, and this discovery has important implications for ascertaining the chronic pathophysiology of glaucoma.

Group	T1	T2	T3	T4	T5		A1	A2	A3	A4	A5		S1	S2	S3	S4	S5
Duration (days)	1 - 7	11 - 19	20 - 27	33 - 46	47 - 65	Area (mmHg)	0.9 - 22.7	24.3 – 96.8	97.2 – 151.1	165.3 – 256.1	271.9 – 469.3	SD	0 - 1.511	1.52 - 2.96	3.20 - 3.75	3.81 - 5.57	6.02 - 12.76
% RGC Apoptosis	2.04	1.89	5.38	4.47	1.46		1.71	2.78	3.27	3.75	4.65		3.15	1.48	4.24	3.13	5.28
GFAP		*	***						***						*		
OX33											*						
MHCII																	
CD45	*	*		***	***		***			*	**		*	***	*		
OX42		**	***	**					***						*	*	*
OX41			***	**													
CD200L	***						*										
CD200R			***						*								
NOS1			**	***					*	*	*					**	
NOS2	*		**	***	*		*		*		**			*	*	***	*
NOS3																	

Table 7.1 Summary of results This table summarises the main findings of the present study. Ocular hypertensive groups T1-T5, A1-A5 and S1-S5 are shown, together with their defining IOP variables. Apoptosis data for the retina is also shown for each group. Significant elevations of immunohistochemically probed proteins are indicated by * ($P<0.01$), ** ($P<0.05$) and *** ($P<0.001$).

Other aspects of IOP elevation were also examined with respect to microglial, astrocyte and NOS upregulation. These findings are summarised in Table 7.1, and are described in detail in Chapters V and VI. In short, it is apparent that all aspects of IOP investigated had complex effects on the optic nerve head markers used. Duration, severity and fluctuation of IOP elevation all have important roles to play in the reaction of the optic nerve head cellular component to increased IOP.

7.2 Neurodegeneration and death of the optic nerve in context

The study of neurodegeneration and regeneration can be easily facilitated in the visual system. The optic nerve, derived from the central nervous system (CNS), is a spatially and anatomically distinct CNS tract. This distinction allows easy identification and manipulation of the optic nerve. Optic nerve alterations can be measured in many ways, from clinical assessment to electron microscopy. Access to other CNS areas is far more restricted than the optic nerve. Therefore optic nerve manipulation can provide neurodegenerative changes representative of other central diseases, as well as those in glaucoma.

7.2.1 Potential of rodent model of ocular hypertension in the study of human disease

Despite the lack of a lamina cribrosa, the rat shares many optic nerve characteristics with the primate, rat glaucoma models are potentially representative of the human disease, highlighted by the histological techniques used in this study.

Experimental rat glaucoma resulted in progressive RGC loss, as in the human disease. Therefore effects of IOP elevation and/or glial activity are likely to be similar on RGC survival between species. However, despite this relationship, experimental results cannot be directly correlated to human disease.

Moderate pressure elevation in the rat may represent more severe clinical disease due to a lack of resistance to pressure induced damage at the nerve head, while severe pressure elevation in the rodent may represent a clinical situation that is rarely

encountered. This is supported by the results of this study, which show cavernous degeneration typical of relatively mild rodent glaucoma, which is also typical of only the most severe human disease (Quigley *et al.*, 1981). Similarly the glial response documented in this study may therefore represent the glial response during severe human glaucoma, and thus limit the therapeutic implications of inhibiting this response.

7.2.2 Neurodegeneration in glaucoma

This study showed reduced immunohistochemical detection of neurofilament protein (TUJ-1) following ocular hypertension in the episcleral drainage model of glaucoma. Cytoskeletal components of the optic nerve, such as TUJ-1 are transported both retrogradely and anterogradely (Roy *et al.*, 2000). Therefore a reduction in neurofilament protein is a good indication of the state of axonal transport. Cytoskeletal alteration of the optic nerve has implications for axonal transport, particularly retrograde transport of neurotrophins, a lack of which may adversely affect cell survival (Roy *et al.*, 2000). Indications are that retrogradely transported neurotrophic factors are essential for RGC survival and thus have particular interest in glaucoma. (reviewed by Caleo and Cenni, 2004).

Superior colliculus ablation, therefore loss of transportation, results in rapid apoptosis in about 50% RGC population within 48 hours (Cui and Harvey, 1995; Dreher et al., 1983; Harvey and Robertson, 1992; Harvey *et al.*, 1994; Rabacchi *et al.*, 1994). Optic nerve transection is similarly associated with loss of trophic support but also has a later onset and rate of cell death (Berkelaar et *al.*, 1994; Garcia-Valenzuela *et al.*, 1995; Isenmann and Bahr, 1997). Consequently loss of neurotrophin at the level of the retina is a good indicator of glaucomatous damage to the RGC. Loss of axonal transportation is implicated by reduction of neurofilament in the present study. This raises similarities between the episcleral drainage vessel sclerosis model of glaucoma, and other models of neurodegeneration, as well as the usefulness of TUJ-1 in studies of degeneration.

7.2.3 Neurotrophins, apoptosis and IOP

Loss of neurotrophic factors occurs initially in the superior retina during experimental glaucoma (Johnson *et al.*, 2000), and is associated with a slow onset and rate of RGC apoptosis of 8% per week. Despite the initial loss of neurotrophins in the superior retina (Johnson *et al.*, 2000), RGC loss begins in the inferior retina following moderate pressure elevations (a mean daily elevation of 6.55 mmHg) and low apoptotic rate (an average of 3.47% total per retina) induced in the present study.

Loss of neurotrophic support may therefore not be involved during initiation of RGC loss in mild glaucoma. Compensation, by paracrine or autocrine signalling, may occur in superior regions such that retrograde delivery of factors may not be as essential to survival following mild insult.

7.3 RGC death as a function of IOP variables

Mean daily IOP was raised by 6.55 mmHg, and induced a mean apoptotic rate of 3.47% per retina in the present study. In comparison to other studies of experimental glaucoma this is a relatively mild manifestation of disease (for a discussion of the clinical relevance see Section 7.2.1). In the majority, a wide range of higher IOP elevations and apoptotic rates are reported in experimental glaucoma.

Apoptosis generally appeared to increase with duration of pressure elevation (T1-T4), with a decrease at the highest durations (T5). Severity of pressure elevation as indicated by the area under the IOP elevation/duration curve related well to apoptotic rate, and increased with increasing apoptosis throughout. Percentage apoptosis fluctuated with standard deviation of pressure elevation, and a clear relationship was not apparent.

Several studies of ocular hypertension report the pattern and rate of RGC loss in relation to both duration and degree of pressure elevation. However, this is the first study to investigate the role of standard deviation of pressure elevation, or pressure

fluctuation on RGC loss. Hence one of the most interesting results of this investigation was the correlation of high pressure fluctuations with the greatest degree of apoptosis observed. Consequently, during clinical glaucoma a fluctuating IOP may predispose to a more vigorous disease progression.

Also, peak apoptosis and pressure fluctuations coincided with increases in pan-microglial marker (OX42) as well as increased optic nerve head NOS2 protein. This indicates that not only does fluctuation of IOP induce RGC death, it is also involved with microglial proliferation, and possible activation. These findings have important implications for future glaucoma investigations and treatment.

In relation to other studies on apoptosis, RGC death was at very low levels in the present study. A total apoptotic rate of 15.24% occurred over a maximum of 65 days of ocular hypertension, resulting in a weekly RGC loss of 1.64%. Laquis *et al.* (1998) induced ocular hypertension for 70 days, resulting in a weekly RGC loss of 4%. An average IOP elevation 2.55 mmHg greater than the present study, partially accounts for the generation of higher apoptotic rates by Laquis *et al.* (1998). However, it is also likely that the use of a different method to generate hypertension (episcleral vein cautery) may also have resulted in greater levels of apoptosis.

Previous studies of the episcleral drainage vessel model of glaucoma indicate that RGC apoptosis occurs from day 1 post-IOP elevation (Johnson *et al.*, 2000), with an overall rate of 0.142% per retina. However, much higher pressures were generated by Johnson *et al.* (2000), and comparison with the present study highlights how IOP alteration, duration, fluctuation and severity can all contribute to apoptotic levels.

In conclusion, a lack of correlation between the many studies of RGC apoptosis following IOP elevation may be explained by several factors. The use of different glaucoma models, in terms of species and strain of animal, as well as the technique used to elevate IOP may affect apoptotic rate. Also, the present study shows that IOP variables of duration, fluctuation and severity can affect RGC death.

7.4 New perspectives on the primary and secondary insults of glaucoma

Glaucomatous optic nerve degeneration begins with an initial insult to the RGCs of optic nerve. This insult initiates RGC damage and/or death. In the rodent glaucoma model developed in the present study, the initial insult of pathologically raised IOP was used to induce RGC death. However, many studies indicate that even following the removal of the primary insult, for example, reduction of IOP to normal levels, RGC degeneration and death continues (Bakalash *et al.*, 2002). It is thought that this continued cell loss, or secondary degeneration, results from numerous reactions derived from the cellular response to the initial insult (Abbas *et al.*, 1996; Matsubara *et al.*, 1999; Mosmann and Sad, 1996; Raibon *et al.*, 2002). These reactions may propagate RGC damage, and induce a hostile optic nerve microenvironment conducive to cell death. These reactions may include formation of the astroglial scar, microglial activation and/or infiltration of peripheral immune cells (Abbas *et al.*, 1996; Matsubara *et al.*, 1999; Mosmann and Sad, 1996; Raibon *et al.*, 2002; Wang *et al.* 2002a), the former of which have both been identified and investigated in the present study.

7.4.1 Primary damage

Previous studies have not examined the effects of duration of pressure elevation, area under the IOP curve (combined effect of IOP level and duration) and standard deviation (fluctuations) of pressure elevation on the optic nerve. The effects of these variables on several optic nerve cellular markers were quantified. Indications are that there is a complex relationship between pressure variables, other than duration, and cellular alterations in the glaucomatous optic nerve.

Standard deviation of pressure elevation and area under the IOP curve affected onset and time course of glaucoma pathology. This is likely to be of particular interest in management of glaucoma treatment. Differences in pressure fluctuations and degree of pressure elevation all affected disease progression.

7.4.2 Resultant secondary degeneration

Glaucoma is not generally regarded as an inflammatory disease. With new research, evidence is gradually being accumulated implicating a role for the immune system in secondary degeneration of glaucomatous RGCs (Becher *et al.*, 2000; Tezel *et al.*, 1999; Wax *et al.*, 1994). This opens a door for new avenues in glaucoma treatment. For instance, the use of microglial inhibitors, such as tuftsin-1,3 or minocycline (Baptiste *et al.*, 2005), may abrogate unfavourable microglial responses in glaucomatous pathophysiology.

The glial response has been correlated with aspects of pressure elevation under experimental glaucoma conditions. For efficacy of microglial down-regulation, as a treatment, the IOP attributes which affect microglial activation need to be clear. This study showed that microglial activation appeared to occur via the CD200 axis during the initiation of disease, before significant RGC death. At this stage, duration of clinical pressure elevation is relatively mild. Activation, via the CD200 axis, also seems likely to occur during moderate pressure durations and area under the pressure curve, when apoptosis was relatively high. CD200 axis disruption coincided with upregulation of the myeloid cell marker CD45 (indicating possible microglial upregulation) and was followed by an increase in microglial cells (marked by the pan-microglial marker, OX42), and thereafter microglial activation.

A glaucoma patient presenting with elevated IOP, before the onset of visual field loss, is very likely to benefit from inhibition of the CD200 axis disruption. However, an individual with some visual field loss would likely still benefit from inhibitors of microglial activation.

Inhibition of microglial activation, as a method of therapeutic intervention in glaucoma, may have considerable positive patient outcomes. However, regain of visual function and optic nerve regeneration should also be addressed in any future glaucoma therapy.

7.5 Implications of astrocytic changes in secondary degeneration

Astrocytes are transiently upregulated following 11 days of ocular hypertension in conjunction with significant elevation of RGC apoptosis. It is therefore unlikely that the astrocytic response is involved in initiation of optic nerve damage. However, during activation, from days 11-27 (T2 and T3), A2, and S2 the astrocytic response may affect RGC survival.

Many studies have reported GFAP alterations under conditions of ocular hypertension. In particular Johnson *et al.* (2000) investigated the astroglial response from 3 to 14 days of IOP elevation in the same model as used in the present study. From 7 to 14 days of ocular hypertension, astrocytic labelling with GFAP was reduced, and after 14 days normal levels of labelling returned. GFAP elevation would have been affected differently at an average IOP elevation of 16 mmHg (induced by Johnson *et al.*, 2000), rather than the 6.55 mmHg elevation induced in the present study.

Astrocytic reactivity is also recorded in studies of primate experimental glaucoma (Yucel *et al.*, 1999) and human glaucoma (Varela and Hernandez, 1997). This is a good indication that the present study produced astrocytic alterations more similar to the human disease, and it can therefore be inferred that the mild pressure elevations produced are more representative of the human condition.

Astrocytic alterations produced in this study are analogous to those of human glaucoma (Varela and Hernandez, 1997). Due to the upregulation of these cells during the initiation of cell death, and at fairly low IOP fluctuations and severity, these cells are likely to be involved in a transient response to RGC apoptosis. It is likely that upregulation of astrocytes is in some way an attempt to prevent either the effects of pressure alterations or to limit RGC death (reviewed by Fitch and Silver).

7.6 Implications of microglial changes in secondary degeneration

Lack of a cell-specific marker that can distinguish microglia from peripheral macrophages is a major problem in studies of central pathophysiology (Guillemin and Brew, 2004). However, the present study showed how combinations of cellular markers can be used to clarify the microglial reaction in a disorder that also may involve compromise of the blood-retinal barrier.

7.6.1 Parallels with other disease

Microglial alterations are not specific to glaucomatous neurodegeneration. Activation of these cells is found in Parkinson's disease (Ouchi *et al.*, 2005), multiple sclerois (Ayers *et al.*, 2004), as well as nerve crush (Frank and Wolberg, 1996) and axotomy (Baptiste *et al.*, 2005). Identification and inhibition of microglial activation therefore has far-reaching implications for many pathological mechanisms and the treatment of several neurological conditions. Efficacy of treatment may be improved by combination therapies specific to the particular disease and the stage of pathology. For example, preventative therapy (such as CD200 axis inhibition), and if disease onset has occurred, preventative measures (such as microglial activation inhibitors) together with damage limitation and regenerative treatments.

Glaucoma does not only have correlations to other types of neurodegeneration in terms of microglial activation. Similarities can be draw between glaucoma and Alzheimer's disease through an association of the inheritance of the apolipoprotein epsilon4 allele (Vickers *et al.*, 2002). Mice expressing a human neurofilament gene develop neurofilamentous accumulations in RGC perikarya, useful in studying both Alzheimer's disease and glaucomatous pathophysiology (Vickers *et al.*, 1995a). In order to determine the exact role of microglia during glaucomatous pathophysiology, potential points of neuroglial interactions need to be further explored. Inhibition of these cellular pathways or knock-out of particular genes will further facilitate the study of glaucoma.

7.6.2 The immune system in glaucoma: peripheral and central

Controversy exists over the role of the immune response in glaucoma (Tezel and Wax, 2004). There is compelling evidence to suggest that the peripheral immune system can actually alleviate RGC loss during glaucoma (Bakalash *et* al., 2002), particularly as compromise of the immune system can lead to enhanced RGC death.

It is likely that, to a certain degree, both central and peripheral immune responses function to eliminate debris from RGC degeneration following glaucoma. However, exacerbation of this immune response is a candidate for causing the continued secondary degeneration observed following reduction of IOP during glaucoma.

During optic nerve regeneration through peripheral nerve grafts, nerve injury induces apoptosis accompanied by microglial activation and removal of axonal debris (Schuetz and Thanos, 2004). This does not significantly affect neuronal survival, indicating that microglial activation may not have an important role in degeneration (Schuetz and Thanos, 2004). The microglial response in glaucoma may parallel the response in such axotomy models. Elevated microglial responses during peak RGC death, followed by reduced response during alleviation of RGC death (as shown in the present study) may similarly indicate a clearing function.

However, microglial upregulation during glaucoma may indicate a role for these cells, other than clearing debris during disease. Microglia activation involves many changes culminating in an immune response that may involve secretion of cellular toxins. If unregulated, the latter may damage RGCs. Microglia may signal to recruit and regulate T cell-mediated immune responses which target self-antigens at the site of damage. It has been suggested that boosting this reaction in neurodegeneration may be used as a vaccination therapy for therapeutic intervention (Schwartz, 2003). There is a fine line, however, between protective and degenerative autoimmunity.

Microglial cells can be isolated and identified by OX42 positivity for investigations of pathophysiological mechanisms in cell culture (Chen *et al.*, 2002). Cell culture investigation of microglial responses suffer from a propensity of cellular activation

through culture techniques (Sergent-Tanguy *et al.*, 2003). It is therefore very difficult to determine the exact cellular pathways that lead to and result in microglial activation following hypertension. *In vitro* investigations into microglial activation should consequently be approached with caution. *In vivo* studies do not share these problems, as microglia are maintained in their natural environment in the CNS.

Following initial insult of elevated IOP, retinal ganglion cell damage may be mediated through mechanisms such as aberrant immune signalling (reviewed by Tezel and Wax, 2004), excitotoxicity (reviewed by Lotery, 2005), neurotrophin deprivation or free radical damage (Ko *et* al., 2005) to name but a few. The peripheral and central immune systems may affect, or be affected by these other responses to IOP elevation. It is likely that the role of resident optic nerve microglia during glaucoma illustrated in this study serves to alter nerve pathophysiology in combination with other mechanisms. Some of the immune mechanisms likely to be affected during glaucoma are described in Figure 7.1. The role of each of these pathways needs to be determined in order to accurately ascribe a function to the peripheral and central immune response in glaucomatous optic nerve degeneration.

7.6.3 Neuroregeneration and immunity

Due to the low capacity of central nerves to regenerate fully, regain of visual function is unlikely to be achieved through conventional glaucoma treatment, or the inhibition of microglial activation. Manipulation of immune reaction in glaucoma is likely to induce an optic nerve microenvironment more conducive to nerve survival and regrowth (Reviewed by Schwartz, 2004 and Stoll *et al.*, 2002). Following the application of such a therapy, it is likely that any attempts to regenerate the nerve would be more successful. However, it is likely that there is a fine line between destructive and constructive autoimmunity.

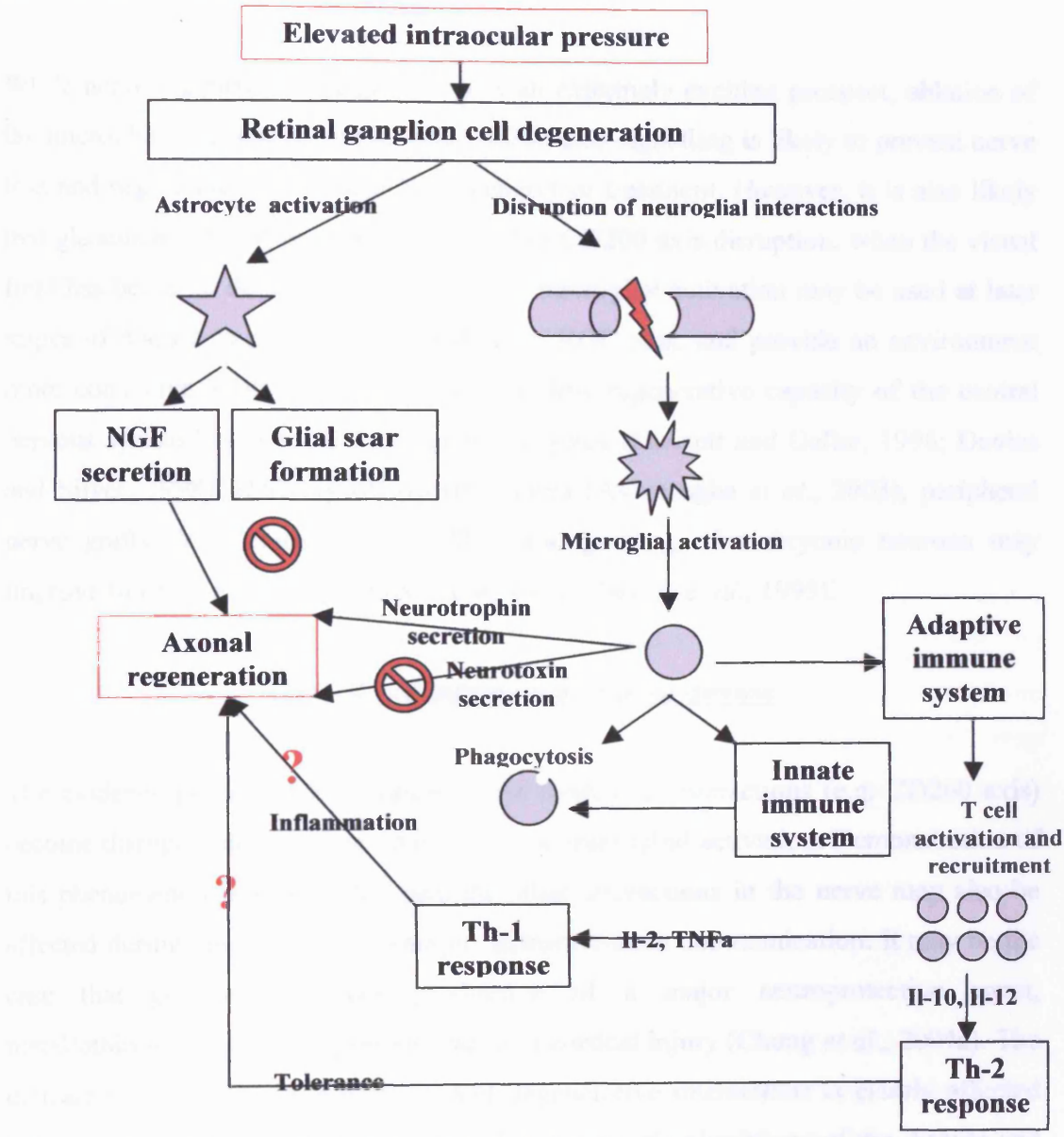

Figure 7.1 Glial mediated pathways following ocular hypertension *Astrocytes and microglia may induce neuroprotective or degenerative pathways. Astrocytes may be neuroprotective by the secretion of nerve growth factors (NGF), while astroglial scar formation prevents regeneration. Disruption of neuroglial signalling may induce microglial activation involving morphological changes, phagocytosis, and secretion of signalling factors, with direct consequences for axonal regeneration. It is also possible that microglia interact with innate and adaptive immune systems to exacerbate phagocytosis or T-cell activation / recruitment, respectively. T cell maturation into Th1 cells will further exacerbate immune reaction and may prevent axonal regeneration. However, induction of the Th2 response may cause tolerance, and prevent further axonal damage.*

While nerve regeneration in glaucoma is an extremely exciting prospect, ablation of the microglial response by preventing CD200 axis signalling is likely to prevent nerve loss and negate the requirement for regenerative treatment. However, it is also likely that glaucoma will not be detected until after CD200 axis disruption, when the visual field has begun to deteriorate. Inhibitors of microglial activation may be used at later stages of disease to prevent exacerbation of RGC loss, and provide an environment more conducive to RGC regeneration. The low regenerative capacity of the central nervous system has been diffused in recent years (Fawcett and Geller, 1998; Davies and Silver, 1998). Delivery of growth factors (Avwenagha *et al.*, 2003), peripheral nerve grafts (Vidal-Sanz *et al.*, 1987), and grafting of embryonic neurons may improve function following neurodegeneration (Shewan *et al.*, 1995).

7.7 Cell:cell interactions during disease

The evidence presented here suggests that neuroglial interactions (e.g. CD200 axis) become disrupted during glaucoma leading to microglial activation. Demonstration of this phenomenon indicates that perhaps other interactions in the nerve may also be affected during glaucoma, for example, astrocyte-axon communication. It may be the case that glaucoma induces production of a major neuroprotective agent, metallothionen, from astrocytes similar to in cortical injury (Chung *et al.*, 2004a). The delicate balance of neuroprotective and degenerative interactions is clearly affected during glaucoma. The determination of the exact pathophysiology of the disease and the cellular interactions involved should provide suitable targets for high efficacy treatment.

There are many other pathways that may be affected through neuroglial interactions to influence retinal ganglion cell health and survival. The specific phosphatidylserine receptor (PtdSerR) present on active and quiescent microglia can be activated to eliminate neuronal debris, through neuroprotective and anti-inflammatory pathways (DeSimone *et al.*, 2004). Recognition of neuronal debris through this receptor does not induce inflammation (DeSimone *et al.*, 2004).

It is interesting therefore to note that loss of retinal CD200-mediated down-regulation of microglial activation elevated microglial numbers (Dick *at el.*, 2003), indicated in the present study by elevation of OX42 labelling in the optic nerve head These microglia express NOS2, a recognised marker of microglial activation (Dick *at el.*, 2003), which was also elevated in this study from the initiation of RGC death and onwards. However, following CD200 axis disruption retinal microglial cells retain a resting morphology and consequently, conventional microglial activation was not observed through CD200 axis disruption in the retina (Dick *at el.*, 2003). This may indicate induction of an alternative signalling pathway through CD200 receptor activation, which is involved in microglial-mediated neuronal death by release of NO.

In contradiction, the findings of thesis have demonstrated that, following CD200 axis disruption, microglia resident in the optic nerve head do become activated (shown by elevated OX41 labelling). Microglial-mediated neuronal death, by release of NO, may also be involved in glaucomatous optic nerve head degeneration. However, due to the presence of conventional active microglia, it is possible that a slightly different cellular reaction is produced, or other signalling pathways are involved at the glaucomatous optic nerve head.

Potential candidates in such pathways are prostanoids, produced by cyclooxygenases (Cox-1 and Cox-2), which are involved in microglial activation and Wallerian degeneration of peripheral nerves (Durrenberger *et al.*, 2004). It is possible that these chemical mediators of inflammation also have a role to play in the cellular interactions of glaucoma at the optic nerve head (Yuan and Neufeld, 2001.

7.8 Molecular mediators of neurodegeneration? NOS

During experimental glaucoma, NOS isoforms 1 and 2 were upregulated in the optic nerve. This discovery is particularly controversial. These isoforms are upregulated in some glaucoma models (Shareef *et al.*, 1999) and the human disease (Neufeld *et al.*, 1997), while other models show no NOS2 upregulation (Pang *et al.*, 2005). Also,

inhibition of NOS2 can result in reduction of cell loss in some experimental glaucoma models (Neufeld *et al.*, 1999) but not others (Pang *et al.*, 2005).

NOS1 upregulation is less controversial. Upregulation of this isoform of the NOS enzyme occurred after initial cell death, when apoptotic levels were at their peak (T3 and T4). Therefore NOS1 upregulation can be associated with RGC apoptosis after the initial astrocytic reaction (T1 and T2), and during alterations in microglial cells at the optic nerve head.

However, this is not the case when looking at the duration/IOP elevation effects on NOS1. Upregulation of NOS1 appeared at the lowest apoptotic levels when correlated with IOP elevation/duration, however upregulation was still associated with microglial alterations. In contrast only the lowest levels of apoptosis produced NOS1 elevation when results were grouped according to IOP fluctuation. Although NOS1 did not appear to have a clear relationship with RGC apoptosis, NOS1 elevation always corresponded with CD200 axis modulation and/or upregulation of microglial markers, and frequently followed GFAP elevation. It is therefore likely that NOS1 upregulation was mediated by optic nerve head astrocytes or microglia, and was not directly involved in RGC apoptosis.

To date, only NOS2 protein and mRNA expression have been investigated in the episcleral vessel sclerosis model of glaucoma (Pang *et al.*, 2005). Indications are that NOS2 is not upregulated following 35 days of episcleral drainage vessel sclerosis-induced ocular hypertension, from stages of disease without damage, through to severe optic nerve damage (Pang *et al.*, 2005). This study however, does not take into account several important aspect of ocular hypertension. These include the duration and fluctuation of IOP elevation, both of which are correlated with NOS2 levels in the present study.

Disagreement between results of the present study and that of Pang *et al.* (2005) can be easily accounted for by IOP variables. Expression of NOS2 was not detected following a full range of optic nerve damage following 35 days of hypertension by Pang *et al.* (2005). However, each hypertensive eye had endured pressure elevation of

varying degrees for exactly 35 days, and as indicated by the present study, duration of IOP elevation, as well as severity and fluctuation of elevation can all affect NOS2 levels. These other aspects of IOP are not accounted for by Pang *et al.* (2005).

Levels of IOP elevation (7.04 mmHg) similar to the present study (6.55 mmHg) were produced by Shareef *et al.* (1999). Episcleral vein cautery in the rat, results in upregulation of all NOS isoforms from 4 days to 3 months post-induction of ocular hypertension (Shareef *et al.*, 1999). An enhanced response, without any return to normal levels of NOS, and with the apparent upregulation of NOS3 (Shareef *et al, 1999)*, may indicate a different response to vein cautery and sclerosis. It is possible that vascular stress caused by vein cautery combines with the effects of elevated IOP to enhance NOS levels. However, upregulation of all NOS isoforms has been reported in the human condition (Neufeld *et al.*, 1997). Unfortunately, NOS levels in human glaucoma optic nerve tissue have not been correlated with any aspects of IOP. Therefore it is not possible to put these results into context of the present study.

It is likely that NOS produced by either astrocytes or microglia as a response to the initial insult is involved in production of neurotoxic levels of NO. Disruption of cell:cell interactions are likely to induce NOS upregulation. For example, RGC mediated regulation of microglial activation may participate in NOS regulation in the retina (for example via the CD200 axis). Similarly astrocyte:endothelial cell interactions are thought to affect NOS levels in glaucoma (Neufeld *et al.*, 1997).

The CD200 axis appears to be in part responsible for upregulation of NOS. Indeed, upregulation stems from microglial activation, which occurs as a consequence of cellular signalling. Aberrant signalling may therefore exacerbate microglial activation and consequently the elevation of NOS levels. It is possible that the signalling pathways involved in microglial activation and NOS regulation either run in parallel, or are identical. These pathways may be represented by any of those shown in Figure 7.1. However, at this early stage of investigation into the microglial-mediated alteration of the optic nerve microenvironment, the CD200 axis was positively identified as being involved in microglial activation, as well as NOS production.

7.9 The future for glaucoma

7.9.1 Models

This study highlighted the importance of the development of animal models of glaucoma to study the pathophysiological mechanisms of disease. The development of novel animal models for glaucoma research will assist in the treatment of the human disease. Certain animals, for example primates are particularly suited to the study of the optic nerve head, due to structural parallels with the human. However, it is more convenient to use small animal models in research. Popular laboratory species such as the mouse, guinea pig and rabbit are all used to generate experimental glaucoma. However, currently, rat models are increasingly popular due to several factors, including the variety of well-documented methods for generating glaucoma, as well as a wealth of information on the optic nerve structure. The aforementioned laboratory species, excluding the rat all suffer from a paucity of structural components at the optic nerve head. In particular, the mouse used frequently for modelling glaucoma does not even posses a true equivalent to the human nerve head. Hopefully, future glaucoma models will take into account the crucial role of the cells and tissues of the optic nerve head in the pathophysiology of glaucoma.

7.9.2 Research

The present study has demonstrated the importance of glia and the immune response in glaucomatous damage. Glaucoma is not traditionally thought of as an inflammatory condition. However, the evidence both here and in the current literature, suggests that the immune system is likely to play a role, at least in part, in the progression of glaucoma. The inhibition of the immune and microglial response are both interesting avenues for future research. The precise mechanisms of microglial activation during disease, including the disruption of NOS regulation will no doubt predominate in the future of glaucoma research.

7.9.2.1 Neuroprotection studies

A major current target for glaucoma research is not only to ascertain the exact pathophysiologies of glaucomatous degeneration, but also to achieve adequate neuroprotection of the RGC in the diseased optic nerve. In the episcleral drainage vessel sclerosis model neuroprotection studies with respect particularly to NOS2 inhibition should continue due to conflicting evidence regarding this enzyme in glaucoma (see data presented here and Pang *et al.*, 2005). It may also prove useful to investigate the effects of inhibiting microglial activation and/or proliferation on RGC protection. This would ascertain the exact role of microglia at each disease stage, as well as provide a strong platform on which potential clinical therapies might be based.

7.9.2.2 Future assessment of regeneration

Following neuroprotection, neuroregeneration of the RGC is a desirable target for glaucoma research. Reformation of the dendritic field, as well as the axon following cell rescue will need to be quantitatively measured. A promising technique for such measurements is biolistic RGC labelling followed by Scholl analysis, however, the prospects of quantification of immunoreactivity in the assessment of regeneration are less promising.

TUJ-1 immunoreactivity, used as a measure of RGC degeneration (Cui and Harvey, 1995), is phosphorylated in the growth gone of regenerating nerves (Fournier and McKerracher, 1997; Mason *et al.*, 2000). Therefore TUJ-1 immunoreactivity, while a useful indicator of neurodegeneration, may not be a good indicator of regeneration as phosphorylation may prevent antibody-antigen interaction. Similarly silver staining may be of limited use in regeneration studies. Staining could be used to indicate cessation of degeneration, but not nerve regeneration. The prevention of degeneration is likely to involve alterations in optic nerve microenvironment which are supportive to growth. Silver staining is a quick, reliable and potentially quantitative measure that can be used to indicate when neuroregeneration might be supported in the nerve.

7.9.3 Therapy

The compelling evidence presented here suggests that modulation of the local immune response and glial activity may potentially be of benefit to the glaucoma sufferer. There is also an increasing mass of literature that suggests these responses have a crucial role to play in neurodegeneration. Hopefully future glaucoma treatment and research will yield preventative and restorative treatments for some of the debilitating neurodegenerative diseases that share a common pathway with glaucoma, as well as the disease itself.

7.10 Conclusions

The pathophysiology of glaucomatous optic atrophy is extremely complex. There are a multitude of primary insults that can be applied to cells or animals to facilitate the study of the disease. The pressure-dependent form of glaucoma can be attributed to temporal aspects of chronic pressure elevation as well as the degree of actual pressure achieved, and how much this pressure varies.

The effects of pressure elevation include neurodegeneration and apoptosis of the retinal ganglion cell, as well as the induction of secondary insults. It is likely that these insults stem from aberrant cell signalling as a consequence of disease. The resulting disruption of glial regulation may influence retinal ganglion cell survival, and even regeneration. Manipulation of the glial reaction following hypertension may assist in the production of neuroprotection, and eventually regeneration of the RGC. However, the complete nature of the glial reaction remains unclear, and it is unknown whether inhibition of glial activation will exacerbate or alleviate degeneration. Due to parallels between glaucoma and other central nervous system disorders any progress made in either research area has the potential for far reaching implications in the treatment of CNS dysfunction.

7.11 Future work

Apoptotic RGC death as a function of IOP variables are clearly very important with respect to the future treatment and monitoring of the disease process regardless of other factors involved. Any future work using the episcleral drainage vessel sclerosis model should take into account these factors. It is also possible that IOP variables not investigated in the present study are of importance to the progression of glaucoma pathophysiology. Correlation of mean daily IOP, or total IOP elevation with apoptotic levels, neurodegeneration, expression of optic nerve head cellular markers and NOS levels may provide additional information on the pathological mechanisms of glaucoma.

Activation of astrocytes occurs in conjunction with the onset of RGC death. Implications of preventing astrocytic activation could be investigated in the future in order to determine whether neuronal death occurs independently of this process. Also, the neuroglial interactions between astrocytes and RGCs that might influence activation and cell survival could be probed. Indications are that astrocytic cell death does not occur in this model of glaucoma, and are fairly resistant to IOP alterations. Future investigations could identify which aspects of astrocytic morphology and biochemistry are involved in this resistance. The implications of astrocytic activation at the optic nerve head with respect to efficacy of neuroregeneration also needs to be addressed in future studies. Active astrocytes form a potential barrier to neuroregeneration across the optic nerve head.

Microglia are likely to play a role in RGC degeneration during glaucoma. Indications are that CD200 axis signalling in involved. Inhibition of microglial activation, and consequent effects on RGC viability and regeneration is essential to future investigations. If possible, microglial proliferation and activation could be inhibited independently to show the effects on neurodegeneration and RGC death. Manipulation of the CD200 axis may also prove useful in future research using the episceral drainage vessel sclerosis model of glaucoma, in order to determine whether prevention of signalling through this axis can indeed prevent microglial activation and RGC degeneration. It may also be of interest to prevent the peripheral immune

response in this model of glaucoma, similar to Bakalash *et al* (2002) in order to verify whether this response does indeed play any role in glaucoma, and to absolutely segregate the peripheral and central responses to elevation of IOP.

This study clearly correlates raised NOS protein levels with ocular hypertension. Due to the controversy surrounding this issue, future work should include consolidation of this result. Detection of NOS mRNA, in both homogenates and tissue sections of optic nerve could be used to indicate transcriptional upregulation of the NOS genes, as well as the location of any alterations. Additionally verification of NOS dimerisation (and therefore activation) should also be investigated to confirm the involvement of NOS in glaucoma. Should NOS dimerisation increase it would be desirable to investigate NO and superoxide production in order to confirm the role of NOS in neurodegeneration.

There remains a multitude of potential investigations that could stem from this one study into the pathogenesis of glaucoma. As befits such a multifaceted disease, a huge amount of investigation is ongoing, worldwide, into one of the leading causes of irreversible blindness. Hopefully this thesis and future publications will assist in defining glaucoma pathophysiology and the development of clinically relevant glaucoma medications.

Bibliography

Abbas AK, Murphy, KM and Sher, A. **Functional diversity of helper T lymphocytes.** *Nature.* 1996;383:787-93

Adams S, van der Laan LJ, Vernon-Wilson E, Renardel de Lavalette C, Dopp EA, Dijkstra CD, Simmons DL, van den Berg TK. **Signal-regulatory protein is selectively expressed by myeloid and neuronal cells.** *J Immunol.* 1998;161:1853-9.

Aguayo AJ, Bray, GM, Rasminsky, M, Zwimpfer, T, Carter, D and Vidal-Sanz, M. **Synaptic connections made by axons regenerating in the central nervous system of adult mammals.** *J Exp Biol.* 1990;153:199-224

Aguayo AJ, Rasminsky, M, Bray, GM, Carbonetto, S, McKerracher, L, Villegas-Perez, MP, Vidal-Sanz, M and Carter, DA. **Degenerative and regenerative responses of injured neurons in the central nervous system of adult mammals.** *Philos Trans R Soc Lond B Biol Sci.* 1991;331:337-43

Ahmed FA, Ingoglia, NA and Sharma, SC. **Axon resealing following transection takes longer in central axons than in peripheral axons: implications for axonal regeneration.** *Exp Neurol.* 2001;167:451-5

Ahmed F, Brown, KM, Stephan, DA, Morrison, JC, Johnson, EC and Tomarev, SI. **Microarray analysis of changes in mRNA levels in the rat retina after experimental elevation of intraocular pressure.** *Invest Ophthalmol Vis Sci.* 2004;45:1247-58

Airaksinen PJ, Mustonen, E and Alanko, HI. **Optic disc hemorrhages. Analysis of stereophotographs and clinical data of 112 patients.** *Arch Ophthalmol.* 1981;99:1795-801

Albon J, Karwatowski, WS, Avery, N, Easty, DL and Duance, VC. **Changes in the collagenous matrix of the aging human lamina cribrosa.** *Br J Ophthalmol.* 1995;79:368-75

Albon J, Purslow, PP, Karwatowski, WS and Easty, DL. **Age related compliance of the lamina cribrosa in human eyes.** *Br J Ophthalmol.* 2000;84:318-23

Aloisi F, Ria, F and Adorini, L. **Regulation of T-cell responses by CNS antigen-presenting cells: different roles for microglia and astrocytes.** *Immunol Today.* 2000;21:141-7

Alvarado J, Murphy, C and Juster, R. **Trabecular meshwork cellularity in primary open-angle glaucoma and nonglaucomatous normals.** *Ophthalmology.* 1984;91:564-79

Anderson DR, Hoyt, WF and Hogan, MJ. **The fine structure of the astroglia in the human optic nerve and optic nerve head.** *Trans Am Ophthalmol Soc.* 1967;65:275-305

Anderson DR. **Itrastructure of meningeal sheaths. Normal human and monkey optic nerves.** *Arch Ophthalmol.* 1969;82:659-74

Anderson DR and Hoyt, WF. **Ultrastructure of intraorbital portion of human and monkey optic nerve.** *Arch Ophthalmol.* 1969;82:506-30

Anderson DR and Davis, EB. **Retina and optic nerve after posterior ciliary artery occlusion. An experimental study in squirrel monkeys.** *Arch Ophthalmol.* 1974;92:422-6

Anderson DR and Hendrickson, A. **Effect of intraocular pressure on rapid axoplasmic transport in monkey optic nerve.** *Invest Ophthalmol.* 1974;13:771-83

Anderson MG, Smith, RS, Savinova, OV, Hawes, NL, Chang, B, Zabaleta, A, Wilpan, R, Heckenlively, JR, Davisson, M and John, SW. **Genetic modification of glaucoma associated phenotypes between AKXD-28/Ty and DBA/2J mice.** *BMC Genet.* 2001;2:1

Armaly MF. **On the distribution of applanation pressure. I. Statistical features and the effect of age, sex and family history of glaucoma.** Arch Ophthalmol. 1965;73:11-8.

Armaly MF, Krueger, DE, Maunder, L, Becker, B, Hetherington, J, Jr., Kolker, AE, Levene, RZ, Maumenee, AE, Pollack, IP and Shaffer, RN. **Biostatistical analysis of the collaborative glaucoma study. I. Summary report of the risk factors for glaucomatous visual-field defects.** *Arch Ophthalmol.* 1980;98:2163-71

Arvin KL, Han, BH, Du, Y, Lin, SZ, Paul, SM and Holtzman, DM. **Minocycline markedly protects the neonatal brain against hypoxic-ischemic injury.** *Ann Neurol.* 2002;52:54-61

Asrani S, Zeimer, R, Wilensky, J, Gieser, D, Vitale, S and Lindenmuth, K. **Large diurnal fluctuations in intraocular pressure are an independent risk factor in patients with glaucoma.** *J Glaucoma.* 2000;9:134-42

Bakalash S, Kipnis, J, Yoles, E and Schwartz, M. **Resistance of retinal ganglion cells to an increase in intraocular pressure is immune-dependent.** *Invest Ophthalmol Vis Sci.* 2002;43:2648-53

Bakalash S, Kessler, A, Mizrahi, T, Nussenblatt, R and Schwartz, M. **Antigenic specificity of immunoprotective therapeutic vaccination for glaucoma.** *Invest Ophthalmol Vis Sci.* 2003;44:3374-81

Banati RB, Gehrmann, J, Schubert, P and Kreutzberg, GW. **Cytotoxicity of microglia.** *Glia.* 1993;7:111-8

Barclay AN, Wright, GJ, Brooke, G and Brown, MH. **CD200 and membrane protein interactions in the control of myeloid cells.** *Trends Immunol.* 2002;23:285-90

Bellezza AJ, Rintalan, CJ, Thompson, HW, Downs, JC, Hart, RT and Burgoyne, CF. **Deformation of the lamina cribrosa and anterior scleral canal wall in early experimental glaucoma.** *Invest Ophthalmol Vis Sci.* 2003;44:623-37

Bennis M, El-Hassni, M, Rio, JP, Lecren, D, Reperant, J and Ward, R. **A quantitative ultrastructural study of the optic nerve of the chameleon.** *Brain Behav Evol.* 2001;58:49-60

Bishop A, Anderson JE. **NO signaling in the CNS: from the physiological to the pathological.** *Toxicology.* 2005;208:193-205.

Bo L, Dawson, TM, Wesselingh, S, Mork, S, Choi, S, Kong, PA, Hanley, D and Trapp, BD. **Induction of nitric oxide synthase in demyelinating regions of multiple sclerosis brains.** *Ann Neurol.* 1994;36:778-86

Boger RH, Ron ES. **L-Arginine improves vascular function by overcoming deleterious effects of ADMA, a novel cardiovascular risk factor.** *Altern Med Rev.* 2005;10:14-23.

Bonfoco E, Krainc, D, Ankarcrona, M, Nicotera, P and Lipton, SA. **Apoptosis and necrosis: two distinct events induced, respectively, by mild and intense insults with N-methyl-D-aspartate or nitric oxide/superoxide in cortical cell cultures.** *Proc Natl Acad Sci U S A.* 1995;92:7162-6

Bredt DS, Hwang, PM, Glatt, CE, Lowenstein, C, Reed, RR and Snyder, SH. **Cloned and expressed nitric oxide synthase structurally resembles cytochrome P-450 reductase.** *Nature.* 1991;351:714-8

Broderick C, Hoek, RM, Forrester, JV, Liversidge, J, Sedgwick, JD and Dick, AD. **Constitutive retinal CD200 expression regulates resident microglia and activation state of inflammatory cells during experimental autoimmune uveoretinitis.** *Am J Pathol.* 2002;161:1669-77

Brubaker RF. **Delayed functional loss in glaucoma. LII Edward Jackson Memorial Lecture.** *Am J Ophthalmol.* 1996;121:473-83

Brune B, Mohr S, Messmer UK. **Protein thiol modification and apoptotic cell death as cGMP-independent nitric oxide (NO) signaling pathways.** *Rev Physiol Biochem Pharmacol.* 1996;127:1-30.

Burgoyne CF, Quigley, HA, Thompson, HW, Vitale, S and Varma, R. **Early changes in optic disc compliance and surface position in experimental glaucoma.** *Ophthalmology.* 1995;102:1800-9

Burgoyne CF, Downs JC, Bellezza AJ, Hart RT. **Three-dimensional reconstruction of normal and early glaucoma monkey optic nerve head connective tissues.** *Invest Ophthalmol Vis Sci.* 2004 45:4388-99.

Calzada JI, Jones BE, Netland PA, Johnson DA. **Glutamate-induced excitotoxicity in retina: neuroprotection with receptor antagonist, dextromethorphan, but not with calcium channel blockers.** *Neurochem Res.* 2002;27:79-88.

Carter D, Murphy D. **Molecular Neuroscience**, 1999. Pearson Education Limited, Dorset, UK.

Caprioli J, Sears, M and Miller, JM. **Patterns of early visual field loss in open-angle glaucoma.** *Am J Ophthalmol.* 1987;103:512-7

Caprioli J, Miller JM. **Correlation of structure and function in glaucoma. Quantitative measurements of disc and field.** *Ophthalmology.* 1988;95:723-7.

Carson MJ. **Microglia as liaisons between the immune and central nervous systems: functional implications for multiple sclerosis.** *Glia.* 2002;40:218-31

Carter-Dawson L, Crawford, ML, Harwerth, RS, Smith, EL, 3rd, Feldman, R, Shen, FF, Mitchell, CK and Whitetree, A. **Vitreal glutamate concentration in monkeys with experimental glaucoma.** *Invest Ophthalmol Vis Sci.* 2002;43:2633-7

Cartwright MJ, Grajewski, AL, Friedberg, ML, Anderson, DR and Richards, DW. **Immune-related disease and normal-tension glaucoma. A case-control study.** *Arch Ophthalmol.* 1992;110:500-2

Cellerino A, Carroll P, Thoenen H, Barde YA. **Reduced size of retinal ganglion cell axons and hypomyelination in mice lacking brain-derived neurotrophic factor.** *Mol Cell Neurosci.* 1997;9(5-6):397-408.

Chao CC, Hu, S, Molitor, TW, Shaskan, EG and Peterson, PK. **Activated microglia mediate neuronal cell injury via a nitric oxide mechanism.** *J Immunol.* 1992;149:2736-41

Chauhan BC, Pan J, Archibald ML, LeVatte TL, Kelly ME, Tremblay F. **Effect of intraocular pressure on optic disc topography, electroretinography, and axonal loss in a chronic pressure-induced rat model of optic nerve damage.** *Invest Ophthalmol Vis Sci.* 2002;43:2969-76.

Chauhan BC, LeVatte, TL, Jollimore, CA, Yu, PK, Reitsamer, HA, Kelly, ME, Yu, DY, Tremblay, F and Archibald, ML. **Model of endothelin-1-induced chronic optic neuropathy in rat.** *Invest Ophthalmol Vis Sci.* 2004;45:144-52

Chee P and Hamasaki, DI. **The basis for chymotrypsin-induced glaucoma.** *Arch Ophthalmol.* 1971;85:103-6

Chen HS, Pellegrini, JW, Aggarwal, SK, Lei, SZ, Warach, S, Jensen, FE and Lipton, SA. **Open-channel block of N-methyl-D-aspartate (NMDA) responses by memantine: therapeutic advantage against NMDA receptor-mediated neurotoxicity.** *J Neurosci.* 1992;12:4427-36

Cheon EW, Park, CH, Kang, SS, Cho, GJ, Yoo, JM, Song, JK and Choi, WS. **Nitric oxide synthase expression in the transient ischemic rat retina: neuroprotection of betaxolol.** *Neurosci Lett.* 2002;330:265-9

Chew SJ and Ritch, R. **Neuroprotection: the next breakthrough in glaucoma? Proceedings of the Third Annual Optic Nerve Rescue and Restoration Think Tank.** *J Glaucoma.* 1997;6:263-6

Chierzi S, Fawcett JW. **Regeneration in the mammalian optic nerve.** *Restor Neurol Neurosci.* 2001;19(1-2):109-18.

Chung RS, Vickers, JC, Chuah, MI, Eckhardt, BL and West, AK. **Metallothionein-III inhibits initial neurite formation in developing neurons as well as postinjury, regenerative neurite sprouting.** *Exp Neurol.* 2002;178:1-12 (a)

Chung YH, Means, RE, Choi, JK, Lee, BS and Jung, JU. **Kaposi's sarcoma-associated herpesvirus OX2 glycoprotein activates myeloid-lineage cells to induce inflammatory cytokine production.** *J Virol.* 2002;76:4688-98 (b)

Chung RS, Adlard, PA, Dittmann, J, Vickers, JC, Chuah, MI and West, AK. **Neuron-glia communication: metallothionein expression is specifically up-regulated by astrocytes in response to neuronal injury.** *J Neurochem.* 2004;88:454-61

Ciancaglini M, Carpineto P, Costagliola C, Matropasqua L. **Perfusion of the optic nerve head and visual field damage in glaucomatous patients.** *Graefes Arch Clin Exp Ophthalmol.* 2001 Aug;239(8):549-55.

Cioffi GA and Sullivan, P. **The effect of chronic ischemia on the primate optic nerve.** *Eur J Ophthalmol.* 1999;9 Suppl 1:S34-6

Cockburn DM. **Does reduction of intraocular pressure (IOP) prevent visual field loss in glaucoma?** *Am J Optom Physiol Opt.* 1983;60:705-11.

Columba-Cabezas S, Serafini B, Ambrosini E, Aloisi F. **Lymphoid chemokines CCL19 and CCL21 are expressed in the central nervous system uring experimental autoimmune encephalomyelitis: implications for the aintenance of chronic neuroinflammation.** *Brain Pathol.* 2003;13:38-51.

Cotrina ML, Gao, Q, Lin, JH and Nedergaard, M. **Expression and function of astrocytic gap junctions in aging.** *Brain Res.* 2001;901:55-61

Cui Q, Yip, HK, Zhao, RC, So, KF and Harvey, AR. **Intraocular elevation of cyclic AMP potentiates ciliary neurotrophic factor-induced regeneration of adult rat retinal ganglion cell axons.** *Mol Cell Neurosci.* 2003;22:49-61

Cui Q, Cho, KS, So, KF and Yip, HK. **Synergistic effect of Nogo-neutralizing antibody IN-1 and ciliary neurotrophic factor on axonal regeneration in adult rodent visual systems.** *J Neurotrauma.* 2004;21:617-25

Damji KF, Muni, RH and Munger, RM. **Influence of corneal variables on accuracy of intraocular pressure measurement.** *J Glaucoma.* 2003;12:69-80

Danias J, Lee, KC, Zamora, MF, Chen, B, Shen, F, Filippopoulos, T, Su, Y, Goldblum, D, Podos, SM and Mittag, T. **Quantitative analysis of retinal ganglion cell (RGC) loss in aging DBA/2NNia glaucomatous mice: comparison with RGC loss in aging C57/BL6 mice.** *Invest Ophthalmol Vis Sci.* 2003;44:5151-62

Davanger M, Ringvold, A and Blika, S. **The probability of having glaucoma at different IOP levels.** *Acta Ophthalmol (Copenh).* 1991;69:565-8

Davies TG. **Tonographic survey of the close relatives of patients with chronic simple glaucoma.** *Br J Ophthalmol.* 1968;52:32-9

Dawson TM, Bredt DS, Fotuhi M, Hwang PM, Snyder SH. **Nitric oxide synthase and neuronal NADPH diaphorase are identical in brain and peripheral tissues.** *Proc Natl Acad Sci U S A.* 1991;88:7797-801

Dawson TM and Snyder, SH. **Gases as biological messengers: nitric oxide and carbon monoxide in the brain.** *J Neurosci.* 1994;14:5147-59

De Simone R, Ajmone-Cat, MA and Minghetti, L. **Atypical antiinflammatory activation of microglia induced by apoptotic neurons: possible role of phosphatidylserine-phosphatidylserine receptor interaction.** *Mol Neurobiol.* 2004;29:197-212

Dick AD, Broderick, C, Forrester, JV and Wright, GJ. **Distribution of OX2 antigen and OX2 receptor within retina.** *Invest Ophthalmol Vis Sci.* 2001;42:170-6

Dick AD, Carter, D, Robertson, M, Broderick, C, Hughes, E, Forrester, JV and Liversidge, J. **Control of myeloid activity during retinal inflammation.** *J Leukoc Biol.* 2003;74:161-6

Dickson TC, Adlard, PA and Vickers, JC. **Sequence of cellular changes following localized axotomy to cortical neurons in glia-free culture.** *J Neurotrauma.* 2000;17:1095-103

Drance SM, Sweeney VP, Morgan RW, Feldman F. **Studies of factors involved in the production of low tension glaucoma.** *Arch Ophthalmol.* 1973;89:457-65.

Drance SM, Fairclough, M, Butler, DM and Kottler, MS. **The importance of disc hemorrhage in the prognosis of chronic open angle glaucoma.** *Arch Ophthalmol.* 1977;95:226-8

Drance SM. **Disc hemorrhages in the glaucomas.** *Surv Ophthalmol.* 1989;33:331-7

Dreyer EB, Zurakowski D, Schumer RA, Podos SM, Lipton SA. **Elevated glutamate levels in the vitreous body of humans and monkeys with glaucoma.** *Arch Ophthalmol.* 1996;114:299-305

Durrenberger PF, Facer, P, Gray, RA, Chessell, IP, Naylor, A, Bountra, C, Banati, RB, Birch, R and Anand, P. **Cyclooxygenase-2 (Cox-2) in injured human nerve and a rat model of nerve injury.** *J Peripher Nerv Syst.* 2004;9:15-25

Eclancher F, Kehrli P, Labourdette G, Sensenbrenner M. **Basic fibroblast growth factor (bFGF) injection activates the glial reaction in the injured adult rat brain.** *Brain Res.* 1996;737:201-14

Egbert PR. **Glaucoma in West Africa: a neglected problem.** *Br J Ophthalmol.* 2002;86:131-2

Elkington AR, Inman, CB, Steart, PV and Weller, RO. **The structure of the lamina cribrosa of the human eye: an immunocytochemical and electron microscopical study.** *Eye.* 1990;4 (Pt 1):42-57

Emre M, Orgul S, Haufschild T, Shaw SG, Flammer J. **Increased plasma endothelin-1 levels in patients with progressive open angle glaucoma.** *Br J Ophthalmol.* 2005;89:60-3.

Ernest JT and Potts, AM. **Pathophysiology of the distal portion of the optic nerve. I. Tissue pressure relationships.** *Am J Ophthalmol.* 1968;66:373-80

Evans K and Bird, AC. **The genetics of complex ophthalmic disorders.** *Br J Ophthalmol.* 1996;80:763-8

Farinelli SE and Nicklas, WJ. **Glutamate metabolism in rat cortical astrocyte cultures.** *J Neurochem.* 1992;58:1905-15

Fawcett JW, Asher RA. **The glial scar and central nervous system repair.** *Brain Res Bull.* 1999;49:377-91.

Fitch MT and Silver, J. **Glial cell extracellular matrix: boundaries for axon growth in development and regeneration.** *Cell Tissue Res.* 1997;290:379-84

Flammer J and Orgul, S. **Optic nerve blood-flow abnormalities in glaucoma.** *Prog Retin Eye Res.* 1998;17:267-89

Forrester J and Peters, A. **Nerve fibres in optic nerve of rat.** *Nature.* 1967;214:245-7

Fraser S, Bunce, C, Wormald, R and Brunner, E. **Deprivation and late presentation of glaucoma: case-control study.** *Bmj.* 2001;322:639-43

Furuyoshi N, Furuyoshi, M, Futa, R, Gottanka, J and Lutjen-Drecoll, E. **Ultrastructural changes in the trabecular meshwork of juvenile glaucoma.** *Ophthalmologica.* 1997;211:140-6

Furuyoshi N, Furuyoshi, M, May, CA, Hayreh, SS, Alm, A and Lutjen-Drecoll, E. **Vascular and glial changes in the retrolaminar optic nerve in glaucomatous monkey eyes.** *Ophthalmologica.* 2000;214:24-32

Garcia-Valenzuela E, Shareef, S, Walsh, J and Sharma, SC. **Programmed cell death of retinal ganglion cells during experimental glaucoma.** *Exp Eye Res.* 1995;61:33-44

Garcia-Valenzuela E and Sharma, SC. **Laminar restriction of retinal macrophagic response to optic nerve axotomy in the rat.** *J Neurobiol.* 1999;40:55-66

Garthwaite J and Boulton, CL. **Nitric oxide signaling in the central nervous system.** *Annu Rev Physiol.* 1995;57:683-706

Gasser P, Flammer J. **Influence of vasospasm on visual function.** *Doc Ophthalmol.* 1987;66:3-18.

Gehrmann J, Matsumoto Y, Kreutzberg GW. **Microglia: intrinsic immuneffector cell of the brain.** *Brain Res Brain Res Rev.* 1995;20:269-87

Gennarelli TA, Thibault LE, Tipperman R, Tomei G, Sergot R, Brown M, Maxwell WL, Graham DI, Adams JH, Irvine A. **Axonal injury in the optic nerve: a model simulating diffuse axonal injury in the brain.** *J Neurosurg.* 1989;71:244-53.

Georgopoulos G, Andreanos, D, Liokis, N, Papakonstantinou, D, Vergados, J and Theodossiadis, G. **Risk factors in ocular hypertension.** *Eur J Ophthalmol.* 1997;7:357-63

Gharagozloo NZ, Larson, RS, Kullerstrand, LJ and Brubaker, RF. **Terbutaline stimulates aqueous humor flow in humans during sleep.** *Arch Ophthalmol.* 1988;106:1218-20

Giuliani F, Goodyer CG, Antel JP, Yong VW. **Vulnerability of human neurons to T cell-mediated cytotoxicity.** *J Immunol.* 2003;171:368-79.

Goldberg I. **Relationship between intraocular pressure and preservation of visual field in glaucoma.** *Surv Ophthalmol.* 2003;48 Suppl 1:S3-7

Goldblum D and Mittag, T. **Prospects for relevant glaucoma models with retinal ganglion cell damage in the rodent eye.** *Vision Res.* 2002;42:471-8

Gonzalez P, Epstein, DL and Borras, T. **Characterization of gene expression in human trabecular meshwork using single-pass sequencing of 1060 clones.** *Invest Ophthalmol Vis Sci.* 2000;41:3678-93

Gorczynski RM, Chen Z, Fu XM, Zeng H. **Increased expression of the novel molecule OX-2 is involved in prolongation of murine renal allograft survival.** *Transplantation.* 1998;65:1106-14.

Gorczynski RM, Cattral MS, Chen Z, Hu J, Lei J, Min WP, Yu G, Ni J. **An immunoadhesin incorporating the molecule OX-2 is a potent immunosuppressant that prolongs allo- and xenograft survival.** *J Immunol.* 1999;163:1654-60.

Gorczynski RM, Chen, Z, Yu, K and Hu, J. **CD200 immunoadhesin suppresses collagen-induced arthritis in mice.** *Clin Immunol.* 2001;101:328-34

Goss JR, O'Malley ME, Zou L, Styren SD, Kochanek PM, DeKosky ST. **Astrocytes are the major source of nerve growth factor upregulation following traumatic brain injury in the rat.** *Exp Neurol.* 1998;149:301-9.

Graeber MB, Lopez-Redondo, F, Ikoma, E, Ishikawa, M, Imai, Y, Nakajima, K, Kreutzberg, GW and Kohsaka, S. **The microglia/macrophage response in the neonatal rat facial nucleus following axotomy.** *Brain Res.* 1998;813:241-53

Greenberg JH, Uematsu, D, Araki, N, Hickey, WF and Reivich, M. **Cytosolic free calcium during focal cerebral ischemia and the effects of nimodipine on calcium and histologic damage.** *Stroke.* 1990;21:IV72-7

Grimelius L. **Silver stains demonstrating neuroendocrine cells.** *Biotech Histochem.* 2004;79:37-44

Grodum K, Heijl, A and Bengtsson, B. **Refractive error and glaucoma.** *Acta Ophthalmol Scand.* 2001;79:560-6

Groves JT, Wang CC. **Nitric oxide synthase: models and mechanisms.** *Curr Opin Chem Biol.* 2000;4:687-95.

Grozdanic SD, Betts, DM, Sakaguchi, DS, Kwon, YH, Kardon, RH and Sonea, IM. **Temporary elevation of the intraocular pressure by cauterization of vortex and episcleral veins in rats causes functional deficits in the retina and optic nerve.** *Exp Eye Res.* 2003;77:27-33

Grozdanic SD, Kwon, YH, Sakaguchi, DS, Kardon, RH and Sonea, IM. **Functional evaluation of retina and optic nerve in the rat model of chronic ocular hypertension.** *Exp Eye Res.* 2004;79:75-83

Grunwald JE, DuPont, J and Dreyer, EB. **Effect of chronic nitrate treatment on retinal vessel caliber in open-angle glaucoma.** *Am J Ophthalmol.* 1997;123:753-8

Guillemin GJ and Brew, BJ. **Microglia, macrophages, perivascular macrophages, and pericytes: a review of function and identification.** *J Leukoc Biol.* 2004;75:388-97

Guy J, Fitzsimmons, J, Ellis, EA, Beck, B and Mancuso, A. **Intraorbital optic nerve and experimental optic neuritis. Correlation of fat suppression magnetic resonance imaging and electron microscopy.** *Ophthalmology.* 1992;99:720-5

Haefliger IO, Fleischhauer, JC and Flammer, J. **In glaucoma, should enthusiasm about neuroprotection be tempered by the experience obtained in other neurodegenerative disorders?** *Eye.* 2000;14 (Pt 3B):464-72

Hanninen VA, Pantcheva MB, Freeman EE, Poulin NR, Grosskreutz CL. **Activation of caspase 9 in a rat model of experimental glaucoma.** *Curr Eye Res.* 2002 ;25:389-95.

Harbuz MS. **Chronic inflammatory stress.** *Baillieres Best Pract Res Clin Endocrinol Metab.* 1999;13:555-65

Hausladen A, Privalle CT, Keng T, DeAngelo J, Stamler JS. **Nitrosative stress: activation of the transcription factor OxyR.** *Cell.* 1996;86:719-29.

Hayreh SS, March W, Anderson DR. **Pathogenesis of block of rapid orthograde axonal transport by elevated intraocular pressure.** *Exp Eye Res.* 1979;28:515-23.

Healey PR, Mitchell, P, Smith, W and Wang, JJ. **Optic disc hemorrhages in a population with and without signs of glaucoma.** *Ophthalmology.* 1998;105:216-23

Hernandez MR, Igoe, F and Neufeld, AH. **Cell culture of the human lamina cribrosa.** *Invest Ophthalmol Vis Sci.* 1988;29:78-89

Hernandez J and Condes-Lara, M. **Brain Na+/K(+)-ATPase regulation by serotonin and norepinephrine in normal and kindled rats.** *Brain Res.* 1992;593:239-44

Hernandez MR and Ye, H. **Glaucoma: changes in extracellular matrix in the optic nerve head.** *Ann Med.* 1993;25:309-15

Hernandez MR, Pena JD, Selvidge JA, Salvador-Silva M, Yang P. **Hydrostatic pressure stimulates synthesis of elastin in cultured optic nerve head astrocytes.** *Glia.* 2000 Nov;32(2):122-36.

Hirji N, Lin TJ, Befus AD. **A novel CD8 molecule expressed by alveolar and peritoneal macrophages stimulates nitric oxide production.** *J Immunol.* 1997;158:1833-40.

Hitchings RA and Spaeth, GL. **The optic disc in glaucoma. I: Classification.** *Br J Ophthalmol.* 1976;60:778-85

Hoek RM, Ruuls SR, Murphy CA, Wright GJ, Goddard R, Zurawski SM, Blom B, Homola ME, Streit WJ, Brown MH, Barclay AN, Sedgwick JD. **Down-regulation of the macrophage lineage through interaction with OX2 (CD200).** *Science.* 2000;290:1768-71.

Hofman P, Hoyng, P, vanderWerf, F, Vrensen, GF and Schlingemann, RO. **Lack of blood-brain barrier properties in microvessels of the prelaminar optic nerve head.** *Invest Ophthalmol Vis Sci.* 2001;42:895-901

Hollander H, Makarov, F, Stefani, FH and Stone, J. **Evidence of constriction of optic nerve axons at the lamina cribrosa in the normotensive eye in humans and other mammals.** *Ophthalmic Res.* 1995;27:296-309

Huang Z, Huang, PL, Panahian, N, Dalkara, T, Fishman, MC and Moskowitz, MA. **Effects of cerebral ischemia in mice deficient in neuronal nitric oxide synthase.** *Science.* 1994;265:1883-5

Huang Z, Huang, PL, Ma, J, Meng, W, Ayata, C, Fishman, MC and Moskowitz, MA. **Enlarged infarcts in endothelial nitric oxide synthase knockout mice are attenuated by nitro-L-arginine.** *J Cereb Blood Flow Metab.* 1996;16:981-7

Hughes A. **The pigmented-rat optic nerve: fibre count and fibre diameter spectrum.** *J Comp Neurol.* 1977;176:263-8

Ikonomidou C, Turski L. **Why did NMDA receptor antagonists fail clinical trials for stroke and traumatic brain injury?** *Lancet Neurol.* 2002;1:383-6.

Inoue-Matsuhisa E, Sogo, S, Mizota, A, Taniai, M, Takenaka, H and Mano, T. **Effect of MCI-9042, a 5-HT2 receptor antagonist, on retinal ganglion cell death and retinal ischemia.** *Exp Eye Res.* 2003;76:445-52

Javitt JC, Spaeth, GL, Katz, LJ, Poryzees, E and Addiego, R. **Acquired pits of the optic nerve. Increased prevalence in patients with low-tension glaucoma.** *Ophthalmology.* 1990;97:1038-43; discussion 1043-4

Jia L, Cepurna, WO, Johnson, EC and Morrison, JC. **Patterns of intraocular pressure elevation after aqueous humor outflow obstruction in rats.** *Invest Ophthalmol Vis Sci.* 2000;41:1380-5

Johansson JO. **Inhibition of retrograde axoplasmic transport in rat optic nerve by increased IOP in vitro.** *Invest Ophthalmol Vis Sci.* 1983;24:1552-8.

John SW, Smith, RS, Savinova, OV, Hawes, NL, Chang, B, Turnbull, D, Davisson, M, Roderick, TH and Heckenlively, JR. **Essential iris atrophy, pigment dispersion, and glaucoma in DBA/2J mice.** *Invest Ophthalmol Vis Sci.* 1998;39:951-62

John SW, Anderson, MG and Smith, RS. **Mouse genetics: a tool to help unlock the mechanisms of glaucoma.** *J Glaucoma.* 1999;8:400-12

Johnson EC, Morrison, JC, Farrell, S, Deppmeier, L, Moore, CG and McGinty, MR. **The effect of chronically elevated intraocular pressure on the rat optic nerve head extracellular matrix.** *Exp Eye Res.* 1996;62:663-74

Johnson EC, Deppmeier, LM, Wentzien, SK, Hsu, I and Morrison, JC. **Chronology of optic nerve head and retinal responses to elevated intraocular pressure.** *Invest Ophthalmol Vis Sci.* 2000;41:431-42

Jonas JB, Gusek, GC and Naumann, GO. **Optic disc morphometry in chronic primary open-angle glaucoma. II. Correlation of the intrapapillary morphometric data to visual field indices.** *Graefes Arch Clin Exp Ophthalmol.* 1988;226:531-8

Jonas JB, Nguyen, XN and Naumann, GO. **Parapapillary retinal vessel diameter in normal and glaucoma eyes. I. Morphometric data.** *Invest Ophthalmol Vis Sci.* 1989;30:1599-603

Jonas JB, Fernandez, MC and Sturmer, J. **Pattern of glaucomatous neuroretinal rim loss.** *Ophthalmology.* 1993;100:63-8

Jonas JB and Papastathopoulos, KI. **Optic disc shape in glaucoma.** *Graefes Arch Clin Exp Ophthalmol.* 1996;234 Suppl 1:S167-73

Karali A, Russell, P, Stefani, FH and Tamm, ER. **Localization of myocilin/trabecular meshwork--inducible glucocorticoid response protein in the human eye.** *Invest Ophthalmol Vis Sci.* 2000;41:729-40

Karatsoreos IN, Yan, L, LeSauter, J and Silver, R. **Phenotype matters: identification of light-responsive cells in the mouse suprachiasmatic nucleus.** *J Neurosci.* 2004;24:68-75

Kashiwagi K, Iizuka, Y, Araie, M, Suzuki, Y and Tsukahara, S. **Effects of retinal glial cells on isolated rat retinal ganglion cells.** *Invest Ophthalmol Vis Sci.* 2001;42:2686-94

Kawahara K, Oyadomari, S, Gotoh, T, Kohsaka, S, Nakayama, H and Mori, M. **Induction of CHOP and apoptosis by nitric oxide in p53-deficient microglial cells.** *FEBS Lett.* 2001;506:135-9

Keirstead SA, Rasminsky, M, Fukuda, Y, Carter, DA, Aguayo, AJ and Vidal-Sanz, M. **Electrophysiologic responses in hamster superior colliculus evoked by regenerating retinal axons.** *Science.* 1989;246:255-7

Kermer P, Klocker N, Labes M, Bahr M. **Inhibition of CPP32-like proteases rescues axotomized retinal ganglion cells from secondary cell death in vivo.** *J Neurosci.* 1998;18:4656-62.

Kermer P, Klocker, N, Weishaupt, JH and Bahr, M. **Transection of the optic nerve in rats: studying neuronal death and survival in vivo.** *Brain Res Brain Res Protoc.* 2001;7:255-60

Kerrigan-Baumrind LA, Quigley, HA, Pease, ME, Kerrigan, DF and Mitchell, RS. **Number of ganglion cells in glaucoma eyes compared with threshold visual field tests in the same persons.** *Invest Ophthalmol Vis Sci.* 2000;41:741-8

Kim HJ, Ifergan, I, Antel, JP, Seguin, R, Duddy, M, Lapierre, Y, Jalili, F and Bar-Or, A. **Type 2 monocyte and microglia differentiation mediated by glatiramer acetate therapy in patients with multiple sclerosis.** *J Immunol.* 2004;172:7144-53

Kim KY, Ju, WK and Neufeld, AH. **Neuronal susceptibility to damage: comparison of the retinas of young, old and old/caloric restricted rats before and after transient ischemia.** *Neurobiol Aging.* 2004;25:491-500

Kitano S, Morgan J, Caprioli J. **Hypoxic and excitotoxic damage to cultured rat retinal ganglion cells.** *Exp Eye Res.* 1996;63:105-12

Kitazawa Y, Taniguchi, T and Sugiyama, K. **Use of apraclonidine to reduce acute intraocular pressure rise following Q-switched Nd:YAG laser iridotomy.** *Ophthalmic Surg.* 1989;20:49-52

Kitazawa Y, Yamamoto T. **Glaucomatous visual field defects: their characteristics and how to detect them.** *Clin Neurosci.* 1997;4(5):279-83

Klocker N, Cellerino A, Bahr M. **Free radical scavenging and inhibition of nitric oxide synthase potentiates the neurotrophic effects of brain-derived neurotrophic factor on axotomized retinal ganglion cells In vivo.** *J Neurosci.* 1998;18:1038-46

Konobu T, Sessler, F, Luo, LY and Lehmann, J. **The hNT human neuronal cell line survives and migrates into rat retina.** *Cell Transplant.* 1998;7:549-58

Kotikoski H, Moilanen, E, Vapaatalo, H and Aine, E. **Biochemical markers of the L-arginine-nitric oxide pathway in the aqueous humour in glaucoma patients.** *Acta Ophthalmol Scand.* 2002;80:191-5

Kugler S, Klocker N, Kermer P, Isenmann S, Bahr M. **Transduction of axotomized retinal ganglion cells by adenoviral vector administration at the optic nerve stump: an in vivo model system for the inhibition of neuronal apoptotic cell death.** *Gene Ther.* 1999;6:1759-67.

Kreutzberg GW. **Microglia: a sensor for pathological events in the CNS.** *Trends Neurosci.* 1996;19:312-8

Krishna R, Mermoud, A, Baerveldt, G and Minckler, DS. **Circadian rhythm of intraocular pressure: a rat model.** *Ophthalmic Res.* 1995;27:163-7

Lam DY, Kaufman, PL, Gabelt, BT, To, EC and Matsubara, JA. **Neurochemical correlates of cortical plasticity after unilateral elevated intraocular pressure in a primate model of glaucoma.** *Invest Ophthalmol Vis Sci.* 2003;44:2573-81 (a)

Lam TT, Kwong, JM and Tso, MO. **Early glial responses after acute elevated intraocular pressure in rats.** *Invest Ophthalmol Vis Sci.* 2003;44:638-45 (b)

Lamas S, Marsden, PA, Li, GK, Tempst, P and Michel, T. **Endothelial nitric oxide synthase: molecular cloning and characterization of a distinct constitutive enzyme isoform.** *Proc Natl Acad Sci U S A.* 1992;89:6348-52

Lampert PW, Vogel, MH and Zimmerman, LE. **Pathology of the optic nerve in experimental acute glaucoma. Electron microscopic studies.** *Invest Ophthalmol.* 1968;7:199-213

Lambert W, Agarwal R, Howe W, Clark AF, Wordinger RJ. **Neurotrophin and neurotrophin receptor expression by cells of the human lamina cribrosa.** *Invest Ophthalmol Vis Sci.* 2001;42:2315-23.

Lancaster JR, Jr. **A tutorial on the diffusibility and reactivity of free nitric oxide.** *Nitric Oxide.* 1997;1:18-30

Lang R, Lustig M, Francois F, Sellinger M, Plesken H. **Apoptosis during macrophage-dependent ocular tissue remodelling.** *Development.* 1994;120:3395-403.

Laquis S, Chaudhary, P and Sharma, SC. **The patterns of retinal ganglion cell death in hypertensive eyes.** *Brain Res.* 1998;784:100-4

Lassmann H, Ammerer, HP and Kulnig, W. **Ultrastructural sequence of myelin degradation. I. Wallerian degeneration in the rat optic nerve.** *Acta Neuropathol (Berl).* 1978;44:91-102

LaVail MM, Gorrin GM. **Protection from light damage by ocular pigmentation: analysis using experimental chimeras and translocation mice.** *Exp Eye Res.* 1987;44:877-89.

Le A, Mukesh, BN, McCarty, CA and Taylor, HR. **Risk factors associated with the incidence of open-angle glaucoma: the visual impairment project.** *Invest Ophthalmol Vis Sci.* 2003;44:3783-9

Lee EW, Render, JA, Garner, CD, Brady, AN and Li, LC. **Unilateral degeneration of retina and optic nerve in Fischer-344 rats.** *Vet Pathol.* 1990;27:439-44

Lee SH, Kim, WT, Cornell-Bell, AH and Sontheimer, H. **Astrocytes exhibit regional specificity in gap-junction coupling.** *Glia.* 1994;11:315-25

Leret ML, San Millan, JA, Fabre, E, Gredilla, R and Barja, G. **Deprenyl protects from MPTP-induced Parkinson-like syndrome and glutathione oxidation in rat striatum.** *Toxicology.* 2002;170:165-71

Levkovitch-Verbin H, Quigley, HA, Martin, KR, Valenta, D, Baumrind, LA and Pease, ME. **Translimbal laser photocoagulation to the trabecular meshwork as a model of glaucoma in rats.** *Invest Ophthalmol Vis Sci.* 2002;43:402-10

Levkovitch-Verbin H, Quigley, HA, Martin, KR, Zack, DJ, Pease, ME and Valenta, DF. **A model to study differences between primary and secondary degeneration of retinal ganglion cells in rats by partial optic nerve transection.** *Invest Ophthalmol Vis Sci.* 2003;44:3388-93

Ling EA. **Electron microscopic studies of macrophages in Wallerian degeneration of rat optic nerve after intravenous injection of colloidal carbon.** *J Anat.* 1978;126:111-21

Lipton SA, Kater SB. **Neurotransmitter regulation of neuronal outgrowth, plasticity and survival.** *Trends Neurosci.* 1989;12:265-70

Lipton SA, Choi, YB, Pan, ZH, Lei, SZ, Chen, HS, Sucher, NJ, Loscalzo, J, Singel, DJ and Stamler, JS. **A redox-based mechanism for the neuroprotective and neurodestructive effects of nitric oxide and related nitroso-compounds.** *Nature.* 1993;364:626-32

Ling EA, Shieh JY, Wen CY, Yick TY, Wong WC. **Neural degeneration and non-neuronal cellular reactions in the hypoglossal nucleus following an intraneural injection of toxic ricin.** *Arch Histol Cytol.* 1989 Oct;52(4):345-54

Liu T, van Rooijen, N and Tracey, DJ. **Depletion of macrophages reduces axonal degeneration and hyperalgesia following nerve injury.** *Pain.* 2000;86:25-32

Liu B, Neufeld AH. **Nitric oxide synthase-2 in human optic nerve head astrocytes induced by elevated pressure in vitro.** *Arch Ophthalmol.* 2001;119:240-5

Lumme P, Tuulonen, A, Airaksinen, PJ and Alanko, HI. **Neuroretinal rim area in low tension glaucoma: effect of nifedipine and acetazolamide compared to no treatment.** *Acta Ophthalmol (Copenh).* 1991;69:293-8

Lyons CR, Orloff, GJ and Cunningham, JM. **Molecular cloning and functional expression of an inducible nitric oxide synthase from a murine macrophage cell line.** *J Biol Chem.* 1992;267:6370-4

Mabuchi F, Aihara, M, Mackey, MR, Lindsey, JD and Weinreb, RN. **Optic nerve damage in experimental mouse ocular hypertension.** *Invest Ophthalmol Vis Sci.* 2003;44:4321-30

Maeda H, Nakamura, M and Yamamoto, M. **Morphometric features of laminar pores in lamina cribrosa observed by scanning laser ophthalmoscopy.** *Jpn J Ophthalmol.* 1999;43:415-21

Maeda K, Sawada, A, Matsubara, M, Nakai, Y, Hara, A and Yamamoto, T. **A novel neuroprotectant against retinal ganglion cell damage in a glaucoma model and an optic nerve crush model in the rat.** *Invest Ophthalmol Vis Sci.* 2004;45:851-6

Majno G, Joris I. **Apoptosis, oncosis, and necrosis. An overview of cell death.** *Am J Pathol.* 1995;146:3-15.

Manni G, Lambiase, A, Centofanti, M, Mattei, E, De Gregorio, A, Aloe, L and de Feo, G. **Histopathological evaluation of retinal damage during intraocular hypertension in rabbit: involvement of ganglion cells and nerve fiber layer.** *Graefes Arch Clin Exp Ophthalmol.* 1996;234 Suppl 1:S209-13

Marques SA, Taffarel, M and Blanco Martinez, AM. **Participation of neurofilament proteins in axonal dark degeneration of rat's optic nerves.** *Brain Res.* 2003;969:1-13

Martinez-Bello C, Chauhan BC, Nicolela MT, McCormick TA, LeBlanc RP. **Intraocular pressure and progression of glaucomatous visual field loss.** *Am J Ophthalmol.* 2000;129:302-8.

Martinou JC, Dubois-Dauphin, M, Staple, JK, Rodriguez, I, Frankowski, H, Missotten, M, Albertini, P, Talabot, D, Catsicas, S, Pietra, C and et al. **Overexpression of BCL-2 in transgenic mice protects neurons from naturally occurring cell death and experimental ischemia.** *Neuron.* 1994;13:1017-30

Maruyama W and Naoi, M. **Neuroprotection by (-)-deprenyl and related compounds.** *Mech Ageing Dev.* 1999;111:189-200

Matsubara T, Pararajasegaram, G, Wu, GS and Rao, NA. **Retinal microglia differentially express phenotypic markers of antigen-presenting cells in vitro.** *Invest Ophthalmol Vis Sci.* 1999;40:3186-93

Maxwell WL, Islam MN, Graham DI, Gennarelli TA. **A qualitative and quantitative analysis of the response of the retinal ganglion cell soma after stretch injury to the adult guinea-pig optic nerve.** *J Neurocytol.* 1994;23:379-92.

May CA, Hayreh, SS, Furuyoshi, N, Ossoinig, K, Kaufman, PL and Lutjen-Drecoll, E. **Choroidal ganglion cell plexus and retinal vasculature in monkeys with laser-induced glaucoma.** *Ophthalmologica.* 1997;211:161-71

May CA and Lutjen-Drecoll, E. **Morphology of the murine optic nerve.** *Invest Ophthalmol Vis Sci.* 2002;43:2206-12

May CA. **The optic nerve head region of the aged rat: an immunohistochemical investigation.** *Curr Eye Res.* 2003;26:347-54

McKinnon SJ, Lehman DM, Kerrigan-Baumrind LA, Merges CA, Pease ME, Kerrigan DF, Ransom NL, Tahzib NG, Reitsamer HA, Levkovitch-Verbin H, Quigley HA, Zack DJ. **Caspase activation and amyloid precursor protein cleavage in rat ocular hypertension.** *Invest Ophthalmol Vis Sci.* 2002;43:1077-87.

McLeod D. **Retinal ischaemia, disc swelling, and axoplasmic transport.** *Trans Ophthalmol Soc U K.* 1976;96:313-8.

Mellough CB, Cui, Q, Spalding, KL, Symons, NA, Pollett, MA, Snyder, EY, Macklis, JD and Harvey, AR. **Fate of multipotent neural precursor cells transplanted into mouse retina selectively depleted of retinal ganglion cells.** *Exp Neurol.* 2004;186:6-19

Mermoud A, Baerveldt, G, Minckler, DS, Prata, JA, Jr. and Rao, NA. **Aqueous humor dynamics in rats.** *Graefes Arch Clin Exp Ophthalmol.* 1996;234 Suppl 1:S198-203

Messmer UK, Ankarcrona M, Nicotera P, Brune B. **p53 expression in nitric oxide-induced apoptosis.** *FEBS Lett.* 1994;355:23-6.

Messmer UK, Brune B. **Nitric oxide-induced apoptosis: p53-dependent and p53-independent signalling pathways.** *Biochem J.* 1996;319 (Pt 1):299-305.

Messmer UK, Reed UK, Brune B. **Bcl-2 protects macrophages from nitric oxide-induced apoptosis.** *J Biol Chem.* 1996;271:20192-7.

Miller JM and Caprioli, J. **Videographic quantification of optic disc pallor.** *Invest Ophthalmol Vis Sci.* 1988;29:320-3

Minckler DS and Spaeth, GL. **Optic nerve damage in glaucoma.** *Surv Ophthalmol.* 1981;26:128-48

Mittag TW, Danias, J, Pohorenec, G, Yuan, HM, Burakgazi, E, Chalmers-Redman, R, Podos, SM and Tatton, WG. **Retinal damage after 3 to 4 months of elevated intraocular pressure in a rat glaucoma model.** *Invest Ophthalmol Vis Sci.* 2000;41:3451-9

Mo JS, Anderson, MG, Gregory, M, Smith, RS, Savinova, OV, Serreze, DV, Ksander, BR, Streilein, JW and John, SW. **By altering ocular immune privilege, bone marrow-derived cells pathogenically contribute to DBA/2J pigmentary glaucoma.** *J Exp Med.* 2003;197:1335-44

Moore CG, Epley, D, Milne, ST and Morrison, JC. **Long-term non-invasive measurement of intraocular pressure in the rat eye.** *Curr Eye Res.* 1995;14:711-7

Moore CG, Johnson, EC and Morrison, JC. **Circadian rhythm of intraocular pressure in the rat.** *Curr Eye Res.* 1996;15:185-91

Moreno MC, Sande P, Marcos HA, de Zavalia N, Keller Sarmiento MI, Rosenstein RE. **Effect of glaucoma on the retinal glutamate/glutamine cycle activity.** *FASEB J.* 2005;19:1161-2.

Morris MM, Dyson, H, Baker, D, Harbige, LS, Fazakerley, JK and Amor, S. **Characterization of the cellular and cytokine response in the central nervous system following Semliki Forest virus infection.** *J Neuroimmunol.* 1997;74:185-97

Morrison J, Farrell, S, Johnson, E, Deppmeier, L, Moore, CG and Grossmann, E. **Structure and composition of the rodent lamina cribrosa.** *Exp Eye Res.* 1995;60:127-35

Morrison JC, Moore, CG, Deppmeier, LM, Gold, BG, Meshul, CK and Johnson, EC. **A rat model of chronic pressure-induced optic nerve damage.** *Exp Eye Res.* 1997;64:85-96

Morrison JC, Nylander, KB, Lauer, AK, Cepurna, WO and Johnson, E. **Glaucoma drops control intraocular pressure and protect optic nerves in a rat model of glaucoma.** *Invest Ophthalmol Vis Sci.* 1998;39:526-31

Morrison JC. **Elevated intraocular pressure and optic nerve injury models in the rat.** *J Glaucoma.* 2005;14:315-7.

Mosmann TR and Sad, S. **The expanding universe of T-cell subsets: Th1, Th2 and more.** *Immunol Today.* 1996;17:138-46

Mueller M, Leonhard, C, Wacker, K, Ringelstein, EB, Okabe, M, Hickey, WF and Kiefer, R. **Macrophage response to peripheral nerve injury: the quantitative contribution of resident and hematogenous macrophages.** *Lab Invest.* 2003;83:175-85

Nagasubramanian S, Rahi, AH and Gloster, J. **Immunological investigations in chronic simple glaucoma.** *Trans Ophthalmol Soc U K.* 1978;98:22-7

Narciso MS, Hokoc, JN and Martinez, AM. **Watery and dark axons in Wallerian degeneration of the opossum's optic nerve: different patterns of cytoskeletal breakdown?** *An Acad Bras Cienc.* 2001;73:231-43

Naskar R, Wissing, M and Thanos, S. **Detection of early neuron degeneration and accompanying microglial responses in the retina of a rat model of glaucoma.** *Invest Ophthalmol Vis Sci.* 2002;43:2962-8

Nathan C and Xie, QW. **Regulation of biosynthesis of nitric oxide.** *J Biol Chem.* 1994;269:13725-8

Negishi H, Dezawa, M, Oshitari, T and Adachi-Usami, E. **Optic nerve regeneration within artificial Schwann cell graft in the adult rat.** *Brain Res Bull.* 2001;55:409-19

Netland PA, Chaturvedi, N and Dreyer, EB. **Calcium channel blockers in the management of low-tension and open-angle glaucoma.** *Am J Ophthalmol.* 1993;115:608-13

Neufeld AH, Hernandez, MR and Gonzalez, M. **Nitric oxide synthase in the human glaucomatous optic nerve head.** *Arch Ophthalmol.* 1997;115:497-503

Neufeld AH. **Microglia in the optic nerve head and the region of parapapillary chorioretinal atrophy in glaucoma.** *Arch Ophthalmol.* 1999;117:1050-6

Neufeld AH, Liu B. **Comparison of the signal transduction pathways for the induction of gene expression of nitric oxide synthase-2 in response to two different stimuli.** *Nitric Oxide.* 2003;8:95-102.

Neumann H. **Molecular mechanisms of axonal damage in inflammatory central nervous system diseases.** *Curr Opin Neurol.* 2003;16:267-73

Nguyen T, Brunson D, Crespi CL, Penman BW, Wishnok JS, Tannenbaum SR. **DNA damage and mutation in human cells exposed to nitric oxide in vitro.** *Proc Natl Acad Sci U S A.* 1992;89:3030-4.

Nickells RW. **Retinal ganglion cell death in glaucoma: the how, the why, and the maybe.** *J Glaucoma.* 1996;5:345-56

Nicotera P, Ankarcrona, M, Bonfoco, E, Orrenius, S and Lipton, SA. **Neuronal necrosis and apoptosis: two distinct events induced by exposure to glutamate or oxidative stress.** *Adv Neurol.* 1997;72:95-101

Nii H, Ikeda, H, Okada, K, Yoshitomi, T and Gregory, DS. **Circadian change of adenylate cyclase activity in rabbit ciliary processes.** *Curr Eye Res.* 2001;23:248-55

Norenberg MD. **Astrocyte responses to CNS injury.** *J Neuropathol Exp Neurol.* 1994;53:213-20

Nunokawa Y, Ishida, N and Tanaka, S. **Cloning of inducible nitric oxide synthase in rat vascular smooth muscle cells.** *Biochem Biophys Res Commun.* 1993;191:89-94

Ogden TE and Miller, RF. **Studies of the optic nerve of the rhesus monkey: nerve fiber spectrum and physiological properties.** *Vision Res.* 1966;6:485-506

Ogden TE, Duggan, J, Danley, K, Wilcox, M and Minckler, DS. **Morphometry of nerve fiber bundle pores in the optic nerve head of the human.** *Exp Eye Res.* 1988;46:559-68

Osborne NN, Ugarte, M, Chao, M, Chidlow, G, Bae, JH, Wood, JP and Nash, MS. **Neuroprotection in relation to retinal ischemia and relevance to glaucoma.** *Surv Ophthalmol.* 1999;43 Suppl 1:S102-28

Pang IH, Johnson EC, Jia L, Cepurna WO, Shepard AR, Hellberg MR, Clark AF, Morrison JC. **Evaluation of inducible nitric oxide synthase in glaucomatous optic neuropathy and pressure-induced optic nerve damage.** *IOVS* 2005;46(4):1313-21

Parra B, Hinton, DR, Lin, MT, Cua, DJ and Stohlman, SA. **Kinetics of cytokine mRNA expression in the central nervous system following lethal and nonlethal coronavirus-induced acute encephalomyelitis.** *Virology.* 1997;233:260-70

Pearson R, Catsicas, M, Becker, D and Mobbs, P. **Purinergic and muscarinic modulation of the cell cycle and calcium signaling in the chick retinal ventricular zone.** *J Neurosci.* 2002;22:7569-79

Pederson JE, Gaasterland DE. **Laser-induced primate glaucoma. I. Progression of cupping.** *Arch Ophthalmol.* 1984;102:1689-92

Perkins ES and Phelps, CD. **Open angle glaucoma, ocular hypertension, low-tension glaucoma, and refraction.** *Arch Ophthalmol.* 1982;100:1464-7

Pointer JS. **The diurnal variation of intraocular pressure in non-glaucomatous subjects: relevance in a clinical context.** *Ophthalmic Physiol Opt.* 1997;17:456-65

Potts AM, Hodges, D, Shelman, CB, Fritz, KJ, Levy, NS and Mangnall, Y. **Morphology of the primate optic nerve. I. Method and total fiber count.** *Invest Ophthalmol.* 1972;11:980-8 (a)

Potts AM, Hodges, D, Shelman, CB, Fritz, KJ, Levy, NS and Mangnall, Y. **Morphology of the primate optic nerve. II. Total fiber size distribution and fiber density distribution.** *Invest Ophthalmol.* 1972;11:989-1003 (b)

Prasanna G, Krishnamoorthy, R, Clark, AF, Wordinger, RJ and Yorio, T. **Human optic nerve head astrocytes as a target for endothelin-1.** *Invest Ophthalmol Vis Sci.* 2002;43:2704-13

Privat A. **Astrocytes as support for axonal regeneration in the central nervous system of mammals.** *Glia.* 2003;43:91-3

Quigley HA. **Gap junctions between optic nerve head astrocytes.** *Invest Ophthalmol Vis Sci.* 1977;16:582-5

Quigley HA and Anderson, DR. **Distribution of axonal transport blockade by acute intraocular pressure elevation in the primate optic nerve head.** *Invest Ophthalmol Vis Sci.* 1977;16:640-4

Quigley HA and Addicks, EM. **Chronic experimental glaucoma in primates. II. Effect of extended intraocular pressure elevation on optic nerve head and axonal transport.** *Invest Ophthalmol Vis Sci.* 1980;19:137-52

Quigley HA, Flower, RW, Addicks, EM and McLeod, DS. **The mechanism of optic nerve damage in experimental acute intraocular pressure elevation.** *Invest Ophthalmol Vis Sci.* 1980;19:505-17

Quigley HA. **Long-term follow-up of laser iridotomy**. *Ophthalmology.* 1981;88:218-24

Quigley HA and Addicks, EM. **Regional differences in the structure of the lamina cribrosa and their relation to glaucomatous optic nerve damage**. *Arch Ophthalmol.* 1981;99:137-43

Quigley HA, Addicks, EM, Green, WR and Maumenee, AE. **Optic nerve damage in human glaucoma. II. The site of injury and susceptibility to damage**. *Arch Ophthalmol.* 1981;99:635-49

Quigley HA, Addicks, EM and Green, WR. **Optic nerve damage in human glaucoma. III. Quantitative correlation of nerve fiber loss and visual field defect in glaucoma, ischemic neuropathy, papilledema, and toxic neuropathy**. *Arch Ophthalmol.* 1982;100:135-46 (a)

Quigley HA, Hohman, RM and Addicks, EM. **Quantitative study of optic nerve head capillaries in experimental optic disk pallor**. *Am J Ophthalmol.* 1982;93:689-99 (b)

Quigley HA. **Reappraisal of the mechanisms of glaucomatous optic nerve damage**. *Eye.* 1987;1 (Pt 2):318-22

Quigley HA, Dorman-Pease ME, Brown AE. **Quantitative study of collagen and elastin of the optic nerve head and sclera in human and experimental monkey glaucoma.** *Curr Eye Res.* 1991;10:877-88.

Quigley H, Pease, ME and Thibault, D. **Change in the appearance of elastin in the lamina cribrosa of glaucomatous optic nerve heads**. *Graefes Arch Clin Exp Ophthalmol.* 1994;232:257-61

Quigley HA, Nickells, RW, Kerrigan, LA, Pease, ME, Thibault, DJ and Zack, DJ. **Retinal ganglion cell death in experimental glaucoma and after axotomy occurs by apoptosis**. *Invest Ophthalmol Vis Sci.* 1995;36:774-86

Quintero JE, Kuhlman, SJ and McMahon, DG. **The biological clock nucleus: a multiphasic oscillator network regulated by light.** *J Neurosci.* 2003;23:8070-6

Rabacchi SA, Ensini, M, Bonfanti, L, Gravina, A and Maffei, L. **Nerve growth factor reduces apoptosis of axotomized retinal ganglion cells in the neonatal rat.** *Neuroscience.* 1994;63:969-73

Rader J, Feuer, WJ and Anderson, DR. **Peripapillary vasoconstriction in the glaucomas and the anterior ischemic optic neuropathies.** *Am J Ophthalmol.* 1994;117:72-80

Radius RL and Pederson, JE. **Laser-induced primate glaucoma. II. Histopathology.** *Arch Ophthalmol.* 1984;102:1693-8

Rahman R, Casson RJ, Gouveia SM, Salmon JF. **Optic disc morphology on presentation of chronic glaucoma.** *Eye.* 2002;16:665-7.

Raibon E, Sauve, Y, Carter, DA and Gaillard, F. **Microglial changes accompanying the promotion of retinal ganglion cell axonal regeneration into peripheral nerve grafts.** *J Neurocytol.* 2002;31:57-71

Rao NA, Kimoto, T, Zamir, E, Giri, R, Wang, R, Ito, S, Pararajasegaram, G, Read, RW and Wu, GS. **Pathogenic role of retinal microglia in experimental uveoretinitis.** *Invest Ophthalmol Vis Sci.* 2003;44:22-31

Rauen T, Taylor WR, Kuhlbrodt K, Wiessner M. **High-affinity glutamate transporters in the rat retina: a major role of the glial glutamate transporter GLAST-1 in transmitter clearance.** *Cell Tissue Res.* 1998;291:19-31.

Richards JE, Ritch, R, Lichter, PR, Rozsa, FW, Stringham, HM, Caronia, RM, Johnson, D, Abundo, GP, Willcockson, J, Downs, CA, Thompson, DA, Musarella, MA, Gupta, N, Othman, MI, Torrez, DM, Herman, SB, Wong, DJ, Higashi, M and Boehnke, M. **Novel trabecular meshwork inducible glucocorticoid response mutation in an eight-generation juvenile-onset primary open-angle glaucoma pedigree.** *Ophthalmology.* 1998;105:1698-707

Richardson PM, Issa, VM and Shemie, S. **Regeneration and retrograde degeneration of axons in the rat optic nerve.** *J Neurocytol.* 1982;11:949-66

Ridet JL, Malhotra SK, Privat A, Gage FH. **Reactive astrocytes: cellular and molecular cues to biological function.** *Trends Neurosci.* 1997;20:570-7

Ripodas A, de Juan, JA, Roldan-Pallares, M, Bernal, R, Moya, J, Chao, M, Lopez, A, Fernandez-Cruz, A and Fernandez-Durango, R. **Localisation of endothelin-1 mRNA expression and immunoreactivity in the retina and optic nerve from human and porcine eye. Evidence for endothelin-1 expression in astrocytes.** *Brain Res.* 2001;912:137-43

Roberts JE. **Light and immunomodulation.** *Ann N Y Acad Sci.* 2000;917:435-45

Rodrigues RW, Gomide, VC and Chadi, G. **Astroglial and microglial reaction after a partial nigrostriatal degeneration induced by the striatal injection of different doses of 6-hydroxydopamine.** *Int J Neurosci.* 2001;109:91-126

Rohen JW. **Why is intraocular pressure elevated in chronic simple glaucoma? Anatomical considerations.** *Ophthalmology.* 1983;90:758-65

Rohrer B, LaVail MM, Jones KR, Reichardt LF. **Neurotrophin receptor TrkB activation is not required for the postnatal survival of retinal ganglion cells in vivo.** *Exp Neurol.* 2001;172:81-91.

Rojanapongpun P, Drance, SM and Morrison, BJ. **Ophthalmic artery flow velocity in glaucomatous and normal subjects.** *Br J Ophthalmol.* 1993;77:25-9

Salvador-Silva M, Ricard, CS, Agapova, OA, Yang, P and Hernandez, MR. **Expression of small heat shock proteins and intermediate filaments in the human optic nerve head astrocytes exposed to elevated hydrostatic pressure in vitro.** *J Neurosci Res.* 2001;66:59-73

Samuelson TW and Spaeth, GL. **Focal and diffuse visual field defects: their relationship to intraocular pressure.** *Ophthalmic Surg.* 1993;24:519-25

Santiago M, Machado, A and Cano, J. **Effect of L-arginine/nitric oxide pathway on MPP(+)-induced cell injury in the striatum of rats.** *Br J Pharmacol.* 1994;111:837-42

Sawada A and Neufeld, AH. **Confirmation of the rat model of chronic, moderately elevated intraocular pressure.** *Exp Eye Res.* 1999;69:525-31

Sawaguchi S, Yue, BY, Abe, H, Iwata, K, Fukuchi, T and Kaiya, T. **The collagen fibrillar network in the human pial septa.** *Curr Eye Res.* 1994;13:819-24

Scharenberg K. **Degeneration, regeneration and readjustment in the human brain.** *J Neuropathol Exp Neurol.* 1953;12:90-2

Schlamp CL, Johnson EC, Li Y, Morrison JC, Nickells RW. **Changes in Thy1 gene expression associated with damaged retinal ganglion cells.** *Mol Vis.* 2001;7:192-201

Schuetz E and Thanos, S. **Neuro-glial interactions in the adult rat retina after reaxotomy of ganglion cells: examination of neuron survival and phagocytic microglia using fluorescent tracers.** *Brain Res Bull.* 2004;62:391-6

Schulze-Osthoff K, Ferrari, D, Los, M, Wesselborg, S and Peter, ME. **Apoptosis signaling by death receptors.** *Eur J Biochem.* 1998;254:439-59

Schwartz M, Belkin M, Yoles E, Solomon A. **Potential treatment modalities for glaucomatous neuropathy: neuroprotection and neuroregeneration.** *J Glaucoma.* 1996;5:427-32

Schwartz M and Yoles, E. **Neuroprotection: a new treatment modality for glaucoma?** *Curr Opin Ophthalmol.* 2000;11:107-11

Schwartz M. **Macrophages and microglia in central nervous system injury: are they helpful or harmful?** *J Cereb Blood Flow Metab.* 2003;23:385-94

Schwartz K and Budenz, D. **Current management of glaucoma.** *Curr Opin Ophthalmol.* 2004;15:119-26

Sears ML. **Visual field loss in glaucoma.** *Am J Ophthalmol.* 1979;88:492-8

Sefton AJ and Lam, K. **Quantitative and morphological studies on developing optic axons in normal and enucleated albino rats.** *Exp Brain Res.* 1984;57:107-17

Sergent-Tanguy S, Chagneau, C, Neveu, I and Naveilhan, P. **Fluorescent activated cell sorting (FACS): a rapid and reliable method to estimate the number of neurons in a mixed population.** *J Neurosci Methods.* 2003;129:73-9

Shaked I, Porat, Z, Gersner, R, Kipnis, J and Schwartz, M. **Early activation of microglia as antigen-presenting cells correlates with T cell-mediated protection and repair of the injured central nervous system.** *J Neuroimmunol.* 2004;146:84-93

Shareef S, Sawada, A and Neufeld, AH. **Isoforms of nitric oxide synthase in the optic nerves of rat eyes with chronic moderately elevated intraocular pressure.** *Invest Ophthalmol Vis Sci.* 1999;40:2884-91

Sheffield VC, Stone, EM, Alward, WL, Drack, AV, Johnson, AT, Streb, LM and Nichols, BE. **Genetic linkage of familial open angle glaucoma to chromosome 1q21-q31.** *Nat Genet.* 1993;4:47-50

Shen CL and Liu, KM. **Neuroglia of the adult rat optic nerve in the course of wallerian degeneration.** *Proc Natl Sci Counc Repub China B.* 1984;8:324-34

Shibuya K, Tajima M, Yamate J. **Unilateral atrophy of the optic nerve associated with retrograde and anterograde degenerations in the visual pathways in Slc: Wistar rats.** *J Vet Med Sci.* 1993 Dec;55(6):905-12.

Shou T, Liu, J, Wang, W, Zhou, Y and Zhao, K. **Differential dendritic shrinkage of alpha and beta retinal ganglion cells in cats with chronic glaucoma.** *Invest Ophthalmol Vis Sci.* 2003;44:3005-10

Siu AW, Leung, MC, To, CH, Siu, FK, Ji, JZ and So, KF. **Total retinal nitric oxide production is increased in intraocular pressure-elevated rats.** *Exp Eye Res.* 2002;75:401-6

Snow RL and Robson, JA. **Ganglion cell neurogenesis, migration and early differentiation in the chick retina.** *Neuroscience.* 1994;58:399-409

Soares AS, Artes, PH, McCormick, TA, LeBlanc, RP, Nicolela, MT and Chauhan, BC. **Retinal arterial diameter changes in progressive and nonprogressive glaucoma.** *J Glaucoma.* 2003;12:243-9

Sommer A, Tielsch, JM, Katz, J, Quigley, HA, Gottsch, JD, Javitt, J and Singh, K. **Relationship between intraocular pressure and primary open angle glaucoma among white and black Americans. The Baltimore Eye Survey.** *Arch Ophthalmol.* 1991;109:1090-5

Sommer A. **Glaucoma risk factors observed in the Baltimore Eye Survey.** *Curr Opin Ophthalmol.* 1996;7:93-8

Spaeth GL, Henderer J, Liu C, Kesen M, Altangerel U, Bayer A, Katz LJ, Myers J, Rhee D, Steinmann W. **The disc damage likelihood scale: reproducibility of a new method of estimating the amount of optic nerve damage caused by glaucoma.** *Trans Am Ophthalmol Soc.* 2002;100:181-5

Stamler JS. **Redox signaling: nitrosylation and related target interactions of nitric oxide.** *Cell.* 1994;78:931-6.

Stephan FK and Zucker, I. **Circadian rhythms in drinking behavior and locomotor activity of rats are eliminated by hypothalamic lesions.** *Proc Natl Acad Sci U S A.* 1972;69:1583-6

Stone J, Makarov, F and Hollander, H. **The glial ensheathment of the soma and axon hillock of retinal ganglion cells.** *Vis Neurosci.* 1995;12:273-9

Streit WJ, Graeber, MB and Kreutzberg, GW. **Functional plasticity of microglia: a review.** *Glia.* 1988;1:301-7

Streit WJ, Walter SA, Pennell NA. **Reactive microgliosis.** *Prog Neurobiol.* 1999;57:563-81.

Sugiyama K, Bacon DR, Morrison JC, Van Buskirk EM. **Optic nerve head microvasculature of the rabbit eye.** *Invest Ophthalmol Vis Sci.* 1992;33:2251-61.

Sugiyama T, Moriya, S, Oku, H and Azuma, I. **Association of endothelin-1 with normal tension glaucoma: clinical and fundamental studies.** *Surv Ophthalmol.* 1995;39 Suppl 1:S49-56

Sung VC and Barton, K. **Management of inflammatory glaucomas.** *Curr Opin Ophthalmol.* 2004;15:136-40

Swanson RA. **Astrocyte glutamate uptake during chemical hypoxia in vitro.** *Neurosci Lett.* 1992;147:143-6

Takeuchi A, Isobe, KI, Miyaishi, O, Sawada, M, Fan, ZH, Nakashima, I and Kiuchi, K. **Microglial NO induces delayed neuronal death following acute injury in the striatum.** *Eur J Neurosci.* 1998;10:1613-20

Tan J, Town T, Mori T, Wu Y, Saxe M, Crawford F, Mullan M. **CD45 opposes beta-amyloid peptide-induced microglial activation via inhibition of p44/42 mitogen-activated protein kinase.** *J Neurosci.* 2000;20:7587-94

Tezel G, Kass MA, Kolker AE, Becker B, Wax MB. **Plasma and aqueous humor endothelin levels in primary open-angle glaucoma.** *J Glaucoma.* 1997;6:83-9.

Tezel G, Hernandez, R and Wax, MB. **Immunostaining of heat shock proteins in the retina and optic nerve head of normal and glaucomatous eyes.** *Arch Ophthalmol.* 2000;118:511-8

Tezel G, Chauhan, BC, LeBlanc, RP and Wax, MB. **Immunohistochemical assessment of the glial mitogen-activated protein kinase activation in glaucoma.** *Invest Ophthalmol Vis Sci.* 2003;44:3025-33

Tezel G and Wax, MB. **The immune system and glaucoma.** *Curr Opin Ophthalmol.* 2004;15:80-4

Tezel G, Yang, J and Wax, MB. **Heat shock proteins, immunity and glaucoma.** *Brain Res Bull.* 2004;62:473-80 (a)

Tezel G, Yang, X, Yang, J and Wax, MB. **Role of tumor necrosis factor receptor-1 in the death of retinal ganglion cells following optic nerve crush injury in mice.** *Brain Res.* 2004;996:202-12

Thanos S and Thiel, HJ. **Mechanisms governing neuronal degeneration and axonal regeneration in the mature retinofugal system.** *J Cell Sci Suppl.* 1991;15:125-34

Thanos S and Naskar, R. **Correlation between retinal ganglion cell death and chronically developing inherited glaucoma in a new rat mutant.** *Exp Eye Res.* 2004;79:119-29

Tikka TM and Koistinaho, JE. **Minocycline provides neuroprotection against N-methyl-D-aspartate neurotoxicity by inhibiting microglia.** *J Immunol.* 2001;166:7527-33

Toriu N, Sasaoka M, Shimazawa M, Sugiyama T, Hara H. **Effects of lomerizine, a novel Ca2+ channel blocker, on the normal and endothelin-1-disturbed circulation in the optic nerve head of rabbits.** *J Ocul Pharmacol Ther.* 2001;17:131-49.

Town T, Tan J, Mullan M. **CD40 signaling and Alzheimer's disease pathogenesis.** *Neurochem Int.* 2001;39:371-80.

Trivino A, Ramirez, JM, Salazar, JJ, Ramirez, AI and Garcia-Sanchez, J. **Immunohistochemical study of human optic nerve head astroglia.** *Vision Res.* 1996;36:2015-28

Tsukita S and Ishikawa, H. **The movement of membranous organelles in axons. Electron microscopic identification of anterogradely and retrogradely transported organelles.** *J Cell Biol.* 1980;84:513-30

Turmaine M, Raza, A, Mahal, A, Mangiarini, L, Bates, GP and Davies, SW. **Nonapoptotic neurodegeneration in a transgenic mouse model of Huntington's disease.** *Proc Natl Acad Sci U S A.* 2000;97:8093-7

Tuulonen A, Nagin, P, Schwartz, B and Wu, DC. **Increase of pallor and fluorescein-filling defects of the optic disc in the follow-up of ocular hypertensives measured by computerized image analysis.** *Ophthalmology.* 1987;94:558-63

Ueda J, Sawaguchi S, Hanyu T, Yaoeda K, Fukuchi T, Abe H, Ozawa H. **Experimental glaucoma model in the rat induced by laser trabecular photocoagulation after an intracameral injection of India ink.** *Jpn J Ophthalmol.* 1998;42:337-44.

van der Zypen E. **Experimental morphological study on structure and function of the filtration angel of the rat eye.** *Ophthalmologica.* 1977;174:285-98

Varela HJ and Hernandez, MR. **Astrocyte responses in human optic nerve head with primary open-angle glaucoma.** *J Glaucoma.* 1997;6:303-13

Vickers JC, Lazzarini, RA, Riederer, BM and Morrison, JH. **Intraperikaryal neurofilamentous accumulations in a subset of retinal ganglion cells in aged mice that express a human neurofilament gene.** *Exp Neurol.* 1995;136:266-9 (a)

Vickers JC, Schumer, RA, Podos, SM, Wang, RF, Riederer, BM and Morrison, JH. **Differential vulnerability of neurochemically identified subpopulations of retinal neurons in a monkey model of glaucoma.** *Brain Res.* 1995;680:23-35 (b)

Vickers JC. **The cellular mechanism underlying neuronal degeneration in glaucoma: parallels with Alzheimer's disease.** *Aust N Z J Ophthalmol.* 1997;25:105-9

Vickers JC, Hof, PR, Schumer, RA, Wang, RF, Podos, SM and Morrison, JH. **Magnocellular and parvocellular visual pathways are both affected in a macaque monkey model of glaucoma.** *Aust N Z J Ophthalmol.* 1997;25:239-43

Vickers JC. **A vaccine against Alzheimer's disease: developments to date.** *Drugs Aging.* 2002;19:487-94

Vickers JC, Craig, JE, Stankovich, J, McCormack, GH, West, AK, Dickinson, JL, McCartney, PJ, Coote, MA, Healey, DL and Mackey, DA. **The apolipoprotein epsilon4 gene is associated with elevated risk of normal tension glaucoma.** *Mol Vis.* 2002;8:389-93

Villegas-Perez MP, Vidal-Sanz, M, Bray, GM and Aguayo, AJ. **Influences of peripheral nerve grafts on the survival and regrowth of axotomized retinal ganglion cells in adult rats.** *J Neurosci.* 1988;8:265-80

Vorwerk CK, Gorla MS, Dreyer EB. **An experimental basis for implicating excitotoxicity in glaucomatous optic neuropathy.** *Surv Ophthalmol.* 1999:43 Suppl 1:S142-50.

Wang RF, Schumer, RA, Serle, JB and Podos, SM. **A comparison of argon laser and diode laser photocoagulation of the trabecular meshwork to produce the glaucoma monkey model.** *J Glaucoma.* 1998;7:45-9

Wang X, Tay, SS and Ng, YK. **An immunohistochemical study of neuronal and glial cell reactions in retinae of rats with experimental glaucoma.** *Exp Brain Res.* 2000;132:476-84

Wang L, Cioffi, GA, Cull, G, Dong, J and Fortune, B. **Immunohistologic evidence for retinal glial cell changes in human glaucoma.** *Invest Ophthalmol Vis Sci.* 2002;43:1088-94 (a)

Wang X, Tay, SS and Ng, YK. **An electron microscopic study of neuronal degeneration and glial cell reaction in the retina of glaucomatous rats.** *Histol Histopathol.* 2002;17:1043-52 (b)

Wang CX, Yang, T and Shuaib, A. **Effects of minocycline alone and in combination with mild hypothermia in embolic stroke.** *Brain Res.* 2003;963:327-9

Waniewski RA and Martin, DL. **Exogenous glutamate is metabolized to glutamine and exported by rat primary astrocyte cultures.** *J Neurochem.* 1986;47:304-13

Wax MB, Tezel, G, Kobayashi, S and Hernandez, MR. **Responses of different cell lines from ocular tissues to elevated hydrostatic pressure.** *Br J Ophthalmol.* 2000;84:423-8

Weber AJ, Kaufman, PL and Hubbard, WC. **Morphology of single ganglion cells in the glaucomatous primate retina.** *Invest Ophthalmol Vis Sci.* 1998;39:2304-20

Weber AJ, Zelenak D. **Experimental glaucoma in the primate induced by latex microspheres.** *J Neurosci Methods.* 2001;111:39-48.

Wiggs JL, Haines, JL, Paglinauan, C, Fine, A, Sporn, C and Lou, D. **Genetic linkage of autosomal dominant juvenile glaucoma to 1q21-q31 in three affected pedigrees.** *Genomics.* 1994;21:299-303

Wilson MR, Hertzmark, E, Walker, AM, Childs-Shaw, K and Epstein, DL. **A case-control study of risk factors in open angle glaucoma.** *Arch Ophthalmol.* 1987;105:1066-71

Wizemann AJ and Wizemann, V. **Organic nitrate therapy in glaucoma.** *Am J Ophthalmol.* 1980;90:106-9

Wolf S, Arend, O, Sponsel, WE, Schulte, K, Cantor, LB and Reim, M. **Retinal hemodynamics using scanning laser ophthalmoscopy and hemorheology in chronic open-angle glaucoma.** *Ophthalmology.* 1993;100:1561-6

Wright GJ, Puklavec, MJ, Willis, AC, Hoek, RM, Sedgwick, JD, Brown, MH and Barclay, AN. **Lymphoid/neuronal cell surface OX2 glycoprotein recognizes a novel receptor on macrophages implicated in the control of their function.** *Immunity.* 2000;13:233-42

Wright GJ, Jones, M, Puklavec, MJ, Brown, MH and Barclay, AN. **The unusual distribution of the neuronal/lymphoid cell surface CD200 (OX2) glycoprotein is conserved in humans.** *Immunology.* 2001;102:173-9

Yamadori T and Yamauchi, KE. **An experimental anatomical study on the optic nerve fibers in the rat: courses of the accessory optic tract.** *Brain Res.* 1983;269:41-6

Yang J, Patil, RV, Yu, H, Gordon, M and Wax, MB. **T cell subsets and sIL-2R/IL-2 levels in patients with glaucoma.** *Am J Ophthalmol.* 2001;131:421-6 (a)

Yang J, Yang, P, Tezel, G, Patil, RV, Hernandez, MR and Wax, MB. **Induction of HLA-DR expression in human lamina cribrosa astrocytes by cytokines and simulated ischemia.** *Invest Ophthalmol Vis Sci.* 2001;42:365-71 (b)

Ye H and Hernandez, MR. **Heterogeneity of astrocytes in human optic nerve head.** *J Comp Neurol.* 1995;362:441-52

Yoshioka M, Tanaka, K, Miyazaki, I, Fujita, N, Higashi, Y, Asanuma, M and Ogawa, N. **The dopamine agonist cabergoline provides neuroprotection by activation of the glutathione system and scavenging free radicals.** *Neurosci Res.* 2002;43:259-67

Yucel YH, Kalichman, MW, Mizisin, AP, Powell, HC and Weinreb, RN. **Histomorphometric analysis of optic nerve changes in experimental glaucoma.** *J Glaucoma.* 1999;8:38-45

Yucel YH, Zhang, Q, Weinreb, RN, Kaufman, PL and Gupta, N. **Effects of retinal ganglion cell loss on magno-, parvo-, koniocellular pathways in the lateral geniculate nucleus and visual cortex in glaucoma.** *Prog Retin Eye Res.* 2003;22:465-81

Zeiher AM, Fisslthaler B, Schray-Utz B, Busse R. **Nitric oxide modulates the expression of monocyte chemoattractant protein 1 in cultured human endothelial cells.** *Circ Res.* 1995;76:980-6.

Zhang Y, Champagne, N, Beitel, LK, Goodyer, CG, Trifiro, M and LeBlanc, A. **Estrogen and androgen protection of human neurons against intracellular amyloid beta1-42 toxicity through heat shock protein 70.** *J Neurosci.* 2004;24:5315-21

Zietlow R, Dunnett SB, Fawcett JW. **The effect of microglia on embryonic dopaminergic neuronal survival in vitro: diffusible signals from neurons and glia change microglia from neurotoxic to neuroprotective.** *Eur J Neurosci.* 1999;11:1657-67.

Zigmond MJ (Editor), Bloom FE (Editor), Landis SC (Editor), Roberts JL (Editor), Squire LR (Editor), Woolley RS (Illustrator). **Fundamental Neuroscience**, 1999. Academic press, London

References from the world wide web

Eye Institute, Hartford hospital, www.harthosp.org/eyes/ procedures/glaucoma.htm

Merck Frosst, Canada, www.merckfrosst.ca/.../what_is/home.html

Appendices

Appendix 1: Reagents

Sterile saline solutions

Hypertonic saline (1.75M) used during the microinjection procedure to sclerose the episcleral vasculature was made up by adding 1.022g NaCl (Sigma-Aldrich, UK) to 10ml distilled water. The solution was stirred, followed by filtration to remove particles (0.22 μm filters, Millipore, UK), then autoclaved to ensure sterility.

Similarly, 0.9% sterile saline solution consisted of 0.9% (weight/volume) NaCl in distilled water. This solution was autoclaved and used to maintain hydration of the operated eye during surgical procedures.

Phosphate buffered saline (PBS)

PBS was used as a general buffering reagent in several experiments including perfusion and immunohistochemistry. A concentrated (100%) PBS solution was made up as a stock. This was diluted to 10% before use. 100% PBS consisted of 800g NaCl, 142.4g disodium hydrogen orthophosphate, 20g potassium dihydrogen orthophosphate and 20g potassium chloride dissolved in 10 litres of distilled water. pH was adjusted to 7.5.

The composition of 8% paraformaldehyde stock

PFA was used as a tissue fixative. PFA stock was made up by adding 8g of PFA powder (Sigma-Aldrich, UK) to a 100ml volume of PBS. This mixture was warmed and stirred, while 0.1 M NaOH was added drop-wise until a clear solution was obtained. Once cool, pH was adjusted to 7.4 using 0.1 M HCl.

Neutral buffered formalin (NBF)

Neutral buffered formalin (10%) was used as a fixative in some experiments. One litre of solution was made up by adding 100ml 40% formaldehyde, 4g monohydrate monobasic sodium phosphate and 6.5g anhydrous dibasic sodium phosphate, then topping up to one litre with distilled water.

Gelvatol

Gelvatol was used as a mountant for frozen sections with fluorescence labelling. Gelvatol consisted of 0.08 g Na_2HPO_4 and 0.03 g KH_2PO_4 in 40ml double distilled water (pH7.2) to which 0.327 g NaCl, 0.024 g sodium azide and 0.6 g DABCO (1,4-Diazabicyclo[2.2.2]octane) were added. The solution was then protected from light, and polymerised by stirring in 10 g of gelvatol (vinyl alcohol 25) overnight. Glycerol (20ml) was added (pH6-7) and the mountant centrifuged at 12000 rpm for 15 minutes, and then 18000 rpm for 25 minutes. The mountant was stored at 4°C with protection from light.

Tris-buffered saline (TBS)

On occasions when PBS was not used as a general buffer, for example during the optimisation of immunolabelling techniques, TBS was used as an alternative. TBS consisted of 60.0 g Tris, 44.06 g NaCl, 1.39 g Tris base in 500 ml double distilled H_2O, pH was adjusted to 7.5.

Appendix 2: Conference presentations, abstracts and publications

Conference presentations and abstracts

January 2003

Farrant SY, Albon J, Erichsen JT, Boulton ME, Taylor MA, Morgan JE. **Pathophysiology of retinal ganglion cell death in glaucoma.** School of Optometry

and Vision Sciences Postgraduate Poster Sessions, Cardiff University. (Poster presentation)

November 2003

Farrant SY, Albon J, Erichsen JT, Boulton ME, Taylor MA, Morgan JE. **Glial cell activation in a rodent model of glaucomatous optic nerve degeneration.** Society for Neuroscience annual meeting.

April 2004

Farrant SY, Albon J, Erichsen JT, Akhtar S, Boulton ME, Taylor MA, Morgan JE. **Glial cell activation is associated with retinal ganglion cell apoptosis and neurodegeneration in experimental glaucoma.** School of Optometry and Vision Sciences Postgraduate Poster Sessions, Cardiff University. (Poster presentation)

September 2004

Farrant SY, Albon J, Erichsen JT, Akhtar S, Boulton ME, Taylor MA, Morgan JE. **The role of glia during secondary neurodegeneration in experimental glaucoma.** Cardiff Institute for tissue engineering and repair.

September 2004

Boulton ME, Datta A, Farrant S, Albon J, Erichsen JT, Morgan JE. **Evidence for retinal ganglion cell remodelling in experimental glaucoma.** XVI International Congress of Eye Research.

Published Abstracts

S.Y. **Farrant**, J. Albon, J.T. Erichsen, S. Akhtar, M.E. Boulton, M.A. Taylor, and J.E. Morgan **Optic nerve degeneration in experimental glaucoma is associated with microglial activation.** Invest. Ophthalmol. Vis. Sci. 2004 45: E-Abstract 2141.

S. Akhtar, A.V. Datta, J. Albon, S. **Farrant**, M. Taylor, J.T. Erichsen, M. Boulton, and J.E. Morgan **Ultrastructural Analysis of Optic Nerve Axons in Experimental**

Glaucoma: Evidence for Axon Shrinkage Invest. Ophthalmol. Vis. Sci. 2005 46: E-Abstract 1236.

Papers in preparation

Farrant SY, Albon J, Erichsen JT, Akhtar S, Boulton ME, Taylor MA, Morgan JE. **The role of glia during the initiation of retinal ganglion cell death in experimental glaucoma.** Journal of Neuroscience.

Farrant SY, Albon J, Erichsen JT, Akhtar S, Boulton ME, Taylor MA, Morgan JE. **Correlation of retinal ganglion cell death with intraocular pressure during experimental glaucoma.** IOVS.

Farrant SY, Albon J, Erichsen JT, Boulton ME, Taylor MA, Morgan JE. **The role of nitric oxide synthase during retinal ganglion cell death in a glaucoma model.** IOVS.

Farrant SY, Albon J, Erichsen JT, Boulton ME, Morgan JE. **Statistical analyses of fluorescence images to determine microglial activation.** Journal of Neuroscience Methods.